



2025

# PV Reliability Workshop

## Poster Proceedings

This annual conference was held in Golden, Colorado, with the intent of bringing together solar technology experts to discuss current and future issues in PV reliability. Longer-lasting PV systems make lower-cost solar electricity and have less impact on the environment, human health, and natural resources.

This document collects posters that were presented at PVRW 2025. Click the poster titles in the following agenda to jump to each poster. Not all posters listed in the agenda can be found in this document, as not all poster files were provided to PVRW for inclusion in these proceedings.

The content and views contained herein are those of the individual authors only, and are not reviewed or endorsed by NREL.

August 2025

Access PVRW 2025 poster and presentation proceedings  
[on Box](#) or [on GitHub](#)

### Chair:

Chris Deline

### Committee:

Teresa Barnes  
Ken Boyce  
Jennifer Braid  
Evelyn Butler  
Kristopher Davis  
Michael Deceglie  
Tristan Erion-Lorico  
Robert Flottemesch  
Peter Hacke  
Henry Hieslmair  
Will Hobbs  
Cara Libby  
Danielle Merfeld  
Christos Monokroussos  
Colleen O'Brien  
Gernot Oreski  
Michael Owen-Bellini  
Jon Previtali  
Ingrid Repins  
Laura Schelhas  
Eric Schneller  
Adam Shinn  
Colin Sillerud  
Nick de Vries  
Allan Ward  
Kent Whitfield

## Poster Session A – Tuesday, 4 March 2025

**Notes:** Presenter names are in **bold type**.

01. *Dynamic mechanical compatibility of trackers and PV modules (DuraMAT)*, **C. O'Brien**
04. *Steady-state and Sequenced Accelerated Aging to Reveal Degradation Pathways and Inform IEC Testing Standards*, **K. Liu**, D.C. Miller, N. Bosco, J.M. Newkirk, R.H. Dauskardt
07. *Leveling up for big format bifurcals*, **S. Ovatt**, C. Deline, B. McDanold, J. Park, B. Sekulic, T. Silverman, E. Palmiotti
10. *Progress Towards a Universal PV Plug and Socket*, **M. Kempe**
13. *Recommendations and Limitations for Winter PV Capacity Tests*, **A. Dionigi**
16. *Forecasting glass resilience of large format modules*, **M. Springer**, T. Silverman, J. Newkirk, N. Bosco
19. *Critical Role of Incoming Quality in Domestic Module Manufacturing*, **P. Bhatt**
22. *Simulating Wind-Driven Physics and Instabilities in Single-Axis Trackers*, **E. Young**
25. *Field connectors – observations from current construction projects*, **R. Chatelain**, T. Deer
28. *Mapping PV degradation mechanisms and field performance by leveraging large language models*, **B. Li**, M. Springer, D. Jordan, A. Jain
31. *IEC 61724 Standard Overview*, **M. Gostein**
34. *Predicting Degradation Kinetics Occurring During Encapsulant Lifetime*, H. Dedmon, S. Kruse, J. Kustas, J. Braid, M. Chandross, **M. Wilson**
37. *De-Risking EPE Encapsulants: Modeling Polymer-Polymer Interfaces*, **H. Dedmon**, M. Wilson, E. Palmiotti
40. *Applying Geospatial Workflows with "PVDeg"*, **T. Ford**, S. Ovatt, M. Springer, M. Kempe
43. *New Cells, New Issues: Stress Tests for N-Type PV Module Designs*, **A. Sinha**, J.N. Jaubert, D.B. Kern, T. Karin
46. *Module breakage impacts on system availability*, **C. Helms**, N. de Vries
49. *Effect of Cell Cracks on Module Power Loss and Degradation: Modern Module Architectures*, **V. Parikh**
52. *Accelerated stress testing to deconvolute simultaneous-but-distinct degradation pathways under UV illumination*, **R. Wai**, X. Hanna, J. Newkirk, K. Terwilliger, S. Johnston, D. Miller, P. Hacke, D. Kern
55. *Root cause investigation of glass cracking in field-mounted solar modules*, **J. Karas**, R. Flottemesch, V. Parikh
58. *Investigation of inner layer cracking in PPE backsheets*, **S. Mitterhofer**, Z. Li, A. Aiello, K. Jensen, X. Gu, M.D. Kempe, W. Hobbs
61. *Reliability Evaluation of High-Efficiency Double-Glass PV Modules*, **J.M. Kuitche**
64. *Failure modes in modern cell interconnects for PV modules*, **P. Hacke**, N. Bosco, J. Hartley, S. Uličná
67. *Updates to the Variational Auto-encoder for crack parametrization*, **N. Jost**, O. Sanghi, B. Byford, E. Cooper, B. Pierce, I. Deane, J. Braid
70. *Let's Not R-EPE-at Our Mistakes*, **M. Mirzokarimov**, D. Roberts, L. Schelhas, H. Dedmon, M. Wilson, J. Munro, L. Madenjian, M. Issa, **E. Palmiotti**
73. *Emerging Technique for Detecting Damage On Various Module Layouts*, **R.M. Smith**, D.J. Colvin, B.A. Thompson, C.J. West, E.M. Langlois
76. *Gridline wear-out depends on the regime of crack opening*, **S. Rabade**, N. Bosco
79. *Measuring the stress factors for PV back sheet degradation*, **A. Wesley**, S. Ovatt, M. Prilliman, J. Newkirk, R. Arnold, M. Springer, M. Kempe
82. *DuraMAT Data Hub Chat*, **R. White**, S. Zisman, A. Nag, D. Rager
85. *Strengthening PV Thin Glasses Using Salt Pastes*, **J. Rimsza**, J. Nance, K. Strong

- 88.** *Encapsulants for screen-printed copper contacts*, T. Druffel, **D. Williams**, K. Elmer, E. Yenney, A. Nambo, R. Dharmadasa, P. Stradins, P. Hacke, W. Nemeth, S. Theingi, K. Kenney, J. Munro
- 91.** *Steel module frames plus trackers equals cost savings*, **L.B. Ahsler**
- 94.** *Development of version 1 of the National Climate Database (NCDB)*, **J. Yang**, M. Sengupta, A. Habte, Y. Xie, M. Bailey, D. Nychka, S. Bandyopadhyay
- 97.** *Polysilicon issue of TOPCon bottom cells for perovskite/silicon tandem solar cell performance.*, **C. Lee**, J. Hyun, **H. Lee**, D. Kim
- 100.** *Technoeconomic analysis (TEA) support*, **J. Zuboy**, B. Smith, M. Woodhouse
- 103.** *Modeling Crystallization and Melting in EVA and Polyolefin Encapsulation to Augment Stress Predictions in Cracked PV Modules Over a 24-hour Period*, **K. Long**, K. Cundiff, J. Hartley
- 106.** *Unscrambling combiner box SCADA tags using high frequency time series data*, **R. van Haaren**, M. Marosvari, H. Coleman, K. Rhee
- 109.** *Comparative Dust Soiling Assessment for PV systems: Evaluating Multiple Methodologies*, **B. Pendleton**
- 112.** *Distributed Strain Sensing of Solar PV Single-Axis Tracking System Under Dynamic Wind Loads*, **Y.J. Li**, H. Zhang, A. Chutani, P. Dice, G. Robinson, A.R. Dyreson, M.J. DeJong
- 115.** *A Framework for the Multimodal Analysis of Photovoltaic (PV) Data*, **S.N. Venkat**, J. Raby, B. Thompson, D.J. Colvin, M. Liggett, K. Lu, M. Bolen, S. Johnston, D. Kern, G. Horner, K.O. Davis
- 118.** *Outdoor Performance of n-type Modules With and Without Cell Cracks Over One Year*, **T. Karin**
- 121.** *Silicon Module Recycling by High-Power Lasers*, P.K. Kanaujia, M. Owen-Bellini, H. Mirletz, D.L. Young, **M.C. Gupta**
- 124.** *A computationally derived framework for predicting probability of PV module glass breakage by hail impact*, J. Hartley, **S.J. DiGregorio**
- 127.** *Walkable Solar Panels*, **D. Meakin**

## Poster Session B – Wednesday, 5 March 2025

**Notes:** Presenter names are in **bold type**.

02. *Lessons learned from solar PV energy yield assessment validation*, **E. Giacchino**, E. Soderlund, E. DeCristofaro, J. Silhavy, M. Sleiman
05. *Comparison of degradation due to outdoor exposure and accelerated stress testing in perovskite solar cells*, **T. Tayagaki**, S. Hirooka, H. Kobayashi, K. Yamamoto, T.N. Murakami, M. Yoshita
08. *IEC TC 82 Status*, **G. Kelly**
11. *A New Framework for Standardized Assessments of Risk Severity for Issues in Operating Assets*, **D. Penalva**
14. *2000V PV System LCOE Benefit Analysis*, **B. Frazier**
17. *Selecting bankable resource data for solar energy assessments*, **C. Bordonaro**, P. Metaut, A. Berlinsky, T. Romshek
20. *IEC Standard Aging Sequences for Adhesion in PV Modules*, **R. Arnold**, D. Miller, A. Jackson
23. *Going beyond stuck trackers: how well do your trackers work?*, **W. Hobbs**, K. Anderson
26. *Evaluation of front eave loads caused by snow accumulation on PV modules*, **T. Tanahashi**, T. Chiba, S. Adachi, H. Arakawa, Y. Tsuno, K. Ikeda, T. Oozeki
29. *Hail Damage - A Direct Comparison of Glass-Polymer and Glass-Glass Modules*, **A. Hendricks**
32. *Analyzing the Mechanical Resilience of PV Modules with Different Frame Designs*, **T. Billie**
35. *Field Testing of PID-p Susceptible Bifacial PERC Modules: Impact of Light, Voltage and Module History*, **C. Molto**, D.J. Colvin, R. Smith, P. Hacke, F. Li, G. TamizhMani, J. Oh, H. Seigneur
38. *Effect of Salt Mist and DH Preconditioning on PID for Mono and Bi-facial half cell PERC modules*, **C. Bainier**, J. Cano-Garcia, G. Kaur, E. Kam-Lum
41. *Encapsulation selection for TOPCon cells with LECO*, **J. Munro**, Y. Li, L. Madenjian, M. Issa, P. Brigandt
44. *Investigating Temperature Uniformity and Accuracy in PV Module Lamination: A Verification Study*, **A. Jackson**, R.L. Arnold
47. *Wind-Induced Dynamic Loading and PV Module Frame Fatigue Crack Initiation and Propagation*, **F. Oudheusden**, C. Needham, J. Ness
50. *Comparing Outdoor and Indoor I-V Curves on Bifacial PERC PV Modules Experiencing Polarization-Type Potential-Induced Degradation (PID-p)*, **D. Colvin**, C. Molto, R. Smith, M. Matam, P. Hacke, F. Li, G. TamizhMani, H. Seigneur
53. *Hail Kinetic Energy damage thresholds on large scale PV panels*, **J. Carl**
56. *Wind-Induced Dynamic Loading and PV Module Frame Fatigue Crack Initiation and Propagation*, **F. Oudheusden**, **C. Needham**, J. Ness
59. *Module Mounting Design Qualification Challenges*, **J. Sorensen**, S. Lokanath
62. *Incentivizing reliable PV through Revenue Put insurance premium reduction*, **H. Rasmussen**, A. Shinn
65. *Main factors contributing to the underperformance of solar modules in Colombia: high power tolerances and degradation due to inadequate cleaning procedures and improper handling of solar modules*, **R. Naranjo**, L.F.R. Chavez, J. Barrera, K. Visbal, J.S. Conejo
68. *Spectroscopic analysis of water in PV modules: from water detection to water mapping in polymers*, **C. Buerhop-Lutz**, O. Stroyuk, O. Mashkov, S. Vorstoppel, O. Ghaffari, I. Peters
71. *Filtering of Operational Data for Performance Issue Breakdowns*, **B. Pereyra**
74. *A New Vulnerability in Bypass Diodes Under High Temperature, Long Term Operation in Reverse Bias (HTRB)*, **K. Rane**, **N. Shiradkar**
77. *Pre-failure signatures of solar pv inverters: a pathway for improving inverter reliability*, **K. Buch**, R. Dhakal, W. Li

- 80.** *Unraveling the Degradation of SHJ Solar Cells with 82% Less Silver*, **M.W. Martinez-Szewczyk**, O.J. Hildreth, M.I. Bertoni
- 83.** *Classification of Defects in Thin film Silicon Modules for Hotspot Formation Using EL Imaging*, **S.K. Pullayikody**, P. Sluijs, N. Zeiher, V. Venkatesh, G. Mathiazagan, R. Vasudevan, A. Smets
- 86.** *Rapid Screening of SHJ and TOPCon Solar Cells for UV Degradation*, **J.D. Zubieta Sempertegui**, N. Moser-Mancewicz, J.G. Gezelter, S.R. Buffone, S. Cheng, M. Kamperai, N.G. Tshuma, G. Thomas, C. Biaou, J.L. Bryan, K.O. Davis, M.I. Bertoni, L.S. Bruckman, I.T. Martin
- 89.** *PV Equipment Failures: Patterns and Predictions from O&M log data*, **C. Sotero**
- 92.** *Best practices for pv project hail recovery*, **S. Ressler**
- 95.** *An evaluation of operational PV project availability performance*, **K. Mullaney**, A. Chang, B. Grenko
- 98.** *Evaluating the Degradation of Silicon Heterojunction Devices Through Chemical Analysis and Computational Simulation*, **N. Moser-Mancewicz**, J. Ochoa, M. Martinez-Szewczyk, T. Bantle, D. Kern, D. Jordan, S. Johnston, J. Medvedeva, M. Bertoni
- 101.** *Reliable design: establishing a feedback loop between real world and design conditions*, **D. Herron**, A. Lindsay, M. Toro
- 104.** *Module Due Diligence for Procurement by a Developer*, **S.K.L. Xu**
- 107.** *Field Demo Sneak Peak: Side-by-Side Comparison of Hail Damage Mitigation*, **K. Reiter**, M. Bolen, D. Doerner
- 110.** *Fluctuating PV module wind loads*, **Y. Fewless**
- 113.** *Anomaly detection in PV fleet data via interpretable machine learning*, **B. Meyers**, A. Dufour, G. Ogut
- 116.** *Comparative Dust Soiling Assessment for PV systems: Evaluating Multiple Methodologies*, **S. Li**, B. Pendleton, T. Müller
- 119.** *MANTIS: from multiscale analysis to next generation thin film module inspection systems*, **G. Horner**
- 122.** *Inline, Non-contact EL Scanner for Module Inspection and Quality Control*, **K. Lu**, E. Ignatovich, P. Miller, L. Vasilyev, A. Dirriwachter, J. Williams, T. Frank, E. Schneller
- 125.** *Development of meaningful, low-cost Solar PV module and mounting fastener stack testing equipment and procedures*, **G. Robinson**

## Poster Session C – Thursday, 6 March 2025

**Notes:** Presenter names are in **bold type**.

03. *Developing a UV Spot Test for Years of Equivalent Exposure, I. Repins*, T. Silverman, E. Palmiotti, M. Deceglie, A. Gaulding
06. *Residual Effects of Long-Term Vegetation Shading on a Ground Mount PV Array, R. Stromberg*
09. *GroundWork® Eyewitness™ Hail Monitoring and Event Reporting Service: A summary of hail data collected from a dense network of hail monitoring devices, T. Morrison*, J. Chard, A. Bryan, A. Will
12. *What is a polyolefin? A critical overview of ethylene copolymers as PV module encapsulants, G. Oreski*, C. Barretta, P. Christöfl, P. Gebhardt, K.A. Weiss, D. Miller, M. Kempe, S. Ulicna, A. Virtuani, H. Li, B. Habersberger, J. Munro, K. Proost, M. Kühne
15. *Analysis the Performance of PV Modules with Different Failures under Longtime Outdoor Condition, B. Wang*
18. *Low-cost daytime electroluminescence imaging, A.M. Gabor*, R. Landy, J.D. Friedl
21. *Screening early field failure in metal halide perovskite modules through stress testing, N.P. Irvin*, S. Uličná, J. Schall, D.B. Kern, T.J. Silverman, M. Deceglie, C. Fei, X. Shi, R.L. Arnold, B. McDanold, J. Parker, J. Huang, J.J. Berry, J.S. Stein, L.T. Schelhas
24. *A Tool to Create High-Fidelity and Adaptive Finite Element Model for PV Systems, X. He*, W. Arsalane, M.P. Shah
27. *From Hail to Hardware: A Comprehensive Risk Assessment for Solar Asset Resilience, R. Fagan*
30. *PV Standards Activities of IEC, J. Wohlgemuth*
33. *Soiling loss modeling in regions across the US, A. Berlinsky*, P. Metaut, C. Bordonaro, T. Romshek
36. *Adaptable Silicon Solar Cell Metrology in the Age of the Inflation Reduction Act, H. Wilterdink*, A.B. Karpen, N. Degenhart, L. Bruno, W. Dobson, R. Sinton
39. *X-Ray Imaging as a Tool for Understanding Photovoltaic Connector Failures, S. DiGregorio*, L. Burnham, B. King
42. *Performance evaluation of a Brazil research floating PV power plant, D.A. Cassini, A.S.A. Diniz, V.C. Santana, D.S. Braga, L.L. Kazmerski*
45. *Module Mounting Design Qualification Challenges, S. Lokanath*, J. Sorensen
48. *17 Years of Investigating Fires in PV Systems: A Synopsis of Experience, B. Brooks*
51. *Module and tracker deformation, G. Jago*
54. *Low-Cost Vibrational Sensors for in-situ High-wind Detection and Analysis, D.C. Jordan*, R. Smith, B. Sekulic, H. Seigneur
57. *Characterizing PV Modules using Paralleled MOSFET Loads with Active Feedback, A. Mapes, W. Sekulic*
60. *Updates on PV Bio-Soiling in the Southeast U.S., M. Muller*, A. Rivera, M. Valerino
63. *A Comprehensive Test-to-Failure Protocol for PV Module Hail Damage: Integrating Weibull Analysis and Impact Mechanics, T. DeWolf-Moura*, S.A. Far, P. Bostock, R. Fritz, A. Hernandez, M. Kaur, C. Kedir, M. Pilliod, J. Previtali, J.R. Reynolds
66. *Evaluation of Durability and Cracking Propensity of Emerging PV Backsheets after Accelerated Laboratory Weathering, X. Gu*, S. Mitterhofer, Z. Li, A. Aiello, A. Aiello, K. Jensen, H.H. Hsien, A. Kadri, L. Ji
69. *The road to perovskite bankability, F. Dross*, T. Krajewski, L. Crowe
72. *Reliable Module Design Cost Reductions for Vertical Bifacial PV, J. McCabe*
75. *Assessing risk of glass failure during due diligence, B. Weinshenker*
78. *Climate Resilience for Inverter of Utility Scale PV Plant: Strategies and Risk Assessment, R. Dhakal*
81. *Watts the Hype? AI's Role in Powering Solar Reliability, M. Mousou*

- 84.** *Investigating oxygen barrier properties of desiccated edge sealants for protection of perovskite solar modules*, **L. Postak**
- 87.** *Edge sealed modules for improved perovskite stability in 1000 hours of damp heat testing*, **R. Ruhle**, D. Durney, D. McDougall, L. Laxmi, V. Chityala, D. Kabra, W. Sampath
- 90.** *Edge sealed photovoltaic modules: matching thermal and optical properties of traditional encapsulation*, **D. Durney**, R. Ruhle, L. Maple, S. Johnston, D. Kern, W. Sampath
- 93.** *Data-driven insights into solar production performance*, **P. Hwang**
- 96.** *A review of modeled performance of PAN files in PVsyst®*, **E. Westphal**
- 99.** *Recommendations for research-scale mini-module vacuum laminations*, **M. Owen-Bellini**
- 102.** *Diffuse Stow: Maximizing Potential in Photovoltaic Tracking*, **R.A. Borea**, S. Ovaitt, V. Cirimele, F. Melino, G. Maugeri, T. Ford
- 105.** *Observation of High PV Durability Under Harsh Sequential Stress*, **D. Kern**
- 108.** *Sustainable Solar Photovoltaics: Utilising operational characteristics for end-of-life management*, **A.P. Joshi**
- 111.** *Heat and light: reliability testing of perovskite modules*, P. Pasmans, S. Roest, **J. Veloza**
- 114.** *Enhancing performance of solar trackers through wind nowcasting and aerodynamic mitigations*, P. Fatehi, M. Elnahla, Y. Guo, T. Wu, **J. Elsworth**, S. Dana
- 117.** *Photovoltaic module backsheets burns attributed to misaligned busbar wires*, **S. Johnston**
- 120.** *Assessment of frame sealant property to module glass breakage via beam mechanics theory*, **Y. Lai**, G. Beaucarne, V. Hayez
- 123.** *The Transferability of Silicon Photovoltaic Multiscale Diagnostics to Cadmium Telluride Technologies*, **M. Liggett**, D.J. Colvin, S.N. Venkat, G. Horner, M. Bolen, S. Johnston, D. Kern, K.O. Davis
- 126.** *Off track: performance impacts of PV tracker mishaps*, **S. MacAlpine**



# Advancing Steady-State and Sequenced Accelerated Aging for Assessing Adhesion Degradation in Contemporary Encapsulants

Kuan (Alan) Liu<sup>1</sup>, David C. Miller<sup>2</sup>, Nick Bosco<sup>2</sup>, Jimmy M. Newkirk<sup>2</sup>, Reinhold H. Dauskardt<sup>1</sup>

<sup>1</sup>Stanford University; <sup>2</sup>National Renewable Energy Laboratory

Awarded FY22  
Core Modelling Call

Period of Performance:

04/01/23 – 03/31/25

Funding: SUB-2023-10208

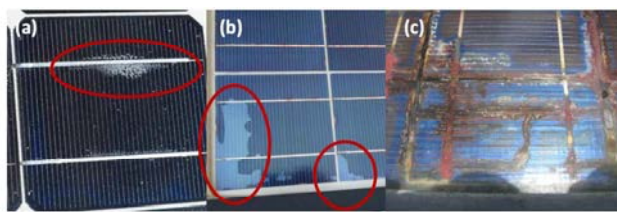
## Contributing to DuraMAT Consortium Goals

- Investigate how environmental stressors induce molecular degradation and crosslinking, affecting the encapsulants' long-term interfacial adhesion and mechanical properties with accelerated aging of up to 10,000 hours.
- Steady-state and sequenced accelerated aging tests inform IEC testing standards to ensure long-term module reliability by capturing the dominant degradation mechanisms and their connection to interfacial degradation.

## Project Overview and Goals

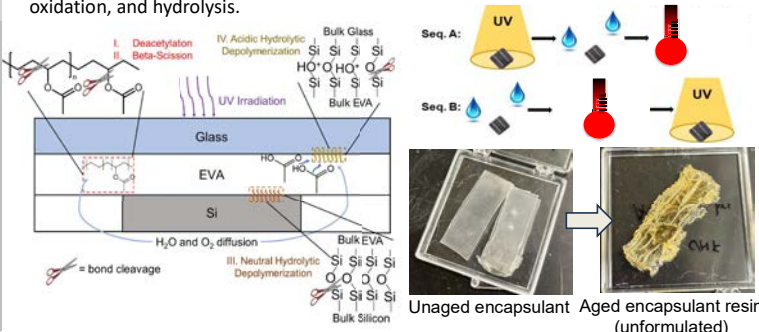
### Motivation:

- Encapsulant degradation leads to embrittlement and delamination in solar modules.
- Delamination could lead to moisture ingress, corrosion, and transmittance losses.

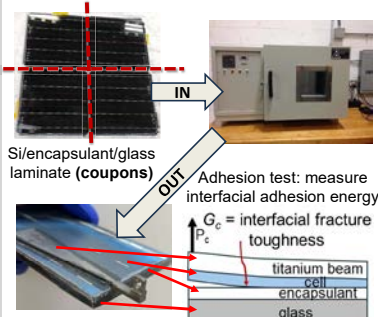


### Goals:

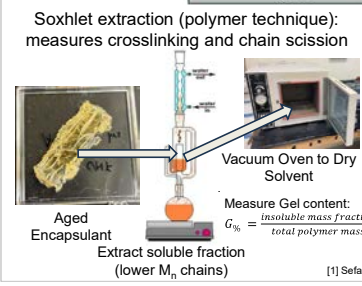
- Identify long-term encapsulant and interfacial degradation mechanisms and kinetics with specific accelerated aging conditions simulating isolated and combined UV, elevated humidity, and elevated temperature (environmental stressors).
- Explain the effects of different sequences of exposures for informing accelerated testing strategies that will ensure 50-year module lifetimes.
- Develop and experimentally validate a module encapsulant degradation model incorporating fundamental degradation pathways and their dependence on photolysis, oxidation, and hydrolysis.



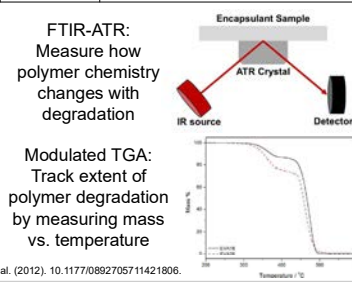
## Aging Conditions and Characterization Techniques



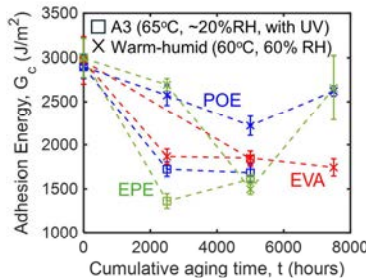
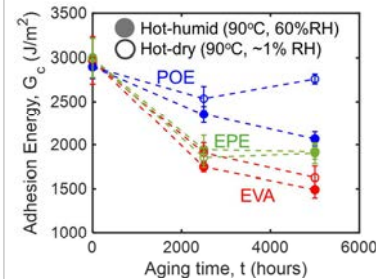
| Name                  | Aging Condition  |
|-----------------------|--|
| Hot-dry (HD)          | Steady state: to 10,000 hours cumulative 90°C, ~1% RH, no UV   |
| Hot-humid (HH)        | Steady state: to 10,000 hours cumulative 90°C, 60% RH, no UV   |
| Warm-humid (WH)       | Steady state: to 10,000 hours cumulative 60°C, 60% RH, no UV   |
| IEC TS 62788-7-2 (A3) | Steady state: to 10,000 hours cumulative 65°C, ~20% RH, UV 0.8 W/(m²·nm) at 340 nm                       |
| IEC TS 62788-7-2 (A5) | Steady state: to 5,000 hours cumulative 85°C, ~20% RH, UV 0.8 W/(m²·nm) at 340 nm                        |
| WH to A3              | Sequenced: (Warm-humid (2500 hours) → A3 UV (2500 hours) → Warm-humid (2500 hours) → A3 UV (2500 hours)) |
| A3 to WH              | Sequenced: A3 UV (2500 hours) → Warm-humid (2500 hours) → A3 UV (2500 hours) → Warm-humid (2500 hours)   |



[1] Sefadi et al. (2012). 10.1177/089205711241806.

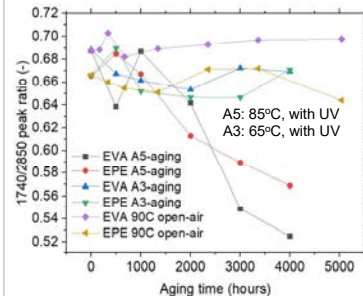


## Results

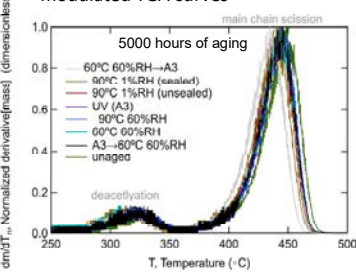


- POE-encapsulated coupons exhibited the best thermal and moisture stability, having the least  $G_c$  degradation under hot-humid, hot-dry, warm-humid conditions.
- Similar degrees of interfacial adhesion degradation in the presence of UV (A3).

### FTIR carbonyl index: deacetylation extent



### EPE (EVA/POE/EPE composite) modulated TGA curves



- FTIR-ATR carbonyl index analysis (left) shows that deacetylation is significant only at combined elevated temperature (>90°C) and UV conditions for EVA and EPE.
- In modulated TGA through 5k-hours of aging, EPE shows that main-chain scission is most prominent under the warm-humid to UV (A3) condition.

## Future Work, Presentations, Publications

### Future work:

- Continue characterizations (adhesion testing, Soxhlet extraction, FTIR-ATR, DMA, MTGA) of coupon and encapsulant samples with up to 10,000 hours of accelerated aging.
- Investigate the effect of sequenced accelerated aging on interfacial adhesion energy.
- Tune and expand the capabilities of the previously developed module encapsulant degradation model with newly acquired accelerated aging results, which serves as a useful delamination predictive tool for the PV community.

### Acknowledgements:

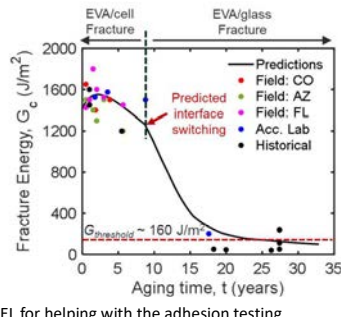
We thank Rachael L. Arnold and Aubrey Jackson of NREL for helping with the adhesion testing technique. Part of this work was performed at the Stanford Nano Shared Facilities, supported by the National Science Foundation under award ECCS-2026822.

### Select Presentations (2024):

- K. Liu, D.C. Miller, N. Bosco, R.H. Dauskardt, "Degradation Mechanisms and the Role of Sequenced Accelerated Testing to Ensure Long-Term Solar Module Encapsulation", Durable Materials Consortium Fall 2024 Workshop, September 17-18, 2024, Oral Presentation.
- K. Liu, D.C. Miller, N. Bosco, R.H. Dauskardt, "Determining the Photochemical Degradation and Crosslinking Kinetics in Photovoltaic Encapsulants Using Accelerated Aging", 2024 IEEE PVSC, June 13, 2024, Oral Presentation.
- K. Liu, D.C. Miller, N. Bosco, R.H. Dauskardt, "Predictive mechanics and photochemical degradation kinetics modeling for polymeric encapsulants", DuraMAT Webinar, April 8, 2024, Oral Presentation. <https://www.duramat.org/news-and-events/webinars>
- K. Liu, D.C. Miller, N. Bosco, R.H. Dauskardt, "Predictive mechanics and photochemical degradation kinetics modeling for polymeric encapsulants", NREL Photovoltaic Reliability Workshop, Lakewood, CO, February 28, 2024, Oral Presentation

### Publications:

- K. Liu, D. C. Miller, N. Bosco, J. M. Newkirk, T. Sakamoto and R. H. Dauskardt, "Investigating the Crosslinking, Degradation, and Adhesion Behavior of Photovoltaic Encapsulants Under Thermal Accelerated Aging," in IEEE JPV, doi: 10.1109/JPHOT.2024.3496512.
- K. Liu, T. Thornton, P. D'hooge DR, Dauskardt RH. Predicting encapsulant delamination in photovoltaic modules bridging photochemical reaction kinetics and fracture mechanics. *Prog Photovolt Res Appl.* 2023; 1-13. doi:10.1002/pip.3771



# Leveling-up for Big-Format Modules

Silvana Ovaitt, Chris Deline, Byron McDanold, Josh Park, Mike Deceglie, Bill Sekulic, Greg Perrin, Kent Terwillinger, Luke McClintok, Ellie Palmiotti, Tim Silverman (NREL)



## Awarded FY25 Core Modelling Call

Period of Performance: FY25  
Funding: \$50k

Like Mario grabbing a super mushroom, PV modules just keep getting bigger! As they grow, so do the challenges of handling, installing, and testing them in the field. At NREL, we've embarked on our own *New Hope*—adapting to this size revolution across our tools, transportation, ergonomics, and field compatibility. Join us as we navigate this galactic expansion and keep PV testing at the cutting edge.

### Project objectives:

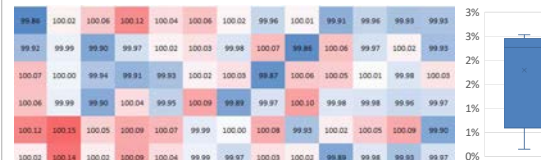
1. Develop capability for measuring large-format bifacial TOPCon modules
2. Conduct initial characterization of modules
3. Engage with industry by recruiting additional module partners and creating initial characterization and commissioning reports for manufacturers



## Contribution to DuraMAT Consortium Goals – Project Overview

Enhance NREL's capability to measure and characterize large-format bifacial TOPCon modules, and establish a reliable baseline for future field comparisons, ensuring precise performance assessment.

## Sintonulator Updates



While we got a flashy new flash-tester that has leveled-up to accommodate these giant power-up modules, we have also worked on upgrading our Sintonulator (solar simulator from Sinton) to ensure we can still provide top-tier testing and reliability measurements for these oversized modules. Tests were run to evaluate the uniformity across the module surface, and attempt to improve it.



### Variables tested:

- **Operator** – Different individuals, different clothing (Stormtrooper), plus no operator (tape)
- **Light Source & Placement** – white light (front, behind, or off), and red-light behind
- **Bulb Condition** – Either left "as is" or "cleaned."
- **Flash Rate**: BPM (30, 45, 60)
- **Curtain Mode** – "Careful mode" consistently used.
- **Repetitions**
- **Area and material type** – module center only; planar steel module

### Takeaways:

1. Precise positioning reduces non-uniformity, with tape achieving the lowest values.
2. Higher flash rates (e.g., 60 bpm) increased non-uniformity, suggesting sensitivity to setup inconsistencies
3. Bulb cleaning and lighting conditions have little impact on non-uniformity.
4. **Proposed improvements:** redesigning the measurement-gig to maintain better contact, adjusting module height for better positioning, and adding a baffle to improve light control.

| Type       | Control 1 | Control 2 | Field 1 | Field 2 | Field 3-16 |
|------------|-----------|-----------|---------|---------|------------|
| Visual     | X         | X         | X       | X       | X          |
| EL         | X         | X         | X       | X       | X          |
| SOMS F+R   | X         | X         | X       | X       |            |
| Sinton F+R | X         | X         | X       | X       |            |
| QE         | X         |           | X       |         |            |
| MSR F      | X         |           |         |         |            |
| TS cbc PL  | X         |           |         |         |            |
| N/C EL     | X         |           |         |         |            |
| UVF        | X         |           |         |         |            |
| BS Optical | X         |           |         |         |            |
| Temper     | X         |           |         |         |            |

Set of baseline measurements for our large-format modules (*ongoing*)

## Field Module Installation

As PV modules continue their *Super Mushroom* growth, their electrical characteristics are also evolving, pushing the limits of existing field components. One key adaptation has been upgrading optimizers, as the voltage of the new, larger modules exceeds the capacity of older models. Previously mounted to the torque tube, the new optimizers required redesigned mounting solutions since they no longer fit the existing brackets. Luckily for us our inverter size did not need to change on this case—no need to *disturb the Force* of our power conversion.

The module size was also not compatible with our racking, so we fabricated a custom jig to redrill the torque tube, referencing existing holes while adding new ones to reposition the mounting arms. Currently the entire row has been stripped down to the bare torque tube before remounting the arms in their new configuration. A filler 'module' will be fabricated to occupy the remaining space at the end of rows where a full module won't fit.



These types of modifications are becoming increasingly common in the repowering of utility-scale PV systems, where older infrastructure must adapt to the latest generation of larger, more powerful modules. However, the need for reengineering—whether it's replacing inverters, cables or other electronics, or adjusting mounting configurations—adds significant costs. In many cases, these expenses make **repowering** economically unfeasible.

(Want to know more? See our PVSC 2025 presentation)

## Call for Industry Participation

- **Data Accessibility:** Once testing is complete, measurement data will be made available on the DataHub.
- **Call for Industry Participation:** We welcome more industry module partners to engage with our field testing efforts and ensure that emerging PV technologies are rigorously evaluated under real-world conditions.



And remember:  
lift with the legs,  
keep the load close,  
engage your core,  
and use a partner—  
Stormtrooper  
safety first!



# Simulating Wind-Driven Physics and Instabilities in Single-Axis Trackers



Ethan Young\*, Xin He, Brooke Stanislawski, Walid Arsalane, Chris Ivanov, Scott Dana, Mike Deceglie

\* Email: ethan.young@nrel.gov

**Awarded FY22  
Core Modelling Call**
**Period of Performance: FY23-FY25  
Funding: \$800K**
**Contributing to DuraMAT Consortium Goals**

We are developing computational tools and case studies to reduce the destructive effects of wind loading on PV panels and in turn minimize degradation effects that can worsen cell cracking and reduce performance over the lifetime of the module. We will identify the exact mechanism(s) by which wind loading leads to the deterioration of modules (e.g., vortex shedding, array layout) to inform design and operation guidelines to reduce degradation and avoid the most damaging phenomena associated with wind loading in PV arrays.

## Project Overview

As PV modules continue to trend toward larger, thinner, and more flexible forms they grow more susceptible to damage from dynamic wind loading. As a result, understanding the impact of wind on PV systems, particularly when mounted on solar-tracking hardware, and identifying robust, stable array layouts and stow strategies is becoming increasingly important for the PV community. We are developing PVade (PV Aerodynamic Design Engineering)<sup>1</sup>, an open-source, fluid-structure interaction (FSI) software to predict unsteady PV loading and dynamic instability due to wind. This software will enable researchers to test hardware, layout, and tracker control changes, leading to enhanced stability, optimized stow strategies, and a reduction in wind-driven damage.

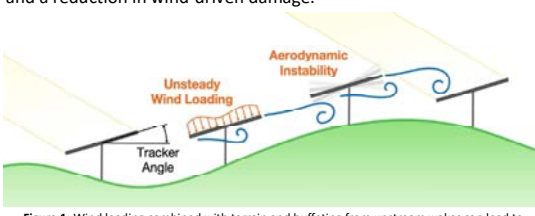


Figure 1: Wind loading combined with terrain and buffeting from upstream wakes can lead to fluttering and instability of panels, particularly when mounted on compliant, solar-tracking hardware.

## Solver Background

PVade is scalable from desktop to high-performance computing hardware with no modification. It makes extensive use of the DOLFINx and Gmsh packages<sup>2,3</sup> and enables easy PV-system problem definitions via yaml input files.

### Physics Solvers

We employ a fractional step method to numerically solve the arbitrary Lagrangian-Eulerian (ALE)<sup>4</sup> incompressible Navier-Stokes equations and an advection diffusion equation for temperature. The response of the structure is obtained by solving the equilibrium equation

### FSI Coupling

PVade uses a partitioned FSI coupling in which fluid and structure are solved separately and coupled through an iteration-free, predictor-corrector algorithm<sup>5</sup>:

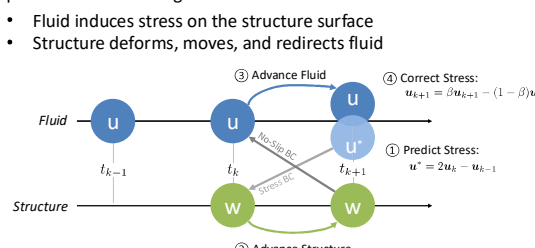


Figure 2: PVade's FSI algorithm: ① predict the next hydrodynamic stress using previous two states, ② advance structure from k to k+1 using this prediction, ③ advance fluid from k to k+1 using the k+1 structural boundary conditions, and ④ correct the predicted stress with the true stress.

## Outcome and Impact

We are developing an open-source FSI simulation tool for PV systems, PVade. We have performed a preliminary validation of our loading and deformation models using single-row experimental data and are in the process of improving agreement and extending validation to multiple-row arrays. We have added new features

including temperature and heat transfer and improved the accuracy of structural properties. PVade is being used to support studies with multiple industry partners and developing more new features to support applications with novel agrivoltaics hardware and floating installations.

Scan to learn more and get started with PVade!

## Heat Transfer Modeling

### Motivation

Solar panels are typically hotter than the surrounding air. In the ensuing heat transfer problem: (1) the flow of wind through the array is affected by the warmer air rising and (2) the panels are cooled by the wind. When the temperature of PV panels decreases, efficiency increases, and module degradation is reduced. Each 10°C increase in module temperature reduces module lifetime by 50%<sup>6</sup>.

### Methodology

By adding in a buoyancy term to the ALE momentum equation and an additional solve for the advection-diffusion equation for temperature, we can simulate two-way coupled convective heat transfer between the PV panels and the surrounding air flow and predict which combinations of tilt angle and weather lead to improved convective cooling and lower operating temperature.

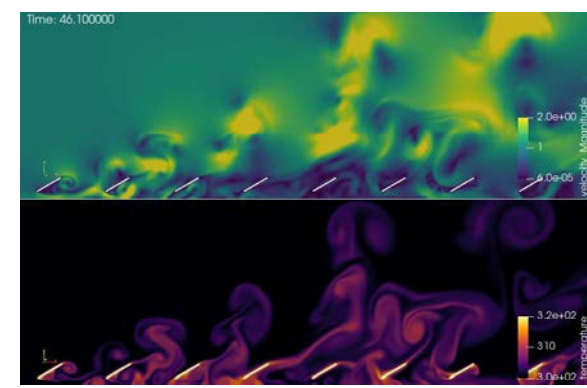
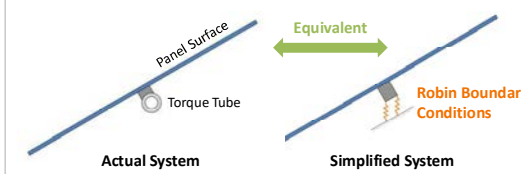


Figure 3: (Top) a snapshot of the velocity magnitude as wind moves through the solar farm from left to right and (Bottom) the corresponding temperature field as heat from the panels is transported into the surrounding air.

## Tracker Hardware Modeling

### Motivation

Directly simulating the torque tube and its attachment points in PVade would require a complicated geometry specification and extremely fine meshing which would significantly increase the overall computational expense. To simplify the simulation while predicting an accurate response from the structure, we exclude the torque tube from the FSI mesh but accurately capture its stiffness and torsional resistance via Robin boundary conditions.



### Methodology

Given a constant torque applied to each of the PV panels sharing a torque tube, the rotation of the actual torque tube should be the same as the rotation of the boundary condition attachment point in the simplified structure.

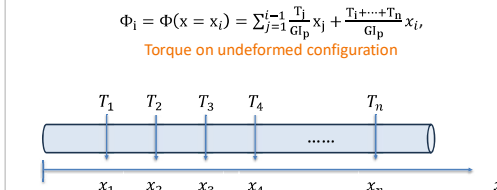
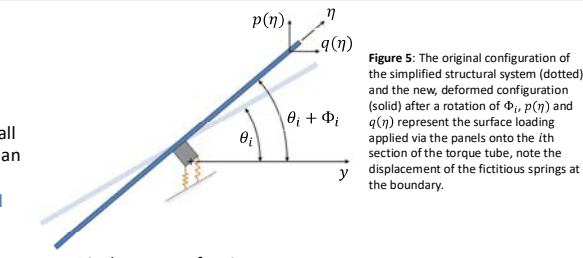


Figure 4: Discretizing the torque tube into per-panel segments and labeling the load per each of these segments allows us to predict both individual and aggregate rotation.



Displacement of springs:

$$u_y = \eta [\sin(\theta_i + \phi_i) - \sin(\theta_i)]$$

Force applied by springs:

$$dF = u_y K_i ds, ds = wd\eta, w: \text{width of spring area}$$

Torque:

$$T_i(\text{deformed}) = \int_0^{l_0} 2\eta \cos(\theta_i + \phi_i) dF$$

Stiffness of Springs:

$$K_i = \frac{12T_i(\text{deformed})}{l_0^3 \cos(\theta_i + \phi_i) [\sin(\theta_i + \phi_i) - \sin(\theta_i)] w} (N/m^3)$$

### Verification

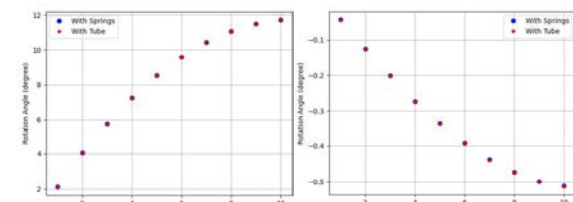


Figure 6: (Left) rigid panels with  $p(\eta) = 1000\text{Pa}$ ,  $q(\eta) = 200\text{Pa}$  at  $\eta > 0$  and  $p(\eta) = -1000\text{Pa}$ ,  $q(\eta) = -200\text{Pa}$  at  $\eta < 0$ , (Right) compliant panels with real wind loading simulated in PVade.

## Future Work

We will focus on understanding how these different physical effects lead to instability, damage, and degradation in multiple-row arrays and identify combinations of tracker angle and array design that increase resilience.

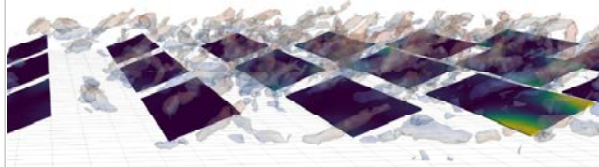


Figure 7: The displacements predicted in a 7x3 array of panels, isosurfaces depict vorticity in the wake, note the large displacements on the array perimeter.

### Acknowledgements

This work was authored by the National Renewable Energy Laboratory, operated by Alliance for Sustainable Energy, LLC, for the U.S. Department of Energy (DOE) under Contract No. DE-AC36-08GQ28308. Funding provided by the U.S. Department of Energy Solar Energy Technologies Office Durable Module Materials Consortium. The views expressed in the article do not necessarily represent the views of the DOE or the U.S. Government. The U.S. Government retains and the publisher, by accepting the article for publication, acknowledges that the U.S. Government retains a nonexclusive, paid-up, irrevocable, worldwide license to publish or reproduce the published form of this work, or allow others to do so, for U.S. Government purposes. A portion of the research was performed using computational resources sponsored by the Department of Energy's Office of Energy Efficiency and Renewable Energy and located at the National Renewable Energy Laboratory.

### References

- E. Young, W. Arsalane, B. Stanislawski, X. He, et al., "PVade (PV Aerodynamic Design Engineering)," 2023
- I. A. Baratta, et al., "DOLFINx: The next generation FEniCS problem solving environment," 2023
- C. Geuzaine and J.-F. Remacle, "Gmsh: a three-dimensional finite element mesh generator with built-in pre- and post-processing facilities," 2009
- J. Donea, A. Huerta, et al., "Arbitrary Lagrangian-Eulerian Methods," 2004
- W. G. Dettmer and D. Perić, "A new staggered scheme for fluid-structure interaction," 2013
- D. H. Ott et al., "Assessing photovoltaic module degradation and lifetime from long term environmental tests," 1983

# DC connectors – Field observations from current construction projects

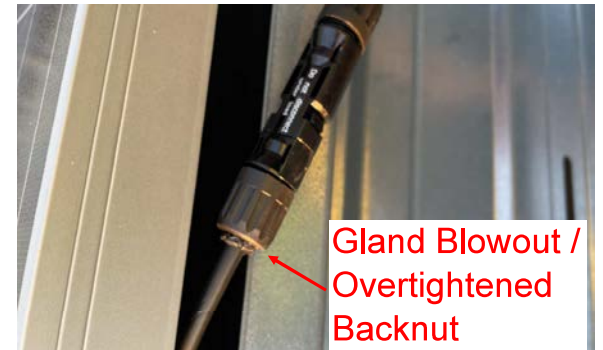
**Authors:** Tanya Deer (Luminace), Rob Chatelain (Luminace); Dustin Becher (Luminace)

During 2024 construction visits, it was discovered that the personnel performing wire management and making field connectors are not trained/qualified, are not aware of manufacturer specifications, and are not supplied with the required tools. There are no quality-control measures. The presented field observations show multiple safety and quality concerns with connectors across newly constructed sites by well-known PV EPCs.

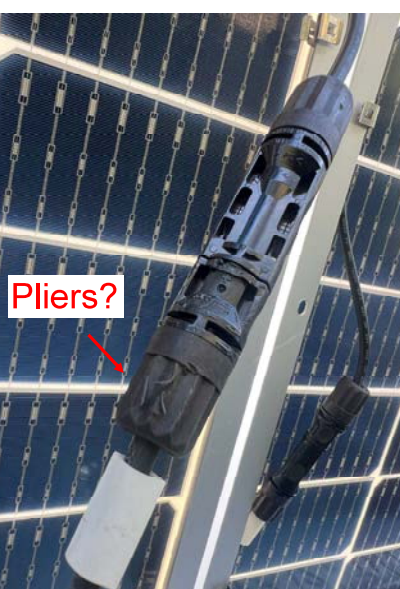
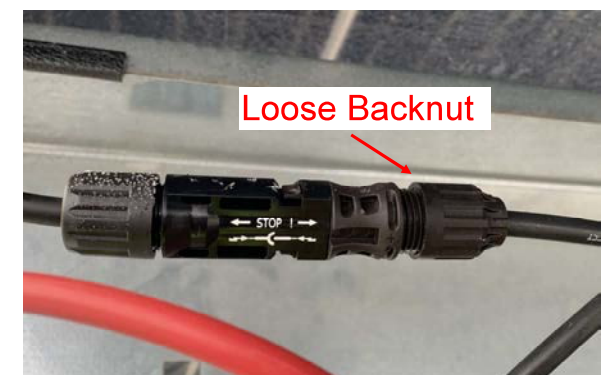
Wrong tools



Mis-matched



Loose Backnut



Uncapped Connector



# Predicting Degradation Kinetics Occurring During Encapsulant Lifetime

Hannah Dedmon, Samantha Kruse, Jessica Kustas, Jennifer Braid, Michael Chandross, Mark A. Wilson  
Sandia National Laboratories, NM, contact: [marwils@sandia.gov](mailto:marwils@sandia.gov)



Multi-Scale, Multi-Physics Model

Awarded FY24  
Core Modelling Call

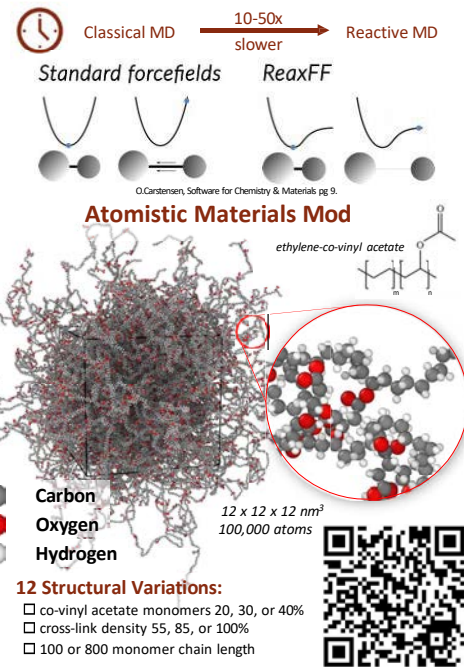
Period of Performance: 18 months  
Funding: \$165K

## Contributing to DuraMAT Consortium Goals

1. Inform understanding of chemical degradation of polymeric encapsulant materials
2. Elucidate concentration dependent degradation in the presence of dissolved species
3. Report chemically specific input parameters for higher length scale models

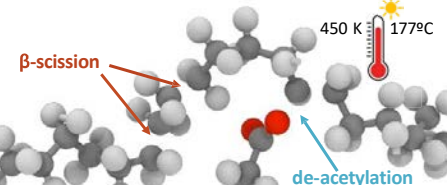
### Simulating Degradation Pathways

Unlike other force fields used in Classical MD simulations, **Reactive Force Field (ReaxFF)** used to model kinetic processes allows for **dynamic bond orders**.



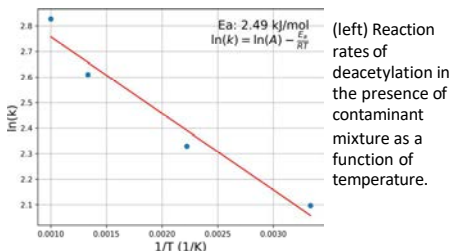
Molecular scale simulations  
reveal increases in degradation  
of EVA encapsulants in the  
presence of contaminants.

### Tracing $\beta$ -Scission and De-Acetylation



### Reaction Activation Energy

Reaction rates were found over a large temperature range to compute activation energies in the presence of various contaminant species.



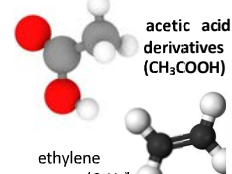
Activation energy (kJ/mol) of de-acetylation in various contaminant environments; no contaminants (EVA), in water, in acetic acid, and in a mixture of water, acetic acid, and oxygen.

| units: kJ/mol  | EVA  | in water | in acetic acid | in mix |
|----------------|------|----------|----------------|--------|
| De-acetylation | 7.49 | 1.99     | 3.25           | 2.49   |

### Reaction By-Products

Small molecule by-products were identified for comparison with MALDI-TOFSM, GCMS, and nano-IR results from experimental aging studies. The top by-products produced from degradation of EVA in water at 450 K are shown below.

- 1) CO<sub>2</sub>
- 2) C<sub>2</sub>H<sub>4</sub>O<sub>2</sub>
- 3) C<sub>2</sub>H<sub>3</sub>O<sub>2</sub>
- 4) C<sub>4</sub>H<sub>4</sub>O<sub>4</sub>
- 5) C<sub>4</sub>H<sub>5</sub>O<sub>4</sub>
- 6) H
- 7) C<sub>2</sub>H<sub>4</sub>
- 8) H<sub>3</sub>O
- 9) H<sub>4</sub>O<sub>2</sub>
- 10) OH



Funding provided as part of the Durable Module Materials Consortium 2 (DuraMAT 2) funded by the U.S. Department of Energy, Office of Energy Efficiency and Renewable Energy, Solar Energy Technologies Office, agreement number 3829.

# De-risking EPE Encapsulants: Modeling polymer-polymer interfaces

Hannah Dedmon<sup>1</sup>, Mark A. Wilson<sup>1</sup>, Dennice Roberts<sup>2</sup>,  
Laura Schelhas<sup>2</sup>, Mirzo Mirzokarimov<sup>2</sup>, Jeff Munro<sup>3</sup>,  
Lisa Madenjian<sup>3</sup>, Marola Issa<sup>3</sup>, Elizabeth Palmiotti<sup>2</sup>

<sup>1</sup> - Sandia National Laboratories, <sup>2</sup> - National Renewable Energy Laboratory, <sup>3</sup> - Dow Chemical



Module Materials Solutions

Awarded FY25      Period of Performance: 10/24-09/27  
Core Call              Funding: \$1.25 M

## Contributing to DuraMAT Consortium Goals

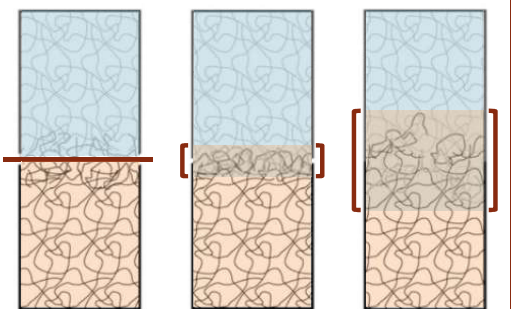
1. De-risk modules from unknown degradation factors introduced by novel EVA/POE composite encapsulant materials.
2. Multi-technique analysis to identify, test, and model material degradation modes and effects.

EVA-POE based composite encapsulants make up **20% of global market share** as of 2023, despite lack of reliability testing and fielded history to understand **risks and degradation modes**.

Underlying the lack of reliability testing of EPE encapsulants, is the **complexity of the polymer-polymer interface**. In this work we employ atomistic molecular dynamics (MD) simulations to elucidate polymer features impacting the formation and preservation of the encapsulant's interfaces.

## Polymer-Polymer Interfaces

Co-extrusion and lamination procedures create variable **chain entanglements** at the interface.



Material properties dictate **strength of adhesion** between entangled chains.

| T <sub>g</sub> (°C) | Density (g/cm <sup>3</sup> ) |
|---------------------|------------------------------|
| EVA -20 (250 K)     | 0.95                         |
| POE -53 (220 K)     | 0.87                         |



Take a picture  
to visit our  
project site

See Poster #70 For Full Project Details

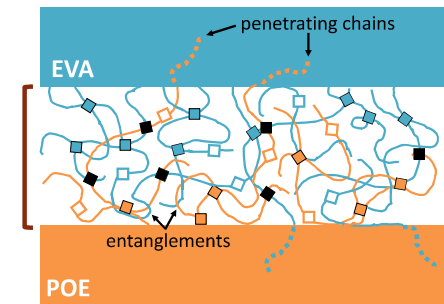


Sandia National Laboratories is a multimission laboratory managed and operated by National Technology & Engineering Solutions of Sandia, LLC, a wholly owned subsidiary of Honeywell International Inc., for the U.S. Department of Energy's National Nuclear Security Administration under contract DE-NA0003525.

SAND2025-02468C



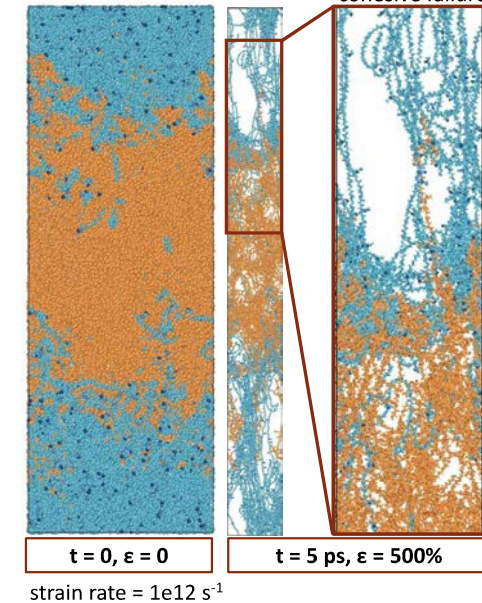
Funding provided as part of the Durable Module Materials Consortium 2 (DuraMAT 2) funded by the U.S. Department of Energy, Office of Energy Efficiency and Renewable Energy, Solar Energy Technologies Office, agreement number 38259.



□ crosslinking unit    ■ intra-crosslink    ▨ inter-crosslink

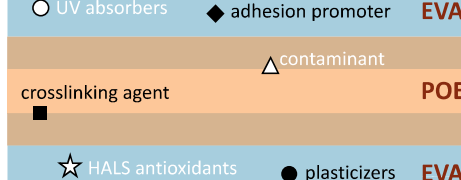
The key features impacting interfacial adhesion are the polymer **chain length** (molecular weight), chain **entanglements** across the interface and **crosslinking** between EVA and POE chains.

## Predicting Adhesive and Mechanical Properties



strain rate = 1e12 s<sup>-1</sup>

## Additive Migration in EPE Encapsulants



# PV Degradation Modeling: Applying Geospatial Workflows with “PVDeg”

Tobin Ford, Silvana Ovaitt, Martin Springer, Michael Kempe (NREL)



**Awarded FY22  
Core Modelling Call**

**Period of Performance: FY23-26  
Funding: \$750k**

## Contribution to DuraMAT Consortium Goals – Project Overview

The goal of this work is to create an online tool that can be used to search for degradation information and extrapolate PV module performance and durability to field exposure. A graphical user interface will aid in the understanding of the results. The prediction tool will be built as a module and published as open-source, allowing users to expand on the existing framework.

## Project Highlights

- PVDeg: open-source tool for degradation analysis.
- Searchable database of degradation parameters.
- Geospatial analysis via high-performance computing (HPC) and in AWS.
- Multivariate Monte Carlo methods to quantify error in calculations.

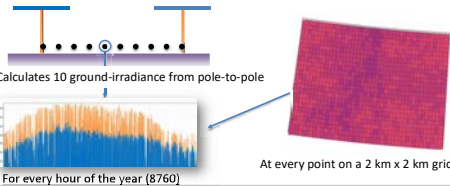
## Impact

- Degradation occurs due to many different modes and mechanisms, each with different dependencies on stress factors. To develop a 50-year module, one must individually address every failure mode and eliminate or minimize it.
- The most difficult task in performance prediction is determining a degradation model and obtaining relevant degradation parameters. Next, extrapolation is performed using time-consuming, repetitive and standardized methods.

## SAM Integration

PVDeg seamlessly integrates the latest SAM versions and modules into geospatial workflows using PySAM. Its coding structure closely follows PySAM's, minimizing the learning curve and eliminating the need to learn a new platform or package. Additionally, it is designed to easily incorporate future updates, ensuring continuous compatibility. PVDeg supports both **pvsam1** and **pvwatts8**, enabling detailed geospatial workflows with a wide range of configurable parameters. Users can define setups in the SAM GUI and seamlessly integrate them into their analyses.

### PVDeg+PySAM Agrivoltaics example

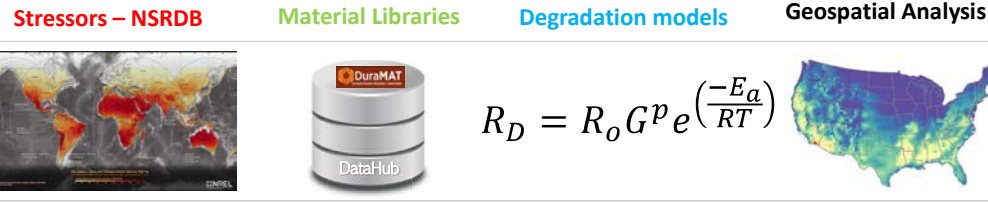


## GeoGridFusion: Local Geospatial

GeoGridFusion enables users outside of NREL, particularly those without access to HPC resources, to utilize and store gridded geospatial data from datasets like NSRDB and PVGIS. The goal of this project is to make our advancements widely accessible.



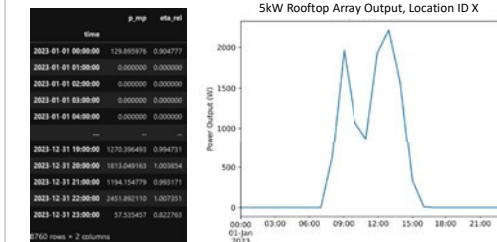
## PV Degradation Tools – The PV-focused, open-source, integration pipeline for PV degradation analysis!



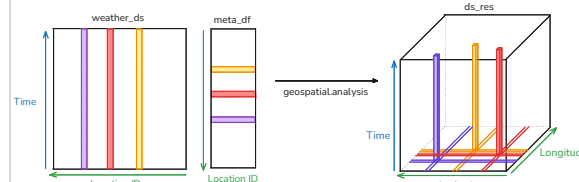
## PVDeg Geospatial Workflow

As a simple example for our geospatial framework, we calculate PV system DC output using the ADR module efficiency model with PVLB<sup>1</sup>. Our goal is to demonstrate how existing tools like the functions in PVLB can be integrated with PVDeg for geospatial calculations.

This framework requires a function that accepts weather data (as a Pandas Dataframe) and metadata (as a dictionary), including latitude, longitude and other relevant details, and produces a result with uniform structure.

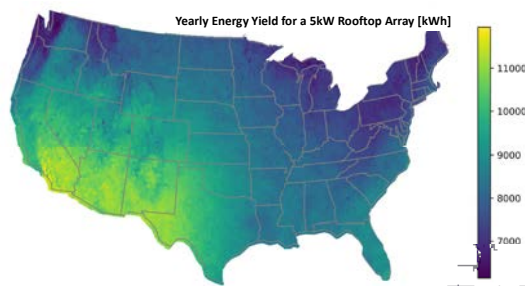


Example output from a function calculating the performance of a 5kW rooftop PV System. The output is in DataFrame format, but PVDeg also supports single or multiple variables in numeric or time-series form. The plot on the right shows the data for a single day at one location



The figure above illustrates the input data structure and transformation for geospatial calculations. The weather dataset has two axes: Location ID and Time, with each Location ID containing all weather data for that location over time. Bars represent TMY data for the three locations. Metadata is stored in a DataFrame, where each row corresponds to a location's metadata.

The mapping process transforms these inputs into a structured output with latitude and longitude dimensions. Depending on the model, the dataset may include additional dimensions such as time.



### Example: 5kW Rooftop Performance

```
def dc_output(weather_df, meta):
    solpos = pvdg.spectral.solar_position(
        weather_df['meta']['lat'],
        weather_df['meta']['lon'],
        weather_df['meta']['date'],
        weather_df['meta']['time']
    )
    weather_df['poa_global'] = total_irrad.poa_global

    # Estimate PV module temperature
    weather_df['temp_pv'] = pvlb.temperature.faisan(
        weather_df['poa_global'], weather_df['temp_air'], weather_df['wind_speed']
    )

    # Adm model parameters
    adm_params = {
        'k_a': 0.99924, 'k_d': -5.49097, 'tc_d': 0.01918,
        'k_r': 0.06999, 'k_rsh': 0.26144
    }

    # Compute efficiency
    weather_df['eta_rel'] = pvefficiency.adr(
        weather_df['poa_global'], weather_df['temp_pv'], **adm_params
    )

    # Compute power output
    weather_df['G_STC'] = 500.0, 1000.0 # Standard conditions (W/m²)
    weather_df['P_mp'] = P_STC * weather_df['eta_rel'] *
    (weather_df['poa_global'] / G_STC)

    return weather_df[['P_mp', 'eta_rel']]
```

## Geospatial Calculation

To adapt the function above for geospatial calculations on Terabyte-scale datasets, we must describe a mapping of the input data to the output in the form of a template.

```
from pvdeg.decorators import geospatial_quick_shape
@geospatial_quick_shape('timeseries', ['p_mp', 'eta_rel'])
def dc_output(weather_df, meta):
    ...
    template=pvdg.geospatial.output_template(
        ds_gids=geo_weather,
        shapes = {
            'p_mp': ('gid','time'),
            'eta_rel': ('gid','time')
        }
    )
```

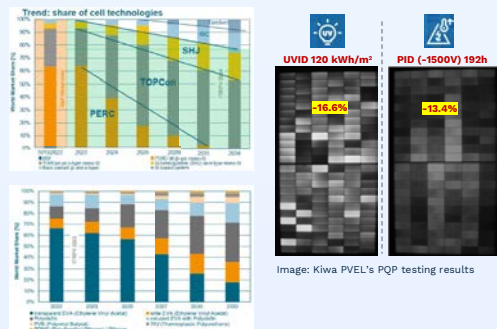
Finally, we provide an Xarray Dataset of weather data and a Pandas DataFrame of metadata containing meteorological data for all locations and perform calculations in parallel.

## Takeaways

- Simplify geospatial calculations with PVDeg.
- Apply single-site functions across geospatial data.
- Run geospatial PySAM models natively.
- Store and merge multiple geospatial datasets locally, using GeoGridFusion.

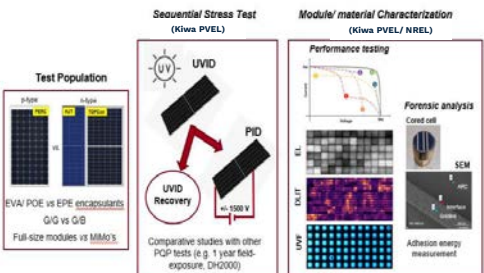
## INTRODUCTION

- Rapid adoption worldwide of n-type cell topologies and new encapsulants.
- Growth is driven by desire for higher efficiency, improved bifaciality, and better resilience to LID LETID.
- These cell types are found susceptible to
  - UV-induced degradation (UVID) - passivation loss
  - Potential induced degradation (PID) – shunting, contact corrosion, delamination
- Higher risk for module performance and warranty, as the first year of degradation may exceed -2%.



## PROJECT GOALS

- Benchmark state-of-the-art reliability for n-type cells and new encapsulants against UVID and PID of industrial full-size modules.
- Understand the root-cause mechanisms behind UVID and PID.
- Develop UVID recovery techniques.
- Correlate accelerated stress tests with field-exposure and other tests (DH2000, LETID).
- Deposit test results in the DuraMAT DataHub.



## CORE OBJECTIVES

- Disruptive Acceleration Science
- Fielded Module Forensics

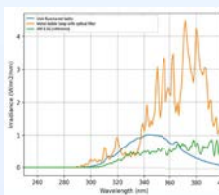
## UVID MECHANISMS

UVID mechanism is different from other light-induced degradation modes (BO-LID and LETID). Expected causes:

- 1) Recombination at SixNy/Si interface [2]
- 2) Recombination in Si bulk [3]
- 3) Hot-carrier effect [4, 5]

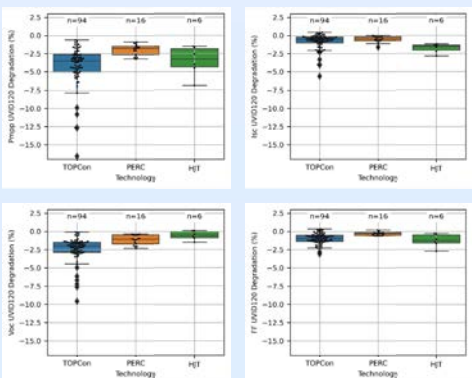
## KIWA PVEL's UVID TESTING

- Modules preconditioned outdoor for LID stabilization.
- Front-side irradiation at module temperature 60°C, under short-circuit condition. Total UV dose is 120 kWh/m² (280–400 nm) when using metal halide lamps. Equivalent dose is ~55 kWh/m² when using UV fluorescent bulbs.
- Total UV dose is equivalent to 1–2 years of outdoor exposure, depending on location.
- Use of MH lamps (Suzhou, China) and UVF bulbs (Napa, USA).
- Test modules are characterized with flash STC front and rear, EL, and wet leakage current test.



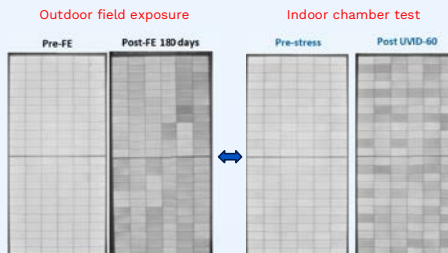
## RESULTS: ACCELERATED UVID TESTING

- More than 100 n-type modules subjected to UVID testing, primarily TOPCon.
  - n-type TOPCon: wide range of power loss -0.8% to -16%.
  - n-type HJT: moderate power loss (-2 to -7%).
  - p-type PERC: lower power degradation (<-3%).
- More than 50% of TOPCon BOMs exhibited power degradation >-3%.
- Deg is mainly due to Voc loss (passivation loss). Some BOMs showed Isc loss, while FF is stable.
  - Different UVID failure mechanisms occurring concurrently.
- Checkerboard pattern in EL images.



## OUTDOOR TESTING

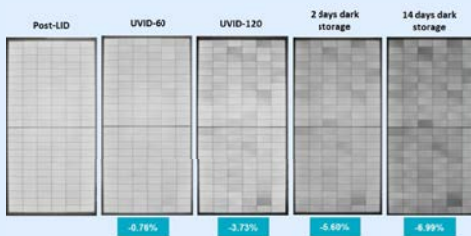
- TOPCon fielded modules at different sites in the US and China showed higher Voc losses in first 5–11 months of deployment.
- Power loss was more prominent on front side.
- Rear-side parameters also severely degraded in some highly sensitive UVID modules.
- Checkerboard pattern visible in field-exposed (FE) module is similar to that seen in UVID stressed module, indicating **UVID is a real problem**.



## DARK DEGRADATION & METASTABILITY

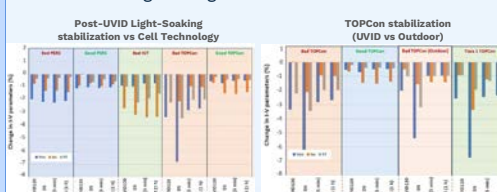
- Post UVID-120 modules stored in dark exhibit significant power degradation – signs of metastability.
- Checkerboard UVID signature in EL images becomes more pronounced with dark storage duration.
- Extent of dark degradation depends on
  - Higher in UVID-sensitive modules.
  - Lower at warmer dark storage room.
- All technologies exhibited dark degradation.
  - TOPCon: Extensive, HJT: Moderate, PERC: Minimal.
  - Parameters affected differently. Greater Voc loss in TOPCon, while HJT suffer from Isc and FF losses.
- Metastability also seen in fielded modules.
- A stabilization step is important to ensure accurate and reliable flash measurements following UVID testing.

| Step#                      | Pmp%  | Voc%  | Vmp%  | Isc%  | Imp%  | FF%   |
|----------------------------|-------|-------|-------|-------|-------|-------|
| Post-LID                   |       |       |       |       |       |       |
| UVID-60                    | -0.76 | -0.84 | -1.02 | 0.60  | 0.31  | -0.52 |
| UVID-120                   | -3.73 | -2.31 | -3.24 | -0.17 | -0.45 | -1.29 |
| After 2 days dark storage  | -5.60 | -3.39 | -4.98 | -0.47 | -0.60 | -1.83 |
| After 14 days dark storage | -6.99 | -4.18 | -5.66 | -1.28 | -1.42 | -1.68 |

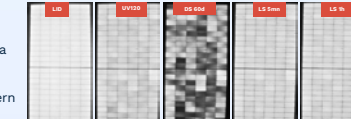


## UVID RECOVERY METHODS

- Experimented different recovery methods on UVID modules using current injection and light exposure.
  - Light exposure method offers faster recovery.
- Results show white LED/ UVF/outdoor sunlight (or full spectrum) can cause significant power recovery.
- Recovery observed with front illumination, suggesting the degradation occurs near passivation/Si interface.
- Recovery is only partial with some degree of permanent damage remaining.
- Module degrades again when left in the dark.



**TOPCon:**  
Significant improvement after a very short light exposure.  
Checkerboard pattern is vanished



**HJT:**  
No obvious changes on EL image, except slight increase in brightness

- Kiwa PVEL's proposed stabilization method involves post UVID-120 test modules to undergo full-spectrum light-soak indoor or outdoors for 0.1 kWh/m² (for TOPCon) and 0.5 kWh/m² (for HJT).

## SUMMARY & FUTURE WORK

- Few TOPCon and HJT BOMs exhibited high susceptibility to UVID as evidenced by both lab and field test data.
- Growing concerns exist regarding their metastability behavior in the dark. Stabilization method needs to be standardized.
- Forensic analysis of UVID samples will be performed using coring and advanced characterization.
- Testing and data analysis will be employed to assess the PID-sensitivity of different BOMs.

## ACKNOWLEDGMENT

Funding provided by the Durable Module Materials Consortium 2 (DuraMAT 2), an Energy Materials Network Consortium funded by the U.S. Department of Energy, Office of Energy Efficiency and Renewable Energy, Solar Energy Technologies Office agreement number 38259. The views expressed in the article do not necessarily represent the views of the DOE or the U.S. Government.

## REFERENCES

- [1] ITRPV Report 2024; [itrpv.vdmaa.org](http://itrpv.vdmaa.org)
- [2] R. Witteck et al., *physica status solidi*, 11 (8), p. 1700178, 2017.
- [3] F. Ye et al., *Sol Energy*, 170, pp. 1009–1015, 2023.
- [4] P. E. Gruenbaum, et al., *J Appl Phys*, 66 (12), pp. 6100–6114, 1989.
- [5] A. Sinha et al., *Prog in Photovolt.*, 31 (1), pp. 36–51, 2023.

# Module Breakage Impacts on System Availability

**Clay Helms**

clay.helms@siliconranch.com

**Nick de Vries**

nick.devries@siliconranch.com

## Overview

A growing concern among long-term PV owners and operators is the impact of module defects, particularly broken modules, on system availability beyond the direct loss of module capacity.

One underestimated root cause of system-wide energy loss is the occurrence of ground faults triggered by physical module defects. These faults can propagate beyond the affected module, extending to entire inverter arrays and significantly reducing plant performance.

Silicon Ranch operates 180+ projects totaling 3,550+ MWdc and has leveraged historic operating data to:

1. Analyze the relationship between ground faults and module health
2. Define, quantify, and identify key contributing factors to **Ground Fault Availability (GFA)**
3. Use these insights to inform and improve commissioning, maintenance, procurement, and site design



This module is cracked.

What is the impact?

## Data Collection

Silicon Ranch captured and analyzed critical ground fault details from maintenance logs to quantify root causes and establish focus areas for field investigations.

Module breakage was quantified through annual aerial scans & post-construction site walks to correlate with Ground Fault Availability.

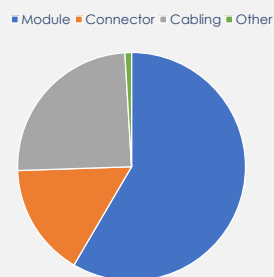


Figure 1: SRC Maintenance Logs – 2022 GF Root Causes

## Ground Fault Availability

Silicon Ranch defined and calculated Ground Fault Availability (GFA) to track array- and plant-level energy impacts from module breakage.

$$\text{Ground Fault Availability} = \frac{\text{Measured Energy}}{\text{Measured Energy} + \text{GF Lost Energy}}$$

Ground Fault Availability in subsequent analyses was calculated for only those faults determined to have been caused by modules.

## Broken Modules vs Ground Fault Availability

For a subset of projects, Silicon Ranch analyzed Ground Fault Availability for one year of operation against the relative percentage of identified broken modules in the same period.

Figure 2 (right) presents a linear fit illustrating the inverse relationship between the increasing quantity of broken modules and the decreasing plant-level Ground Fault Availability.

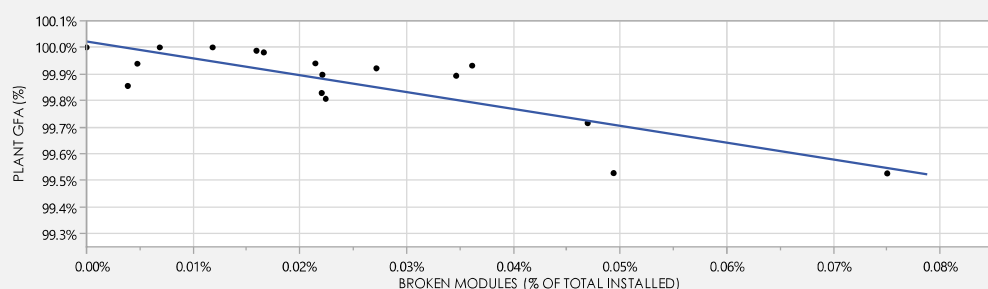


Figure 2: Plant Ground Fault Availability vs Broken Modules

## Ground Fault Availability vs Array Size

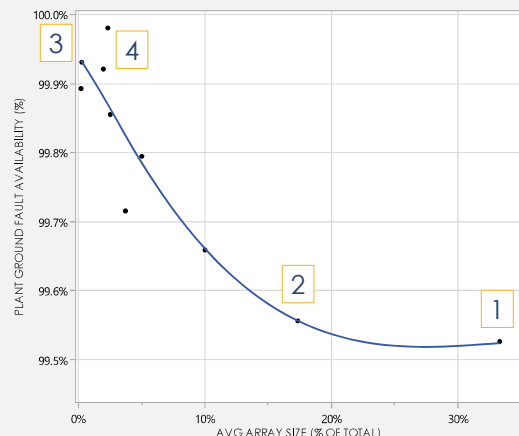


Figure 3: Plant Ground Fault Availability vs Average Array Size

Figure 3 (left) displays a filtered dataset of sites with comparable percentages of broken modules, plotting Ground Fault Availability on the y-axis against average array size (average DC capacity of inverter arrays relative to total system capacity) on the x-axis.

To assess the impact of array size on GFA, four systems – spanning multiple regions, inverter technologies, and array configurations – were analyzed. Table 1 (below) details these systems and their respective differences in Ground Fault Availability.

| System | State | Inv Type | No. Inverters | Avg Array Size | GFA    |
|--------|-------|----------|---------------|----------------|--------|
| 1      | CO    | Central  | 3             | 33%            | 99.52% |
| 2      | TN    | Central  | 6             | 17%            | 99.56% |
| 3      | GA    | String   | 400           | 0.3%           | 99.93% |
| 4      | MS    | Central  | 51            | 2%             | 99.92% |

Table 1: System Metadata

## Findings & Conclusions

Module breakage was the leading cause of recorded ground fault energy loss.

On average, **a 0.01% increase in broken modules led to 6x the loss in plant-level Ground Fault Availability**.

**Reducing the average array size has a direct positive impact on Ground Fault Availability** for the same relative percentage of broken modules. While SRC's string inverter sites generally exhibit higher GFA, this is primarily due to their smaller average array sizes, not the inverter technology itself.

**Ground Fault Availability is recoverable and controllable** through thoughtful system design, breakage prevention, and proactive mitigation strategies, as demonstrated by SRC's continuously-improving Operations to Design feedback loop.

# Effect of Cell Cracks on Module Power Loss and Degradation: Modern Module Architectures

Viral Parikh\*, Robert Flottemesch\*, Martin Springer†, Michael Gostein\$, Will Hobbs#, Jim Rand%

\*Electric Power Research Institute, †National Renewable Energy Laboratory, \$Atonometrics Inc., #Southern Company Services, %Core Energy Works

## BACKGROUND AND MOTIVATION

- Environmental stressors such as wind loading, thermal cycling and exposure to colder temperatures can make benign PV cell cracks turn into harmful cracks that can be linked to substantial power loss and safety issues
- EPRI in partnership with NREL is seeking to understand the direct correlation between lab-based accelerated stress testing of cell cracks using NREL's state-of-the-art DMX device with real-world aging of cell cracks/modules deployed at EPRI's outdoor test facility in Colorado
- Linking lab-based accelerated stress testing for cell cracks to field performance will have high impact across the industry and provides a method to understand power loss mechanism due to cell cracks in modern modules

## IV, EL IMAGING & DROP TEST RESULTS ON GLASS//GLASS MODULES

### Baseline IV:

- Module A: Baseline IV data show Pmax between 530W to 540 W
- Module B: Baseline IV data show Pmax between 600W to 610W

### Baseline EL:

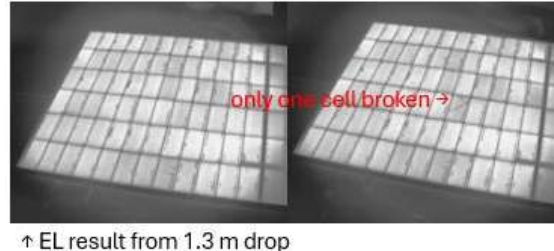
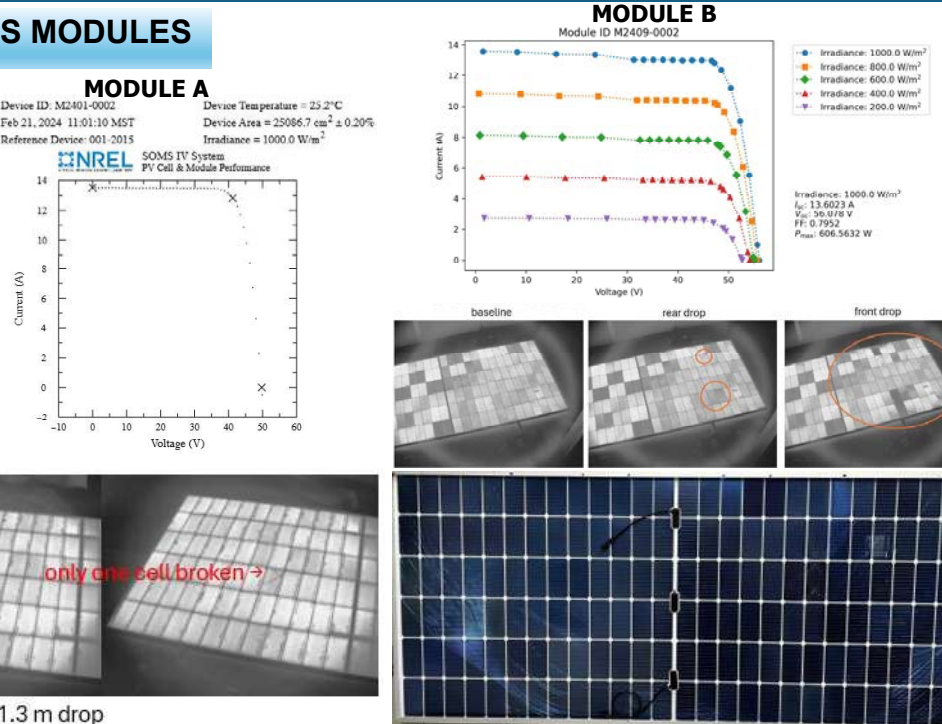
- Both Module A & Module B shows no abnormalities in Baseline EL

### DROP TEST SEQUENCE:

- Drop test onto mock racking
- One-time exposure to -40°C, repeat drop test
- Drop test while module is still at low temperature
- Static load test
- Static load test on never-frozen module

### RESULTS OF DROP TEST

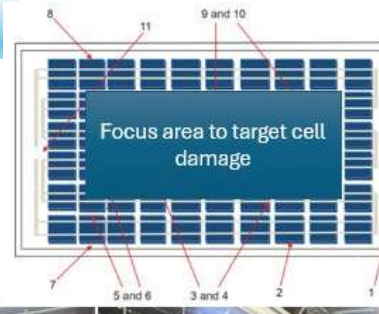
- Module A: Post EL imaging shows only 1 cell crack at step1; no further damage for rest of the drop sequence
- Module B: Post EL imaging does show multiple cell cracks; prob. damage not significant to detect power loss



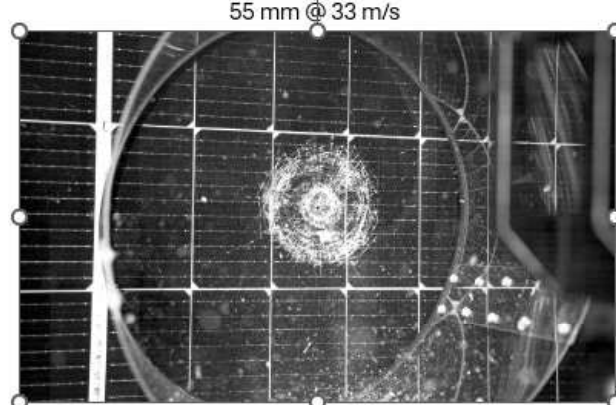
↑ EL result from 1.3 m drop

## HAIL TESTING RESULTS ON GLASS//GLASS MODULES

- Module A: EL shows no cell cracks up to 45mm hail size; glass breakage @55mm
- Module B: EL shows no cell cracks up to 55mm hail size; glass breakage @65mm
- In general, almost impossible to induce cell micro-cracks in the lab in G/G modules without breaking of glass



| Shot No. | Location  |
|----------|---|
| 1        | Any corner of the module window, not more than one radius of ice-ball from the module edge.   |
| 2        | Any edge of the module, not more than one radius of ice-ball from the module edge.  |
| 3, 4     | Over the circuit near interconnects (i.e. cell interconnects and bus ribbons)   |
| 5, 6     | Over edges of the circuit (e.g. individual cells)   |
| 7, 8     | On the module window, not more than half diameter of ice ball from one of the points at which the module is mounted to the supporting structure |
| 9, 10    | On the module window, at points farthest from the points selected above   |
| 11       | Any points which may prove especially vulnerable to hail impact like over the junction box.   |



**MODULE A:** 25, 35, 45, launches showed no cell cracking; 55 mm @33 m/sec broke back glass



**MODULE B:** 25, 35, 45, 55mm launches on four locations showed no cell cracking; 65mm @36m/s hail launch broke glass at first location

## SHAKER TABLE EXPERIMENTS

- Looks exactly like a tracker along with laser displacement sensors (measurement range of 50-150 mm) test fitted on front and back of each module
- Module mounting process along with other hardware (tube, piles) remains the same
- Driven by a large motor and a crankshaft to produce oscillations at 2Hz frequency
- IV tracers from Atonometrics to be installed on these modules
- Inclinometer to ensure shaker table and tracker tube are at the same angles before IV data is collected;
- EL imaging to evaluate the effects of cell cracks



**ACKNOWLEDGEMENTS:** This material is based on work supported by the U.S. Department of Energy's DuraMAT Consortium, under Agreement Number SUB-2023-10206.

# Accelerated Stress Testing to Deconvolute Simultaneous-But-Distinct Degradation Pathways Under UV Illumination

PI: Dana Kern & Peter Hacke Team: David C. Miller, Dennice M. Roberts, Steve Johnston, **Rebecca B. Wai**, Kent Terwilliger, Jimmy M. Newkirk, Rachael L. Arnold, **Xavier M. Hanna**



Disruptive Acceleration Science

## Contributing to DuraMAT Consortium Goals

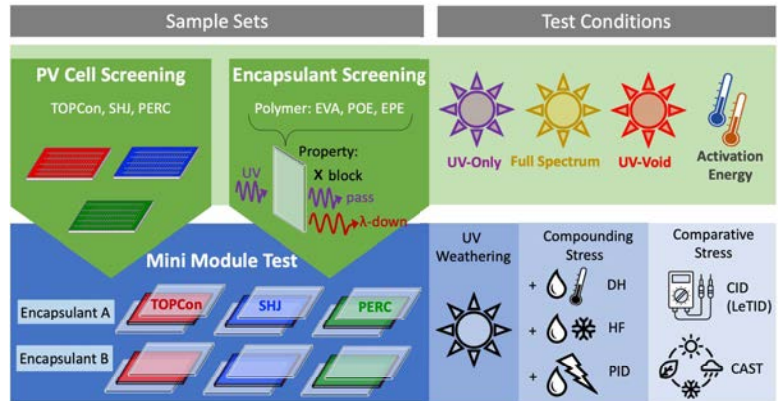
The effects of ultraviolet-induced degradation (UV-ID) on modern module designs remains unclear. One major hurdle in forecasting PV module reliability with accelerated stress testing is that multiple degradation modes can occur simultaneously from the same stressor. Here, we address simultaneous-but-distinct degradation pathways that result from UV illumination in bifacial PV modules with various encapsulants and advanced cell technologies.

## Key Results

For the subset of cells tested thus far, minimal UV-ID has been observed. Wire delamination adversely affects some bare cells, which lack the protection normally provided by other package materials.

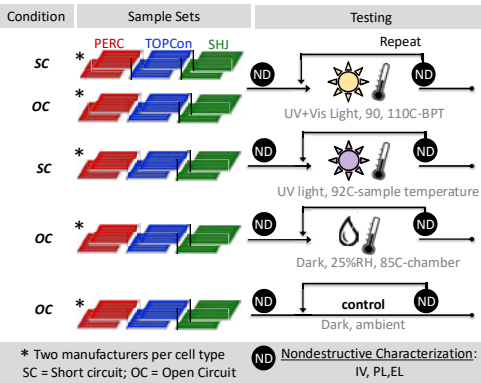
## Project Overview

In this project, we seek to separately understand the simultaneous-but-distinct degradation pathways under UV illumination at the bare cell, package, and combined cell+package (i.e. module) level. Our method will identify differing degradation rates of components by separately screening multiple cell types and package materials. This data set will then be used to identify appropriate combinations of cell+package systems (mini-modules) to test. We will evaluate compounding stressors in addition to UV at the mini-module level. We anticipate that these results will inform (1) the important materials degradation pathways that must be accounted for when deploying new technologies and (2) the appropriate accelerated stress testing conditions needed to identify degradation mechanisms (e.g. UV light vs tests using only charge injection).



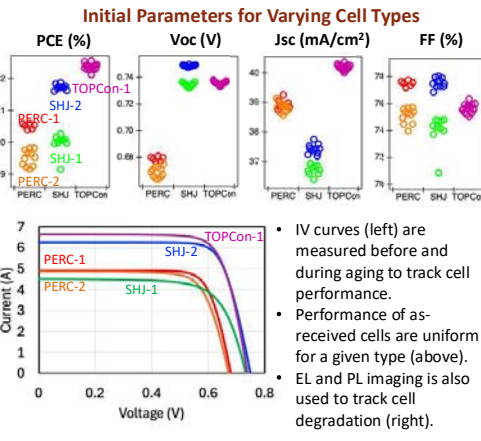
Please See Dennice Roberts's talk "Performance and Degradation of PV Encapsulants for UV Induced Degradation Study" 11:00 am, Wednesday, 3/5/25, NREL/PR-5F00-93382

## Bare Cell Stress Test Overview

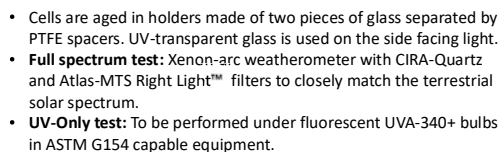
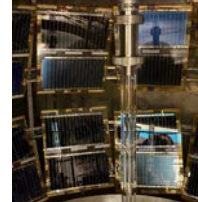


## Non-destructive Characterization

Current-voltage (IV) and imaging (PL/EL) are used during aging tests to monitor cell degradation

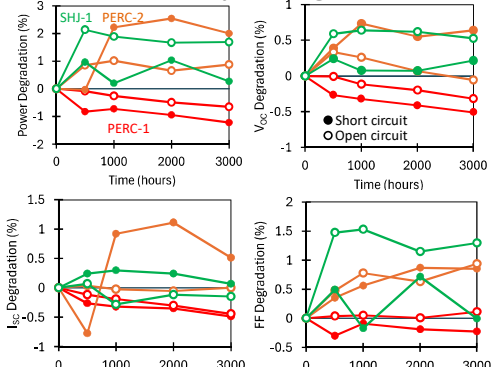


## Weathering Light Conditions

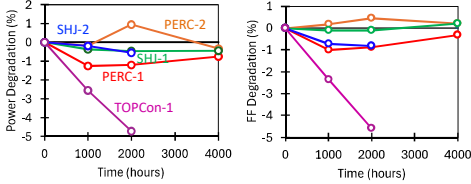


## Full-spectrum Light Aging

A3 weathering of the subset of cells tested thus far results in minimal power degradation

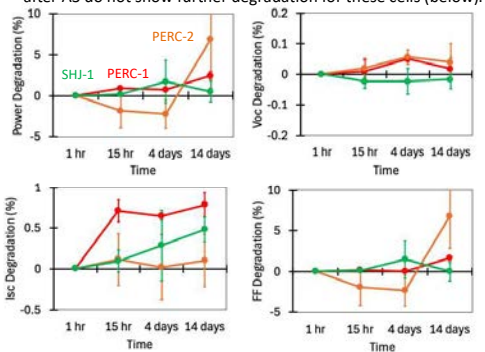
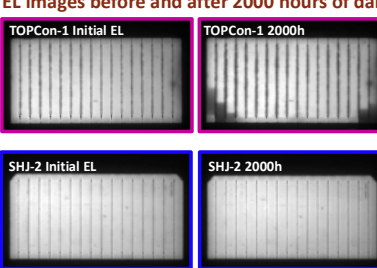


## Moderate Dark Humidity Test



Dark, 25% RH, 85C-chamber aging tests degradation under heat and humidity conditions comparable to our light-aging conditions. TOPCon-1 suffers a 5% power loss, due to losses in fill factor.

### EL images before and after 2000 hours of dark, moist aging



This work was authored by the National Renewable Energy Laboratory, operated by Alliance for Sustainable Energy, LLC, for the U.S. Department of Energy (DOE) under Contract No. DE-AC36-08GO28300. Funding provided by U.S. Department of Energy Office of Energy Efficiency and Renewable Energy, 3020 Program. The article does not necessarily represent the views of the DOE or the U.S. Government. The U.S. Government retains a nonexclusive, paid-up, irrevocable, worldwide license to publish or reproduce the published form of the work, or allow others to do so, for U.S. Government purposes.

# Failure modes in modern cell interconnects for PV modules

Peter Hacke<sup>1</sup>, David C. Miller<sup>1</sup>, Nick Bosco<sup>1</sup>, James Hartley<sup>2</sup>, Soňa Uličná<sup>1</sup>, Akash Kumar<sup>3</sup> and Govindasamy Tamizhmani<sup>3</sup>

<sup>1</sup>National Renewable Energy Laboratory

<sup>2</sup>Sandia National Laboratories

<sup>3</sup>Arizona State University



Disruptive Acceleration Science

Awarded FY21  
Disruptive Acceleration Science

Period of Performance: 9/21-6/24

Funding: \$977 K

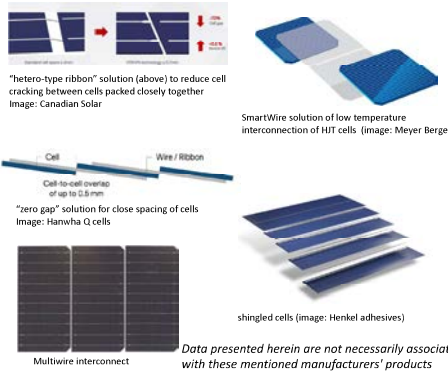
## Contributing to DuraMAT Consortium Goals

- We evaluate strengths and weaknesses of modern cell interconnect designs with combined-accelerated stress testing (CAST) to screen multiple climates along with dynamic mechanical cycling, finite element, and failure analysis to determine potential for a 50-year life.
- We examine to what extent factors like stress and temperature can lead to cell interconnect failure depending on the interconnect type.
- This poster focuses on low temperature solder (SnBi, SnBiPb) wire interconnect.

## Project Overview

### Interconnect types

Novel interconnect designs of the type in focus in this work



### What we do

ACCELERATED TESTING  
CAST: stress factors applied at extremes and in combinations of natural environment: Heat, light, humidity, mechanical pressure, system voltage

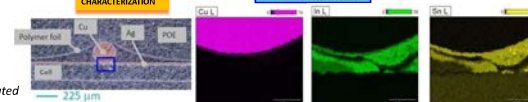


FEA MODELING  
Model for full wire-interconnected module

New Tool:  
Remote Source Dynamic Mechanical Acceleration  
The module may be placed within an environmental chamber while the speaker enclosure remains in ambient laboratory conditions.



CHARACTERIZATION  
Characterization of interconnects and cells



## Outcome & Impact

We examined the degradation modes of PV module wire interconnects, focusing on those using low temperature (SnBi, SnBiPb) solder, alongside conventional solder (PbSn).

### We tested with:

- Combined-accelerated stress testing (CAST)
- Temperature cycling (TC)
- Field exposure (Phoenix AZ, Fairbanks AK)

### We modeled with:

- Finite element analysis (FEA)

### We performed failure analysis with

- Electroluminescence (EL), Photoluminescence (PL)
- Optical microscopy, SEM, EDS

### Findings:

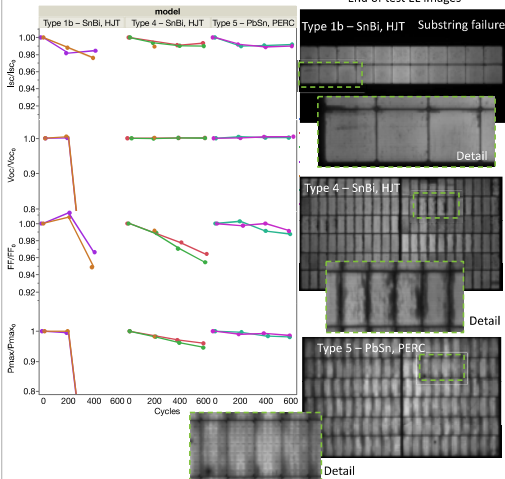
Separation occurs at interfaces: both between the solder-coated wire and the Ag cell metallization (no metallurgical bond) and between the Ag grid finger metallization and the Si cell.

- Interface failures predominant at elevated temperature
  - Hot climate CAST
  - rooft-mounted modules in the hot outdoor climate
- Encapsulant expands, pulling off the embedded interconnect wire. The wire locally pulls the Ag grid finger metallization off the cell during heating, leading to grid finger breaks and a 'digital,' asymmetric EL pattern.
- If the wire contacts the grid finger on one side of the grid finger break, a 'digital' pattern in the EL is also observed.

Low process temperature solder interconnects and Ag grid finger metallization are particularly vulnerable to failure in high temperature environments, which may guide design choices.

### -40 °C/85 °C IEC 61215 MQT 11 thermal cycling

End of test EL images



### Publications

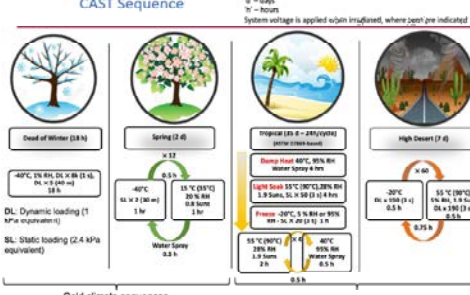
- Hacke, P., Miller, D.C., Bosco, N., and Wu, T., 2025, Performance and Durability of Electrically Conductive Tape for Modern Solar Interconnect Technology, *Cells, Progress in Photovoltaics: Research and Applications*, 33(1), pp. 16-26.
- Jones, Y., Hartley, D.C., Miller, S., Uličná, N., Bosco, P., Hacke, "Characterization, Accelerated Life Testing, and Finite Element Modeling of Low Temperature Solder Wire Interconnect Degradation Mechanisms, in review: *Progress in Photovoltaics: Research and Applications*
- Nick Bosco, James Hartley, David Miller and Peter Hacke, Accelerated Testing to Assess Low-temperature Soldered Wire Interconnect Durability in review: *IEEE PESC (2025)*.

Sample description and stress tests applied. 1a and 1b are the same technology in different module sizes. All samples are glass/backsheet construction. ✓ represents one module in the table category.

| Type # | Solder type, cell technology, module size | All climate CAST | Cold climate CAST | Hot climate CAST | -40/85 °C cycling | Fielded |
|--------|---|------------------|-------------------|------------------|-------------------|---------|
| 1a     | SnBi, HJT, mini                           | ✓                |                   | ✓                |                   |         |
| 1b     | SnBi, HJT, full                           |                  |                   |                  | ✓✓                | ✓✓      |
| 2      | SnBiPb, HJT, mini                         | ✓                | ✓                 | ✓                |                   |         |
| 3      | PbSn, PERC, mini                          | ✓                |                   |                  |                   |         |
| 4      | SnBi, HJT, full                           |                  |                   |                  | ✓✓                | ✓✓      |
| 5      | PbSn, PERC, full                          |                  |                   |                  | ✓✓                | ✓✓      |

### Combined-accelerated stress testing (CAST)

#### CAST Sequence



#### Cold climate sequences

#### Hot climate sequences

### Field testing: Phoenix, AZ (Hot climate)

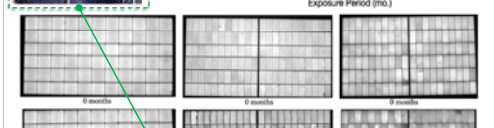
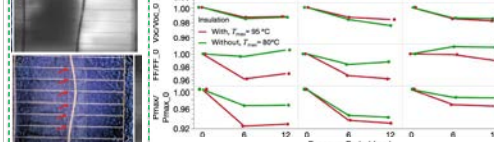
#### Detail of digital EL pattern

Type 1b - SnBi, HJT, G/B

Type 1b - SnBi, HJT, G/B

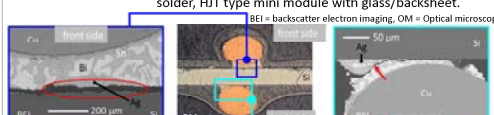
Type 4 - SnBi, HJT, G/B

Type 5 - PbSn, PERC, G/B



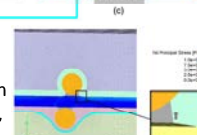
### Metallography

Metallography of a cross-section of a dark region in EL after two cycles of all climate CAST of type 1a - SnBi solder, HJT type mini module with glass/backsheet.



### Finite element analysis

Visualization of stress and displacement at 90 °C assuming an unconstrained solder-Ag interface, where delamination occurs.



# Updates to the Variational Auto-encoder for crack parametrization

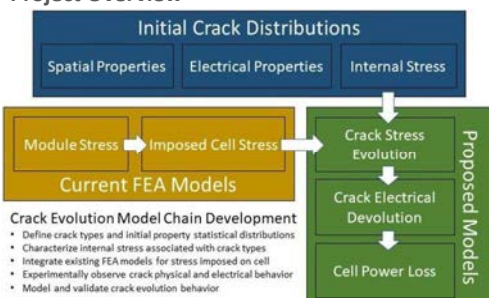


Multi-Scale, Multi-Physics Model

Norman Jost, Ojas Sanghi, Brandon Byford, Emma Cooper, Benjamin G. Pierce, Isaiah Deane and Jennifer L. Braid

Awarded FY22  
Core Modelling CallPeriod of Performance: 10/22-9/25  
Funding: \$1M**Contributing to DuraMAT Consortium Goals**

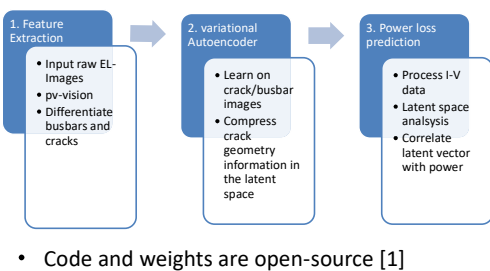
This work will develop **modular, open-source model and analysis** components including crack detection workflow and parameterization for **quantitative inspection of large EL large datasets**. These tools will allow users to quickly and accurately assess the **extent and types of cracking** in their modules. Measured statistical distributions of crack parameters, together with the imposed stress and electrical properties will be used to generate models to predict future crack behavior and power loss.

**Probabilistic Predictive Models for Si PV Cell Crack Stress and Power Loss****Project Overview**

This project will establish comprehensive, physics-informed models and tools to quantify cell crack spatial, mechanical, and electrical properties, and predict future crack power loss. We will combine in-situ measurement of internal cell stress, finite element modeling of modules/cells, image and electrical characterization techniques, dynamic mechanical loading, and automated image analysis and parameterization to build a predictive model for cell crack behavior in PV modules.

**Workflow for Power Loss Prediction**

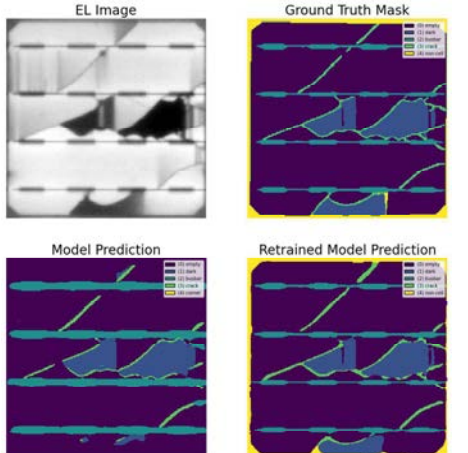
- pv-vision for cell crack image extraction from electroluminescence (EL)
- Variational autoencoder (VAE) for crack parametrization and generation
- Power loss model from latent space (VAE res.)



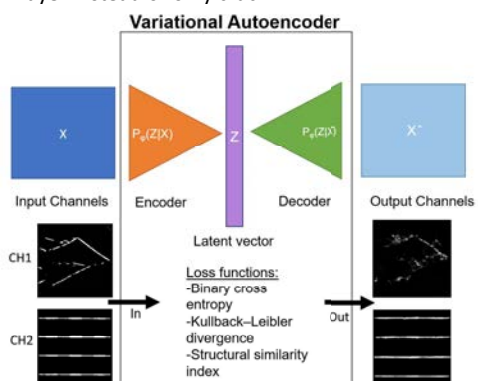
• Code and weights are open-source [1]

**pv-vision**

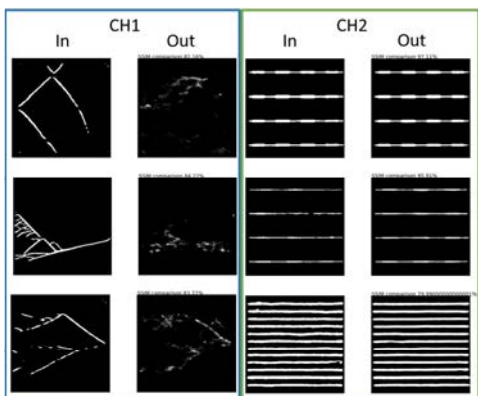
- Open source model for feature extraction [2]
- Retraining for multi-busbar, no-cell area, busbar and crack intersection [1]

**Variational Autoencoder (VAE)**

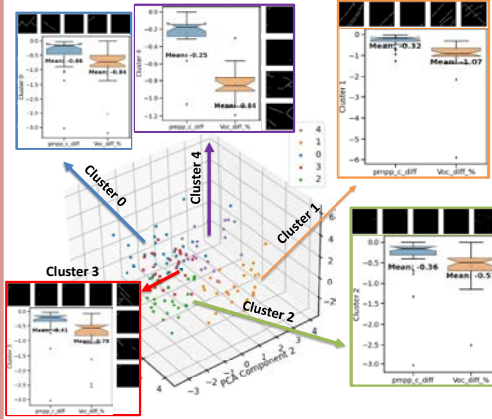
- 6 convolutional layers with kernel of 7x7
- Latent dimension is 50, trained with 500 epochs on a HPC
- Updating to use 2 channels, busbar and crack layer instead of only crack



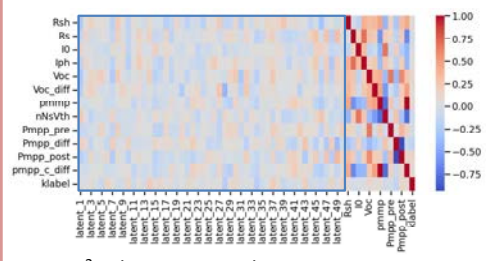
- Further training is necessary, busbars are replicated but cracks are still not recognized
- Currently modifying weights for the loss functions and hyperparameters (latent dim...)

**Latent space analysis**

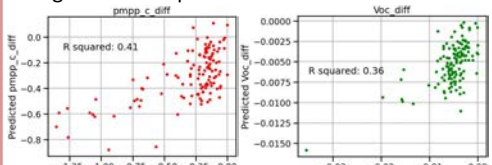
- Principal component analysis and k-means to plot latent space
- Results are from 1 Channel VAE

**Power loss**

- 150 Solar Cell EL – IV Pairs, expanding soon to over 400. Looking for contributors to build a larger dataset
- Correlating latent vector (dimension 50) with a multilinear regression to IV parameters including  $\Delta V_{OC}$ ,  $\Delta P_{MPP}$ , and single diode model parameters
- Pearson correlation for all variables



- Low  $R^2$  values, current data is not progressive in nature. Future EL – IV data will have multiple degradation steps for the same cell

**References**

- [1] N. Jost, et al. (Mar. 12, 2024). Python. Sandia National Lab. (SNL-NM), doi: 10.11578/dc.20240606.4.
- [2] X. Chen et al., "Automatic Crack Segmentation and Feature Extraction in Electroluminescence Images of Solar Modules," doi: 10.1109/JPHOTOV.2023.3249970.

# Emerging Technique for Detecting Damage on Various Module Layouts



Ryan M. Smith<sup>1</sup>, Dylan J. Colvin<sup>2</sup>, Brent Thompson<sup>2</sup>, Collin West<sup>2</sup>, Ethan M. Langlois<sup>2</sup>

<sup>1</sup> Pordis LLC, Austin, Texas, USA

<sup>2</sup> Florida Solar Energy Center (FSEC), University of Central Florida, Cocoa, Florida, USA

## INTRODUCTION

V10 is a new damage identification and quantification metric based on the voltage required to pass 10mA through a module in the dark. It is sensitive to minor cracking in PV modules due to transportation, handling, extreme weather, and vibrations [1]. This work presents additional experimental validation of the V10 technique in modules with different cell architectures, cell cut, and module/substring layouts, showing the extensibility of the technique. Location dependence and the impact of cell string mismatch on V10 crack detection is explored.

## OBJECTIVES

- 1) Confirm that V10 measurement is a valid damage identification metric in multiple cell architectures
- 2) Explore V10 response when damaged is induced in different substrings of a module

## METHODS

This study includes three module types not previously explored:

- a) Half-cell PERC, butterfly layout (Fig. 1)
  - 144 half-cell monofacial, glass/backsheet
  - Multiwire (9) interconnection
- b) Heterojunction, standard layout (Fig. 2)
  - 96 cell monofacial, glass/backsheet
  - Busbar (3) interconnection
  - 4 bypass diodes
- c) Half-cell PERC, standard layout (Fig. 3)
  - 126 half-cell monofacial, glass/backsheet
  - Back contact interconnection (metal wrap-through)
  - 3 bypass diodes

Damage was introduced in steps with a sequence of measurements between each step:

1. Baseline measurement of EL, light I-V, and V10
2. Induce damage to rear side of module
3. Take measurement of EL, light I-V, and V10
4. Repeat steps 2-3 through all damage iterations

Measurements were performed at standard test conditions (STC: 1,000 W/m<sup>2</sup>, AM1.5G spectrum, module temperature 25 ± 2°C).

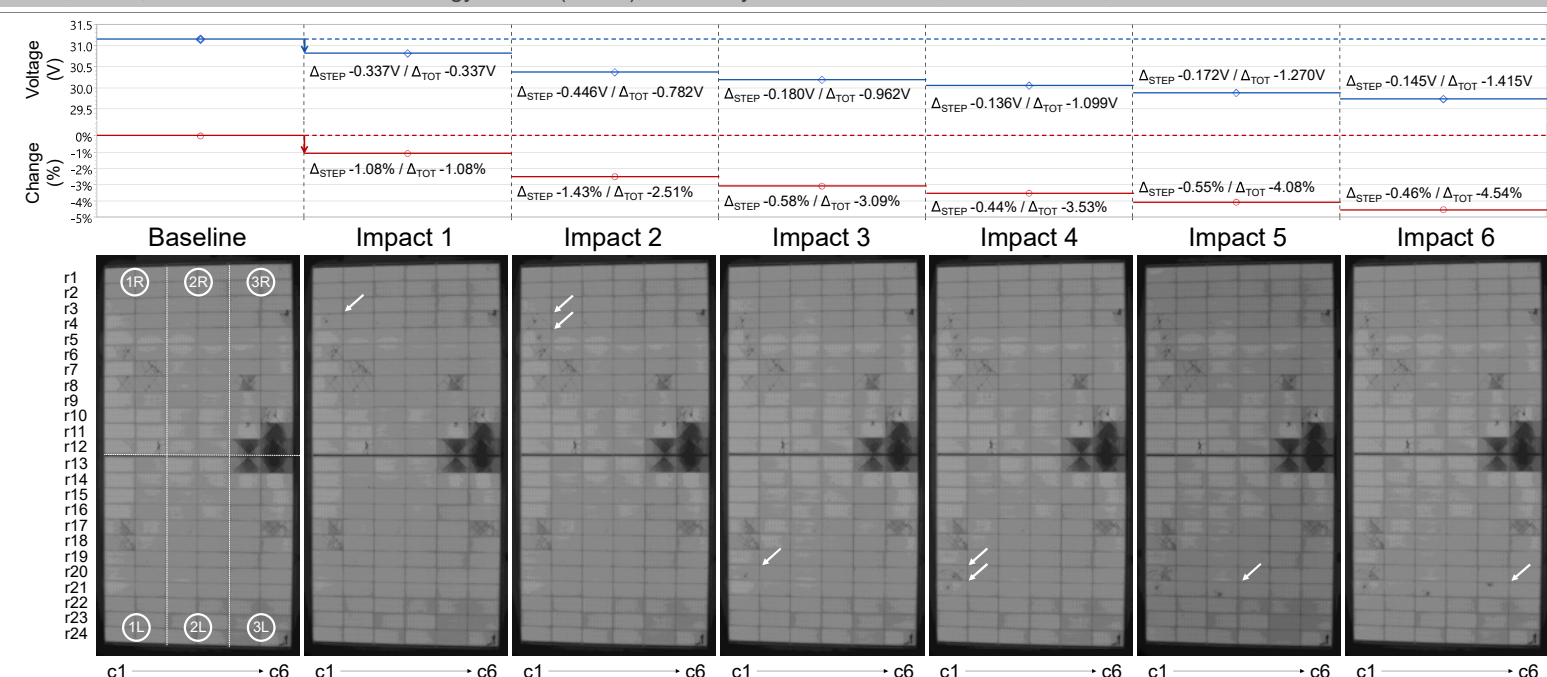


Fig. 1 - Damage was induced on a previously-tested (unrelated experiment) monofacial module ('a') with 144 half-cut PERC cells in a 'butterfly' layout. Substrings are delineated and marked on the baseline EL image. (Top) Damage events result in a drop in the voltage required to pass 10mA in the dark, V10, and the relative change from the baseline. (Bottom) High injection (1.0 nameplate  $I_{SC}$ ) electroluminescence images at baseline and after six impact events; impacted cells at each event are marked with arrows. The baseline condition EL pattern is due to the unrelated previous experiment. Cells affected by impact events: [#1] c1r4 (R), [#2] c1r4, c1r5 (R), [#3] c1r20 (L), [#4] c1r20, c1r21 (L), [#5] c3r21 (L), and [#6] c5r21 (L).

## RESULTS AND DISCUSSION

- A module's previous damage history does not limit the ability of V10 to detect further damage (Fig. 1)
- The results do not suggest that similar mechanical damage on different substrings induces any especially greater damage than in different cells within the same substring. (Figs. 1, 2, 3)
- V10 changes are detectable with confidence before they are with traditional light I-V (Table I)

Table I: Summary of relative changes due to damage. Cells are coded where a change from the baseline value for each parameter is confidently detectable (green, \*) or undetectable (red, #) based on commonly accepted uncertainty of the measurement equipment (LIV: 3% [2]; V10: < 1% [3]).

| Step | Module (a) |                  |                  | Module (b) |                  |                  | Module (c) |                  |                  |
|------|------------|------------------|------------------|------------|------------------|------------------|------------|------------------|------------------|
|      | LIV        | $\Delta P_{MAX}$ | % $\Delta V10$ % | LIV        | $\Delta P_{MAX}$ | % $\Delta V10$ % | LIV        | $\Delta P_{MAX}$ | % $\Delta V10$ % |
| 0    | —          | —                | —                | —          | —                | —                | —          | —                | —                |
| 1    | +0.11      | #                | -1.08 *          | +0.11      | #                | -0.56            | -0.41      | #                | -0.31            |
| 2    | -0.11      | #                | -2.51 *          | -1.30      | #                | -1.63 *          | -0.17      | #                | -0.65            |
| 3    | -0.22      | #                | -3.09 *          | -1.50      | #                | -1.94 *          | -0.09      | #                | -1.04 *          |
| 4    | -0.35      | #                | -3.53 *          | -1.42      | #                | -2.05 *          | -0.11      | #                | -1.08 *          |
| 5    | -0.45      | #                | -4.08 *          | -1.73      | #                | -3.24 *          |            |                  |                  |
| 6    | -0.45      | #                | -4.54 *          |            |                  |                  |            |                  |                  |

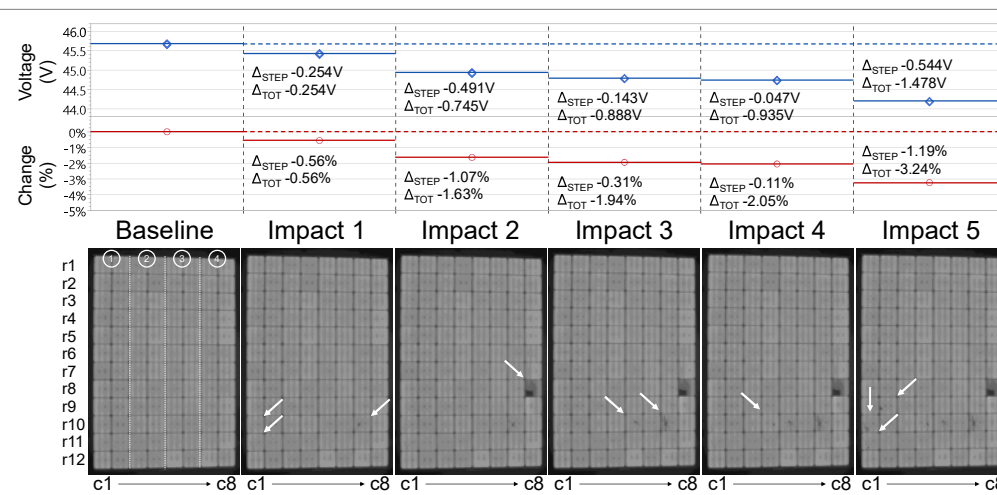


Fig. 2 - Damage was induced on a monofacial module ('b') with 96 Panasonic heterojunction cells in a 'standard' layout. Substrings are marked on the baseline EL image. (Top) Damage events result in a drop in V10. (Bottom) High injection (1.0 nameplate  $I_{SC}$ ) images are marked with damage introduction locations. Cells affected by impact events: [#1] c1r10, c1r11 (1), c7r10 (4), [#2] c8r8 (4), [#3] c5r10 (3), c7r10 (4), [#4] c4r10 (2), and [#5] c1r10, c1r11, c2r9 (1).

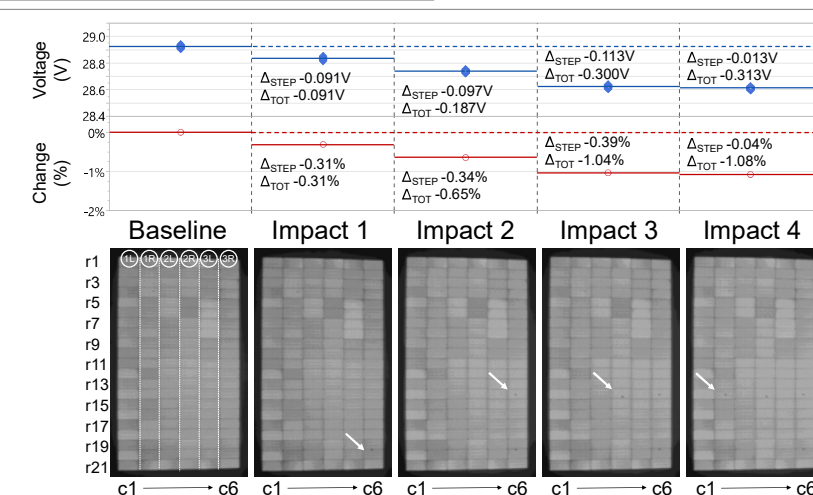


Fig. 3 - Damage was induced on a monofacial module ('c') with 126 half-cut PERC cells with metal wrap-through interconnection in a 'standard' layout. Substrings are marked on the baseline EL image. (Top) Damage events result in a drop in V10. (Bottom) High injection (1.0 nameplate  $I_{SC}$ ) images are marked with damage introduction locations. Cells affected by impact events: [#1] c6r20 (3R), [#2] c6r14 (3R), [#3] c4r14 (2R), and [#4] c2r14 (1R).

## CONCLUSIONS

- V10 reliably captures damage independent of crack location in the module and if pre-existing damage exists.
- V10 is applicable to the modules, cell architectures, and layouts tested
- Module design (e.g., glass-glass architectures, multiwire interconnections) can reduce the impact of damage events by preventing or limiting cell cracking, thus limiting the reduction in V10.

## REFERENCES

- [1] Smith RM, Colvin DJ. V10: Fixed dark bias current as a photovoltaic module damage assessment metric. *Solar Energy*. 2025 Mar 1;288:113271.
- [2] Kortes M, Kurtz S, et al. Review of failures of photovoltaic modules. Report IEA-PVPS T13-01. 2014 Mar:1-40.
- [3] Keithley. 2700/2701/2750 multimeter/data acquisition/systems datasheet, 2018

# Measuring the stress factors for photovoltaic (PV) backsheets degradation

Aidan M. Wesley\*, Silvana Ovaitt, Matthew Prilliman Jimmy M. Newkirk, Rachael L. Arnold, Martin Springer, and Michael D. Kempe | NREL; Minnesota State University Mankato\* | [awesley@nrel.gov](mailto:awesley@nrel.gov)

**Awarded FY22  
Core Modelling Call**

**Period of Performance: FY24-26**  
**Funding: \$350k**

## Contribution to DuraMAT Consortium Goals – Project Overview

This work has two parallel efforts: (1) raytracing to model backside UV exposure and (2) environmental chamber tests to validate degradation parameters. We will test backsheets materials of known quality under varying heat, UV, and RH conditions, using band-pass filters to assess spectral dependence. Degradation metrics include elongation loss, adhesion, tensile strength, color change, and transmittance. Outputs include open-access Python code on PVdeg (GitHub) and industry-relevant degradation parameters.



Multi-Scale, Multi-Physics Model

## Background

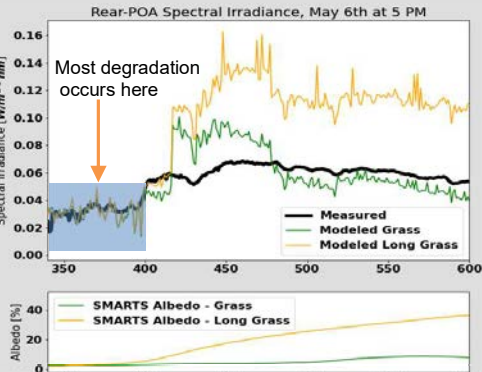
Backsheet failure has resulted in power loss and large-scale recall of photovoltaic modules, resulting in billions of dollars in lost revenue [1-6]. This project aims to study how various backsheets and junction box materials degrade under different conditions and to develop Python code to help model and predict degradation [8].



Visual representation of UV radiation hitting the back sheets

## Challenges:

- This project is gathering data and behaviors to reduce the uncertainty in the spectral and modeling models.
- Spectral distribution is dependent on albedo (sunlight that is diffusely reflected)
- Albedo drops off in the UV range where damage occurs
- Different irradiance levels (chambers are 10 times the intensity of outdoors); differences in spectral characteristic further complicate the extrapolation from chamber to outdoor conditions
- Degradation usually occurs in a sub-linear manner, thus models are needed for sub-linear degradation



## Degradation Model

$$D = D_0 \int_0^t RH(t)^n \cdot e^{-\frac{E_a}{RT(t)}} \int_{\lambda} \left[ e^{-C_2 \lambda} \cdot G(\lambda, t) \right]^P d\lambda dt$$

**D** - damage

**RH** - relative humidity

**t** - time

**RT** - gas constant

**G** - irradiance

**λ** - wavelength

**C<sub>2</sub>** - empirical value describing spectral sensitivity to damage

**P** - reciprocity factor describing effect of higher intensity.  
Between ~0.4-0.8

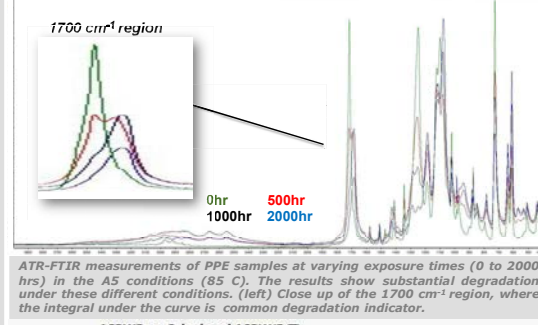
**E<sub>a</sub>** - Arrhenius activation energy

**n** - Dependence of degradation on humidity, can range from negative to positive values

## Test Materials

| Alias    | Description  |
|----------|--|
| T-PVDF   | Transparent PVDF Frontsheet/Backsheet                      |
| T-PVF    | Transparent PVF Frontsheet/Backsheet                       |
| CPC      | Fluorocoat/PET/fluorocoat with Fluororesin BO-C2 Backsheet |
| O-PVF    | Opaque PVF Backsheet                                       |
| PPE      | PET/PET/low-VA EVA Backsheet                               |
| PO       | Polyolefin Backsheet                                       |
| J-BOX #1 | Thin film polyamide. Junction box Housing                  |
| J-BOX #2 | x-Si polycarbonate blend Junction box Housing              |

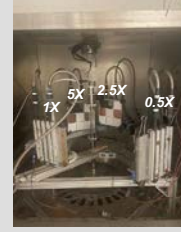
## Preliminary Results



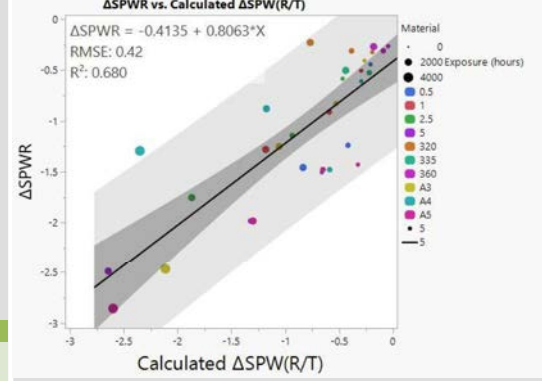
ATR-FTIR measurements of PPE samples at varying exposure times (0 to 2000 hrs) in the A5 conditions (85 C). The results show substantial degradation under these different conditions. (left) Close up of the 1700 cm⁻¹ region, where the integral under the curve is common degradation indicator.

## Exposures Variables

We investigate the stress factors influencing the PV backsheets degradation by exposing samples to controlled environmental conditions. The testing setup includes multiple chambers with varying irradiance levels, temperature dependencies, and glass filter effects.



Samples loaded into a Ci4000 weatherization chamber



Results of a nonlinear regression analysis fitting the degradation model to the data for the change in solar weighted reflectance ( $\Delta SPWR$ ) for the PPE backsheets. The regression analysis is weighted by the exposure time of the different measurements. The integration of the degradation model was achieved using a summation with 5 nm bins from 385 nm to 450 nm. The dark grey is a standard deviation, and the light grey is the 95% confidence interval.

| Parameter             | Condition   | Purpose   |
|-----------------------|---|---|
| <b>Temperature</b>    | A3 (65°C), A4 (75°C), A5 (85°C) chamber settings                  | Test the Arrhenius temperature dependency of the backsheets |
| <b>Irradiance</b>     | 0.5X, 1X, 2.5X, 5X UV-suns in xenon weathering chamber at 70°C    | Test backsheets degradation dependence on irradiation       |
| <b>UV Filter</b>      | 50% UV cut off at 360nm, 335nm, 320nm. In A3 setting for exposure | Test how UV cut off impacts' degradation of backsheets      |
| <b>Read intervals</b> | 0, 500 h, 1000 h, 2000 h, 4000 h                                  | Monitor the degradation process                             |

## Correlation of Estimates

| Values      | Ea      | P       | C2      | Do      |
|-------------|---------|---------|---------|---------|
| 10.7±8.9    | 1.0000  | 0.5015  | -0.2637 | -0.0329 |
| 0.501±0.106 | 0.5015  | 1.0000  | -0.3700 | 0.0483  |
| 0.117±0.107 | -0.2637 | -0.3700 | 1.0000  | -0.9334 |
| 11.6±16.1   | -0.0329 | 0.0483  | -0.9334 | 1.0000  |

Nonlinear regression fit parameters for the polyethylene terephthalate (PET) based backsheets PPE.

## Evaluation Methods

To assess degradation, four different tests were conducted on all samples after exposure:

### Spectrophotometer (Cary 7000)

- Used to evaluate optical degradation and material aging.
- Measures: Photon weighted transmittance/reflectance and yellowness index

### Gloss measurements (BYK Micro-TRI-Gloss meter)

- Used to assess surface wear and gloss retention
- Measures: gloss measurements at 20° 60° 85°

### Nanoidentation (KLA iNano Nanoindenter)

- Used to determine mechanical property changes.
- Measures: Modulus & Hardness

### ATR-FTIR (Attenuated total internal reflectance Fourier transform infrared spectroscopy)

- Used to identify degradation pathways and chemical changes in the composition (structure)
- Measures: Wavenumber, Bond type

## Current Status and Future Work

- Finalizing exposure testing and continuing data analysis.
- Developing an FTIR Python tool for clearer deconvolution of spectra for analysis
- Upcoming phase 2 of exposure will focus on humidity dependence of degradation.
- Raytracing integration (bifaciallfv and bifacial\_radiance) is in progress for geospatial evaluation with PVDeg

## Citations

- Hirotsuchi, A., "Formation of Surface Cracks in Polymeric Backsheets Using Fragmentation and Finite Element Simulation," *IEEE Journal of Photovoltaics*, vol. 14, no. 2, pp. 31-38, 2024, doi: 10.1109/JPHOTOV.2023.3359119.
- Eden, Y., Vovk, A., et al., "Possible repair strategies to PV modules with cracked backsheets," 2019 IEEE Photovoltaic Specialists Conference (PVSC), 25-26 June 2019 2019, pp. 328-332, doi: 10.1109/PVSC48424.2019.8830010.
- Kempe, M. D., et al., "Survey of Mechanical Durability of PV Backsheets," in 2017 IEEE 44th Photovoltaic Specialists Conference (PVSC), 25-26 June 2017 2017, pp. 328-332, doi: 10.1109/PVSC.2017.8029020.
- X, G., et al., "Cracking and Microstructural changes of PVDF-Based Backsheets During Aging," 2020 IEEE Photovoltaic Reliability Workshop (PVRIW), 16-21 June 2020 2020, pp. 2411-2416, doi: 10.1109/PVRC4733.2020.9300874.
- Y, H., et al., "Aging and Degradation of PV Modules Used in Photovoltaic Modules - Part 7-2: Environmental exposure - Accelerated weathering of Polymeric materials," 2022 IEEE Photovoltaic Reliability Workshop (PVRIW), 5-10 June 2022, Philadelphia, Pennsylvania, United States, 2022 [Online]. Available: <https://ieeexplore.ieee.org/document/9810070/>

# An AI-Enabled Chat Bot for DuraMAT

Robert White<sup>1</sup>, Sagi Zisman<sup>1</sup>, David Rager<sup>1</sup>, Ambarish Nag<sup>1</sup>, Harrison Goldwyn<sup>1</sup>, Nicholas Wunder<sup>1</sup>, and Dan Horton<sup>1</sup>
<sup>1</sup>National Renewable Energy Laboratory;

**Awarded FY17 - FY25  
Central Data Resource**
**Period of Performance:  
Active**

## Goals

Since the early 2000s, virtual laboratories have been at the forefront of scientific innovation, driven by increasingly distributed resources, global expertise, and pioneering initiatives like the Materials Genome Initiative. For a virtual laboratory consortium to truly excel, it must establish a robust framework for data management, secure communication, and seamless sharing, dissemination, and demonstration, all while empowering remote researchers to collaborate effectively. Our rapidly evolving data hub embodies this vision. It not only meets these demanding requirements but also delivers fresh, high-quality data to the public and the broader research community. By rigorously adhering to the **FAIR principles**: ensuring data is Findable, Accessible, Interoperable, and Reusable, we are setting a new standard for excellence in scientific data management.

## Accomplishment and Publications

The data hub has now been fully operational for eight years. During that time, we have seen the number of users and amount of data archived grow steadily. We have discovered new ways to help improve the researchers' experience on the data hub, by adding functionality and fine tuning the performance.

Energy Material Network Data Hubs: Software Platforms for Advancing Collaborative Energy Materials Research. Robert R. White, Kristin Munch, Nicholas Wunder, et al., IJACSA, 12(6), 2021. <http://dx.doi.org/10.14569/IJACSA.2021.0120677>

## Data Hub

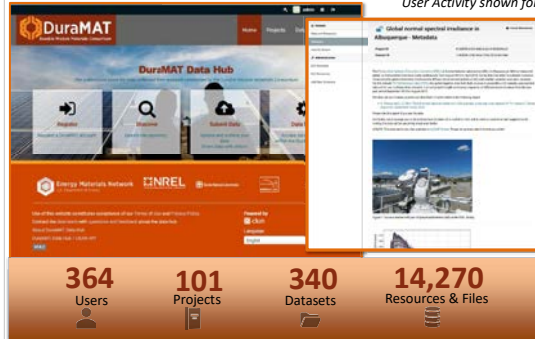
The DuraMat data hub is currently powered by the robust CKAN platform, a highly customizable and widely adopted data-sharing solution trusted by major government portals such as data.gov and data.europa.eu/en. Built with Python and JavaScript and backed by a PostgreSQL database, CKAN seamlessly integrates file archives and a comprehensive security layer, further enhanced by a dynamic ecosystem of open-source plugins.

Our strategic deployment to the AWS FedRAMP cloud has already resolved past accessibility challenges associated with on-premise systems, ensuring secure and efficient collaboration with external partners. However, as research needs progress, the CKAN platform must also evolve to support the advanced capabilities demanded by today's scientists.

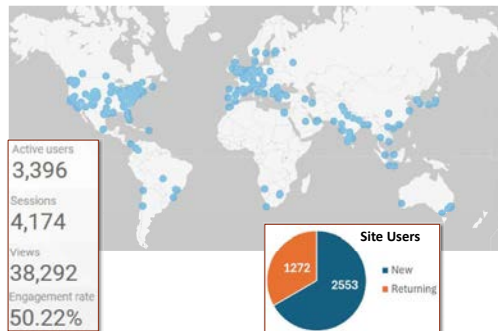
In response, we are launching a multi-Data Hub initiative to design a modern, scalable architecture that not only preserves the strengths of our existing system but also expands its functionality for the future. A cornerstone of this upgrade is an AI-enabled chatbot poised to revolutionize user interactions, transforming how researchers access and engage with our data hub.

## Current Consortium Stats

User Activity shown for Oct 1, 2024, through Feb 10, 2025



## World-Wide Stats



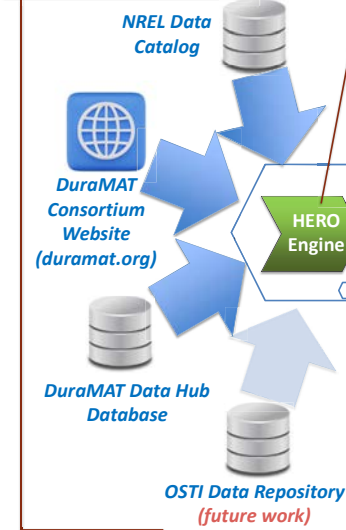
## Anatomy of the DuraMAT AI Chatbot Engine

Data is securely extracted using standardized API frameworks that provide RESTful and other interfaces. The data is extracted and seamlessly formatted and processed through the HERO engine.

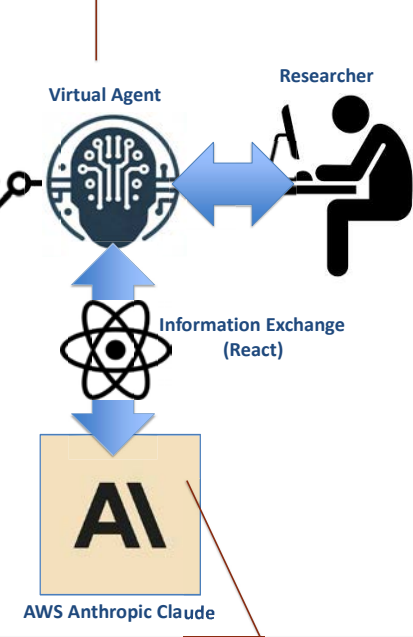
New data is currently ingested weekly, but as operations begin to settle that will be increased to daily harvests.

Our new Chat system leverages NREL's cutting-edge suite of web services, known as Hybrid Environment Resources and Operations (HERO). Built on Amazon Web Services (AWS) and guided by the AWS Well-Architected Framework, HERO delivers secure, reliable, and cost-effective applications. HERO is built on an API-first approach and features user-friendly front-end web applications. Designed as micro front ends (MFEs), these components are not only easy to maintain but also readily reusable across other applications with minimal custom coding.

The agent serves as the central hub for communication and access to the Graph Database, using queries to traverse nodes and edges to assemble comprehensive results. Typically, it begins with an OpenSearch query to generate a broad response to a given question and then iterates between targeted SPARQL or additional OpenSearch queries to refine its findings. This curated information is passed on to ReACT and the AWS Anthropic Claude systems, where advanced natural language processing techniques interpret user queries and results for seamless communication.



Knowledge graphs (KGs) serve as powerful tools to integrate and structure data from diverse sources by capturing detailed information about key entities, whether they be people, places, or abstract concepts, within a specific domain. By extracting metadata from the DuraMAT Data Hub and other sources and then mapping this information through sophisticated ontologies such as spaCy Topics, we can reveal intricate relationships between disparate data elements. These connections are visualized as a topological map, where nodes represent the subjects and edges depict the meaningful associations between them. This dynamic representation not only enhances our understanding of complex data ecosystems but also empowers researchers to uncover hidden patterns and insights.



The DuraMAT Data Hub is continually optimized to adhere to the FAIR Guidelines, ensuring our systems remain state-of-the-art. Our newly developed search and chat interface further enhances the findability and accessibility of DuraMAT's work, empowering users to quickly locate and engage with critical projects and research.

<http://www.go-fair.org/fair-principles>

Acknowledgment: This material is based upon work supported by the U.S. Department of Energy's Office of Energy Efficiency and Renewable Energy (EERE) under the Solar Energy Technologies Office Award Number 52789. This material is based upon work supported by the U.S. Department of Energy's Office of Energy Efficiency and Renewable Energy (EERE) under the Solar Energy Technologies Office Award Number 52789. Legal Disclaimer: The views expressed herein do not necessarily represent the views of the U.S. Department of Energy or the United States Government.

# Encapsulants for screen-printed copper contacts

T. Druffel, D. Williams, K. Elmer, E. Yenney, A. Nambo, R. Dharmadasa, P. Stradins, P. Hacke, W. Nemeth, S. Theingi, K. Kenney, J. Munro

**Awarded FY24  
Core Modelling Call**
**Period of Performance: 10/24-9/25  
Funding: \$400k**

## Contributing to DuraMAT Consortium Goals

This project will develop a library of encapsulants suitable for Tunnel Oxide Passivated Contact (TOPCon) solar cells with copper metallization pastes, ensuring durability and cost-effectiveness. As the industry moves away from EVA due to moisture-related degradation in n-type cells, the transition to copper requires encapsulants that mitigate oxidation. While POE is the current choice, past supply shortages have raised concerns. This study will evaluate encapsulant interactions with copper pastes and their impact on module performance and cost.



Module Materials Solutions

## Project Overview

### Evaluate ENCAPSULANT Compatibility with COPPER PASTE in TOPCon Modules.

- Largest non-silicon cost is silver.
- Copper screen-printed, air-fired pastes.
- Copper can oxidize and diffuse, reducing the performance of a solar cell.
- Assess encapsulant durability, cost-effectiveness, and failure mechanisms.
- Encapsulants to be studied: EVA, POE, EPE, liquid silicone.

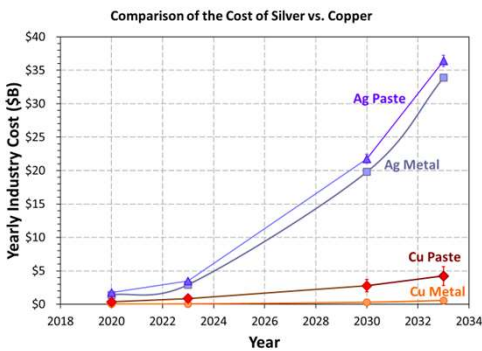


## Printed Cell



## Copper Paste Advantage

Cost projections and sustainability.



## Encapsulants

**EVA (Ethylene Vinyl Acetate)** – good adhesion and low cost, but prone to moisture ingress and acid formation.

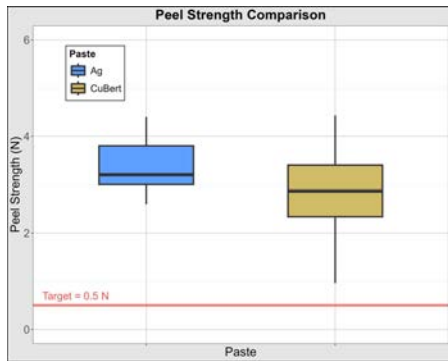
**POE (Polyolefin Elastomer)** – superior moisture barrier with supply constraint concerns.

**EPE (EVA-POE-EVA)** – multilayer encapsulant targeting lower cost of EVA and moisture resistance of POE, but with processing complexity.

**Liquid silicone** – allows for room-temperature lamination using a dam-and-fill approach, requiring different equipment technology. Superior temperature and UV stability, but has a higher water vapor transmission rate.

## Solderability

Paste development for interconnection via soldering.



## Accomplishments & Publications

- Potential for modules containing copper metallized PERC cells demonstrated on the miniature scale.
- Performance and characterization of potential TOPCon degradation pathways in-progress.

### Presentations:

- T. Druffel, "Screen print metallization using Cu-based pastes", Silicon Workshop, August 2023
- T. Druffel, "Durability of Copper Printed Contacts for Silicon Solar Cells", PVRW, February 2024
- T. Druffel, "Copper Pastes for TOPCon Solar Cells", Silicon PV, April 2025

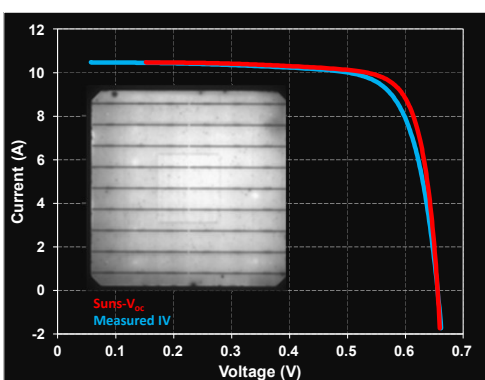


## Mini-Modules



## Performance

Firing improved, but non-uniformities remain.



# STEEL MODULE FRAMES DELIVER TRACKER MOUNT COST SAVINGS AND INCREASED STRUCTURAL RELIABILITY

The Strength and Reliability Benefits of Stronger Steel Frames with Single Axis Trackers

## U. S. SITE COST SAVINGS POTENTIAL WITH SINGLE AXIS TRACKERS



When using weak aluminum-framed M10 modules, 1300-1400 mm tracker rails or clamps are often necessary in the edge wind zone in many US locations.

Even while building in additional factor of safety, Origami steel frames can allow:

- Reducing tracker rails or clamps to 400 mm sitewide for portions of the US (shown in green), delivering 15-20% mounting cost reduction.
- Increasing module mount wind load rating, thereby eliminating custom rail/clamp types in high wind zones, and opening high wind sites to tracker deployment.
- Both mean lower mount cost and less installation complexity.

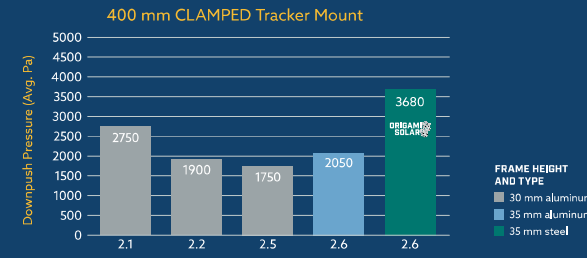
## MECHANICAL STRENGTH TEST TO FAILURE

Aluminum frame strength has been reduced to cut costs, creating module fragility issues.

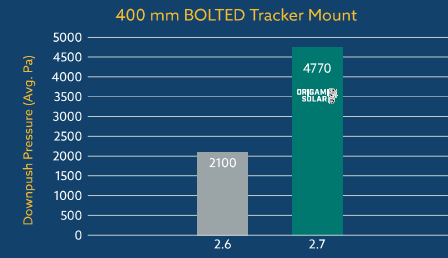
Steel test-to-failure performance is typically 2X that of same aluminum-framed module.

Test to failure informs IEC 61215 mechanical load test potential.

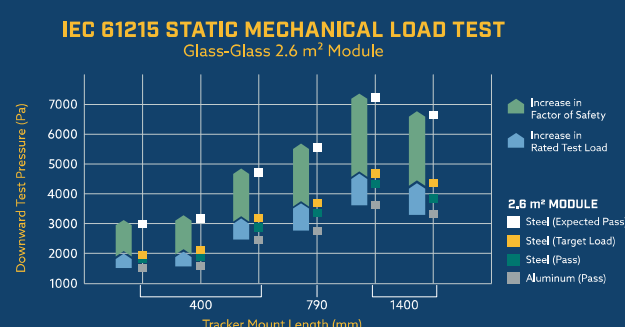
### TEST TO FAILURE: GLASS-GLASS MODULES



### TEST TO FAILURE: GLASS-GLASS MODULE



## STEEL FRAMED MODULES WITH TRACKER MOUNTS IMPROVE BOTH FACTOR OF SAFETY AND RATED TEST LOADS



Expected pass with Origami Steel frames calculated as 70% of test to failure value per industry recommendations.

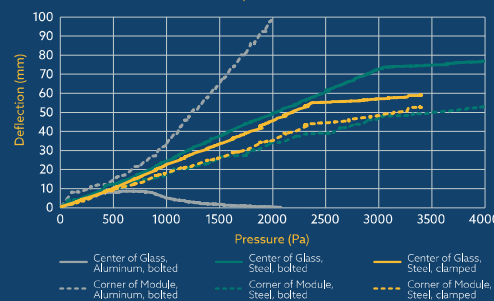
Setting an increased test load rating at 30% above that of the aluminum frame maintains significant margin as an increase in factor of safety.

Factor of safety here equals 2.3, resulting in significant increase in design reliability.

## ALUMINUM VS. STEEL DEFLECTION CURVES WITH TRACKER 400 MM MOUNTS

### DEFLECTION IN DOWNPUSH TEST TO FAILURE

400 mm Tracker Mounts, Glass-Glass 2.6 m<sup>2</sup> Module



Aluminum deflects significantly more at the frame than steel under the same load. The aluminum frame therefore provides very little support to the laminate.

Steel deflects less at the frame, but shows center-of-glass deflection increasing until it touches the torque tube.

Aluminum fails at a load well below where the steel module's glass deflection indicates contact with torque tube.

**ORIGAMI**  
**SOLAR**

### AUTHORS

Lauren Busby Ahsler, SE, VP of Engineering  
Tyler Hudson, Head Product Engineer

[www.origamisolar.com](http://www.origamisolar.com)

# Technoeconomic Analysis (TEA)

Jarett Zuboy, Brittany Smith, and Michael Woodhouse


**Awarded FY22  
Core Modelling Call**
**Period of Performance: 3 years**  
**Funding: \$100,000 per year**
**Contributing to DuraMAT Consortium Goals**

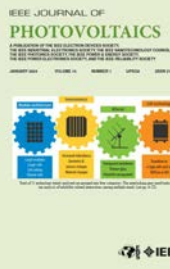
- Provide TEA to Industry Advisory Board (IAB) and researchers to identify research priorities, quantify research value, and enhance publications.
- Track technology changes that could affect PV module reliability.
- Assess changes in module reliability risks over time.
- Identify the need for new research related to reliability.

**Project Overview**

- Link technology trends to reliability implications.
- Provide a framework to calculate technology costs, yielding insights useful for research decision-making, proposals, technology selection, and publications.
- Examine technology tradeoffs considering lifecycle project economics.

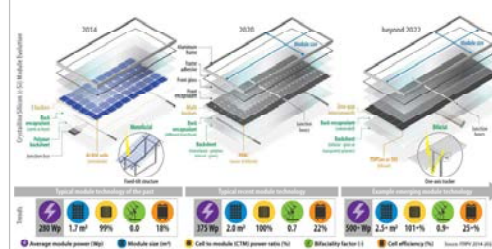
**Outcome & Impact**

- Make TEA data accessible to IAB members & researchers.
- Engage IAB via data and analysis sharing, followed by discussions and review.
- Gather input on current and future DuraMAT research priorities.
- Provide data for proposals, ‘sanity checks,’ publications, evaluating research.

**Tech Scouting 1.0 (c-Si)**


J. Zuboy, M. Springer, E. Palmiotti, J. Karas, B.L. Smith, M. Woodhouse, and T.M. Barnes, "Getting Ahead of the Curve: Assessment of New Photovoltaic Module Reliability Risks Associated With Projected Technological Changes," *IEEE Journal of Photovoltaics* 14(1), 4–22, Jan. 2024, 10.1109/JPHOTOV.2023.333477.

We explore the drivers behind PV technology trends, their interactions, and associated reliability risks and benefits. We identify areas that would benefit from accelerating the PV reliability learning cycle to assess emerging module products and designs more accurately. We also discuss incorporating fundamental knowledge into models that can predict module reliability.

**Module technology trends**

**Evidence-Based Priorities**
**Module architecture**

- Characterize the reliability implications of larger and thinner cells in conjunction with variations in module design, including interconnect type and thinner glass
- Research and develop tests for assessing the effect of larger modules on cell cracking due to weather, shipping, handling, and installation
- Understand multi-step relationships between defects and long-term module degradation causing potential power loss

**Interconnections**

- Research potential new degradation mechanisms associated with conductive adhesives, such as debonding and corrosion of non-silver conductive particles
- Develop accelerated tests and standards to address the change from metallurgical to mechanical contacts

**Evidence-Based Priorities**
**Bifacial**

- Assess whether current PID testing optimized for monofacial modules should be modified for bifacial
- Develop accelerated and field testing to assess the long-term reliability of mixed and co-extruded encapsulants as well as transparent polymer backsheets
- Modify hail testing to account for thinner glass and more hail-prone PV system locations

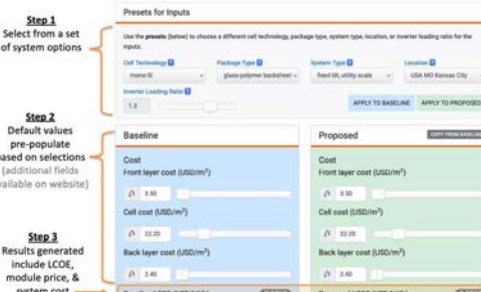
**Cell technology**

- Develop specific stress combinations and sequences for testing the reliability of n-type cells and their ultrathin surface passivation layers
- Develop tests and standards to assess and screen for UV light-induced degradation and PID risk in industrial implementations of bifacial TOPCon and SHJ architectures

**Simplified PV LCOE Calculator**

Available at [pvcoe.nrel.gov](http://pvcoe.nrel.gov)


- Allows users to select system features including: cell type, packaging, racking, location, ILR
- Populates suggested costs for cell, module, BOS, O&M as well as suggested values for discount rate, module efficiency, system energy yield, degradation, service life
- Energy yield data directly from NREL System Advisor Model
- Compares a baseline system to a proposed novel system; break-even buttons automatically adjust the associated input to target an LCOE that matches the opposing system
- Defaults will be updated during 2025 to reflect 2023-2024 market

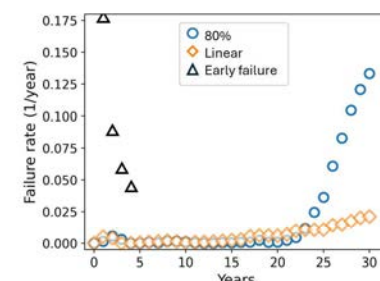
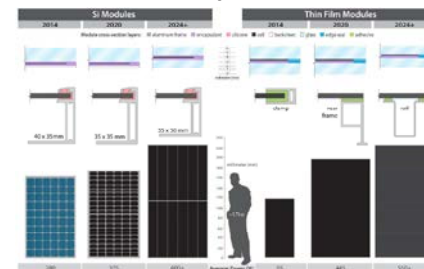
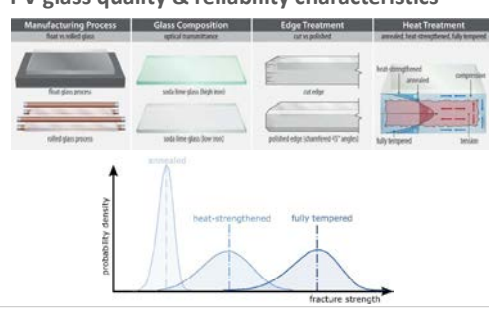
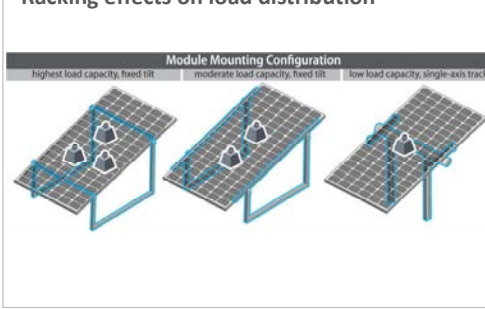
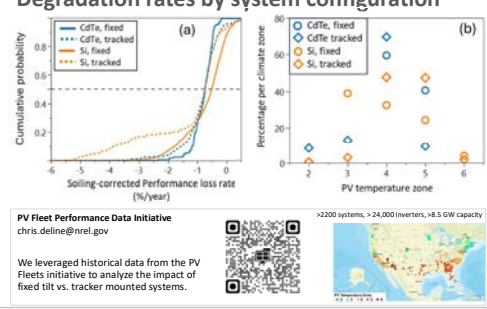


The calculator interface includes dropdown menus for Cell Technology (mono-Si), Package Type (glass/polymer backsheet), System Type (fixed tilt), and Location (USA MO Kansas City). It also includes fields for Inverter Loading Ratio (1.0), Cost Front layer cost (\$/m²), Cost Cell cost (\$/m²), Cost Back layer cost (\$/m²), and Cost Proposed LCOE (\$/kWh).

**Tech Scouting 2.0 (c-Si, TF, glass)**

EC, Palmiotti, M. Springer, J. Zuboy, T.J. Silverman, J.L. Braud, D.C. Jordan, S. Rabade, T.M. Barnes, "Growing Pains: Investigating the PV Technology Trends Behind Frequent Early Failures in Modern Glass-Glass Modules," *IEEE Journal of Photovoltaics*, Jan. 2025, 10.1109/JPHOTOV.2025.3526170.

Silicon and thin film modules are converging toward similar ~3 mm glass-glass designs with thinner glass sheets to increase power output while reducing module weight, and both types are increasingly mounted on single-axis trackers. At the same time, most PV sites have been reporting spontaneous glass breakage in early life systems deployed with these “big, floppy modules.” We discuss the reliability implications of module changes that may be contributing to increased early failure. Larger, thinner glass sheets along with variations in heat treatment and quality may be contributing to glass vulnerability. Trends toward weaker or back-mounted frames may also be contributing to module failures, especially for “extra-extra-large” modules mounted on trackers. Combinations of these trends may have pushed modules to a threshold at which increasing early failures are causing the front edge of the “bathtub curve” to re-emerge. Current qualification testing appears to be ineffective for catching these early failures in new module designs. Additional research is needed to identify the field conditions leading to glass breakage and if there is one or multiple limiting flaws in new module designs causing glass breakage. Early failures may be mitigated by returning to more robust designs or ensuring better module testing and quality assurance.

**Potential module failure rates**

**c-Si and thin film utility-scale module trends**

**PV glass quality & reliability characteristics**

**Racking effects on load distribution**

**Degradation rates by system configuration**


# Unscrambling combiner box SCADA tags using time series data

Rob van Haaren, PhD – rob@proximal.energy



## Mismatched SCADA tags

When utility-scale PV projects are under construction, crews have to meet a tight schedule for completing blocks and have a lot on their minds. Labeling cables properly to make sure they get hooked to the correct central inverter DC input sometimes gets overlooked, leaving an opportunity for conductors to get swapped with one another. Even if cables are labeled correctly, it may happen that the electrical contractor hooks the cable into any arbitrary DC port.

This does not impact the project's energy yield (directly), and when looking at the inverter's expected vs actual power output, there should be no difference. However, when there is an outage that occurs within the DC system of one of these swapped combiner boxes, a technician will be sent to troubleshoot issues in a place where there is none.

Aside from the wasted time and money, this also leads to frustrations with on-site technicians, who sometimes travel for miles at a snail's pace speed limit of typically 15 mph to handle an issue, only to find out that they have to go check every combiner in that block (typically 15), to locate the problem.

This issue of mismatched SCADA tags to GIS elements is more prevalent than one would think. One service provider recalls a project with 70% of its SCADA tags incorrectly mapped:

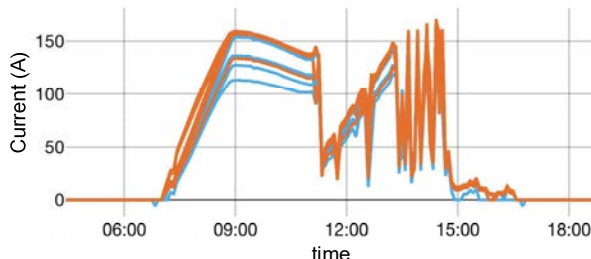
**"We've seen projects with 70% of the DC combiner boxes incorrectly mapped to their GIS elements."<sup>1</sup>**

## Status Quo

The current method to prevent the technician dispatch issue explained above is to unscramble combiner SCADA tags by deploying a team of two people, one remote and one on-site. The remote person is looking at the live data streams, and the on-site person is switching off-and-on one combiner at a time! This way, they can identify each mislabeled SCADA tag and correct it (typically by remapping virtually as opposed to physically swapping conductors). However, this is **extremely time-intensive** as projects sometimes have over 3,000 combiners.

In rare cases, indications of mismatches can be identified more easily if DC combiners of varying DC capacities are swapped. In the figure below, a PCS with 14 combiner boxes is shown with orange lines represent higher DC capacity combiners, and blue lines have lower DC capacity. It is impossible for the blue line to be grouped with the orange as the DC capacity is not capable of producing currents that high.

## Mismatched Combiners Example



## The Idea: Can we solve this with Software?

Prior research shows that irradiance sensor time series data can be used during cloudy conditions for deriving along-wind and cross-wind correlations and its impact on ramps (L. Hinkelman, 2013).

This research is similar, except that we don't work with point-sensors, but PV arrays of roughly 250 kW-DC. Also, we're not looking into ramp rates, but simply trying to find mismatched combiners based on their cross-correlations.

The main premise is:

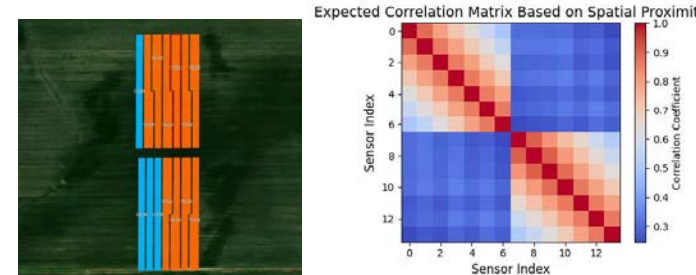
**Time series data of adjacent DC combiners should have a higher cross-correlation than those further separated from each other.**

## Data Source and Pre-processing

The geographic layout and historical time series current (A) production data from a ~500 MW (AC) utility-scale project was collected using the Proximal Energy API. The periodicity varies, but data points are typically 5-10 seconds apart. One block and one day at a time is processed, with data being forward-filled (ffill) and resampled at 1-second.

## 1. Initialization

At first, the layout (i.e. polygons) of all the DC arrays connected to the PCS are turned into a GeoDataFrame. Then, a distance matrix is created from the centroids of those polygons, from which we can derive the "expected correlation matrix" using the numpy.exp() function:



## 2. "Secret Swaps"

In order to stress-test the algorithm, we introduce "secret swaps" to correctly mapped combiner boxes within the same block. This way, we can see the performance as a function of how disorganized the mapping is. Each secret swap switches two random combiner SCADA tags and we test from 1 going up to 10 secret swaps. At each level, we run 20 iterations.

## 3. Unscrambling using Total Square Error (TSE)

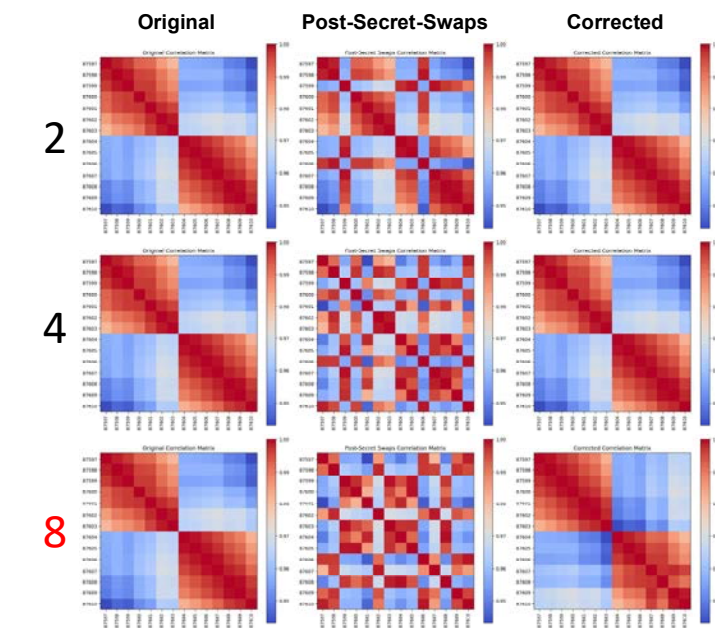
Starting out with the mappings post-secret-swaps, the system iterates over the following steps:

1. Calculate the observed correlation matrix using: df.corr()
2. For each pairwise swap (combinations(n)), calculate the resulting TSE:  $\text{np.sum}((\text{observed\_corr\_matrix} - \text{expected\_corr\_matrix})^2)$
3. Apply the swap with the highest TSE reduction.



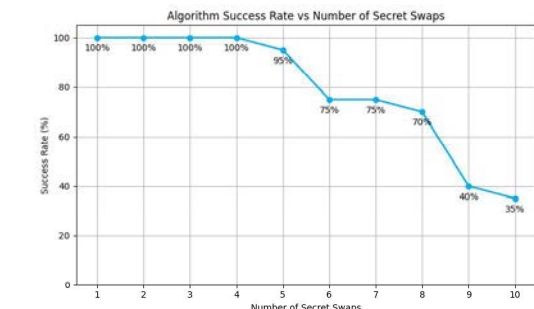
## 100% Success Rate up to Four Secret Swaps

As the number of secret swaps increases, the probability of landing in some local TSE minimum goes up. With this algorithm, mappings with up to four swaps (up to 8 mismatched combiners) were recovered back to their original state 100% of the time. See below the results of 2, 4 and 8 secret swaps unscrambled. Notice the failed outcome on 8 swaps!



## Summary

The poster presents a problem with mismatched SCADA tags in utility-scale PV projects, which leads to inefficient troubleshooting and technician dispatching. The proposed methodology uses time-series data analysis to detect mismatches by analyzing cross-correlations between adjacent DC combiners. By applying a Total Square Error (TSE) optimization algorithm, the system can correctly remap up to four swapped combiners with 100% accuracy. This approach could significantly reduce the time and cost associated with manual tag verification.



# Distributed Strain Sensing of a Solar PV Single-Axis Tracking System

You-Jia (Allen) Li<sup>1</sup>, Hanshu Zhang<sup>1</sup>, Ayush Chutani<sup>2</sup>, Paul Dice<sup>2</sup>, Ana R. Dyreson<sup>2</sup>, Laurie Burnham<sup>4</sup>, Gerald Robinson<sup>3</sup>, and Matthew J. DeJong<sup>1</sup>

<sup>1</sup>Department of Civil & Environmental Engineering, University of California, Berkeley, CA, 94720, USA. <sup>2</sup>Michigan Technological University, Houghton, Michigan, 49931, USA.

<sup>3</sup>Energy Technologies Area, Lawrence Berkeley National Laboratory, Berkeley, CA, 94720, USA. <sup>4</sup>Sandia National Laboratories, Albuquerque, New Mexico, 87185, USA.

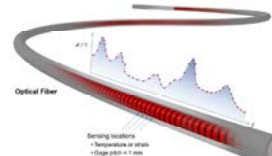
## Motivations and Scope

- Investigates fiber optic sensing (FOS) technology to characterize dynamic wind loading effects on single-axis solar photovoltaic tracking systems, comparing FOS with traditional sensors like accelerometers and strain gauges.
- Utilizes Fiber Bragg Grating (FBG) and Distributed Strain Sensing (DSS) technologies to measure strain on torque tube and solar panel modules, enabling comprehensive analysis of torsional behavior and panel deformation.
- Develops a finite element model using OpenSees to simulate the structure's dynamic response under time-varying wind loads, validating measured results against model predictions.
- Aims to enhance understanding of solar PV tracking systems' dynamic response to realistic wind loads, ultimately improving design methods, operational strategies, and long-term resilience and performance modeling.

## Fiber Optic Sensing

### Distributed Strain (DSS)

- Based on Brillouin scattering, DSS detects strain changes by measuring shifts in Brillouin frequency, allowing for comprehensive monitoring of large structures.
- DSS offers high spatial resolution – 0.5mm to 5cm – with thousands of measurement points along a single fiber.



### Fiber Bragg Grating (FBG)

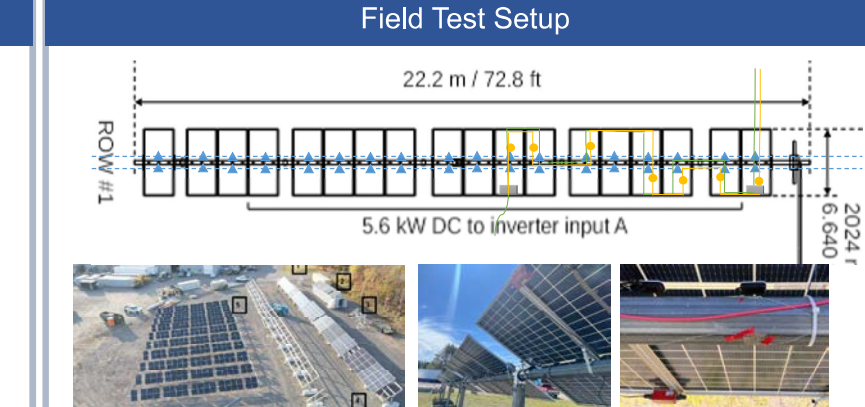
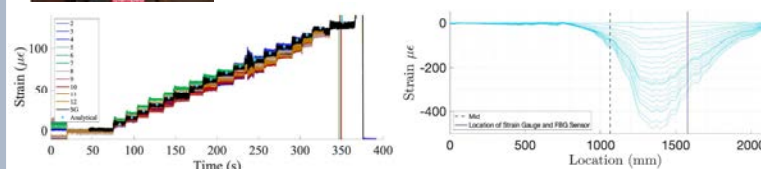
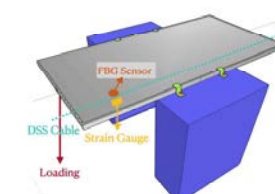
- FBG sensors use light reflection in optical fibers, allowing multiple sensors (18 in this case) on a single fiber or comprehensive strain measurement.
- High sampling rate of up to 2 kHz enables the capturing of dynamic strain events with excellent temporal resolution, surpassing DSS systems.



## Initial Lab Test - Accuracy and Calibration



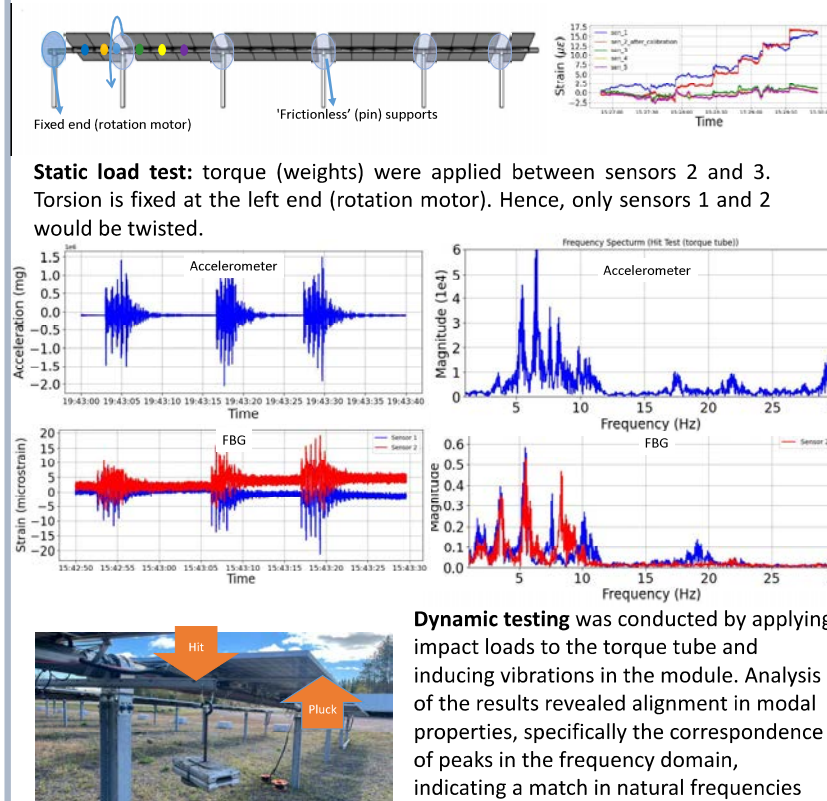
Static and Dynamic loading tests were conducted on both PV module and circular/square torque tube. Results between three strain measuring systems closely agreed.



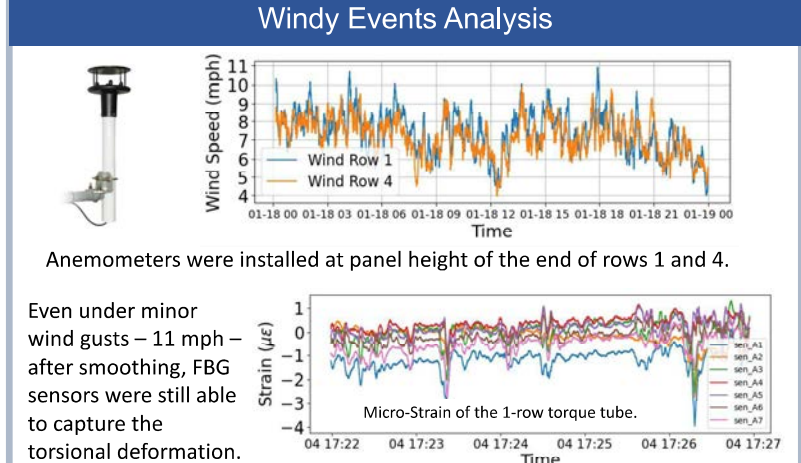
Michigan Regional Test Center for Emerging Solar Technologies at Michigan Tech.

- Sensors were installed at the first and fourth rows of the tracker system.
- 36 FBG sensors were epoxied on the torque tube – 18 on each side.
- DSS cables, along with 7 FBG sensors, were epoxied on the module.
- 2 accelerometers were installed on the modules for dynamic behaviors.
- Several traditional strain gauges were glued along the fiber optic sensors.

## Primary Field Test



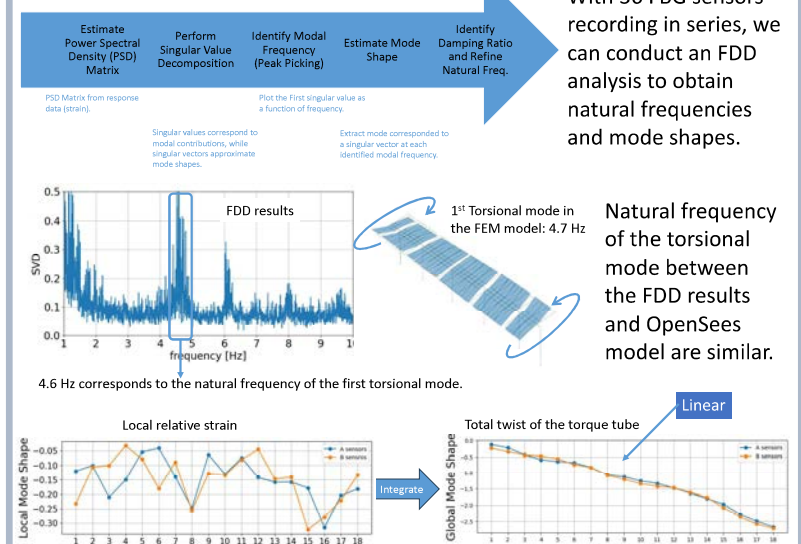
**Dynamic testing** was conducted by applying impact loads to the torque tube and inducing vibrations in the module. Analysis of the results revealed alignment in modal properties, specifically the correspondence of peaks in the frequency domain, indicating a match in natural frequencies between the two components.



Anemometers were installed at panel height of the end of rows 1 and 4.

Even under minor wind gusts – 11 mph – after smoothing, FBG sensors were still able to capture the torsional deformation.

## FDD Analysis of the Strain Data vs. OpenSees

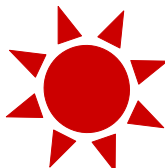


Natural frequency of the torsional mode between the FDD results and OpenSees model are similar.

If the tracker is torsionally fixed at one end and free at the rest, one should expect the angle of twist to be **linear** along the torque tube.

## Discussions

- Fiber optic sensing (FOS) technology, provides an efficient and economical method for structural health monitoring of PV tracker systems.
- FOS captures both static and dynamic structural responses to wind loads, including modal properties, due to its high sampling rate and sensitivity.
- The technology broadens the scope of SHM for PV tracker systems, addressing comprehensive wind load effects.
- This ongoing research will continue with further data collection/analysis, FE model refinement, and stochastic wind load generation based on measured data.



# Walkable Solar Panels!

Author: Lavinia Bunea

Contributors: David Meakin, Nikki Achor, Grusha Lonkar, Mike Kuiper



## Introduction:

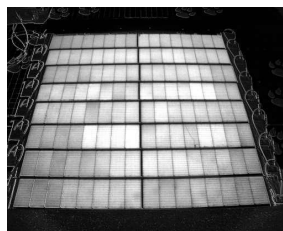
GAF Energy solar panels being able to be walked on offer a convenient dual function, combining energy generation with accessibility for maintenance tasks. This capability not only maximizes space utilization but also simplifies upkeep, making them a practical choice for both residential and commercial application.

## Objectives:

Through the variety of different testing, we will understand the durability and strength of GAF Energy solar panels, as well as the solar panels being able to maintain energy generated in the panels regardless of what conditions the panels may endure.

### How?

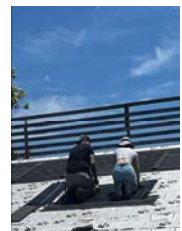
With the combination of glass, jumper modules, wires, thermosets, and many other materials in order for the panels strong factors contribute to the durability of being able to walk on our solar panels as well as maintaining any energy captured in the panels.



The image above is captured by the OPL Tool, and indicates that after walking weighing 230 lbs over panels, there's one new crack in cell 16 at the top, however there was no jurassic change in energy proving the conditions the panels are able to withstand.

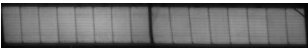


The image above shows Nikki using OPL Tool to scan images of the panels after installation.

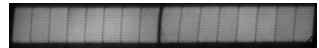


The image above shows Mike and Lavinia installing the panels onto the roof

PJM-COL-13: Original panel before walk



After walk: No new cracks



### Testing used:

EL Scanning before/after roof walk, roofwalk over the installed panels and OPL Tool scanning and image capturing.

### Conclusion:

Through the different components making up the solar panels as well as the variety of testing and scanning in order to ensure how durable these panels are, it's easy to conclude how GAF Energy's solar panels are walkable. Through the variety of scanning there were a few minor cracks, however they formed prior to scanning which could've been caused by transporting the panels, the removal process of the testing from the roof, etc. The large image above with the OPL Tool clearly indicates how no cracks were formed during the installation process as well as during the walking process going over the panels while being 230lbs, the average weight of a contractor installing solar panels. Through this understanding the conclusion of how GAF Energy solar panels being walkable is easily depicted through the durability and testing going into the panels, ensuring that customers are getting the best solar panels there are on the market.

### Why is testing important?

Various types of testing ensures the durability and strength of the panels, regardless of its condition, as well as seeing any fine details missed during previous scanning or tests.

# Key Findings | Solar PV Energy Yield Assessment Validation

**Authors:** Evan Giacchino, Eric Soderlund, Eric DeCristofaro, Jake Silhavy, and Mohamad Sleiman

## Overview

Accurate energy yield prediction is critical for the successful development, financing, commissioning, and operation of solar photovoltaic projects. Over the past decade, there have been significant changes within the industry regarding typical design characteristics, technology, and geographic implications (topography & high wind). These changes merit continuous validation and refinement of the solar energy yield assessment methodology. This white paper presents Sargent & Lundy's comprehensive analysis of five operational solar PV projects to validate our pre-commercial operation energy yield assessments against recent operational data. By examining factors, such as modeling methodology updates, resource variability, and operational losses, we identify key areas for improvement in yield estimation.

## Validation Project Dataset

Number of Projects: 5  
 Total Project Years: 11 years  
 Total Installed Capacity: 554 MW<sub>DC</sub>  
 Module Technologies: Thin Film, c-Silicon  
 Inverter Technologies: Central Inverters  
 Racking Technologies: Fixed Tilt and 1p SAT  
 Battery Energy Storage: AC-Coupled

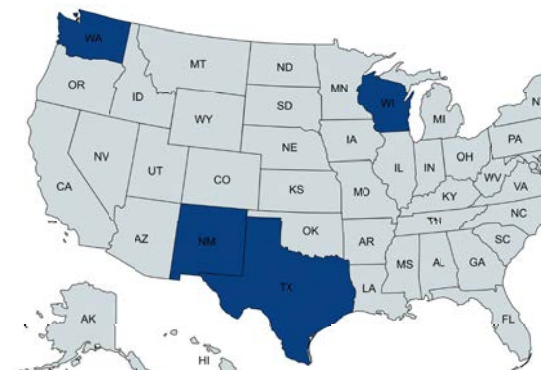
## Validation Methodology

First the original EYAs were adjusted to account for known generation gaps referred to as "indices". The final validation yield that is compared against the reported historical generation is the net impact of all three indices.

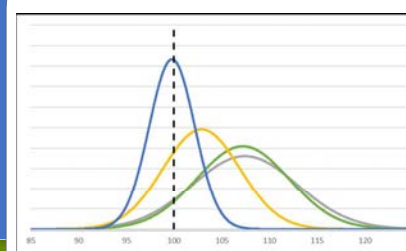
1. Model Index: methodology updates since the time of the original EYA
2. Resource Index: resource variance between operational years and original TMYs
3. Operational Index: operational losses (unavailability + curtailment)

Next, S&L compared the validation EYA results against historical project generation. S&L used the Mean Percentage Deviation (MPD) as the primary metric. The results are therefore based on the mean and median MPD.

## Geographic Diversity



## Validation Results



| Index       | Mean   | Median |
|-------------|--------|--------|
| Model       | -0.13% | -1.56% |
| Resource    | -3.93% | -6.02% |
| Operational | -2.94% | -2.36% |

| Model Iteration | Mean MPD | Median MPD | Standard Deviation |
|-----------------|----------|------------|--------------------|
| Original        | +7.4%    | +5.3%      | 5.5%               |
| Validation      | -0.2%    | +0.4%      | 2.4%               |

## Presented by

**Evan Giacchino**  
 Senior Energy Consultant  
 Sargent & Lundy  
 +1 (312) 269-7480  
 evan.s.giacchino@sargentlundy.co

m  
&

**Maggie Bono**  
 Energy Consultant  
 Sargent & Lundy  
 +1 (312) 269-2502  
 margaret.r.bono@sargentlundy.com



## Solar Resource Findings

The generation gap due to variation in the solar resource was by far the largest driver in S&L's original deviation from the historical production. Investigations were conducted into both the selection of a solar resource dataset as well as measure-correlate-predict methodology. S&L compiled the following lessons:

### Solar Resource Dataset Selection

- Solar resource dataset comparisons should always be conducted inclusive of both bankable and non-bankable datasets to provide as holistic an understanding of the expected solar resource as possible
- Comparisons should include multiple bankable datasets

### Measure-Correlate-Predict

- Robust and thorough data filtering of the measurement campaign is critical to avoid unintended bias in the results.
- Don't always trust measured data as the undisputed indication of true irradiance
- Appropriate rebalancing of irradiance is important

## Model Input Findings

Starting in 2024, S&L incorporated more detailed loss calculations such as wind stow, advanced tracking, terrain losses, and sub-hourly losses. The results of the validation process indicate that these updates did not bridge the entire gap. Based on S&L's investigations, the following losses were flagged as potential causes of overestimation:

- **String Mismatch & Imperfect MPPT:** Using Monte Carlo simulations with the project flash test data, S&L found typical string mismatch loss assumptions (0.0%-0.2%) to be optimistic and often calculated a higher loss (~0.4%). S&L is investigating trends as to whether this loss is at all correlated with module size/capacity.
- **Sub-Array Binning:** Similar to sub-hourly losses, if you group the entire site into a single sub-array in PVsyst, the potential clipping of higher DC:AC blocks is lost.
- **Third-Party Testing:** S&L recommends that more scrutiny and conservatism be placed on the incorporation of third-party test results. For example, create loss floors/ceilings that losses such as LID can drop down to but not below.

## Operational Findings

Behind the resource index, the operational index (generation gap due to unavailability & curtailment) was the second biggest driver for S&L's original deviation from the historical production. This has implications to both loss assumptions as well as uncertainty analysis:

- **Solar PV Availability:** While some data can be found that implies high availability (+99.0%), closer investigation around the definitions and calculations of those availability values to be a source of upward bias, implying lower energy-based availability. Based on S&L's investigations, we recommend a loss of 97.5% for the first year and 98.0% thereafter.
- **Uncertainty Analysis:** There are two important considerations within uncertainty analysis. The first is the sources of uncertainty. Here it is important to not miss aspects such as uncertainty in the unavailability, which averages around 98.0% but ranges anywhere 96% to 99%. Another source of uncertainty that can often be missed is uncertainty in the degradation, which should only increase over time as the project ages. The second consideration is the magnitude of the uncertainty. S&L typically sees a net uncertainty standard deviation of 5.0%-7.0% for bankable EYAs.

## Next Steps

There are still loss considerations and modeling practices that need to be looked at more closely. As part of S&L's ongoing process improvement initiatives, the following areas are being investigated further:

- PV+BESS modeling
- Power factor loss assumptions
- TMY versus historical time series modeling
- DC (LBD's, trackers, modules, etc.) vs AC (inverter/transformer) unavailability

As with any validation effort, the biggest hinderance is the data itself. In future validation efforts and investigations, S&L plans to include more projects as well as more operational data from each project. This relies on cooperation from project owners and sponsors to be more comfortable sharing operational data with independent engineers.



# IEC TC 82 Status

**Reported for  
NREL PV Reliability Workshop**

March 2025

George Kelly, TC 82 Secretary  
Steve Hogan, ARESCA Standards Board





# TC 82 Introduction

- What is IEC?
  - International Electrotechnical Commission
  - Non-profit NGO; national memberships
  - Publishes standards for all types of electrical equipment and applications
- What is TC 82?
  - Technical Committee of experts which covers Solar photovoltaic energy systems
  - Scope includes all the elements in the entire photovoltaic energy system



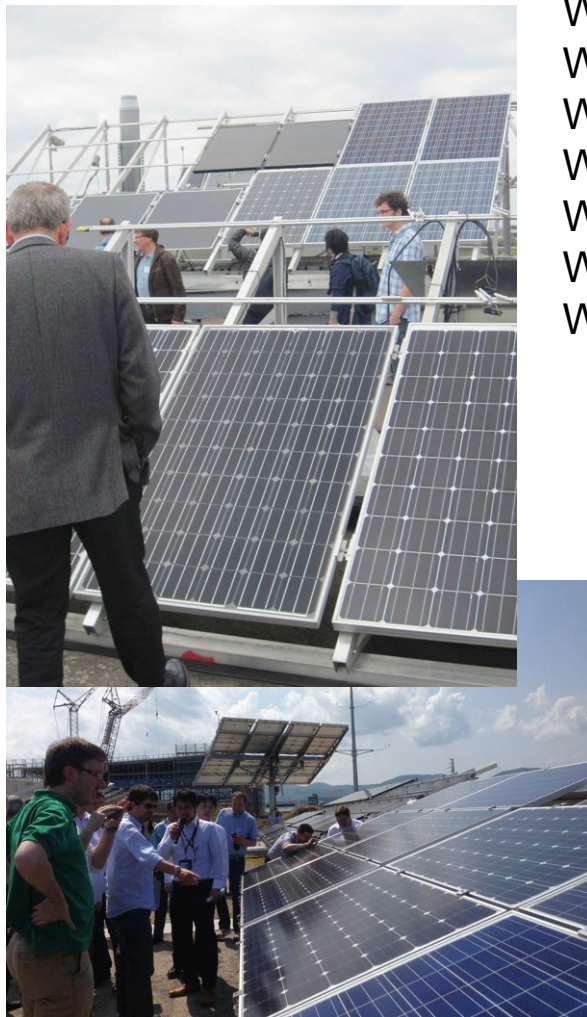
# TC 82 Summary

- Established 1981
- 48 P-member countries
- 9 O-member countries
- 680+ national experts
- 16 working groups
- 207 publications
  - 8 in past 12 months
- 77 active projects





# TC 82 Working Groups



WG 1: Glossary

WG 2: Modules

WG 3: Systems

WG 6: BOS components

WG 7: Concentrators

WG 8: Cells

WG 9: Support Structures

JWG 1: Off-grid systems (TC 88)

JWG 4: Grid code compliance (SC 8A)

JWG 5: System issues regarding integration of wind and PV generation into the grid (SC 8A)

JWG 1: General Planning, Design, Operation and Control of Microgrids (SC 8B)

JWG 10: DER connection with the grid (TC 8)

JWG 32: Electrical safety of PV system installations (TC 64)

JWG 82: Secondary cells and batteries for Renewable Energy Storage (TC 21)

JWG 11: Building Integrated PV (ISO TC 160)

PT 600: Vehicle Integrated PV



# TC 82 Dashboard

Advanced search   Webstore   e-tech   Online learning   Contact us   My IEC

IEC International Electrotechnical Commission Standards development Conformity assessment Where we make a difference Who benefits News & resources Programmes & initiatives Who we are

Home / Standards development / Technical committees and subcommittees / TC 82 Dashboard

## TC 82 Solar photovoltaic energy systems

Scope   Structure   Projects / Publications   Documents   Votes   Meetings   Collaboration Platform

Work programme   Publications   Stability Dates   Project files   Log in   En   Fr

### TC 82 Work programme (72)

| Project Reference  | Document Reference    | Init. Date | Current Stage   | Next Stage      | Working Group | Project Leader        | Fcst. Publ. Date |
|--|-----------------------|------------|-----------------|-----------------|---------------|-----------------------|------------------|
| <b>IEC 63202-2 ED1</b><br>Photovoltaic cells - Part x: Measurement of light and elevated temperature induced degradation of crystalline silicon photovoltaic cells | 82/1797/NP<br>497 kB  | 2021-01    | ACD<br>2021-01  | CD<br>2021-07   | WG 8          | Fangdan Jiang         | 2023-03          |
| <b>PNW TS 82-1782</b><br>Photovoltaic Cells – Part 3: Specifications for electrical characteristics of crystalline silicon wafers                                  | 82/1782/NP<br>429 kB  |            | PRVN<br>2020-10 |                 | WG 8          |                       | 2023-10          |
| <b>IEC TS 63202-2 ED1</b><br>Photovoltaic cells - Part 2: Electroluminescence image for crystalline silicon solar cells  | 82/1703/CD<br>1061 kB | 2018-05    | ADTS<br>2020-06 | TDTS<br>2020-11 | WG 8          | Christos Monokroussos | 2022-01          |
| <b>IEC TS 63202-3 ED1</b><br>Photovoltaic cells - Part y: Measurement of current-voltage characteristics of bifacial photovoltaic cells                            | 82/1800/NP<br>537 kB  | 2021-01    | ACD<br>2021-01  | CD<br>2021-02   | WG 8          | Fangdan Jiang         | 2022-06          |

Information about TC 82 can be found on at this link:

[http://www.iec.ch/dyn/www/f?p=103:23:0::::FSP\\_ORG\\_ID,FSP\\_LANG\\_ID:1276,25](http://www.iec.ch/dyn/www/f?p=103:23:0::::FSP_ORG_ID,FSP_LANG_ID:1276,25)



# Project Details

Advanced search    Webstore    e-tech    Online learning    Contact us    Login My IEC

IEC International Electrotechnical Commission    Standards development    Conformity assessment    Where we make a difference    Who benefits    News & resources    Programmes & initiatives    Who we are   

Home / Standards development / Technical committees and subcommittees / TC 82 Dashboard

## TC 82 Solar photovoltaic energy systems

Scope   Structure   Projects / Publications   Documents   Votes   Meetings   Collaboration Platform

Work programme > Project: IEC 61215-1 ED2

En Fr

| Detail    |                |                  |                |                |                |
|-----------|----------------|------------------|----------------|----------------|----------------|
| Committee | Working Groups | Project Leader   | Current Status | Frcst Pub Date | Stability Date |
| TC 82     | WG 2           | Ms Ingrid Repins | BPUB           | 2021-03        | 2024           |

| Stage | Document    | Downloads        | Decision Date | Target Date |
|-------|-------------|------------------|---------------|-------------|
| ACD   | 82/1332/RR  | 124 kB           | 2017-08-25    |             |
| CD    | 82/1453/CD  | 1022 kB          | 2018-07-27    | 2017-09     |
| PCC   |             |                  | 2018-09-21    | 2018-09     |
| ACDV  | 82/1492/CC  | 847 kB<br>545 kB | 2018-10-26    | 2019-04     |
| ACDV  | 82/1492A/CC | 949 kB<br>568 kB | 2018-10-26    | 2019-04     |
| TCDV  |             |                  | 2019-08-30    | 2019-10     |

### History

| Stage | Document    | Downloads        | Decision Date | Target Date |
|-------|-------------|------------------|---------------|-------------|
| ACD   | 82/1332/RR  | 124 kB           | 2017-08-25    |             |
| CD    | 82/1453/CD  | 1022 kB          | 2018-07-27    | 2017-09     |
| PCC   |             |                  | 2018-09-21    | 2018-09     |
| ACDV  | 82/1492/CC  | 847 kB<br>545 kB | 2018-10-26    | 2019-04     |
| ACDV  | 82/1492A/CC | 949 kB<br>568 kB | 2018-10-26    | 2019-04     |
| TCDV  |             |                  | 2019-08-30    | 2019-10     |

### Project

IEC 61215-1 ED2  
Terrestrial photovoltaic (PV) modules - Design qualification and type approval - Part 1: Test requirements

### Related Projects

Revising - IEC 61215-1:2016 ED1

- Click on the title of any project to find more details and copies of documents circulated at each stage of development

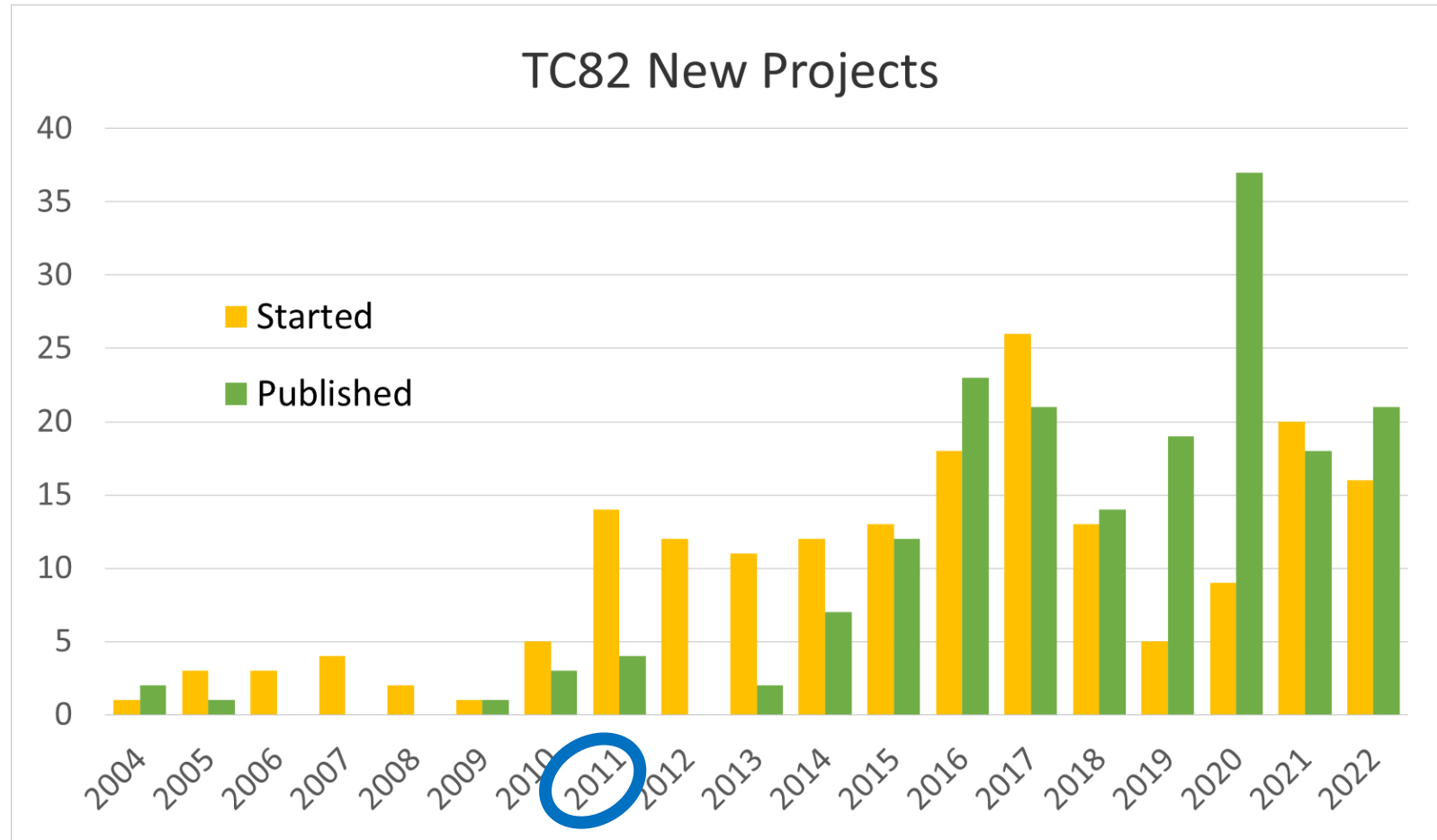


# TC 82 Motivation

- Industry **growth**
  - Demand increasing exponentially worldwide
  - Significant increase in large commercial plants
  - Introduction of new technologies and applications
- Concern for **quality** and **bankability**
  - Need for confidence in existing standards
  - Need for improved understanding of reliability
  - Validation of product lifetime for investors
- International PV Quality Assurance Task Force (**PVQAT**)
  - Formed 2011; currently 15 task groups
  - Mainly focused on scientific methods to characterize and predict possible failure modes
  - Work feeding into TC 82 for new standards and into IECRE for conformity assessment



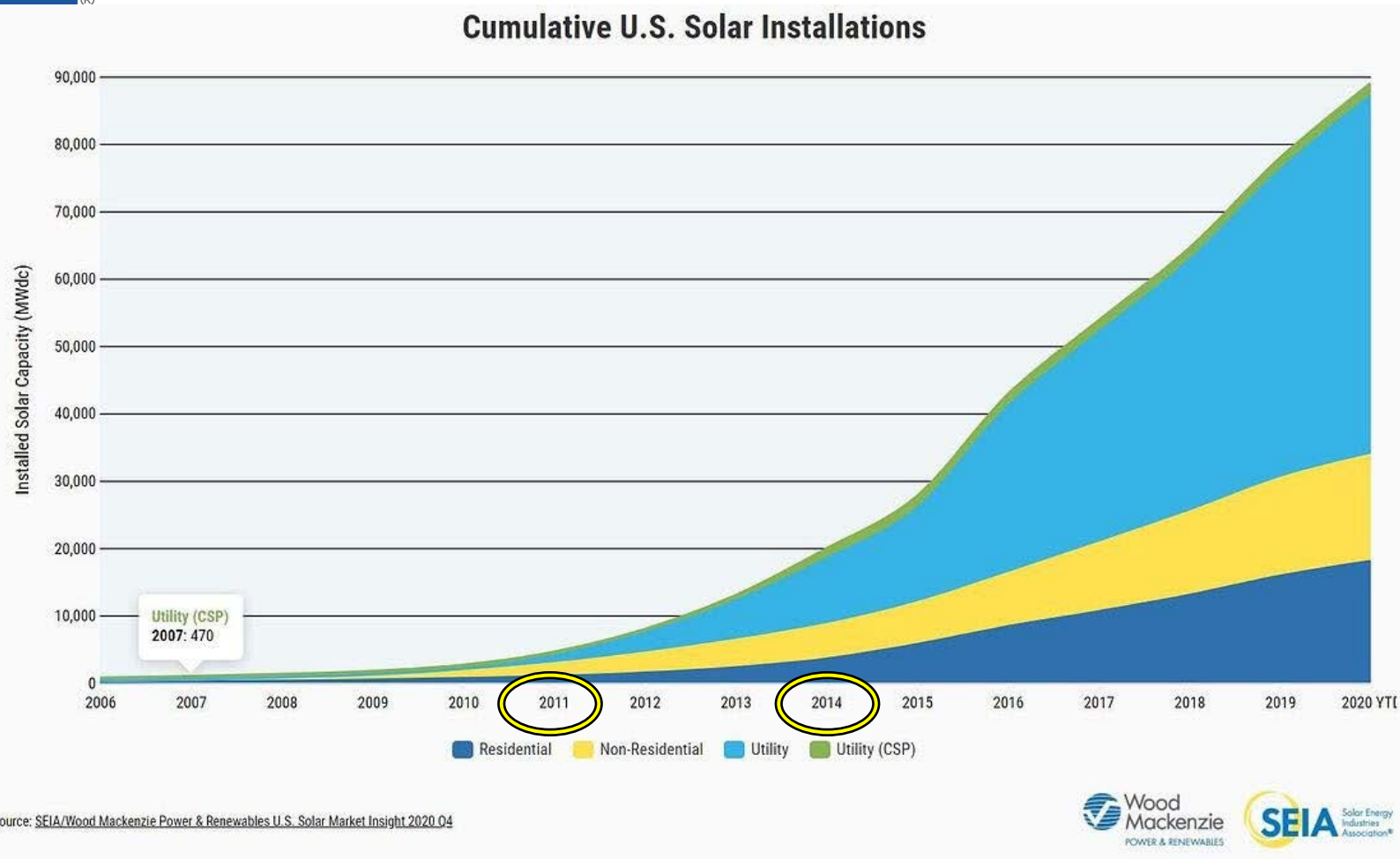
# “PVQAT Effect” on TC 82



- PVQAT formed in 2011; projects initiated in TC 82
- Standards for conformity assessment are now published



# Impact of PV Standards



- PV industry growth is enabled by standards which provide confidence in the technology
- Widespread adoption requires standardization
- Good standards enable wider adoption



# Important New Efforts

- Development of new standards for module safety qualification in systems up to 3000 volts
- Design of “universal” PV connectors to eliminate problems with cross-mating
- Creation of guidelines for module re-use and recycling
- Establishment of grid connection requirements for DERs
  - Goal is to eliminate multiple standards with different requirements and duplication of efforts



# TC 82 Welcomes You



- The strong friendship of TC 82 experts is a key part of what makes us successful
- Happy experts are more productive experts
- We hope to see you in person sometime in 2025



# Thank You



Questions?



Contact [george@sunset-technology.com](mailto:george@sunset-technology.com)

# Standardizing Risk Severity Assessments in Operating PV Assets

**David Penalva**  
Cofounder & CEO  
HelioVolta // SolarGrade

SOLARGRADE  
BY HELIOVOLTA

© 2024 by HelioVolta, LLC.

## Introduction

Most PV system issues do not impact safety, but many impact performance or cause downtime, and some dramatically increase the likelihood of costly, dangerous thermal failures and safety events. Tracking and remediating PV system issues that pose safety or reliability risks is thus vital to profitable portfolios. But the global solar industry lacks common definitions of risk severity. Assessment criteria and processes are also highly variable.

While it is common for solar professionals to use the Failure Modes and Effects Analysis terms to describe risk, such as negligible, minor, major, and critical, they often define them differently. Inconsistent risk definitions have negative consequences:

- When low risks are overstated, time and money is wasted on unnecessarily urgent corrective actions that can wait to be addressed.
- When high risks are overstated, important corrective actions are not undertaken, and safety incidents are more likely.
- When severity levels are disputed, delays in system construction and commissioning, stalled contractor payments, canceled project transactions, and even costly legal action can occur.

Asset owners and operators must balance risks precisely to meet revenue targets. But this balancing act is not simple: risk perception and tolerance varies widely across companies, teams, and technicians. The industry will benefit from a consistent framework for defining the severity of issues observed in the field.

With that goal in mind, David Penalva, CEO and co-founder of HelioVolta, together with HelioVolta's field engineering team, has developed a draft matrix for consistent, empirical risk severity calculations and corrective action timelines. Technicians and inspectors can objectively assign risk severity levels to issues in the field by answering the questions in the flow chart, below left.

Each question assigns points across four key categories: electrical safety, thermal, code and manufacturing specifications, likelihood of catastrophic impact, and frequency. The tool is available as a web-based, mobile-friendly calculator designed for use in the field at PV sites.

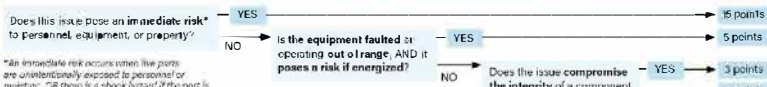
To learn more about this matrix and HelioVolta's findings in the field, download The SolarGrade PV Health Report at <https://solargrade.io/pv-health-report/>

## Risk Severity Matrix

Access this matrix as a mobile calculator with the QR Code →

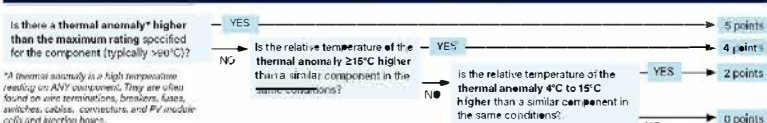


### STEP 1 ELECTRICAL SAFETY: CALCULATE POINTS



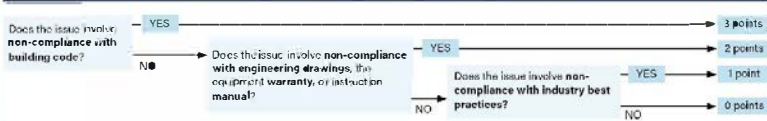
\*An immediate risk occurs when live parts are unintentionally exposed to personnel or equipment. OR there is a shock hazard if the part is contacted.

### STEP 2 THERMAL: CALCULATE POINTS

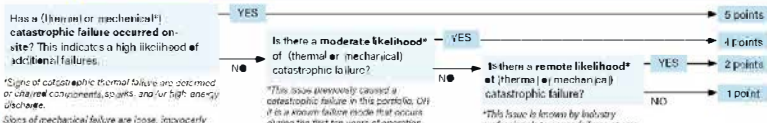


\*A thermal anomaly is a high temperature reading on ANY sensor. This often refers to junctions, connectors, fuses, switches, cables, connectors, and PV module cells and junction boxes.

### STEP 3 CODE & MFG. SPECS: CALCULATE POINTS



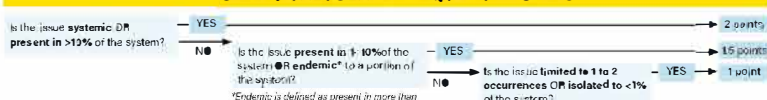
### STEP 4 LIKELIHOOD OF CATASTROPHIC IMPACT: CALCULATE POINTS



\*Signs of catastrophic thermal failure are defined as charred components, smoke, and/or high energy discharge.

Signs of mechanical failure are broken, improper assembly, mis-torqued fasteners, suppressed insulator components, and/or disengaged and malfunctioning equipment that interferes with site operations.

### STEP 5 CALCULATE FREQUENCY POINTS



\*Endemic is defined as present in more than 10% of one portion or area of the system.

### STEP 6 DETERMINE TOTAL SCORE TO ASSIGN RISK

Add up points from Steps 1-4 → Multiply sum by points found in Step 5 → Use table below to assign severity level → Remediate immediately and/or report the issue for ongoing monitoring as appropriate.

| SCORE   | ASSESSMENT             | ACTION   |
|---------|------------------------|--|
| ≥23     | Critical: Extreme risk | Immediate self-isolation; remediate ASAP; ideally before leaving the site  |
| 22 - 13 | Major: High risk       | Remediate ASAP in operating assets or prior to handoff in new construction |
| 12 - 7  | Minor: Medium risk     | Monitor; remediate during next scheduled site visit                        |
| <7      | Negligible: Low risk   | Monitor; okay to skip remediation  |

**DISCLAIMER:** This matrix is intended for use as an informational guide for risk evaluations of issues in PV systems. Individuals who use this matrix are responsible for accurately assessing risk with their own professional judgment. Matrix results may not be accurate for all issues, especially for non-typical project installations and/or environmental conditions.

## Same Issue, Different Risks

### UNDER/OVERTORQUED CONNECTORS

#### CRITICAL

An undertorqued back nut on a field-made home-run connector that was catastrophically damaged due to overheating was found. Undertorqued back nuts were systemic and there were multiple instances of overheating connectors.



#### MAJOR

An undertorqued back nut on a field-made home-run connector was found. Additionally, the connector was cross-torqued, which is a systemic issue at this site.



#### MINOR

Two isolated instances of undertorqued back nuts on field-made home-run connectors were found. No other workmanship or thermal issues were observed.



#### NEGIGIBLE

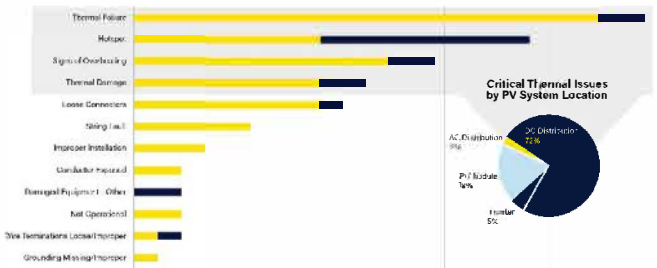
An isolated instance of an overtorqued connector with signs of improper tooling was found. Excessive marks on the back nut indicate tools were most likely used to tighten the back nut.



## Field Observations

HelioVolta's field engineering team applied this matrix during hundreds of PV system inspections conducted with SolarGrade, a field operations app and technical asset management software. Data shown below was collected in inspections that took place from May 2021 through March 2024. Projects ranged in size from 50 kW to 350 MW. 79% of projects are on commercial rooftops, 19% are ground-mounted, and 2% are corporate.

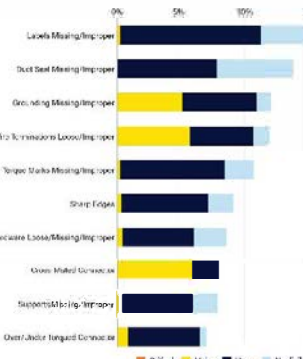
Critical PV System Issues by Project Stage



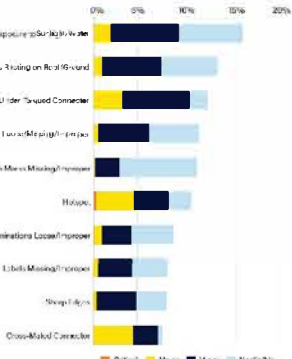
Major PV System Issues by Project Stage



Top 10 Most Common PV System Issues: New Construction



Top 10 Most Common PV System Issues: Operating Assets



## Next Steps

With this poster, we aim to gather feedback from PVW attendees to further refine the draft matrix. Our ultimate goal is to build industry-wide consensus on a standardized set of risk severity definitions and assessment framework.

### Share Your Feedback

**David Penalva**

david@heliovolta.com

In utility solar projects, 1500V DC architecture has been typical for the last few years since it was upgraded from 1000V DC architecture. However, many utilities, plant developers and system designers are considering a shift to 2000V DC architecture, where the operating voltage range would be between 1500V to 2000V. This study assesses the potential cost savings advantages by incorporating a 2000V system design compared to a standard 1500V generic design. The analysis was performed to show the potential impact that the following modules may have on a solar project levelized cost of energy (LCOE):

- TOPCon N-type, Bifacial, half-cut 210mm cell module – 620W
- Generic, N-type, Bifacial, half-cut 210mm cell module – 620W



Trina 210mm cells, N-type module, 620W used in this assessment

Potential cost savings to be observed in inverter count and DC & AC wiring

The primary purpose of moving to higher voltages in PV systems is to reduce the LCOE. Higher voltages can help customers realize lower LCOE in several ways, including cost advantages related to system design, lower component prices, higher power density, and reduced operations and maintenance costs.. All other inputs, which include, but not limited to site conditions, capacity, lifespan, and the PV module type are constant throughout the site. In theory, the 2000V module increases string lengths for utility-scale projects, thus reducing the overall system level component costs and improving end-to-end efficiency with less energy loss and enabling a more competitive leveled cost of energy.

#### Project Scenarios

Two different projects scenarios were created for a hypothetical jobsite using the above-mentioned modules. Using standard industry methods and current market conditions, initial construction costs (civil, electrical, soft costs, labor) were considered for each scenario, and land space was compared. Each system was modeled using PVSYST for the production estimates and the results were obtained for a 30-year operating life of the plant. The site and plant design characteristics are as follows:

- Project site : Gainesville, Florida – Latitude: 30.02 °N, Longitude: -82.30 °W
- Annual GHI: 1,746 kWh/m<sup>2</sup>
- Project size : 125MWdc, 100MWac at point of interconnection
- Project Life: 30 years
- One-in-Portrait tracker configuration
- Central Inverter: Generic 440kVA – 1500Vdc and Generic 5867kVA – 2000Vdc
- Ground coverage ratio (GCR): 0.35, DC/AC ratio: 1.25
- Regular lot shape, flat terrain, no irregular shading.

| System Design Parameter                   | 1500 V System                           | 2000 V System                          |
|---|---|--|
| System DC Capacity [kWp]                  | 125,617                                 | 125,344                                |
| System AC Capacity [kWac]                 | 123,200                                 | 123,207                                |
| System AC Capacity at POI [kWac]          | 100,500                                 | 100,300                                |
| Module Vendor, Model, Rating              | Generic Module, 620[Wp]                 | TSM-620NFG19RC.20, 620[Wp]             |
| Inverter Vendor, Model, Rating            | GENERIC, 4400kVA-1500Vdc, 4400[kWac]    | GENERIC, 5867kVA-2000Vdc, 5867[kWac]   |
| Module Mounting System Type               | Single-Axis Tracking, with backtracking | Single Axis Tracking with Backtracking |
| Tracking Limit [Degrees]                  | +/- 52°                                 | +/- 52°                                |
| Modules per String                        | 28                                      | 37                                     |
| Number of Modules                         | 202,608                                 | 202,168                                |
| Inverter Loading Ratio at Inverter Output | 1.02                                    | 1.02                                   |
| Inverter Loading Ratio at POI             | 1.25                                    | 1.25                                   |
| String DC Voltage [Vdc]                   | 1,500                                   | 2,000                                  |
| Row Pitch [m]                             | 6.81                                    | 6.83                                   |
| Collector Width [m]                       | 2.38                                    | 2.39                                   |
| GCR (%)                                   | 35.0%                                   | 35.0%                                  |
| Module Racking Configuration              | 1 Module in Portrait                    | 1 Module in Portrait                   |

To calculate the LCOE, the Net Present value (NPV) of the project costs were divided by the NPV of the project's generation over the life of the facility, as shown below:

$$\Sigma NPV(Construction + Financing + Lease + O\&M + Insurance + Asset Management)$$

LCOE =

$$\frac{\Sigma [Lifetime MWh Output (1 - Degradation)^t]}{}$$

|                             | 1500V                | 2000V                | Delta              | %Delta       |
|-----------------------------|----------------------|----------------------|--------------------|--------------|
| Module Cost                 | \$55,018,137         | \$55,016,684         | \$1,453            | 0.00%        |
| Inverter Cost               | \$7,042,322          | \$5,809,762          | \$1,232,560        | 17.50%       |
| Rack & Post Cost            | \$14,215,429         | \$14,215,054         | \$375              | 0.00%        |
| Module Install              | \$2,039,858          | \$2,035,375          | \$4,483            | 0.22%        |
| Rack & Post Install         | \$2,908,333          | \$2,927,265          | (\$18,932)         | -0.65%       |
| Civil Cost                  | \$9,749,919          | \$9,749,661          | \$258              | 0.00%        |
| BOS Material                | \$10,495,263         | \$9,630,003          | \$865,260          | 8.24%        |
| BOS Install                 | \$2,955,766          | \$2,911,410          | \$44,356           | 1.50%        |
| Engineering                 | \$2,837,271          | \$2,837,196          | \$75               | 0.00%        |
| Const. Management           | \$4,414,979          | \$4,414,863          | \$116              | 0.00%        |
| Const Equipment & Indirects | \$13,607,274         | \$13,418,286         | \$188,988          | 1.39%        |
| Startup                     | \$814,294            | \$814,272            | \$22               | 0.00%        |
| Project Indirects           | \$3,912,260          | \$3,912,156          | \$104              | 0.00%        |
| Taxes                       | \$892,866            | \$892,842            | \$24               | 0.00%        |
| <b>TOTAL</b>                | <b>\$130,903,971</b> | <b>\$128,584,829</b> | <b>\$2,319,142</b> | <b>1.77%</b> |

Key CAPEX cost savings observed in the following:

- \$1.2M savings in inverter cost, or 17.5% cost difference
- \$865K savings in BOS cost, or 8.2% cost difference
- \$2.3M overall CAPEX saving

Lower LCOE for 2000V System Design:

| System Voltage | LCOE (\$/MWh) |
|----------------|---------------|
| 1500V          | \$54.66       |
| 2000V          | \$53.80       |

- 2000V system design results in \$0.86/MWh less than the traditional 1500V system design
- \$865K savings in BOS cost, or 8.2% cost difference
- \$2.3M overall CAPEX saving

No significant variance was observed for the Energy available at the Point of Metering:

| Contribution Factor                                    | 1500 V System | 2000 V System |
|--|---------------|---------------|
| Medium Voltage Transformer Loss                        | -1.04%        | -1.04%        |
| AC Wire Loss   | -0.32%        | -0.32%        |
| High Voltage Transformer Loss                          | -0.77%        | -0.77%        |
| Auxiliary Loss   | -0.20%        | -0.20%        |
| Gen-Tie Loss   | 0.00%         | 0.00%         |
| Clipping Loss at the Point of Metering                 | -2.62%        | -2.81%        |
| <b>Annual Energy at Point of Metering [kWh/yr/kWp]</b> | <b>1,962</b>  | <b>1,966</b>  |

- **Inverter Count** - Inverters are, in general, sized based on current flow, not power output. In the case of a change from 1500V DC to 2000V DC, an inverter will likely be uprated in power in proportion to the change in voltage, thus requiring 25% fewer inverters for a 2000V system.
- **DC Wiring** - At a higher system voltage, more power will be conveyed at the same current flow. Since wires and other current carrying equipment is sized for current flow, the amount of DC wiring could likely decrease by approximately 25% compared to a similar 1500V system.
- **AC Wiring** - The decrease in inverters will likely result in a reduction in AC fittings, but total AC collector system cable length will not change significantly. Since the AC voltage is the same for both systems, the number of collector circuits and the sized of the AC cables will not change significantly.
- **Voltage Drop** - Losses due to AC voltage drop will likely remain the same. However, the power loss due to DC voltage drop will likely decrease due to the reduction in circuits.

Overall – the significant savings are observed in the Inverter quantity and DC BOS

# Selecting Bankable Resource Data for Solar Energy Assessments



CHRISTINE BORDONARO, PH.D., PIERRE METAUT, ALEX BERLINSKY, TAYLOR ROMSHEK

## Introduction

- It is still current practice among some PV industry stakeholders to use NREL TMY2 and TMY3 weather files as the solar radiation source for energy assessments.
- While these sources may be appropriate for early-stage estimates, there are several limitations that make them less suitable for bankable solar energy estimates compared to satellite site-tuned weather files, as will be discussed below.
- Clearway relies exclusively on satellite site-tuned weather data for developing bankable energy assessments. Site-tuned data consists of measured irradiance and meteorological data at the project location over a 1-2 year period, which is then tuned to satellite data to develop a site-specific TMY for project energy estimates.

## Limitations with NREL TMY2/TMY3 Data and Benefits of Satellite Site-Tuned Data

- A "Typical Meteorological Year" (TMY) data file provides one year of irradiance and meteorological data and is intended to best represent typical conditions over a historic time period. The files are created by piecing together historic individual months from different years that most closely represent the long-term average.
- There are several limitations with NREL TMY2/TMY3 data files that make them less suitable for bankable solar energy estimates compared to satellite site tuned weather files:

### Timeframe and Length of Record

- TMY2 covers 29 years of data, ending in 1990.
- TMY3 extended the record through 2005. However, most of the TMY3 stations are considered "Class II or III" and only include only 12 years of data. A minority of "Class I" stations have a 24-year record.
- Therefore, the NREL TMY datasets are 20-35 years out of date, and most of these stations have relatively short data records.
- In contrast, satellite site-tuned TMY files are developed by scaling the location specific satellite TMY data (which is based on the most recent 20+ years of data) to the on-site measured data over the last 1-2 years. In doing so, a site-specific TMY is created based on the most recent data available.

### Accuracy

- NREL developed these datasets for use with solar heating and cooling system simulations for buildings. As such, meteorological elements including temperature, humidity and wind speed were used in the monthly selection for the TMY file. Global Horizontal Irradiance, the most important variable governing energy production, is only weighted 25%. As a result, the NREL TMY files are not necessarily representative of typical solar radiation.
- Satellite site-tuned TMY files are created using only irradiance, so will provide a more accurate long-term representation of typical solar irradiance.

### Uncertainty

- Of the TMY3 stations, the Class I sites have the longest data record of 24 years, and so have lower uncertainties. Class II and III sites are based on a shorter record, have more interpolated data and have large time periods missing, and therefore tend to have higher uncertainties.
- Uncertainties for all TMY2/3 sites are generally 4% or higher (at 68% CI). In contrast, satellite site tuned data has a solar resource uncertainty on the order of 2% (at 68% CI).
- Higher uncertainties will lead to greater risk in the modeled energy, and will lead to lower project valuation.
- Some examples for different project sites are shown in Figure 3 below.

Figure 1: Time Periods

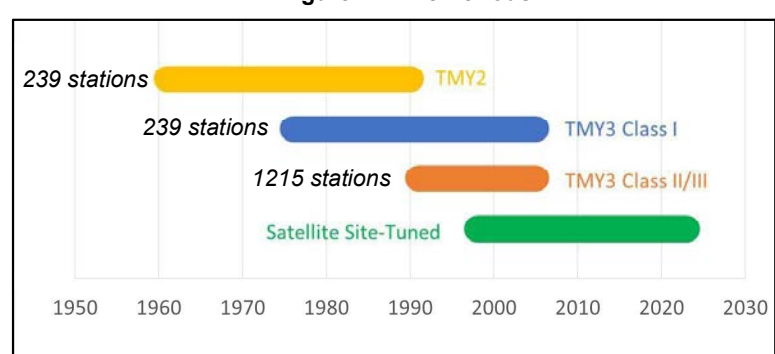


Figure 3: Uncertainty Comparison (%)

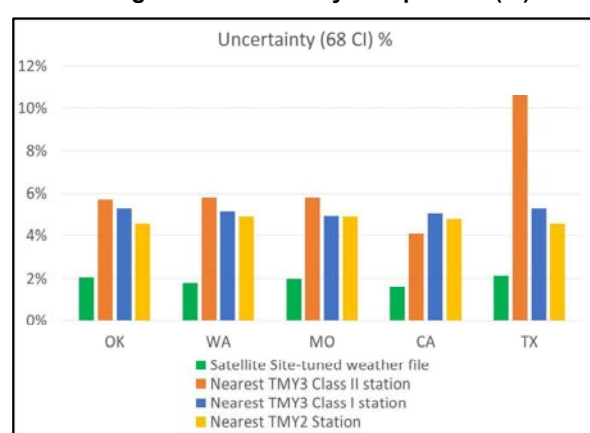
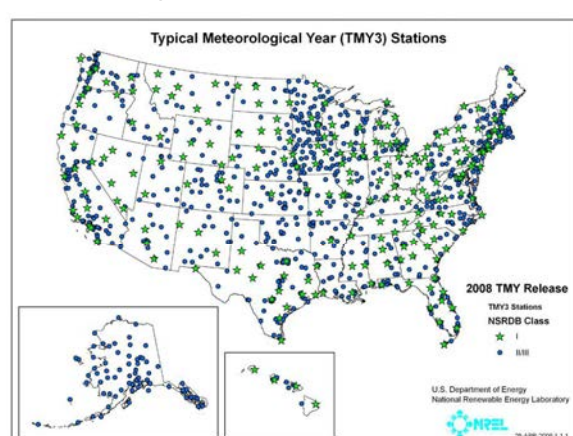


Figure 2: TMY3 Station Map



### Proximity

- Due to the high number of TMY3 Class II/III stations (shown in blue in Figure 2), proximity to any project site will be relatively close, however these tend to be higher uncertainty stations.
- The nearest TMY2/TMY3 Class I station can be many miles away from the project site, some examples are provided in Figure 5 for various project sites.
- In contrast, satellite site-tuned data is based on measured data at the project site
- Relevancy of the irradiance data will be reduced the farther away from the project site, see for example the deltas in Global Horizontal Irradiance in Figure 4 compared to the site-tuned data.

Figure 4: Delta in GHI Comparison

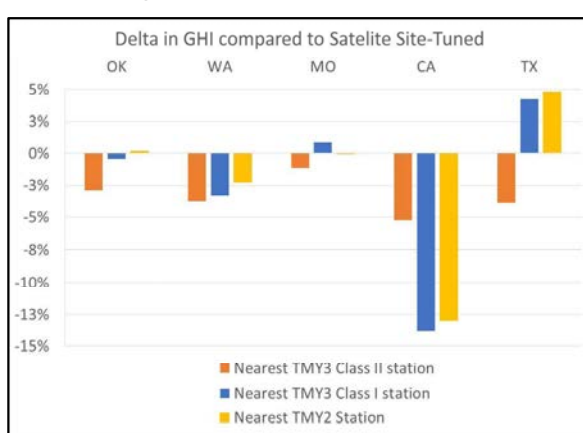
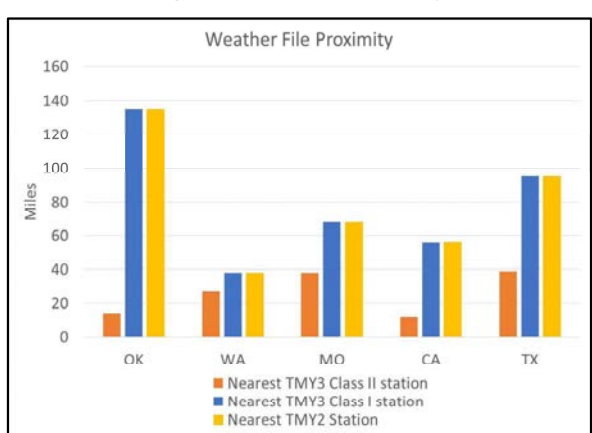


Figure 5: Station Proximity



Sources:

"User's Manual National Solar Radiation Data Base (1961-1990)", NREL, 1992

"User Manual for TMY3 Data Sets", S. Wilcox, et. al., NREL, 2008

"Completing Production of the Updated National Solar Radiation Database for the United States", S. Wilcox, et. al., NREL

"How Misuse of Solar Resource Datasets is Reducing Solar Industry Profits", A. Kankiewicz, et. al., Clean Power Research, 2015

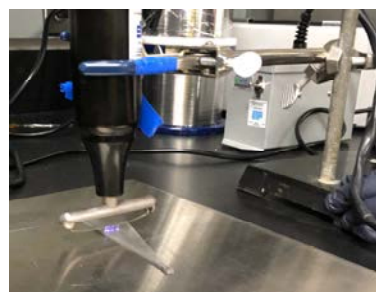
Rachael L. Arnold<sup>1</sup>, David C. Miller<sup>1</sup>, Aubrey Jackson<sup>1</sup>  
<sup>1</sup>National Renewable Energy Laboratory, Golden, CO, USA

## Beam Preparation

Beams are cut from a sheet of titanium: 1.6-mm thick Grade 5 Ti-6Al04V

### Cleaning Methods Examined:

- Sanding → 220 grit, sanding block added for mechanical leverage
- Solvent Clean → Acetone added in addition to IPA
- Plasma Surface Treatment → added
- HF Etch → not recommended
- Thermal Oxidation → reduced adhesion
- Primer EC-3901 → applied to beams and cell surfaces
- Epoxies → DP420 vs DP420NS



Module construction research laboratory surface plasma treater.

**ROUGHER SURFACE → BETTER ADHESION**

**CLEANER SURFACE → BETTER ADHESION**

## Beam Attachment

Epoxy: DP420NS (3M)

Use a dispenser gun and mixing nozzle.

Serpentine pattern (avoid bubbles), scrape to spread, assemble base end first.



Serpentine patterned epoxy on Ti beam.

Invert sample, add weights, and cure at ambient for 10 minutes.

Scrape off squeezed out epoxy then invert, add weights, and cure at ambient for 24 hours.

## Adhesion Testing

Condition samples in 25°C/50%RH for >2 weeks before testing.

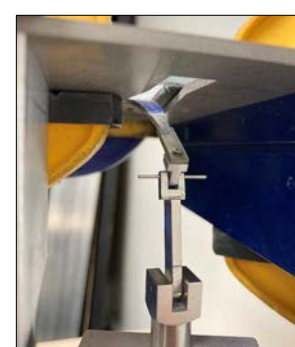
Cut additional material away from test beam using diamond scribe & razor.

Attach to test frame and use clamps to hold sample in place.

Watch load vs position graph during test and mark debond length on sample during plateau.



Top view of sample during test.



Machine:

DTS Company Delaminator

Load Capacity: 180 N

Testing Velocity: 10 µm/s

Bottom view of sample during test.

## Sample Preparation

| Sample Type                                       | Materials   | Sample Preparation   |
|---|---|--|
| Glass/EVA/Glass<br>Test adhesion of EVA to glass. | Substrate Glass: 5.7-mm Low Iron Starphire<br>Superstrate Glass: 0.1-mm willow glass, Corning Precision | Pumice scrub → DI rinse → N2 → IPA clean → N2 → Bilco clean → N2 |
| Glass/EVA/Cell<br>Test adhesion of EVA to cells.  | Substrate Glass: 5.7-mm Low Iron Starphire<br>Cells: >152-mm, Mono-Si, PERC, BiFi Anti-PID front (CSI)  | Sand cell → IPA clean → N2 → primer coat                         |

## Aging Sequence

DH(500h) → UV(A3, 2000h) .... → DH(1000h) → Adhesion test condition... UV durability .... hygrometric durability

Accelerated test sequence in IEC 62788-1-1 and IEC TS 63209-2.

Damp Heat → no UV, 85°C, 85%RH

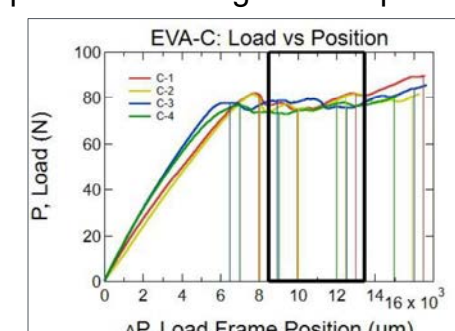
IEC 62788-7-2 A3 → 0.8 W/m<sup>2</sup>, 65°C, 20%RH

## Test Results

Measure the debond lengths that were marked during the test.

Equation A.3 from the IEC 62788-6-3 standard is used to find the debond energy at discrete data segments.

Suspect that the original encapsulants expired in sealed bags.



Load v Position graph of raw data from adhesion test showing marked locations.

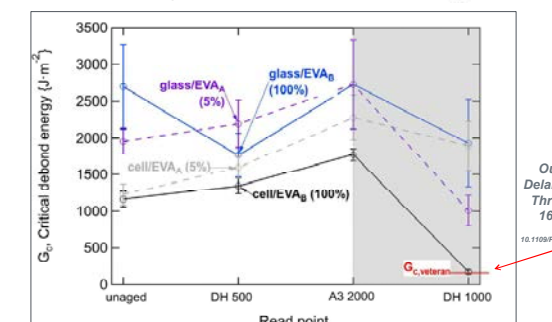
$$G_c = \frac{P_c}{2 \tan(\theta/2)} \frac{\Delta_i}{a_i^2}$$

$P_c$  = critical load

$\theta$  = included beam angle

$\Delta$  = load line displacement

$a$  = debond length



Results from first experiment where the substrate used was float glass. One standard deviation of data shown.

## Future Work & Changes

- Continue testing through aging sequence. Completed A3 2000h.
- Conduct UV aging separately to account for sample temperature differences in A3 (glass/glass is ~75°C and glass/cell is ~95°C). Recommend A3 for glass/glass and A1 for glass/cell.
- Determine different mounting method for UV weathering.
- Thick glass substrate may be bonded in the case of degraded substrate glass.

# Going beyond stuck trackers: how well do your trackers work?

Will Hobbs, Southern Company, [wkhobbs@southernco.com](mailto:wkhobbs@southernco.com)  
Kevin Anderson, Sandia National Laboratories, [ksande@sandia.gov](mailto:ksande@sandia.gov)



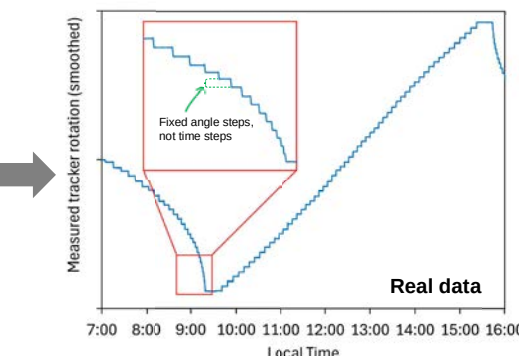
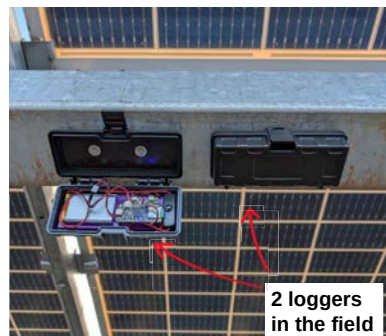
**Stuck & broken trackers** get attention in the industry, but there are additional **issues beyond binary “working/not working”** that can impact performance.

We are working on a cheap temporary datalogger to **measure actual position**, and models to **estimate impacts of “non-idealities.”**

**“Where are my trackers actually pointed?”**

**Non-idealities** that can't be measured with existing plant data: torque-tube twist, torque-tube sag, actuator position calibration error.

**Solution:** cheap, mailable, magnet-mount 3-axis tilt data loggers. Measurements every 1-sec, compare to expected modeled/ideal positions. Eventually open-source.



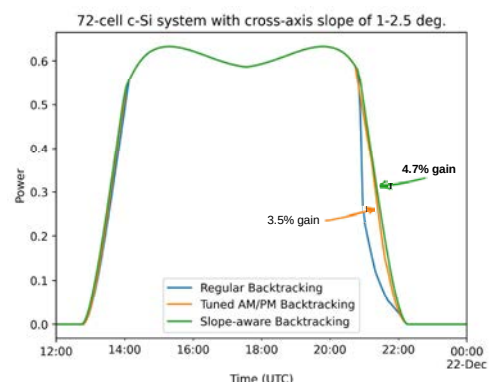
Mail to plant → stick on trackers for a few days → mail back.

**Goal:** assess plant-specific and industry-wide non-idealities. **Contact us if you might want to participate!**

**“How much am I losing?”**

Modeling **non-idealities** isn't always easy, so how much are you losing?

- We presented some self-shade and tracker fault examples/methods in [2].
- Functions in [2] have been **expanded**: now allow cross-axis slope, independent AM/PM backtracking, clock-drift, fixed-tilt shade, others.  
<https://github.com/williamhobbs/pv-system-model>, with examples in  
<https://github.com/williamhobbs/2025-pvrw-trackers>.



## References:

- [1] Anderson, Kevin S., and Clifford W. Hansen. "Simulated Performance Effect of Torque Tube Twisting in Single-Axis Tracking PV Arrays." 2024 IEEE 52nd Photovoltaic Specialist Conference (PVSC). <http://dx.doi.org/10.1109/PVSC57443.2024.10749340>  
[2] Hobbs, W., Anderson, K., Mikofski, M., and Ghiz, M. "An approach to modeling linear and non-linear self-shading losses with pvlib." 2024 PV Performance Modeling Collaborative (PVPMC). [https://github.com/williamhobbs/2024\\_pvpmc\\_self\\_shade](https://github.com/williamhobbs/2024_pvpmc_self_shade)



## Acknowledgements:

Thanks to Will's demo assistant, Liam!



# Evaluation of Front Eave Loads Caused by Snow Accumulation on PV Modules

Tadanori Tanahashi<sup>1</sup>, Takahiro Chiba<sup>2</sup>, Satoru Adachi<sup>3</sup>, Hayato Arakawa<sup>3</sup>, Yuki Tsuno<sup>1</sup>, Kazuaki Ikeda<sup>1</sup>, and Takashi Oozeki<sup>1</sup>

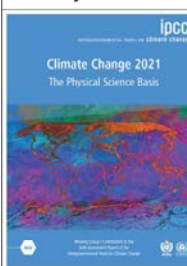
<sup>1</sup> National Institute of Advanced Industrial Science and Technology (AIST), Japan

<sup>2</sup> Hokkaido University of Science, Japan

<sup>3</sup> National Research Institute for Earth Science and Disaster Resilience (NIED), Japan

## Background and Motivation

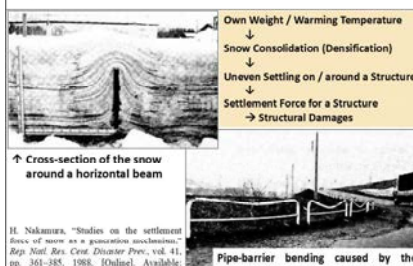
### IPCC Projections: Future Snowfall—More or Less?



North America:  
It is likely that some high-latitude regions will experience an increase in winter snow water equivalent due to the snowfall increase prevailing over the warming trend.

East Asia:  
Decreases have been observed in the frequency, and increases in the mean intensity of snowfall ...  
**Heavy snowfall is projected to occur more frequently in some parts of Japan.**

### Impacts of Settlement Force with Snow Accumulation



H. Nakamura, "Studies on the settlement force of snow as a geotechnical problem," Rep. Natl. Res. Cen. Disaster Prev., vol. 41, pp. 361–385, 1988. [Online]. Available: <https://doi.org/10.2322/rndp.41.361>

Pipe-barrier bending caused by the settlement force with snow accumulation

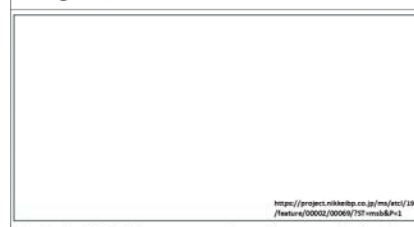
### Snow Settling at Front Eave of PV Array



Cross-section of the snow around front eave of a PV array

"Design Guidelines for Terrestrial PV Facilities 2019 (in Japanese)," 2019. [Online]. Available: <https://www.meteo.go.jp/content/100000757/m002.pdf>

### Damages with Settlement Force at PV Front Eave

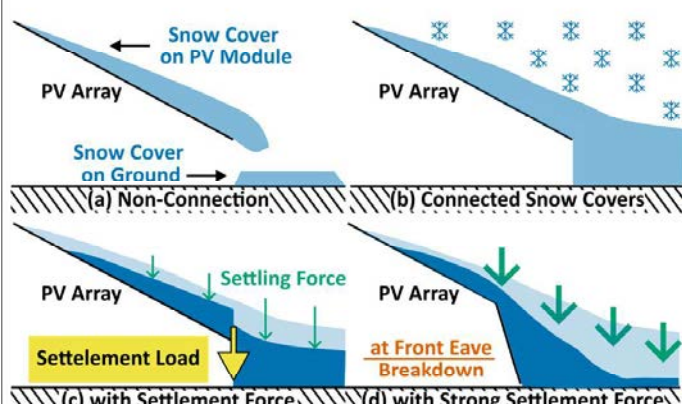


<https://project.meteo.go.jp/m002/127/feature/00002/00006/757/m002.pdf>

During the 2020–2021 snow season, the maximum snow depth on the ground exceeded 2 meters at the nearest meteorological station of the Japan Meteorological Agency (JMA).

## Summary

### Impacts of Snow Settlement at PV Front Eave



In snowy regions, photovoltaic (PV) systems often experience heavy snow accumulation on their modules, which can cause significant damage to both the modules and their mounting structures. The load on the front eave ( $P_e$ ) of the PV module increases significantly when the snow on the modules merges with the snow on the ground. The intensity of  $P_e$  is assumed to greatly exceed the load caused by overhanging accumulated snow on the PV array, a factor considered in IEC 62938 (Non-uniform Snow Load Testing).

To investigate the front eave load during the snowy season, we measured the vertical loads on the 4 pods of a PV mounting structure using load cells installed at the base of each pod [Panel 01]. Based on these vertical load measurements, the linear load at the front eave ( $P'_e$ ) was estimated using a standard mechanical model [Panels 02–04]. The centroid of the accumulated snow was determined through image processing of side-view images of the PV modules [Panel 05]. Using the centroid estimation, we were able to accurately determine  $P_e$  and  $P'_e$  [Panel 07].

Since continuously capturing high-quality side-view images of a PV array is challenging due to snow obstruction and blowing snow, we developed an empirical method for estimating  $P'_e$  that does not rely on such images. By applying baseline correction to the  $P'_e$  trend using a fixed centroid, we obtained  $P'_e$  values comparable to those derived from the actual centroid [Panels 08–09]. As a result, this empirical approach allows  $P'_e$  to be estimated during snowy conditions based solely on the loads measured at the mounting structure's pods. This estimation method contributes to the design and construction of more robust PV systems capable of withstanding snow loads.

In addition, we demonstrated the distinctive evolution of snow loads in the front eave region [Panels 10–12], which decreased due to heating of the PV modules.

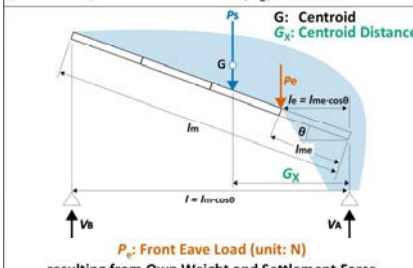
## Results

### [Panel 01] Exp. Setup and Lateral Images



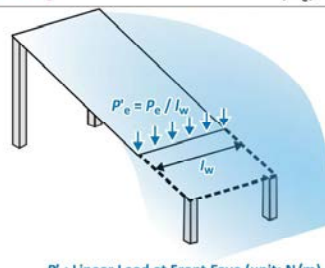
Vertical loads to the respective 4 pods were measured with load cells.

### [Panel 02] Front Eave Load ( $P_e$ )



$P_e$ : Front Eave Load (unit: N)  
resulting from Own Weight and Settlement Force

### [Panel 03] Linear Load at Front Eave ( $P'_e$ )



$P'_e$ : Linear Load at Front Eave (unit: N/m)

### [Panel 04] Calculation of Front Eave Load

$P_e$ : Front Eave Load (unit: N)

$$P_e = \frac{V_A \cdot l - a}{b}$$

where

$$a = \frac{V_B \cdot l \cdot (l - G_X)}{G_X}$$

$$b = (l - l_{me} \cdot \cos \theta) + \frac{l_{me} \cdot \cos \theta \cdot (l - G_X)}{G_X}$$

$P'_e$ : Linear Load at Front Eave (unit: N/m)

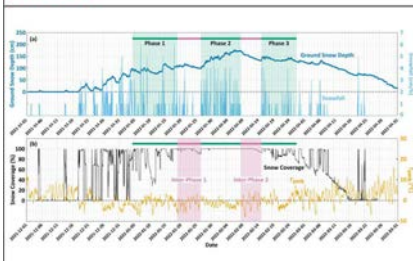
$$P'_e = \frac{P_e}{l_w}$$

### [Panel 05] Estimation of Centroid Distance ( $G_X$ )

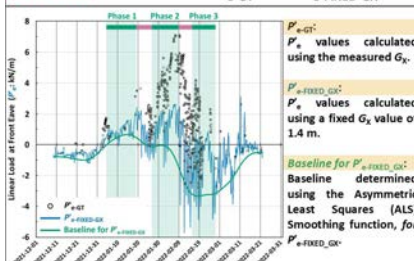


The lateral images, which were captured by a night-vision camera every 1 h, were transformed to grayscale and appropriate thresholding was applied. Then, using the ABSOLVE package integrated into ImageJ software, the area of accumulated snow on the PV modules was extracted (Red contour line), and the centroid of the snow accumulation (Red cross mark) was determined.

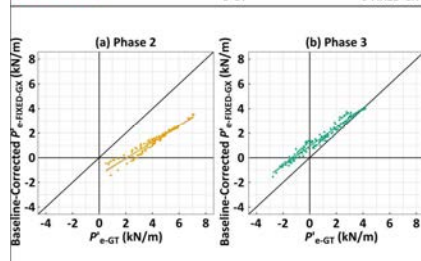
### [Panel 06] Evolution of Weather Parameters



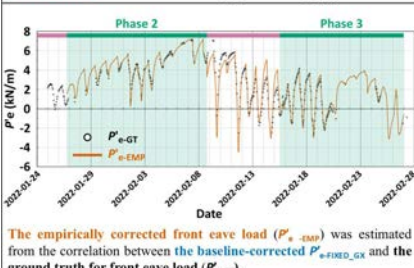
### [Panel 07] Evolution of $P'_{e-GT}$ and $P'_{e-FIXED-GX}$



### [Panel 08] Correlations: $P'_{e-GT}$ & Corrected $P'_{e-FIXED-GX}$

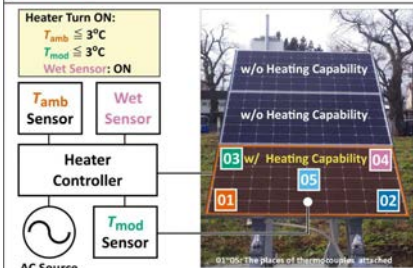


### [Panel 09] Evolution of $P'_{e-GT}$ and $P'_{e-EMP}$

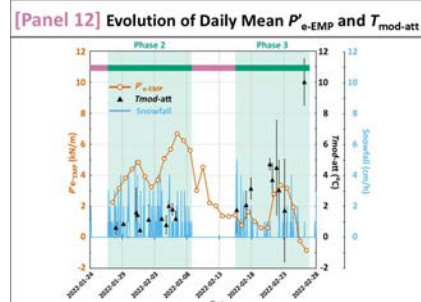
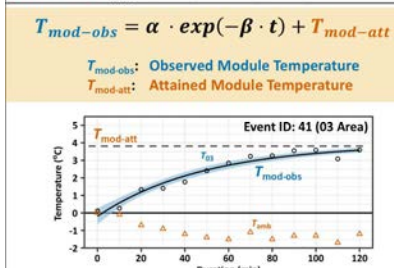


The empirically corrected front eave load ( $P'_{e-EMP}$ ) was estimated from the correlation between the baseline-corrected  $P'_{e-FIXED-GX}$  and the ground truth for front eave load ( $P'_{e-GT}$ ).

### [Panel 10] Control & Monitoring of Heating Ability



### [Panel 11] $T_{mod}$ Fitting to Simple Exp. Curve



This work was supported in part by the "AIST Program for Promoting Technologies Invented by Industries in Disaster Areas in Tohoku (Seeds Support Program)".

# Field Testing of PID-p Susceptible Bifacial PERC Modules: Impact of Light, Voltage and Module History

Cecile Molto<sup>1</sup>, Dylan J. Colvin<sup>1</sup>, Ryan M. Smith<sup>2</sup>, Peter Hacke<sup>3</sup>, Fang Li<sup>4</sup>, Govinda Samy Tamizh Mani<sup>4</sup>, Jaewon Oh<sup>5</sup>, Halima Jahan<sup>5</sup>, and Hubert P. Seigneur<sup>1</sup>



<sup>1</sup>University of Central Florida - Florida Solar Energy Center, Cocoa, FL, 32922, USA

<sup>2</sup>Pordis LLC, Austin, TX, 78729, USA

<sup>3</sup>National Renewable Energy Laboratory, Golden, CO, 80401, USA

<sup>4</sup>Photovoltaic Reliability Laboratory – Arizona State University, Mesa, AZ, 85212, USA

<sup>5</sup>University of North Carolina Charlotte, Charlotte, NC, 28223, USA

## Introduction

Polarization-type Potential-Induced Degradation (PID-p) is drawing more and more attention as it can affect emerging technologies (bifacial p-PERC (Passivated Emitter Rear Contact), PERT (Passivated Emitter Rear Totally diffused), and TOPCon (Tunnel Oxide Passivated Contacts). Degradation is observed at both voltage polarities but is more susceptible for negatively-biased cells (frame grounded) due to the architecture of the bifacial PERC, PERT, TOPCon modules [1]. Most PID-p studies are performed indoors and there is a lack of outdoor data [2-4]. The impact of light has been evidenced [5] but more field data are needed to better understand the underlying mechanisms.

We previously tested commercially available bifacial glass/glass p-type PERC modules in an environmental chamber [4] and their PID-p susceptibility has been evidenced. PID-p occurs on the rear side when cells are negatively-biased relatively to the grounded frame. Under a positive bias, slight PID-p is observed on the front side. Shunting and corrosion-type PID were not observed.

In this study, we performed PID-p field testing on the same make and model of module in a humid subtropical environment (Cfa Köppen climate). The impact of light, voltage and module recovery history are observed and discussed. These results will serve the PV community to better understand PID-p in the field, refine predicting models and develop preventative solutions.

## Methodology

- A high-voltage (HV) testbed was built at the Florida Solar Energy Center (FSEC) in Cocoa, FL with five mounting racks : 3 “Open”, 1 “Near Ground” and 1 “Near Roof” (Fig. 1) to stress PV modules under various voltages and albedo light conditions;
- Modules were light-soaked for at least 1 month before PID stress;
- After one round of testing, modules were recovered via light exposure. These, along with new modules, were stressed in a second round (see Tables 1 and 2);
- Outdoor current voltage (IV) curves were obtained except for modules stressed at -3500V;
- Modules were uninstalled every 3 months for indoor electroluminescence (EL) imaging and IV measurements.



TABLE 1 : Round 1 experimental conditions (1 year stress from June 2023 to June 2024).

| Mounting configuration | Number of new modules tested    | Voltage applied to cells (frame grounded) |
|------------------------|---------------------------------|---|
| Near Ground            | 4 biased - 1 control not biased | - 1500V                                   |
| Open                   | 4 biased - 1 control not biased | - 1500 V                                  |
| Open                   | 2 biased                        | - 3500 V                                  |
| Open                   | 4 biased - 1 control not biased | + 1500 V                                  |
| *Near Roof             | 4 biased - 1 control not biased | - 1500 V                                  |

\*Due to equipment issues on the Near roof rack in Round 1, negative voltage was applied with a delay on this rack, followed by positive bias applied by inadvertence before applying a negative voltage of -1500V until the end of the Round 1.



TABLE 2 : Round 2 experimental conditions (2 weeks stress in September 2024).

| Mounting configuration | Number of new modules tested   | Number of recovered modules tested | Voltage applied to cells (frame grounded) |
|------------------------|--------------------------------|------------------------------------|---|
| Near Ground            | 3 biased<br>1 control unbiased | 4 biased<br>1 control not biased   | - 600V                                    |
| Open                   | 3 biased<br>1 control unbiased | 4 biased<br>1 control not biased   | - 1500 V                                  |
| Open                   | 2 biased                       | -                                  | - 3500 V                                  |
| Open                   | 4 biased<br>1 control unbiased | 4 biased<br>1 control not biased   | - 600 V                                   |
| Near Roof              | 4 biased<br>1 control unbiased | 4 biased<br>1 control not biased   | - 600 V                                   |

Fig.1 : Mounting configurations (5 racks, 25 modules can be installed per rack).

## Experimental Results

### IMPACT OF LIGHT AND VOLTAGE

Round 1 data analysis :

- No PID-p is observed under a positive bias, suggesting the sunlight fully compensates the front degradation (Figs. 2a, c, e).
- Under a negative bias,  $P_{max}$  drops the first 2 weeks (driven by  $I_{sc}$  loss) and then stabilizes at around 5-6% loss respectively to the control module (Figs. 2a, c, e).
- $P_{max}$  is slightly lower in winter, likely due to lower daily irradiance levels (Fig. 2b).
- Degradation is faster for Near Roof (least albedo) than for Open rack (high albedo). More albedo (particularly UV light) likely reduces degradation (Fig. 2c).
- Cells within a module do not degrade at the same rate (Fig. 2e). During PID-p, the Si/dielectric layers' interface transitions from accumulation to flat-band, depletion and inversion states (Fig. 4). Each state differently impacts surface recombination.

Round 2 data analysis :

- The impact of albedo light on PID-p rate is confirmed at -600V (Fig. 3a).
- Degradation occurs more quickly in Round 2 (Fig. 2a v. Fig. 3a), which is mainly attributed to irradiance being ~ 0.38 lower than Round 1 (Fig. 2b v. Fig. 3b).
- Higher voltage increases rate of PID-p degradation (Fig. 3c).

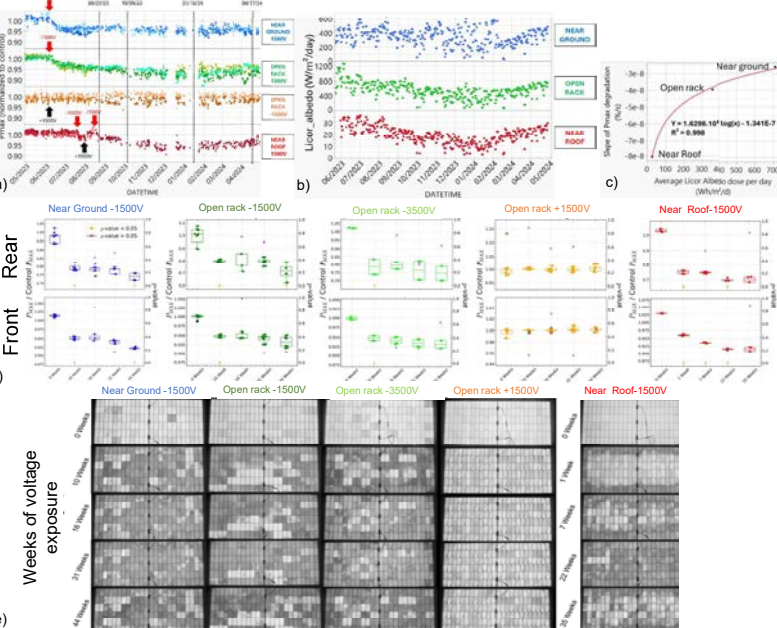


Fig. 2 : Round 1 outdoor & indoor data : a)  $P_{max}$  normalized to control, b) Daily albedo dose, c) slope of  $P_{max}$  the first 2 weeks v. average albedo dose, d) boxplots of  $P_{max}$  measured indoors on both module sides, e) rear side EL images (bias at nameplate 1  $I_{sc}$ ) of one module per rack

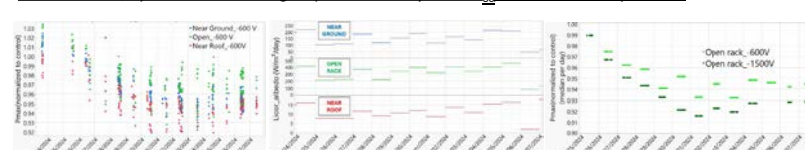


Fig. 3 : Round 2 outdoor data of new modules : a)  $P_{max}$  normalized to control for -600V racks, b) Daily albedo dose, c)  $P_{max}$  normalized to control (median per day) for Open rack at -600V and -1500V.

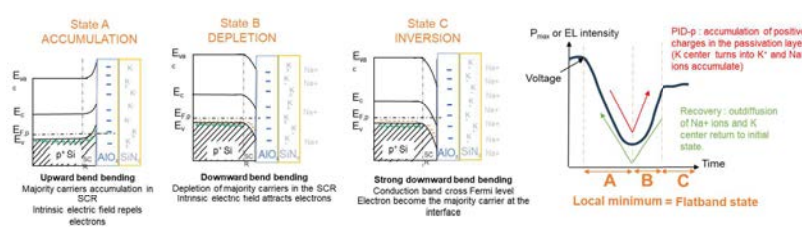


Fig. 4 : a) Accumulation, depletion and inversion states at the p-Si/AIO<sub>2</sub>/SiN<sub>4</sub> interface, and b) impact on the  $P_{max}$  and EL intensity. SCR indicates the Space Charge Region.

### IMPACT OF MODULE HISTORY

- Modules from the 1<sup>st</sup> year deployment that were recovered and stressed during the 2<sup>nd</sup> year deployment degrade faster than brand-new modules (Fig. 5). It is suspected that apparent light-recovery does not mean the accumulated positive charges went back to their initial location. Therefore, they reach the silicon/passivation layers interface faster during a second PID stress.
- On the Near Roof rack, recovered modules stabilize at a higher  $P_{max}$  value. This could be due to a greater number of cells being in depletion/inversion state.

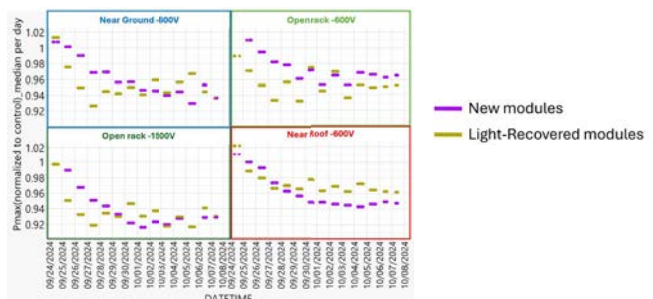


Fig. 5 : Median value per day of outdoor  $P_{max}$  normalized to control module during Round 2 testing.

## Conclusions

- PID-p was evidenced in the field on the rear side of commercial bifacial glass/glass p-PERC modules for voltages as low as -600V;
- $P_{max}$  loss, driven by reduced  $I_{sc}$ , occurs at short time scales (days to 2 weeks) and stabilizes at 5-10% depending on the voltage, irradiance and module history;
- Lower degradation rates are observed with lower voltage and more albedo light;
- Modules with a history of degradation/light-recovery degrade faster;
- EL imaging reveals that cells are not degrading at the same rate. Some cells get darker and then brighter, corresponding to the silicon/passivation layers' interface going through flat-band, depletion and then inversion state.

- [1] C. Molto et al., "Review of Potential-Induced Degradation in Bifacial Photovoltaic Modules," *Energy Technol.*, 2023, doi: 10.1002/ente.202200943.
- [2] P. Hacke et al., "Field-representative evaluation of PID-polarization in TOPCon PV modules by accelerated stress testing," *Prog. Photovolt. Res. Appl.*, 2024, doi: 10.1002/pip.374.

- [3] S. Yamaguchi et al., "Rapid progression and subsequent saturation of polarization-type potential-induced degradation of n-type front-emitter crystalline-silicon photovoltaic modules," *Jpn. J. Appl. Phys.*, 2018, doi: 10.7567/JJAP.57.122301.

- [4] F. I. Mahmood et al., "Susceptibility to polarization type potential induced degradation in commercial bifacial p-PERC PV modules," *Prog. Photovolt. Res. Appl.*, 2023, doi: 10.1002/pip.3724.

- [5] B. M. Haberberger and P. Hacke, "Impact of illumination and encapsulant resistivity on polarization-type potential-induced degradation on n-PERT cells," *Prog. Photovolt. Res. Appl.*, 2021, doi: 10.1002/pip.3505.

# Effect of Salt Mist and DH Preconditioning on PID for Mono and Bi-facial half-cell PERC modules

Camille Bainier, Gurleen Kaur, Jose Cano-Garcia, Elsa Kam-Lum  
TotalEnergies One Tech, Solar R&D

## Abstract

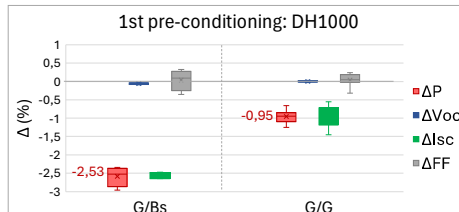
The study investigated the impact of floating photovoltaic (PV) conditions on potential-induced degradation (PID), especially the impact of salt, in half-cell PERC, both monofacial Glass/Backsheet (G/Bs) and bifacial Glass/Glass (G/G). Modules were divided into three groups with different preconditioning treatments before undergoing PID testing: Group A (DH1000 + Salt Mist), Group B (DH2000), and Group C (control, DH1000).

### Key findings:

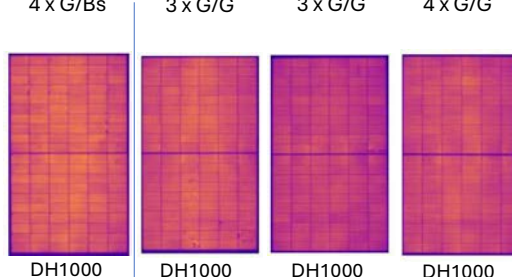
- . G/Bs modules showed greater power loss after 1000 hours DH compared to G/G modules.
- . PID tests revealed 4-7% power losses across all BOMs and preconditionings. G/G modules suffered an additional 1% PID power loss after DH2000 compared to DH1000.
- . Some G/G modules experienced significant insulation resistance drops after Salt Mist exposure.
- . EL imaging showed interconnection failures, more severe on the rear side of G/G modules.
- . PID degradation patterns differed: G/G modules had edge and junction box degradation, while G/Bs modules exhibited uniform degradation, reflecting different moisture penetration paths.

## Results & Discussion

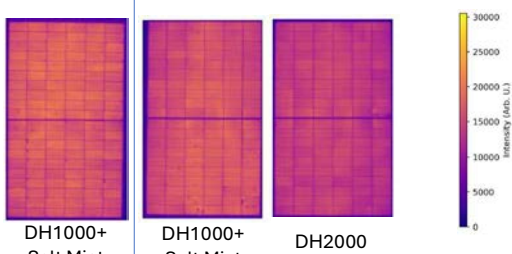
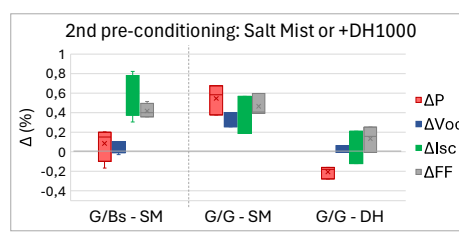
- ① On the first preconditioning step (DH1000), an expected **higher degradation driven by current was observed in G/Bs modules** compared to G/G.



Group A      Group B      Group C

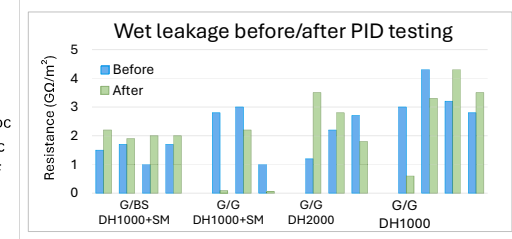
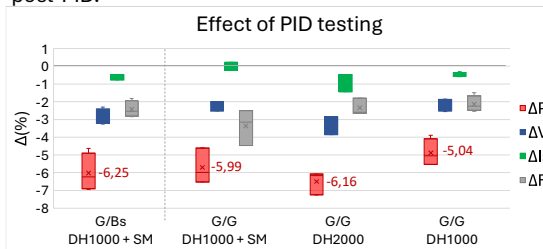


- ② Difference in power loss from additional DH1000 or Salt Mist pre-PID was not discernable from equipment measurement error and small sample sizes.

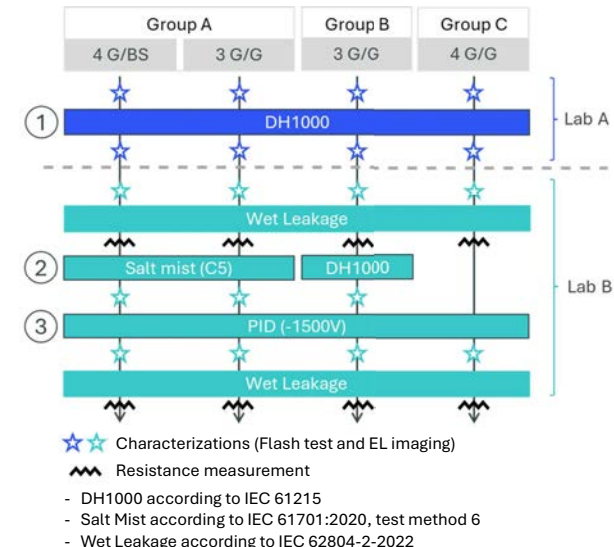


- ③ PID testing (-1500 V), numerical power loss was similar for three groups: G/G, DH2000 and G/G & G/Bs DH1000 + Salt Mist.  
For G/G modules, there was a statistically significant difference of 1% power loss post- PID between DH1000 & DH2000.

Different PID patterns were observed by EL in G/Bs and G/G modules. Some of the G/G modules suffered substantially lower insulation resistance at wet leakage post-PID.



## Experimental Design



## Conclusions & Recommendations

### Preconditioning

Power loss is mostly coming from the first DH1000, esp. G/Bs. Salt mist using IEC 61701:2020, test method 6 (corresponds to C5 conditions) does not result in additional performance loss on G/G as well as G/Bs modules.

### PID testing

Regardless of preconditioning, modules from this manufacturer lost 4 to 7% power after PID testing. While an additional DH1000 on G/G modules did not cause immediate power loss, it led to a 1% increase in power loss post-PID. No additional power loss was observed on the modules subjected to Salt Mist per IEC 61701:2020, test method 6, suggesting that this Salt Mist protocol did not exacerbate PID-s, contrary to expectations of Na<sup>+</sup> ions penetrating the module stack.

Different PID patterns were noted: G/Bs exhibited uniform degradation, while G/G showed degradation primarily at the edges and junction box.

### Future:

Evaluate modules from different manufacturers, incorporate PID without preconditioning, and investigate the post-PID G/G modules' Wet Leakage test for substantial insulation resistance loss.

## Contact

Camille Bainier, TotalEnergies One Tech  
7-9 Boulevard Thomas Gobert  
91120, Palaiseau, France  
[camille.bainier@totalenergies.com](mailto:camille.bainier@totalenergies.com)

## Acknowledgements

Romain Couderc, for Lab B testing and valuable inputs

## Bibliography

Influence of Salt on PID Susceptibility of PV Modules for High Salinity Floating Applications. R. Couderc & L. Sicot. CEA, Le Bourget-du-Lac, France B. Roman & P. Buttin CEA, Bouguenais, France C. Toulemonde Géosel Manosque, Rueil-Malmaison, France – EUPVSEC 2023



# Encapsulation Selection for TOPCon Cells with LECO

Jeff Munro, Paul Brigandi, Lisa Madenjian, Marola Issa, Yuyan Li

## Encapsulation Material Options

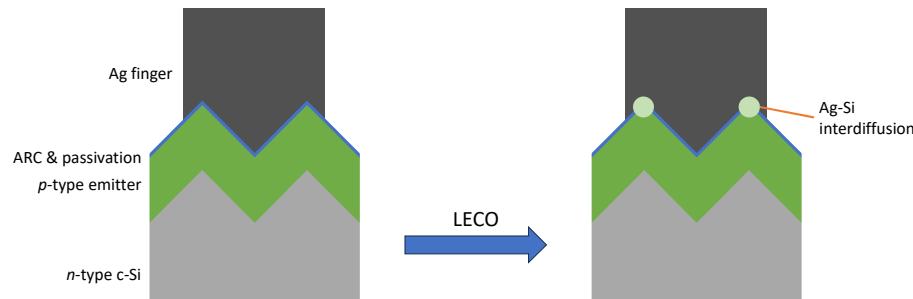
|                                 | POE   | EVA   |
|---------------------------------|---|---|
| (CH <sub>2</sub> ) <sub>n</sub> |   |   |
| WVTR                            | ~3 g/m <sup>2</sup> -day  | ~30 g/m <sup>2</sup> -day   |
| Volume Resistivity              | ~10 <sup>16</sup> Ω·cm  | ~10 <sup>14</sup> Ω·cm  |
| Corrosive Byproducts            | None  | Acetic acid   |
| Attributes                      | <ul style="list-style-type: none"> <li>Na<sup>+</sup> barrier to prevent PID-s</li> <li>High volume resistivity to mitigate PID-p</li> <li>Good moisture barrier</li> </ul> | <ul style="list-style-type: none"> <li>Good processability</li> </ul> |

## Encapsulant Film Structures Evaluated



## LECO Implementation on TOPCon Cells

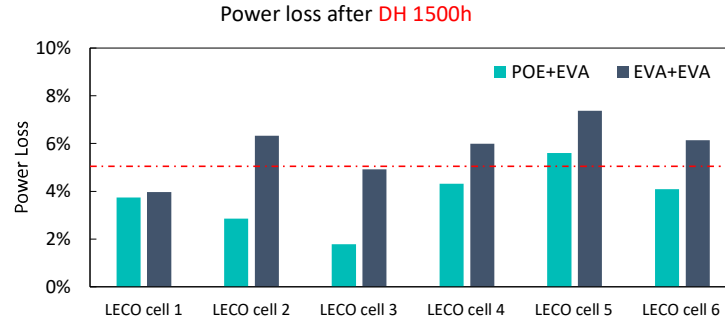
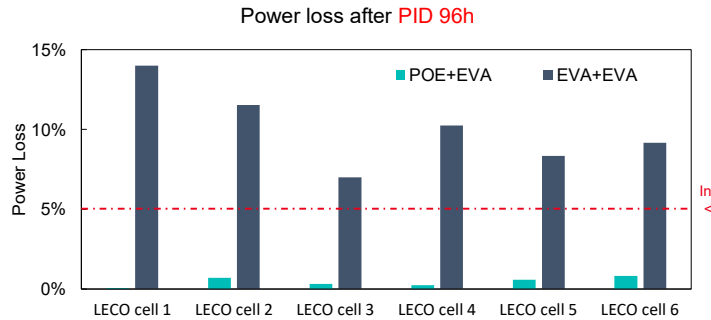
- Laser enhanced contact optimization (LECO) enables higher cell efficiency
- Promotes formation of low-ohmic contacts
- Without LECO → Ag/Al paste often used
- With LECO → Ag with little to no Al content often used
- Use of LECO does not eliminate PID or corrosion issues



Schematic based on "Microscale Contact Formation by Laser Enhanced Contact Optimization," Großer, S., et al. IEEE Journal of Photovoltaics 2022, 12, 26-30.

## Variation in Cell Performance Mitigated by Encapsulant Selection

Evaluated six batches of commercial LECO cells

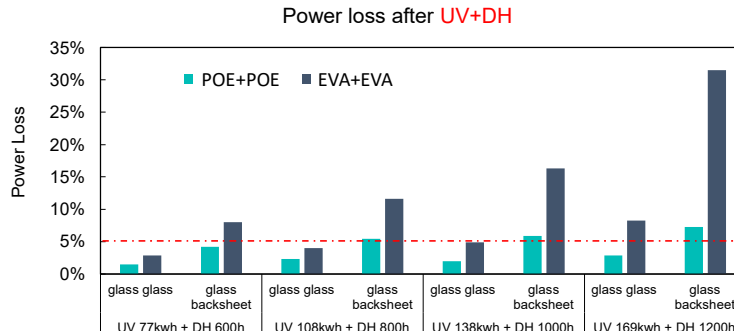
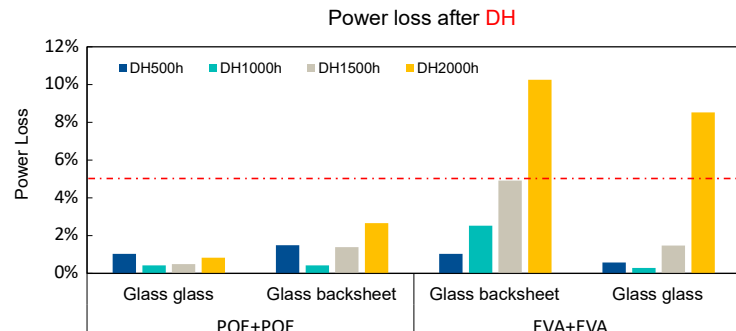


- Significant power loss for all LECO cells after PID test when using EVA+EVA encapsulant structure
- Good performance for POE+EVA across different cell batches

- POE+EVA more robust than EVA+EVA across cell batches
- Failures (>5% power loss) observed for several cell batches with EVA+EVA

## Corrosion Remains Critical Issue for TOPCon Cells with LECO

Selected best performing LECO cell for extended DH aging



- Less power loss with POE+POE versus EVA+EVA at 2000h DH aging
- Significant power loss in both glass-glass and glass-backsheet modules using EVA+EVA after DH 2000h (for glass-glass module, sharp power loss from DH 1500h to DH 2000h may be because of moisture ingress resulting in corrosion and cell failure)

- POE+POE more robust than EVA+EVA
- Less power loss in glass-glass modules than glass-backsheet modules

# Investigating Temperature Uniformity and Accuracy in PV Module Lamination: A Verification Study

Aubrey Jackson<sup>1</sup>, Rachael L. Arnold<sup>1</sup>

<sup>1</sup>National Renewable Energy Laboratory, Golden CO, USA

## Methods

To evaluate temperature distribution, thermocouples (TC) paired with Omega data acquisition software were used to measure temperatures at multiple platen locations and within test samples for a 145°C lamination recipe. All trials ran through entire laminator recipe duration.

### Laminator & Equipment

- 2014 Bent River Laminator, SPL 2828
- Type-T 36-gauge thermocouples (TCs)
- Data Acquisition: Omega TC Central Software

### Samples & Setup

#### 1. Plate Uniformity Test: Direct Laminator Platen Contact

- Plate size: 30" x 30"
- TCs attached using kapton tape at center, surrounding center location (3" from center) and corners (3" from edges).

#### 2. Large Glass/EVA/Glass Sample Uniformity Test

- 18" x 24"x 1/8" tempered solite glass
- 15580P Ethylene vinyl-acetate (EVA) encapsulant
- TCs placed at center and 4 corners (1" from edge)

#### 3. Sample Type Varying Layup

- Glass/EVA/Glass & Glass/EVA/Backsheet
- 8" x 8" x 1/8" tempered solite glass
- TCs placed at center

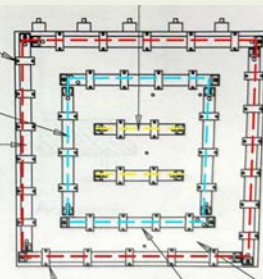


18" x 24" Glass/Glass    8" Glass/Backsheet    8" Glass/Glass

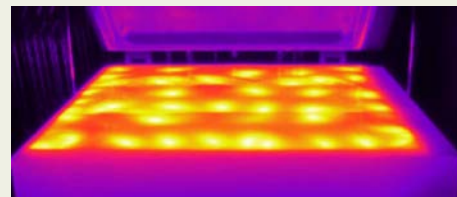
### Laminator Heating Element Specifications

Heaters mounted against bottom platen:

- **Zone 1**  
20A, 4 x 750W = 3000W
- **Zone 2**  
20A, 4 x 500W = 2000W
- **Zone 3**  
20A, 2 x 500W = 1000W

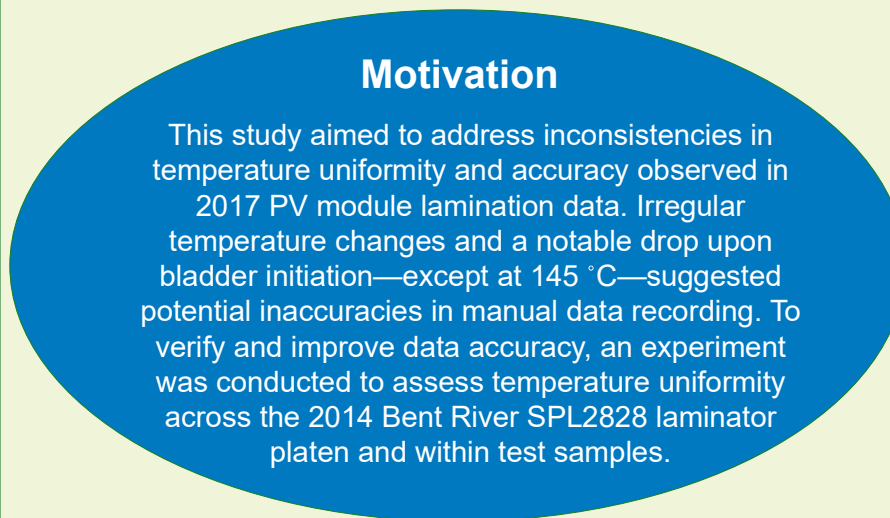


Platen heaters diagram from laminator manual.



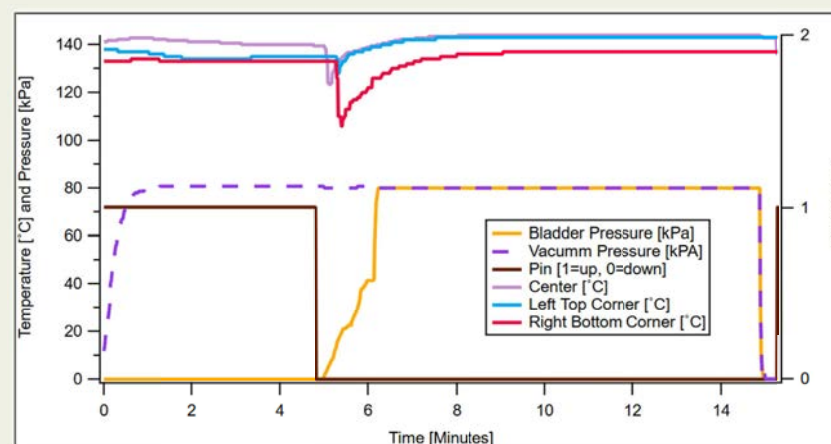
FLIR Image of Laminator Platen

Note: Black aluminum foil was attached to laminator platen to prevent reflection of surroundings.



## Laminator Platen Temperature Uniformity Results

### Laminator Temperature Uniformity and Pressure Profiles



- The bottom section of the platen found to be consistently cooler than the top.
- Right-bottom corner and below center locations experienced the highest temperature drop when the bladder pressure initiates.
- Left and above center location are the hottest.
- Coolest locations are the left-bottom and right-bottom corners.
- Only two locations (above and left of center) reached 145 °C.

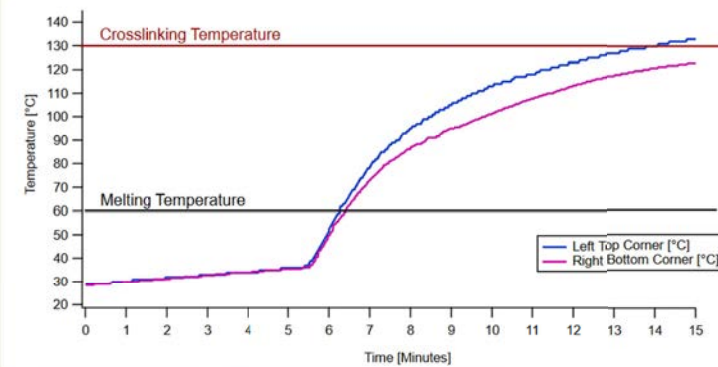


Laminator Platen TC Locations Showing Temperature Distribution

## Glass/EVA/Glass Sample Uniformity Results

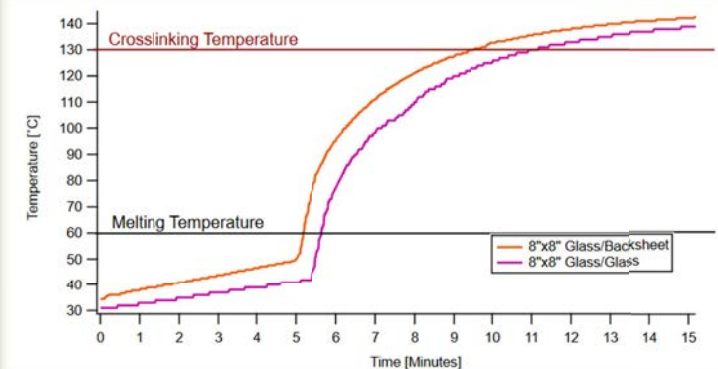
- Right-bottom and left bottom corner showed the lowest temperatures and did not reach crosslinking temperature (130°C)
- Left-top corner was the hottest location. (MAX= 134°C)
- Indicates possible laminator aging or heat distribution issues.

### 18" x 24"x 1/8" Glass Temperature Uniformity



## Glass/Glass vs Glass/Backsheet Results

### Glass/Glass and Glass/Backsheet Lamination Temperature



- Both sample types reached crosslinking temperature.
  - Glass/backsheet finished 5°C hotter than the glass/glass sample as expected due to less material.
- Note: laminator recipe designed for glass/backsheet.

## Future Work

- Investigate temperature compensation strategies and calibrate heat sensors (e.g., setting laminator to a higher temperature to counteract cooling effects).
- Conduct additional tests without Kapton tape (potential insulator affecting TC readings).
- Integrate pressure sensor data to correlate with temperature variations.
- Further analyze ramp rates to understand sample heating behavior and optimize cycle time.

# Wind-Induced Dynamic Loading and PV Module Frame Fatigue Crack Initiation and Propagation

By: Frank Oudheusden & Chris Needham (Azimuth Advisory Services), Jon Ness, Kyle Johnson & Charles Milton (Matrix Engineering Consultants)

## Abstract

### Key Features

Large-format photovoltaic (PV) modules, while offering cost and efficiency advantages, face significant reliability challenges. A key issue stems from their lack of structural rigidity, leading to mechanical failures. A notable mechanism involves the bottom flange of the module frame tearing away under both extreme and moderate wind conditions.

This bottom flange has been reduced in size with the advent of large-format panels, yet identical failures occur in smaller-format modules, highlighting design and material vulnerabilities. Photographs of failures from Hurricane Beryl illustrate the damage, while finite element analysis (FEA) modeling reveals stress points and tear-away conditions. Evidence of frame cracking before failure suggests fatigue crack initiation and propagation as a precursor to catastrophic damage.

Preliminary findings indicate that flange integrity is compromised by cyclical loading and sudden gusts, with wind-induced vibrations amplifying stress in critical areas. These insights underscore the urgent need for improved design standards and testing protocols to ensure durability across diverse climatic conditions.

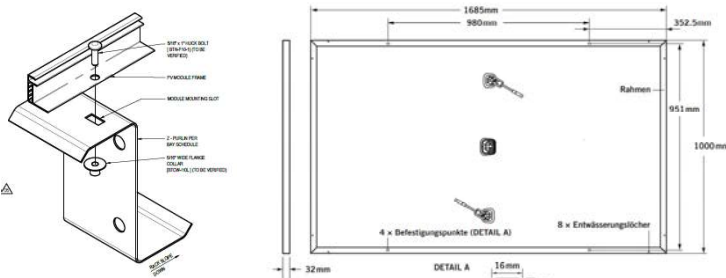
This work has implications for manufacturers, field operators, and policymakers seeking to optimize the reliability and longevity of PV installations. Addressing these reliability concerns will help the industry balance the advantages of large-format modules with the demands of long-term operational resilience.

### Targeted Audience

- Project Developers
- Engineering, Procurement & Construction (EPC) Companies
- Independent Engineering Firms (IE's)
- Standards Committees
- Insurance Companies
- Financiers
- Module Manufacturers
- Solar Racking Manufacturers

## Grenadines Project Information

### Current Design



Installation was performed at the four mounting points utilizing direct bolted connections per the installation manual. It was confirmed in the installation manual that the test load (push/pull) is 4000 PA which after applying the IEC61215-2-2016 and UL61730 safety factor of 1.5, provides a design load (push/pull) of 2670 PA.

Modules were mounted at a low angle (~5 deg) to nominal but were located on a slope (~15 deg) with the leading edge of the module almost perpendicular to the oncoming wind direction. This is an area for future project design improvement and will be outlined in Solar Under Storm III guidance in May 2025.

### Hurricane Beryl

Hurricane Beryl struck the Grenadines on July 2<sup>nd</sup>, 2024. NOAA estimated peak winds of 140mph categorizing Beryl as a dangerous Category 4 storm (on the 1-min Saffir-Simpson scale) at the time of landfall.

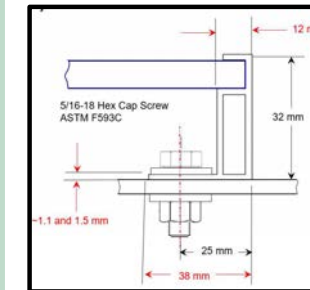


## Site Performance & On-Site Findings

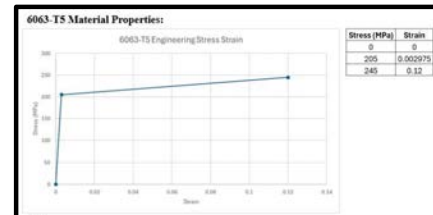


Low-cycle fatigue cracks were found on many remaining modules both on hardware on the low and high-pressure sides of the modules. Propagation led to failures and is the primary failure mode for module liberation.

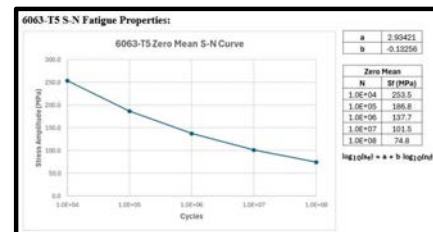
- The project site was modeled after Solar Under Storm 1 recommendations and all accounts performed admirably. To have a test bed for resilience improvements hit by a second hurricane is incredibly improbable and an amazing opportunity to find new paths.
- Racking utilized dual-post foundations and low-angle module mounting, resulting in zero primary failure modes in the racking system.
- 31% of modules remained visibly undamaged.
- No witnessed hardware loosening due to use of Nylock nuts (vibration resistant hardware).
- Mild structural corrosion was present - typical of the region and age.
- Module frame tear-out was the primary cause of module liberation. Photo below >95% of all module hardware



## FEA Model Setup



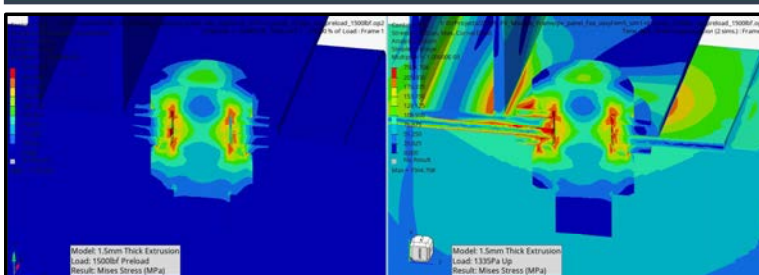
Note:  
• The extension is 6063-T5 aluminum.  
• Ultimate & Yield values from Fatigue Characterization of a VAWT Blade Material measured values.  
• Yield Strength = 205 MPa, Ultimate Strength = 245 MPa.  
• Young's Modulus & Poisson's Ratio from <https://www.matweb.com/search/specmaterial.aspx?accession=6063T5>  
• E = 70 GPa  
• Fasteners use standard steel properties



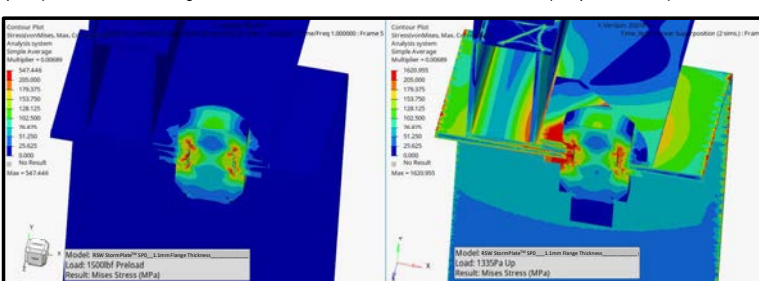
Note:  
• S-N fatigue data from Fatigue Characterization of a VAWT Blade Material.  
• S-N fatigue data from Fatigue Characterization of a VAWT Blade Material.

An area for future improvement in IEC 61215 would be to utilize cyclical loading protocols after a static load test to determine an appropriate amount of static load test plastic deformation in the frame.

## Finite Element Analysis



Industry typical 5/16 bolt stack-up utilizing a round washer at 1335Pa of test load (50% of the rated load of this panel) – Failure shows along the interior wall frame which was observed in the field (see photos above)



RSW StormPlate™ SPO design was tested to distribute the load. FEA Static results showed a 33% reduction in peak stress in the AL frame, drastically improving the frame performance and should (with further IEC61215 testing) improve overall module performance if the primary failure mode was frame buckling (which it often is)

## Results

### Fatigue Life 2 Elements from Edge A (Cycles)

| Model                 | Applied Load         |                      |                      |
|-----------------------|----------------------|----------------------|----------------------|
|                       | 1068 Pa<br>40% Rated | 1335 Pa<br>50% Rated | 1602 Pa<br>60% Rated |
| 1.1mm Thick Extrusion | 198,427              | 14,730               | <b>607</b>           |
| 1.5mm Thick Extrusion | 2,298,817            | 283,000              | 38,958               |
| RSW StormPlate™ SPO   | <b>4,144,299</b>     | <b>1,015,000</b>     | <b>283,169</b>       |
| 1.1mm Thick Extrusion |                      |                      |                      |

The 1.1mm thick frame flange showcased failure at approximately 607 cycles of load at 60% of its rated load (1602 Pa). Assuming the wind comes from the worst-case direction (rear) this could be achieved in the field in a matter of minutes.

The addition of the RSW StormPlate™ SPO in the analysis shows a great area of promise.

RSW StormPlate™ SPO showed a 450x increase in the number of cyclical loads compared to the 1.1mm thick frame utilizing industry-standard hardware stacks.

As modules evolve to become larger and have less rigidity, fastener selection needs to be tailored to the application. RSW StormPlate™ SPO is one example of how to better support these smaller frames against stress concentrations. Application specific mounting innovation and techniques like load distribution are key to reducing module liberations in the field.

Taking this analysis away from smaller-format modules under extremely high wind events is also alarming. The expected performance of a large format module under the same conditions would yield an expected failure pressure of 1000Pa (rather than 1335Pa) for an expected performance of under 1000 cycles. This is an industry wide problem, driven by module frame evolutions across all module platforms.

Multiple module frame flange thicknesses were assessed utilizing industry standard round washers to showcase the cyclical loading difference in simply increasing frame material. 1.1mm was measured in the field in the Grenadines. 1.5mm would cost a 36% increase in material, estimated to cost approximately \$2.00 a module depending on module size (\$0.005/w). 1.5mm brings a meaningful improvement. However, the minimum cycle requirement for 20-year performance (acceptable) is yet to be determined.



Thankfully, industry standards already exist for cyclical load test (IEC 62782-1). Kiwa PVEL (a well-known industry test lab) showcases IEC62782 results as part of its 2024 Module Reliability Scorecard and notes: "...frame fatigue can also be an issue. In this example, the module's mounting hole was ripped out of the frame during tracking-mode testing at 1000Pa and failed again during failure mode testing at 1602Pa, becoming disconnected from racking during high wind events and is likely due to using a thinner frame flange to save cost. This type of defect is typically not replicated during stand-alone SMT or DML testing but has been seen on multiple BOMs subjected to the POP's combination of SMT and DML." The example above shows failure at cycle #962 out of 1000 cycle test, validating that the non-linear FEA model matches both field empirical evidence and lab analytical findings.

## More Information

### Resources:

- International Electrotechnical Commission. (2016). IEC 61215:2016 – Crystalline silicon terrestrial photovoltaic modules – Design qualification and type approval. Geneva, Switzerland: International Electrotechnical Commission.
- International Electrotechnical Commission. (2021). IEC 62782-1:2021 – Photovoltaic (PV) modules - Cyclic (dynamic) mechanical load testing. Geneva, Switzerland: International Electrotechnical Commission.
- Kiwa PVEL. (2024). 2024 Module Reliability Scorecard. Kiwa PVEL.

### Websites:

- <http://www.azimuth-ventures.com>
- <https://www.matrixengrqrq.com>
- <https://www.resilientsolarworks.com>

### Contacts:

- Frank Oudheusden ([frank@azimuth-ventures.com](mailto:frank@azimuth-ventures.com))  
Chris Needham ([chris@azimuth-ventures.com](mailto:chris@azimuth-ventures.com))  
Jon Ness, Matrix Engineering Consultants ([jness@matrixengrqrq.com](mailto:jness@matrixengrqrq.com))

# Comparing Outdoor to Indoor I-V Curves for Bifacial PERC Modules Affected by PID-p

Dylan J. Colvin<sup>1</sup>, Cecile Molto<sup>1</sup>, Ryan M. Smith<sup>2</sup>, Peter Hacke<sup>3</sup>, Fang Li<sup>4</sup>, GovindaSamy TamizhMani<sup>4</sup>, Jaewon Oh<sup>5</sup>, Halima Jahan<sup>5</sup>, and Hubert P. Seigneur<sup>1</sup>



<sup>1</sup>University of Central Florida - Florida Solar Energy Center, Cocoa, FL, 32922, USA | <sup>2</sup>Pordis LLC, Austin, TX, 78729, USA | <sup>3</sup>National Renewable Energy Laboratory, Golden, CO, 80401, USA

<sup>4</sup>Photovoltaic Reliability Laboratory – Arizona State University, Mesa, AZ, 85212, USA | <sup>5</sup>University of North Carolina Charlotte, Charlotte, NC, 28223, USA

## Introduction

Polarization-type Potential-Induced Degradation (PID-p) affects technologies with large market penetration, namely bifacial *p*-PERC (Passivated Emitter Rear Contact and TOPCon (Tunnel Oxide Passivated Contacts). We have tested commercially available bifacial glass/glass *p*-type PERC modules which exhibit PID-p [1], while shunting and corrosion-type PID were not observed. PERC modules are more susceptible to experience PID-p when cell are negatively biased (frame grounded) due to the PERC cell architecture [2], causing the rear side to primarily degrade.

In this study, we performed PID-p field testing on the same make and model of module in a hot-humid environment. The testbed on which these were installed supplied high voltage for accelerated testing and current-voltage (*I*-*V*) curve tracing capabilities on a subset of installed modules. These modules were periodically uninstalled for indoor characterization (*I*-*V* shown here) to assess PID-p evolution.

We compare the indoor *I*-*V* curves (obtained on isolated front and rear sides of the modules) to outdoor traces (with plane-of-array POA and albedo irradiance contributions) to:

1. Assess simple methods of correcting outdoor *I*-*V* curves to standard test conditions (STC) with and without using indoor *I*-*V*.
2. Investigate challenges to analyzing outdoor bifacial *I*-*V* due to PID-p, which can induce severe degradation in rear-side performance.
3. Explore what information emerges from the comparison processes.

## Methodology



Fig. 1: Mounting configurations for high-voltage testbed (5 racks, 25 modules can be installed per rack).

### Outdoor Setup and Tracing

- Clear sky filter: standard deviation of POA irradiance < 3 W/m<sup>2</sup> for a period of 1 min before the trace to 30s after the trace.
- 10,697 *I*-*V* traces pass the filter (~78% of all traces)
- Link meteorological data to outdoor trace to within 15s.
- Maximum albedo irradiance measured ~150 W/m<sup>2</sup>.
- 3 modules from each rack type (see Fig. 1).
- POA irradiance and albedo sensors on each rack type: thermocouples attached to representative control (non-biased) modules per rack.

### Indoor Flash Testing

- *I*-*V* using Sinton FMT-350 flash tester at STC (AM1.5G, 25°C ± 2°C) from ~150 W/m<sup>2</sup> to 1000 W/m<sup>2</sup>.
- Isolate each module side using opaque surface.

- Indoor and outdoor maximum power  $P_{MP}$ , maximum power current  $I_{MP}$ , fill factor  $FF$ , and short-circuit current  $I_{SC}$ .
- Link outdoor traces to indoor *I*-*V* measurements taken within ± 60 days.
- Assume negligible voltage gain from the rear-side.

- Indoor front *I*-*V* at POA irradiance; indoor rear *I*-*V* at 200 W/m<sup>2</sup> due to low-quality indoor *I*-*V* < 150 W/m<sup>2</sup>. Use equations 1 and 2 to get indoor combined current.
- Thresholds of ±0.5%, ±2%, and ±5% chosen to show:

- Excellent matches (<±0.5%, approximate indoor tester  $I_{SC}$  variability);
- Good matches, accounting for sky stability filter and maximum albedo ( $\pm 3$  W/m<sup>2</sup> / 150 W/m<sup>2</sup> → ±2%);
- Moderate fits (<±5%) and poor fits (>±5%).

- Temperature correct voltage and current for STC 25°C. Perform before any other corrections.

- Series resistance  $R_s$  correction: take the negative of the inverse slope of indoor front *I*-*V* curve near  $V_{OC}$ . Use a minimum of 2 data points.

- When  $R_s$  correction applied, omit curves with any  $V > 50$  V due to erroneous  $R_s$  values ( $<0 \Omega, >0 \Omega$ ).

- Irradiance ratio: assume current contribution from albedo is the ratio of albedo to POA multiplied by current, to try isolating the front-side contribution (Eq. 3).

## Results

### Timespan Between Measurements and Albedo Irradiance

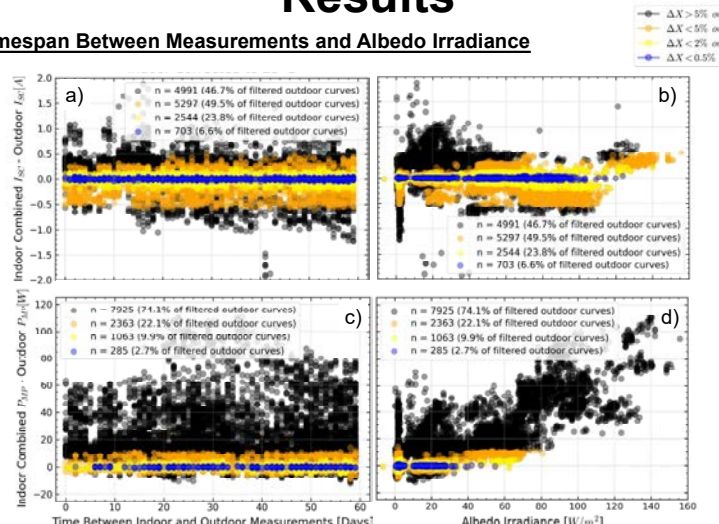


Fig. 2: a) and b) difference between indoor combined  $I_{SC}$  (Eq. 1) and outdoor  $I_{SC}$ ; c) and d) difference between indoor  $P_{MP}$  (calculated after combining current, Eq. 2) and outdoor  $P_{MP}$ .

- PID-p leads to rapid degradation within ~1 month, then reaches a stabilization point. Data shown were taken after stabilization point was reached.
- $P_{MP}$  overestimations driven by low  $FF$  in outdoor data at POA irradiance > 600 W/m<sup>2</sup>.
- Poor  $P_{MP}$  comparisons also could be due to albedo non-uniformity, cell mismatch due to PID-p, spectral mismatch.
- Trend appears for poor (differences >5%)  $P_{MP}$  comparisons and albedo irradiance, but not better (differences <5%).
- No correlation observed for timespan between indoor and outdoor measurements.

### Series Resistance Corrections and Albedo Irradiance

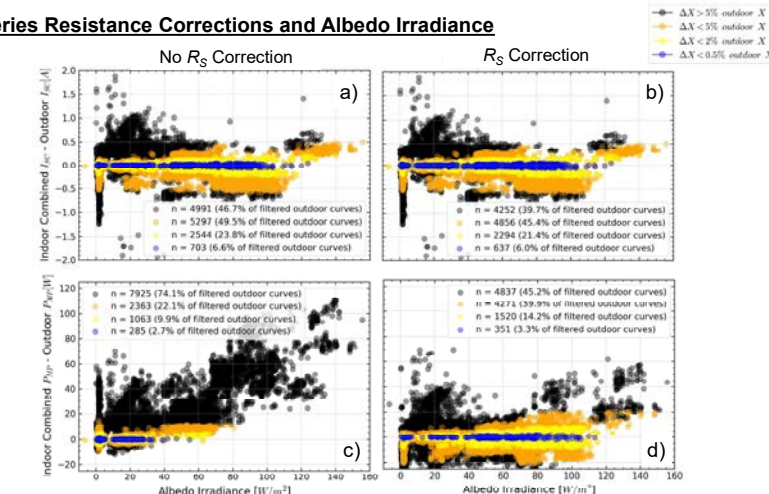


Fig. 3: a) and b) difference between indoor combined  $I_{SC}$  (Eq. 1) and outdoor  $I_{SC}$ ; c) and d) difference between indoor  $P_{MP}$  (calculated after combining current, Eq. 2) and outdoor  $P_{MP}$ .

- $P_{MP}$  and  $FF$  (FF not shown) show major improvement in indoor-outdoor correlation;  $I_{SC}$  and  $I_{MP}$  ( $I_{MP}$  not shown), slightly lower.
- 1908 more curves (17.8 abs% more) within 5% outdoor  $P_{MP}$ ; 457 more curves (4.3 abs% more) within 2%.
- $R_s$  correction shows higher amount of good indoor-outdoor correlations at higher albedo irradiances for  $P_{MP}$  and  $FF$ .
- 441 fewer curves (4.1 abs% fewer) show indoor-outdoor  $I_{SC}$  within 5% outdoor  $I_{SC}$ .

### Irradiance Ratio and Albedo Irradiance – Attempting to Transform Outdoor *I*-*V* to Indoor *I*-*V*

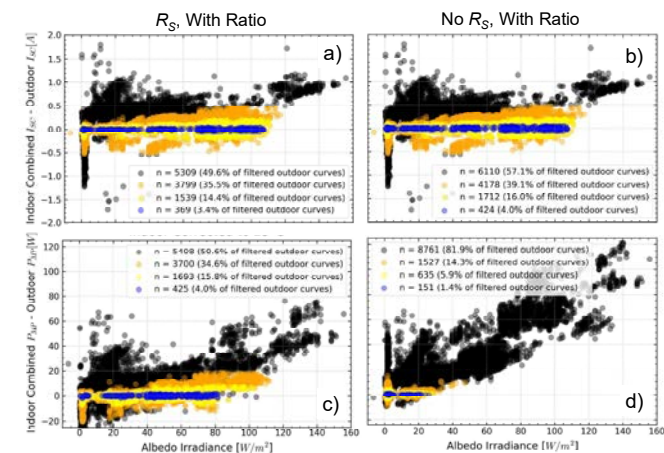


Fig. 3: a) and b) difference between indoor combined  $I_{SC}$  (Eq. 1) and outdoor  $I_{SC}$ ; c) and d) difference between indoor  $P_{MP}$  (calculated after combining current, Eq. 2) and outdoor  $P_{MP}$ .

- Indoor data is not used when making "No  $R_s$ , With Ratio" corrections; front-side indoor used to compare with corrected outdoor *I*-*V* curves.
- No  $R_s$ , With Ratio gave worst indoor-outdoor correlations in  $P_{MP}$  with fewer undercorrections.
- $R_s$  With Ratio and No  $R_s$  With Ratio showed worst indoor-outdoor correlations in  $I_{SC}$  and  $I_{MP}$  ( $I_{MP}$  not shown).
- $P_{MP}$  and albedo in No  $R_s$ , With Ratio demonstrate overcorrections in poor fits correlate with albedo.

## Summary

- Outdoor *I*-*V* is traced on bifacial PERC modules and indoor *I*-*V* curves were measured periodically during high-voltage exposure to evaluate rear-side PID-p.
- Several methods were used to correlate indoor and outdoor data:
  - STC temperature correction,
  - indoor  $R_s$  to shift outdoor curves, and
  - irradiance ratio of  $\frac{G_{POA} - G_{Albedo}}{G_{POA}}$  to see if rear gain is linear on PID-p affected modules
- The difference between indoor and outdoor  $I_{SC}$ ,  $P_{MP}$  is used for indoor-outdoor correlations.
- No difference in correlations found between traces taken ±60 days apart.
- Albedo irradiance shows impact on corrections for  $I_{SC}$ .
- Summary provided in table below of correction impacts on *I*-*V* characteristics using "good" matches: [(indoor – outdoor) / outdoor] < ±2%

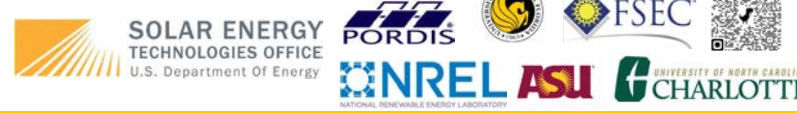
| Parameter | Only 25°C | 25°C + $R_s$ | 25°C + Ratio | 25°C + $R_s$ + Ratio |
|-----------|-----------|--------------|--------------|----------------------|
| $P_{MP}$  | 9.94%     | 14.2%        | 5.94%        | 15.8%                |
| $FF$      | 18.1%     | 26.3%        | 18.1%        | 26.3%                |
| $I_{SC}$  | 23.8%     | 21.4%        | 16.0%        | 14.4%                |
| $I_{MP}$  | 24.1%     | 21.3%        | 13.3%        | 14.3%                |

$P_{MP}$  and  $FF$ : 25°C, then both  $R_s$  and ratio gives best results.

$I_{SC}$  and  $I_{MP}$ : best results with just 25°C correction.

## References

- [1] F. I. Mahmood et al., "Susceptibility to polarization type potential induced degradation in commercial bifacial p-PERC PV modules," *Prog. Photovolt. Res. Appl.*, 2023, doi: 10.1002/pip.3724.
- [2] C. Molto et al., "Review of Potential-Induced Degradation in Bifacial Photovoltaic Modules," *Energy Technol.*, 2023, doi: 10.1002/ente.202200943.



# Hail Kinetic Energy damage thresholds on large scale PV panels

J. Carl<sup>1</sup>, L. Doddipatla<sup>2</sup>

Sr. Lead Research Scientists, FM Research Division, Norwood, Massachusetts, <sup>1</sup>jochen.carl@fmglobal.com, <sup>2</sup>lakshmana.doddipatla@fmglobal.com

## Introduction

Shattering of the glass and creating microcracks in the underlying crystalline silicon layer are the major failure modes of PV panels due to hail impact. Hail impact testing was performed on 4 monofacial and 5 bifacial crystalline silicon, large size, ground-mounted panels.

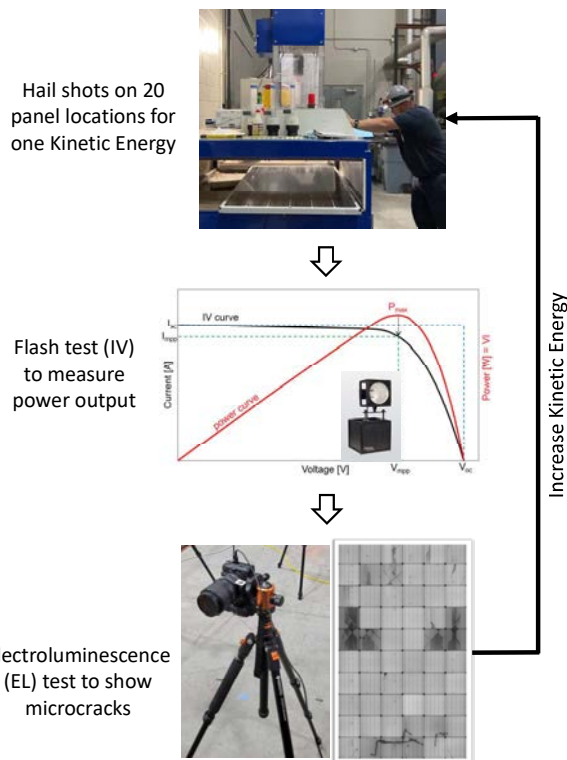
|                        | Monofacial panels          | Bifacial panels           |
|------------------------|----------------------------|---------------------------|
| Glass thickness        | Front: 3.2 mm<br>Back: N/A | Front: 2 mm<br>Back: 2 mm |
| Power output $P_{max}$ | 420 – 545W                 | 485 – 550W                |
| Half cells             | 6 x 22-24                  | 6 x 24-26                 |
| Glass type             | Tempered                   | Heat-strengthened         |
| Width                  | 1.0 – 1.1m                 | 1.0 – 1.1m                |
| Height                 | 2.1 – 2.3m                 | 2.2 – 2.3m                |

## Test matrix and Objective

- 9 different types of PV panels
  - 4 monofacial and 5 bifacial
  - 12 samples per panel type (108 panels total)
- **Objective**  
Determine the Hail Impact Kinetic Energy thresholds for microcracks and glass shattering

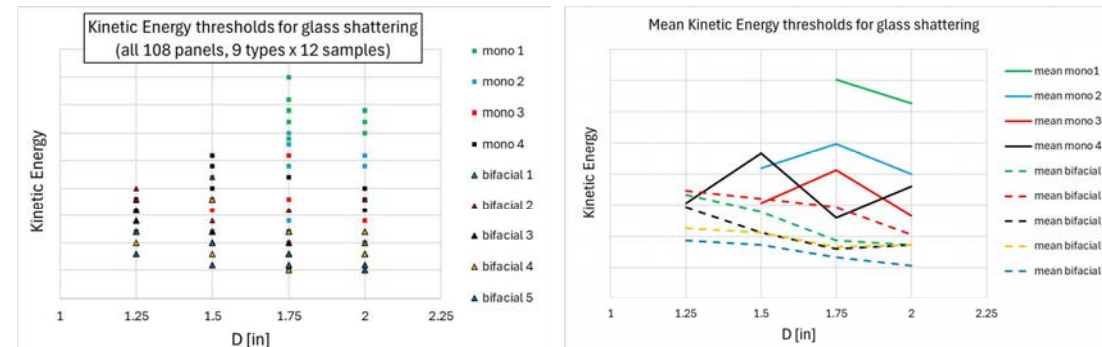
## Test cycles

Before and after the hail tests, electroluminescence (EL) and flash tests (IV) were performed to visualize microcracks and measure the power output degradation.

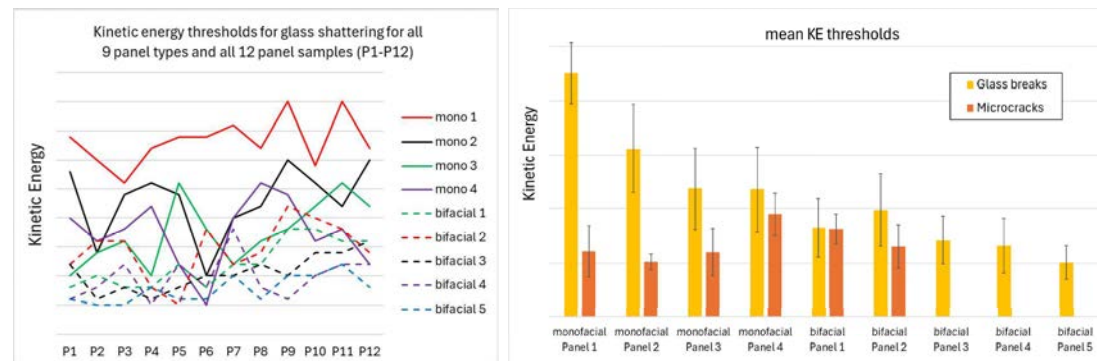


## Test results for Kinetic Energy thresholds

The Kinetic Energy thresholds for microcracks and glass shattering were tested for 1.25 in. (31.8 mm), 1.5 in. (38.1 mm), 1.75 in. (44.5 mm), and 2 in. (50.8 mm) diameter (D) ice balls. As high wind speeds can give small ice balls the same Kinetic Energy as larger ones under no or little wind, we aimed to determine if the hail diameter matters when the Kinetic Energy is equivalent.

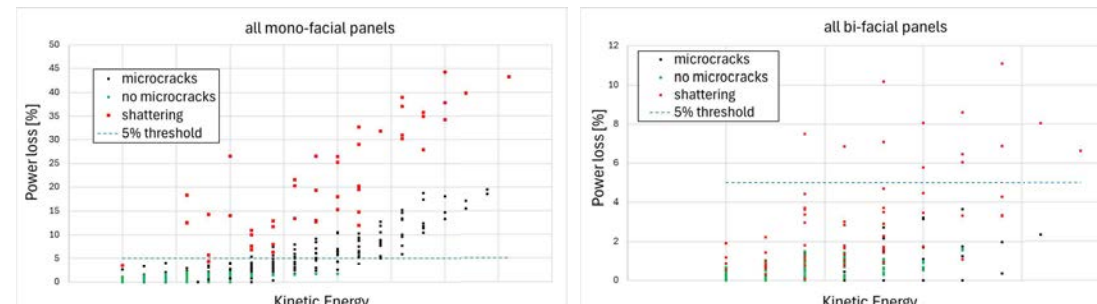


- The study found no significant effect of the ice-ball size on the Kinetic Energy threshold for glass shattering.



- Monofacial panels shattered under a higher Kinetic Energy than bifacial panels.
- Bifacial panels rarely experienced microcracks prior to glass shattering.

## Power loss comparison



### Observations in monofacial panels

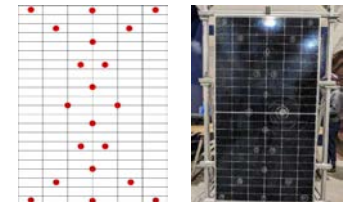
- Microcracks typically occur prior to glass shattering.
- Power loss due to microcracks can be > 5%.

### Observations in bifacial panels

- Microcracks prior to glass shattering were rare.
- Minor power loss due to microcracks prior to glass shattering.

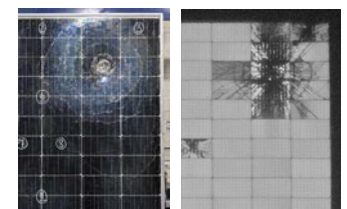
## Hail impact locations and test cycle

We impacted each panel type 20 times following FM Approvals' "Examination Standard for Ground-Mounted or Elevated Photovoltaic Module Systems, Class 4480" that suggests hail impacts on at least 15% of all cells.

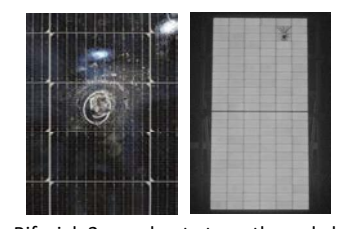


## Differences in failure modes between mono- and bifacial panels

The 3.2 mm tempered glass of the monofacial glass shattered into smaller pieces than the 2 mm heat strengthened glass of the bifacial panels. The microcracks in the bifacial panels remained more localized after glass shattering than in the monofacial panels.



Monofacial, 3.2 mm, tempered glass.



Bifacial, 2 mm, heat-strengthened glass.

## Conclusions

- The test results varied among and within panel types, possibly due to changes in manufacturer quality, installation, and handling.
- The bifacial panels with 2 mm glass thickness shattered under lower Kinetic Energy than the monofacial panels with 3.2 mm glass thickness.
- Bifacial panels experience fewer microcracks than monofacial panels.
- It was unclear whether small ice balls at high velocities or larger ice balls at lower velocities with the same kinetic energy, are more likely to cause glass shattering.

# MODULE MOUNTING DESIGN QUALIFICATION CHALLENGES

Authors: Jim Sorensen and Sumanth Loka Nath

## THE CURRENT SITUATION:

### MODULE MANUFACTURERS

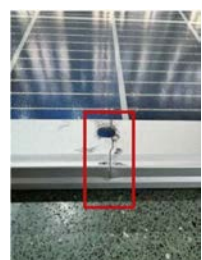
- ▶ Issue mount-specific and sometimes project-specific approvals based on opaque requirements
- ▶ Approval requirements vary by manufacturer, frequently based solely on the module SMLT (IEC 61215, MQT 16)
- ▶ Modules delivered to a project may differ physically from modules tested, but no change in datasheet or model number. For instance: glass thickness, glass stress, frame cross section, material supplier quality, etc.

### TRACKER MANUFACTURERS

- ▶ As experts in wind loading, have little influence on module qualification requirements.
- ▶ Some tracker manufacturers have established high quality standards and rigorous durability protocols demonstrating reliable track records, while other low-cost manufacturers experience much higher failure rates.
- ▶ Unwilling to take module breakage risk
- ▶ Unwilling to make conservative product changes that erode competitiveness. The industry needs to apply consistent requirements.

### FIELD EXPERIENCE

- ▶ Increasing observance of glass breakage at wind conditions well below design wind speeds [1][2]
- ▶ Module frame buckling during strong, but below design wind speeds
- ▶ Module frame fatigue failures [3]
- ▶ Module fastener pull through at mounting points
- ▶ Module fastener loosening



### REFERENCES:

- [1] H. Hieslmair, F. Samara, and M. Jovanovic, "Stress concentrators," DNV, 2023. [Online]. Available: <https://www.dnv.com/article/stressconcentrators/>
- [2] D. Wang, A. Hermawan, and E. Woolard, "Correlation between mid-level wind speed and rear glass breakages on non-large-format bifacial PV modules on trackers in a solar farm," in Proc. IEEE 52nd Photovolt. Specialist Conf., 2024, pp. 0064-0067.
- [3] Y. Yu, "Glass breakage study on large module plus typical tracker system," IEC WG9 committee presentation, 2024
- [4] C. Sillerud, "Modern Methods for Testing Mechanical Durability of PV Modules", NREL PVRW Proceedings, 2024
- [5] S. Van Pelt, "Module wind load resistance: Standards vs Reality", PV Magazine Webinar, 2021, <https://www.pv-magazine.com/webinars/module-wind-load-resistance-standards-vs-reality/>
- [6] M. Hutchins, "Weekend Read: Temper Tantrum, PV Magazine, 2024, <https://www.pv-magazine.com/2024/01/06/weekend-read-temper-tantrum/>
- [7] J. Raoult, B. Dalatre, "Fatigue equivalent load approach for fatigue design", MATEC Web Conf. 300 02003 (2019), DOI: 10.1051/matecconf/201930002003

## TESTING:

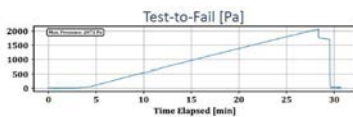
### MOUNTING CONSIDERATIONS:

- ▶ Testing a single module mounted on two mounts, does not represent the typical in-use condition. Mounts are loaded at 50% of expected. Loads are unbalanced. The effect on module can be unpredictable.
- ▶ Must pass component-level testing (not covered here) separate from Module + Mounting testing.
- ▶ Modules also experience stress due to torque tube twist and sag when fixed, or due to movement of the structure. These are currently not considered in testing.

### ASSESSMENT OF TRUE SAFETY FACTOR FOR UNIFORM LOAD:

- ▶ Typical test loads are 1.5X design loads, following IEC 61215...
- ▶ Often testing is conducted only to a desired limit, but not up to failure, due to the time and cost of testing
- ▶ Recommend using TTF method proposal [4]

- **Test-to-Failure**
  - Goal: Bound the issue with a max load
  - Duration: 1 hour



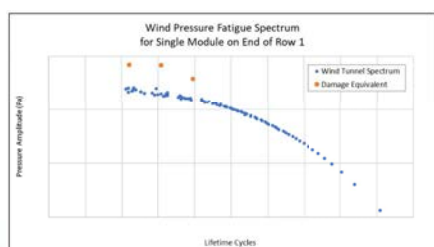
### NON-UNIFORM LOADING:

- ▶ Typical tracker loading is not uniform. It has been assumed that this is adequately captured in the average uniform load requirement and associated safety factor. However, this is widely recognized as inadequate [5][6].
- ▶ With advances in module load test equipment, conducting non-uniform loading is easily performed
- ▶ Industry agreement is needed on universal testing determination and levels



### CYCLICAL FATIGUE LOADING:

- ▶ Most often, no cyclical testing is conducted. In other cases, the DML cycle is used from IEC 61215, which is significantly inadequate for metal fatigue and/or fastener evaluation.
- ▶ Industry agreement is needed on universal testing determination and levels
- ▶ Test equipment now exists for more complex cyclical loading
- ▶ Propose using a damage equivalent approach to setting test levels [7]



## THE PROBLEM

The utility PV industry generally relies on mounting-specific approvals issued by module manufacturers often at pressures well below those required by IEC and UL (61215, 61730, etc). Owner's engineers and project due diligence often require these documents ostensibly to reduce the risk of module breakage and incompatible mounting configurations. However, the process of obtaining these letters and the conditions necessary for satisfactory approval are generally a black box process and not governed by a transparent industry standard.

As an industry, we need to implement a more rigorous qualification testing protocol for different mounting conditions. The reliance on a simple uniform pressure static loading test is insufficient to identify common failure mechanisms seen in the field today.

## PROPOSED TESTING CHANGES

The Interface (Module + Mounting) Test Protocol needs to be expanded:

- ▶ Implement module side-by-side testing
- ▶ Implement a true assessment of safety factor in uniform load testing (TTF)
- Implement baseline non-uniform load testing
- Implement realistic cyclical fatigue loading cycle
- Stop assuming 2400Pa testing is required and necessary

## NEXT STEPS

- Assemble a team of experts committed to contribute to solving this problem.
- Plan to restart IEC Module-Structure Interface standard.

Let us know!

**ARRAY**  
ARRAYTECHINC.COM

# Incentivizing Reliable PV through Insurance Premium Reduction

Hannah Rasmussen, Adam Shinn  
kWh Analytics

## Introduction

The 50-year life initiative, supported by the US Department of Energy (DOE), is principally interested in discovering actionable practices that extend the life of photovoltaic (PV) power plants, and developing incentives that reward the adoption of best practices.

Having insured \$40B in renewable assets, kWh Analytics is well-positioned to work with the DOE to develop insurance incentives with reliability in mind.

The Solar Revenue Put (SRP) is a production insurance product that protects asset owners from downside conditions. The SRP covers a band of production (e.g. P99 to P90), allowing asset owners to achieve more favorable debt financing. In this poster we explore the relationship between availability, inverter quality, and insurance premium.

The SRP model is trained on real-world performance data from the kWh Analytics database, estimating production in a probabilistic manner, such that we can quantify risk for insurance purposes.

## Three Case Studies

Quotes A and B each contain a single utility-scale system, each with an AC capacity over 200 MW. These systems are in Indiana and northwest Texas, respectively. Quote C contains 31 C&I systems. Their locations and AC capacities are described in the table below.

|         | Location               | AC Size    | # Systems |
|---------|------------------------|------------|-----------|
| Quote A | IN                     | > 200 MW   | 1         |
| Quote B | NW TX                  | > 400 MW   | 1         |
| Quote C | CO, HI, IL, MD, MN, NY | 0.5 – 6 MW | 31        |



If I'm not at my poster, scan here to learn more.



Acknowledgement: This material is based upon work supported by the U.S. Department of Energy's Office of Energy Efficiency and Renewable Energy (EERE) under the award number DE-EE0009827.  
Legal Disclaimer: The views expressed herein do not necessarily represent the views of the U.S. Department of Energy or the United States Government. The views expressed herein do not necessarily represent the views of the U.S. Department of Energy or the United States Government.

# Asset owners that achieve high availability deserve a 10-25% deduction on premium.

## Availability as an indicator of best practice adoption

As projected availability increases, SRP premium significantly decreases by 10-25%. By assigning higher availability to projects following best practices, the SRP rewards asset owners with a more affordable SRP quote. By enacting these best practices, the asset owner also develops a more reliable (and profitable) PV plant.

Gross Premium relative to 10 year P50 Revenue

|         | 95%   | 96%   | 97%   | 98%   | 99%   |
|---------|-------|-------|-------|-------|-------|
| Quote A | 4.95% | 4.54% | 4.15% | 3.80% | 3.47% |
| Quote B | 1.25% | 1.15% | 1.07% | 1.01% | 0.96% |
| Quote C | 0.87% | 0.82% | 0.79% | 0.78% | 0.78% |

Gross Premium relative to highest Gross Premium

|         | 95%    | 96%   | 97%   | 98%   | 99%   |
|---------|--------|-------|-------|-------|-------|
| Quote A | 100.0% | 91.7% | 83.9% | 76.7% | 70.1% |
| Quote B | 100.0% | 91.7% | 85.4% | 80.7% | 77.0% |
| Quote C | 100.0% | 93.8% | 90.8% | 89.4% | 88.9% |

## Inverter Manufacturer Matters

Despite less than a 6% difference in annual PI between the most performant and least performant inverter manufacturers (see figure at right), choosing the right inverter manufacturer can yield up to a 35% reduction in premium. Spending time to research reputable inverter manufacturers and investing in these higher quality inverters can save dividends on your SRP premium and improve your portfolio's performance over its lifetime.

Gross Premium relative to 10 year P50 Revenue

|         | W     | X     | Y     | Z     |
|---------|-------|-------|-------|-------|
| Quote A | 3.48% | 3.85% | 5.58% | 4.06% |
| Quote B | 0.96% | 1.02% | 1.47% | 1.05% |
| Quote C | 0.78% | 0.78% | 1.04% | 0.79% |

Gross Premium relative to highest Gross Premium

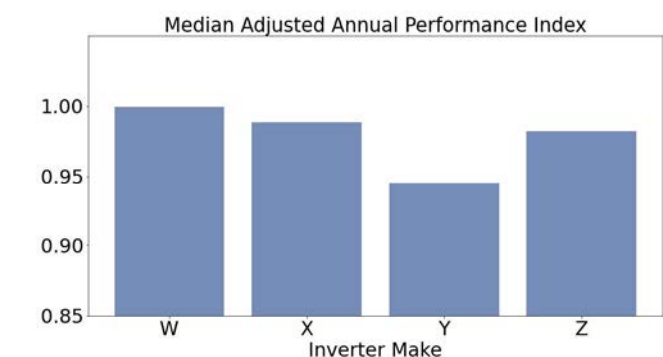
|         | W     | X     | Y      | Z     |
|---------|-------|-------|--------|-------|
| Quote A | 62.4% | 69.0% | 100.0% | 72.8% |
| Quote B | 65.7% | 69.3% | 100.0% | 71.7% |
| Quote C | 74.7% | 75.2% | 100.0% | 75.9% |

## Methods

To explore SRP premium differentiation among the three representative SRP case studies, we needed to settle on variables that would correlate highly with adoption of best practices. We chose availability and inverter make as these key variables.

We used availability as a quantitative indicator that could reflect adoption of qualitative best practices. These best practices could include implementing a spare parts strategy, working with trustworthy OEMs, having a robust preventative maintenance plan.

The kWh Analytics dataset shows that projects with different inverter makes have highly variable performance indices. We chose four common inverter makes and ran all three case studies with these inverter makes to explore their effect on SRP premium.



## Takeaways

- Premium increases as availability decreases
- Portfolio effect: as availability increases, portfolios see less of a deduction on premium than single systems

Diligent asset owners deserve credit for the things they're doing right:

- investing in inverters from high quality manufacturers
- following preventative maintenance best practices (see NREL PV O&M, 3rd edition),
- demonstrating consistent availability,
- working with trustworthy OEMs,
- having an effective spare parts plan, including IGBT and fan/cooling inverter components.

**Asset owners:** open a dialogue with your insurance broker/provider about whether you are getting credit for building resilient assets.



# Rapid Screening of SHJ and TOPCon Solar Cells for UV Degradation



J. Diego Zubieta Sempertegui<sup>1</sup>, Nicholas Moser-Mancewicz<sup>2</sup>, Jonah G. Gezelter<sup>1</sup>, Sophia Buffone<sup>1</sup>, Sijia Cheng<sup>1</sup>, Marina Kamperai<sup>1</sup>, Nqobile Gift Tshuma<sup>1</sup>, Gray Thomas<sup>1</sup>, Evan Jones<sup>1</sup>, Salma Bhar<sup>1</sup>, Carlos Biaou<sup>3</sup>, Jonathan L. Bryan<sup>3</sup>, Kristopher O. Davis<sup>4</sup>, Mariana I. Bertoni<sup>2</sup>, Ina T. Martin<sup>1</sup>, and Laura S. Bruckman<sup>1</sup>

<sup>1</sup> Case Western Reserve University, Cleveland, OH 44106, USA, <sup>2</sup>Arizona State University, Tempe, AZ 85281, USA,

<sup>3</sup>GAF Energy, San Jose, CA 95138, USA, <sup>4</sup>University of Central Florida, Orlando, FL 32816, USA

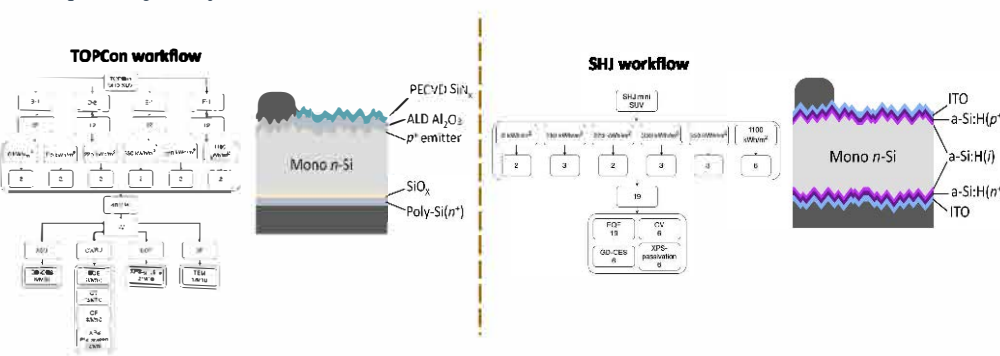
**AIM:** Develop an accelerated screening process for unencapsulated silicon solar cells for UV induced degradation.

## Motivation

Overall PV trends that motivate this work are:

- 1) High-efficiency TOPCon and SHJ cells are entering higher volume production
- 2) UV-transparent front materials are becoming more common

Defining a rapid screening process that includes UV losses is necessary to confidently adopt new materials and architectures.



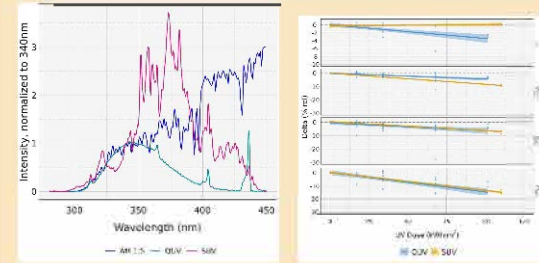
## Protocol Development and Results

### Accelerated Aging

Seek saturation through high intensity chambers (SUV)

| Chamber         | Intensity [W/m <sup>2</sup> ] |         | Hours to 220 kWh/m <sup>2</sup> TUV Dose |
|-----------------|-------------------------------|---------|--|
|                 | <340 nm                       | <400 nm |  |
| AM 1.5          | 9                             | 46      | 4700                                     |
| SUV (60-70 °C)* | 308                           | 2567    | 84                                       |
| QUV (50 °C)     | 16.4                          | 53      | 2600                                     |

\*SUV exposures were of M10 cells; QUV exposures were of diced cells



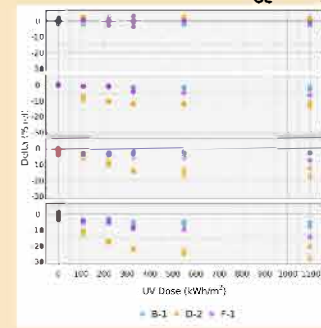
- TOPCon cells exposed to the same total UV dose from a low (QUV) vs. high (SUV) intensity UV source
- Similar degradation with exposure dose, some difference in fill factor and  $V_{oc}$
- Need to further control for chamber temperature and dicing effects

### TOPCon: 3 industrial manufacturers

Large variance between vendors

Electrical performance of SUV-exposed M10 cells

- Largest changes due to losing  $V_{oc}$  and  $I_{sc}$



### Material characterization: GD-OES (left) and XPS (right)

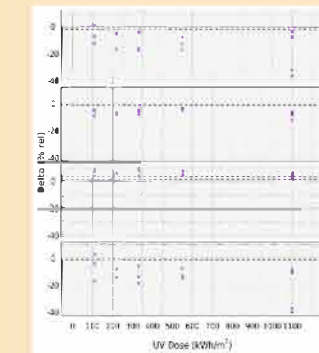
- Vendors B and D have similar  $\text{SiN}_x$  passivation layer compositions
- Largest difference in GD-OES data is the Al signal in  $\text{Al}_2\text{O}_3$ 
  - Separate CV measurements support hypothesis that this is due to difference in fixed negative charges ( $N_s$ )
  - More intense peak → more negative fixed charge within the  $\text{Al}_2\text{O}_3$  layer
- Error between measurements low among most signals (lines average n=5)

### SHJ: 1 laboratory-manufactured set

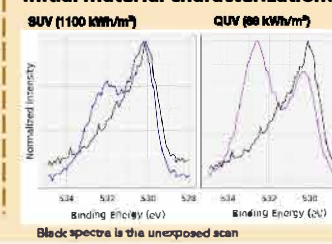
Lesser impact from UV exposure

Electrical performance of 1 x 1" cells fabricated at ASU

- Decrease in efficiency: losses in FF and  $V_{oc}$ ,  $I_{sc}$  remained stable
- Variation between samples



### Initial material characterization: XPS of ITO



- High resolution scan of O1s shows changes in bonding
- Increases in the peak at 533 eV associated with degradation products and adsorbates linked to degradation
- GD-OES will provide additional compositional information throughout the layers

## Next Steps

### Experimental:

- Exposure of industrial SHJ samples.
- Comparison of SUV to QUV, diced and undecided, up to 330 kWh/m<sup>2</sup>.
- Incorporate physics-based modeling and materials characterization data as mechanistic variables in modelling.

### Industrial application:

- Vetting accelerated exposure techniques for transferability to encapsulated modules and outdoor exposure.
- Recommendations to manufacturers on mitigating sources of degradation.

## Acknowledgments

Materials and device characterization at CWRU were performed in the CSE Swagelok Center for Surface Analysis of Materials, the Solar Durability and Lifetime Extension Center, and the CWRU Materials for Optoelectronics Research and Education (MORE) Center.

The authors acknowledge resources and support from the Advanced Electronics and Photonics Core Facility at Arizona State University

This material is based upon work supported by the U.S. Department of Energy's Office of Energy Efficiency and Renewable Energy (EERE) under Solar Energy Technologies Office (SETO) Agreement Number DE-E0010250. The views expressed herein do not necessarily represent the views of the U.S. Department of Energy or the United States Government.

## References

- [1] Iqbal et al. (2022) "Accelerate Cycles of Learning: Unencapsulated Silicon Photovoltaic Cells to Environmental Stressors." 2022 IEEE 49th PVSC, 0668-74.
- [2] Sinha et al. (2023) "UV-Induced Degradation of High-Efficiency Silicon PV Modules with Different Cell Architectures." *Prog. Photovolt. Res. Appl.*, 31, no. 1: 36-51.
- [3] Gebhardt et al. (2025) "Reliability of Commercial TOPCon PV Modules - An Extensive Comparative Study." *Prog. Photovolt. Res. Appl.*
- [4] Thome et al. (2024) "UV-Induced Degradation of Industrial PERC, TOPCon, and HJT Solar Cells: The Next Big Reliability Challenge?." *solar R&R*, 8: 2400628.
- [5] Veldt-Wolf et al. (2018) "Specie-Dependent Stability of the Passivation Quality of  $\text{Al}_2\text{O}_3/\text{Si}$  Interfaces." *IEEE J. Photovolt.*, 8, no. 1: 96-102.

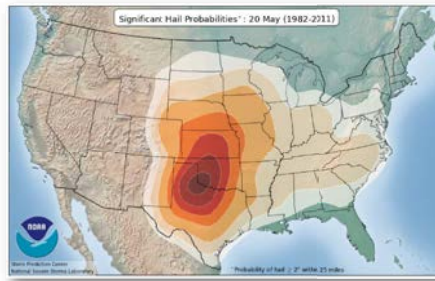
# Best practices for hail damage recovery

Technology Advisory Practice, ICF Inc.

Stephen Ressler and Leah Holton, ICF



Over the past decade, U.S. PV projects have been increasingly built in states with a history of severe hail events. Texas, parts of which have significant risk of storms producing hail over 35 mm diameter, had PV facilities totaling almost 38 GW through Q3 2024. Increasing electric demand to support data center growth suggests non-traditional PV markets may be expected to develop in other regions with high hail risk. While equipment suppliers and system operators are developing new solutions to improve severe hail survivability, portions of the existing installed base will continue to be at risk for the remainder of their typical 30-to-40-year useful lives.



But hail damage restoration is usually not as simple as ordering new equipment...

## Assessing the damage

A visual aerial survey typically provides the fastest assessment but may only capture gross damage.

An aerial IR survey provides a fast and more granular assessment but may miss unusual damage like broken back glass on modules with unbroken front glass.

A ground based visual inspection can provide a detailed assessment but requires significant time, labor, and knowledgeable inspectors.

EL imaging provides the highest resolution assessment and likely the best tool to identify cell-level impact damage, but time and cost currently limits it to random sampling.

## Sourcing replacement equipment

Matching original crystalline silicon PV modules may be challenging once a site is several years old.

For alternate modules (brands or models) one must match electrical specifications (being sure to account for original module degradation), dimensional and structural specifications (compatible with mounting system), wiring length, and of course, ensure the module connectors are compatible!

If procuring warehoused or old stock, consider engaging a third-party inspector to ensure modules were built to expected quality specifications and have not been damaged in storage.

## Planning

Hail damage can be chaotic and randomly dispersed, should (apparently) nondamaged modules be consolidated?

Consider every handling of a module adds labor cost plus introduces a nonzero risk of module damage. But mixing original and replacement modules may complicate O&M. If replacement modules are a different power class or original modules have significant degradation, mixing replacement and original modules likely increases mismatch losses.

Should modules with unbroken glass be replaced if there is a future reliability risk from hail-damaged cells?

Account for partial facility operation in timeline and costs.

## Restoration

If replacement modules are unavailable, it may present an opportunity to repower the facility with updated equipment, effectively resetting to original or higher capacity.

Validate the updated facility generation model using experienced subject matter experts to ensure the restored facility will meet stakeholder expectations.

Look for contractors whose experience includes restoration work as labor cost and scheduling for restoration work is typically not the same as greenfield construction.

Expect to find unexpected damage once underway!

## About ICF

ICF is one of the world's leading independent management and analytical consulting firms with more than 9,000 employees across the globe. With over 2,000 experts working on energy and environmental issues, ICF draws on extensive industry knowledge and innovative forecasting tools to develop solutions to complex energy issues. ICF's technical advisory practice provides independent engineering, owner's advisory, and expert testimony services. The core team has supported over \$90B in generation and infrastructure transactions and is made up of engineers, scientists, and technical experts that have served financial institutions, power producers, and project developers for decades through detailed technical diligence on a wide array of power projects. Learn more at [icf.com/energy](http://icf.com/energy).

Get in touch with us:

**Stephen Ressler**  
Stephen.Ressler@icf.com

**Leah Holton**  
Leah.Holton@icf.com

# Reliable design: establishing a feedback loop between real-world and design conditions



Daniel Herron, Andrew Lindsay, Marc Toro

## Introduction

- Site conditions included in project design often differ from the conditions EPCs encounter when civil activities are finished and pile install is set to begin
- This is true for projects located on flat land, but it is especially true for projects designed on uneven terrain
- Deviations create unique challenges and potential delays during the design and construction phase of a solar project
- If deviations are not addressed in the early stages of project construction, they create a reliability risk once the site becomes operational
- Nevados has instituted several process and product solutions to minimize deviations and mitigate reliability risk when deviations are present

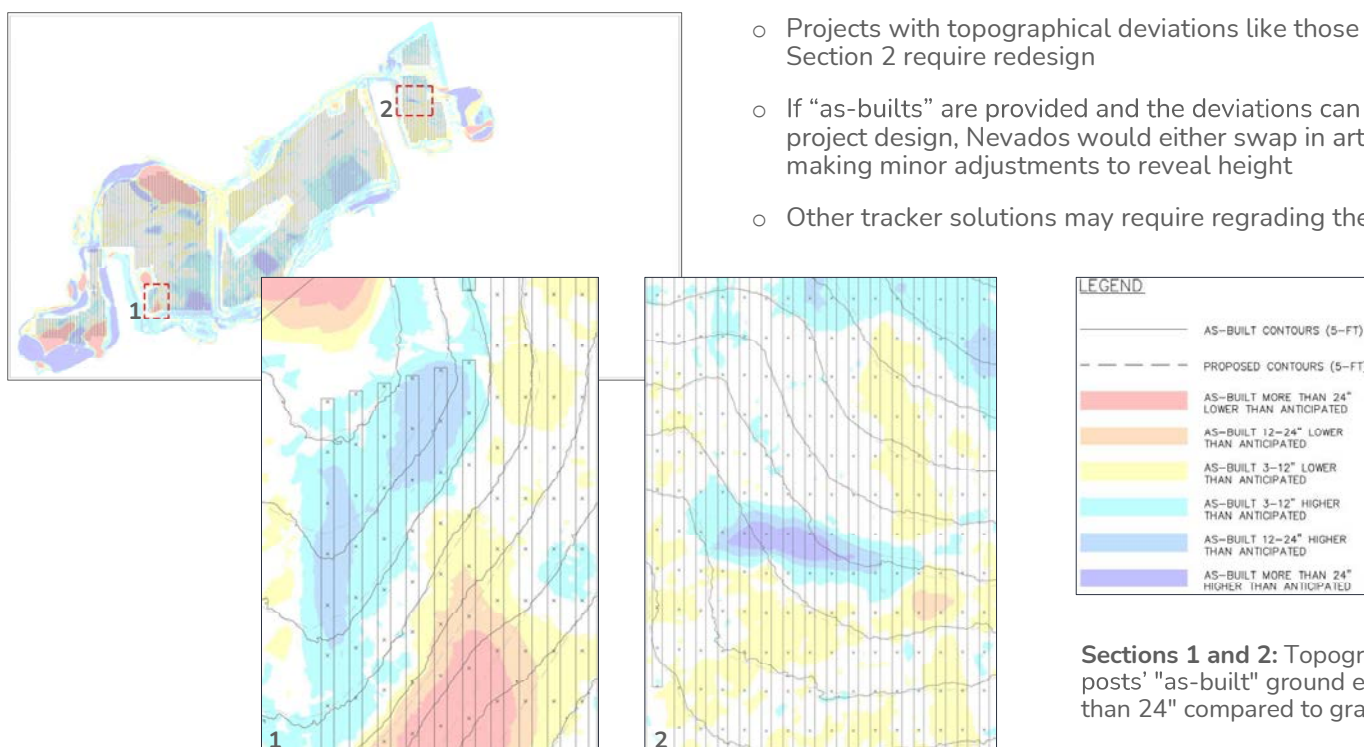
## Methods

- Inputs provided by the on-site installation team define the topographical layout of the site at multiple points during the project design and construction timeline
- Project design would consider topographical inputs in (at least) three stages:

| Stage | Grade    | Description                            |
|-------|----------|--|
| 1     | Existing | Baseline for initiating project design |
| 2     | Proposed | Confirm project design matches civil   |
| 3     | As-built | Topo after completion of civil work    |

- Nevados used the data from Stages 2 and 3 to complete a comparative grading analysis to evaluate the differences between anticipated and real-world topography for a sample project site

## Results



**Sections 1 and 2:** Topographical view of tracker posts' "as-built" ground elevations which vary more than 24" compared to grading plan

## Reliability Impacts

When site conditions are not accurately represented in the final project design, this can create several potential reliability risks, including but not limited to:

- Tracker equipment (couplers, torque tubes) utilized outside of their design tolerance and load capacity
- Improper module clearance which creates module and tracker reliability risk during flood or snow conditions
- Performance risk created by suboptimal tracking schedules that do not appropriately account for terrain

## Conclusions

- To establish a feedback loop, the industry needs to include the collection and distribution of LiDAR "as-built" conditions to relevant project design partners as a standard project design step
- Incorporating "as-builts" in project design is a key part of mitigating the potential reliability risk associated with building on challenging terrain
- As new developers enter the market while we shift towards developing terrain-challenged solar projects, it is especially important to educate the industry on best practices to avoid creating unnecessary reliability risk

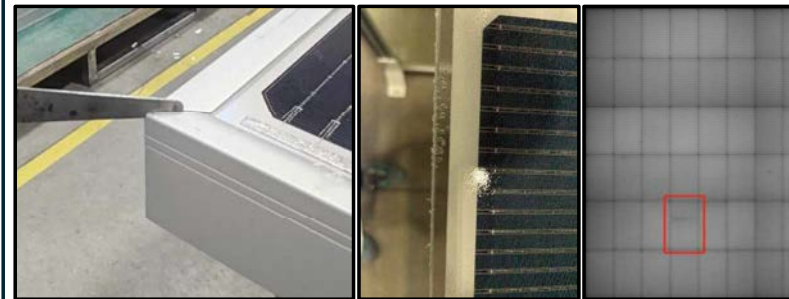
## Introduction

### What do we do at RWE Clean Energy?

RWECE is a renewables developer, owner, and operator focused on building utility-scale solar, wind, BESS and green hydrogen systems across the United States.

### Why are we concerned with module due diligence?

RWECE achieves economies of scale by procuring modules for all its solar PV projects. This means multi-year, bulk procurement purchases to meet the project pipeline, or one-off purchase orders to meet project CODs due to geopolitics and availabilities. In both scenarios, as an owner/operator, RWECE faces module reliability issues in production, transportation, construction, and operation, prompting the need to perform due diligence to de-risk any systematic module related issues. Some examples of issues we experienced are frame gaps, bubbles, cracked connectors, scratched cells, misalignment of connectors, etc.



## Methodology

### How do we tackle module due diligence at scale?

We broke down the challenge into three sub-categories:

#### 1. OEM Assessment

- Leverage the internal procurement team for their commercial knowledge and relationship with OEMs.
- Reference the annually released PVEL Scorecard and subscribe to quarterly reports such as BloombergNEF and PVTECH Bankability.
- Create a rubric to rate the OEMs based on industry standing and supply chain capabilities.

#### 2. Product Qualification

- Update the technical exhibit in the module procurement MSA, indicating classes of acceptable modules.
- Introduce more rigorous QA/QC for factory audits, in-line production monitoring, and pre-shipment inspections.

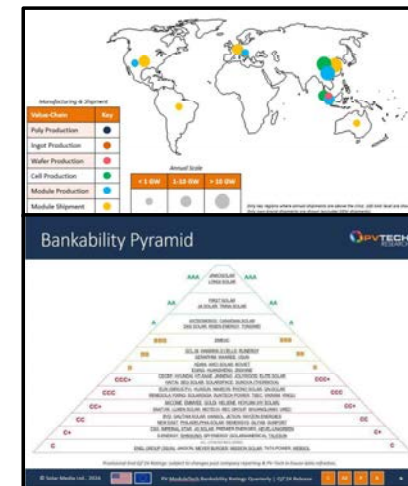
#### 3. Technical Diligence

- Create a standard for tracking and reviewing documentation provided by OEMs, focused on certifications and test reports.
- Use the provided documentation to score modules based on product specific risk parameters and 3<sup>rd</sup> party ranking scorecards.

## OEM Assessment

The OEM criteria takes **6 different metrics**, equally weighted, and classifies the OEMs into **4 categories** – **Proven, Established, Qualified, and Not Qualified**. “Industry Standing” metrics are developed using ratings provided for the OEMs from three different sources – BloombergNEF, PVEL Scorecard, and PVTECH’s Bankability Report. The three “Supply Chain” metrics focuses on domestic content, importability and tariff implications, and global presence. Lastly, the scoring logic shown below is used to score the OEM, ultimately placing it in one of the four categories. Based on this scoring and of the Tier 1 vendors that RWECE works with, **50% are Qualified, 40% are Established, and 10% are Proven**. Quarterly review of the OEMs industry standing and supply chain enables RWECE to assess the continuous viability of the OEMs.

| Scoring Logic |                                   |
|---------------|-----------------------------------|
|               | Score out of 24, equally weighted |
| 6             | 25%                               |
| 7             | 29%                               |
| 8             | 33%                               |
| 9             | 38%                               |
| 10            | 42%                               |
| 11            | 46%                               |
| 12            | 50%                               |
| 13            | 54%                               |
| 14            | 58%                               |
| 15            | 63%                               |
| 16            | 67%                               |
| 17            | 71%                               |
| 18            | 75%                               |
| 19            | 79%                               |
| 20            | 83%                               |
| 21            | 88%                               |
| 22            | 92%                               |
| 23            | 96%                               |
| 24            | 100%                              |
|               | Proven                            |
|               | Proven                            |



## Product Qualification

In collaboration with DNV, the technical exhibit that is a part of every module procurement contract was overhauled to reflect more stringent requirements for certifications, testing, and auditing. Naturally, **3 classes** of module procurement emerged, ranking from highest quality to acceptable quality. Other updates to the exhibit include detailed BOM specifications, extended reliability testing requirements, stricter factory audits, and production monitoring sampling requirements. The table below shows a high-level snapshot of the requirements of the 3 classes:

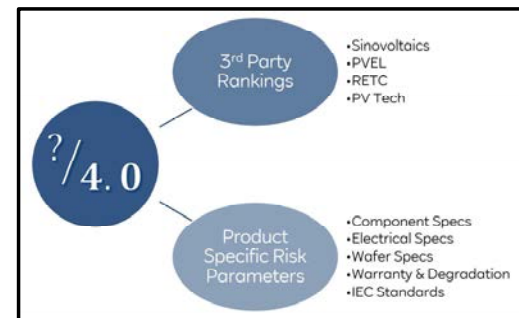
|                                   | Class A                                  | Class B                                 | Class C                                 |
|-----------------------------------|--|---|---|
| Certification requirements        | ISO 9001<br>ISO 14001<br>OHSAS 18001     | ISO 9001<br>ISO 14001<br>OHSAS 18001    | ISO 9001<br>ISO 14001<br>OHSAS 18001    |
| Testing requirements              | IEC 63209+ <2%<br>IEC 61215<br>IEC 61730 | IEC 63209 <2%<br>IEC 61215<br>IEC 61730 | IEC 63209 <5%<br>IEC 61215<br>IEC 61730 |
| Factory audit                     | leading                                  | leading & in-line                       | leading & in-line                       |
| In-line production monitoring     | ✓  | ✓                                       | ✓                                       |
| Pre-shipment inspection           | ✓  | ✓                                       | ✓                                       |
| BOM(s) details and specifications | Detailed BOM for all modules             | Detailed BOM for all modules            | High level BOM(s)                       |

## Technical Diligence

The first step of the technical diligence process is to collect the correct and latest set of documentation for the module models. RWECE requests the following list of documents from the module OEMs:

- Datasheet
- Installation Manual
- 3rd Party PAN File
- IEC 61215 Certification
- IEC 61730 Certification
- LID + LeTID Test Report
- PID Test Report
- Hail Test Report
- Extended Reliability Test Report
- Additional Testing Program
- 3rd Party Bankability Report
- Authorization to mark
- Performance Warranty
- Product Warranty
- Packaging Manual
- Additional Technical Papers

Using the documentation listed above, the second step of technical diligence process is to score the module models. A **score out of 4** is generated against product specific risk parameters, which is given a weight of 85%, and 3<sup>rd</sup> party product rankings, which is given a weight of 15%. The inputs for both risk parameters and 3<sup>rd</sup> party ranking providers is shown below:



## Conclusion

In summary, the outlined process significantly improves RWECE’s chances of procuring more robust and reliable modules. A three-pronged approach evaluating the OEM’s company at large, manufacturing processes, and module offerings allows reliability issues to be caught earlier and remediated or avoided altogether. This poster was prepared in efforts to provide a framework for module procurement and driving the industry towards requesting higher quality of our PV module suppliers.

Next steps for RWECE includes the following:

- Quarterly refreshes of this standardized process
- Incorporation of OEM/client relationship as a metric towards OEM assessment. This aims to target the OEM’s transparency, attention to problems, response rate, etc.
- Integration of LCOE in order to provide a financial ranking for the various product offerings.

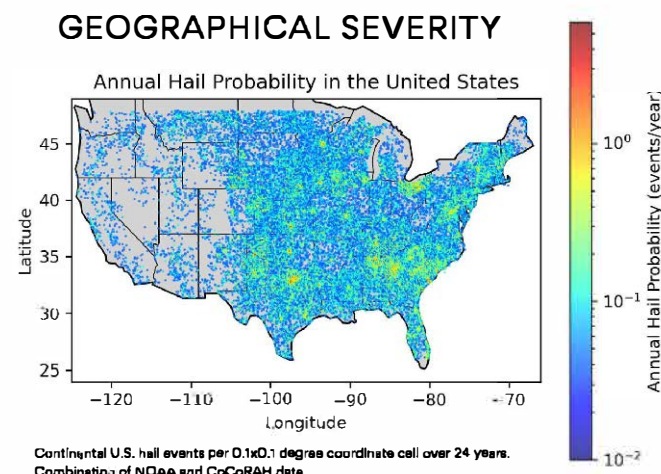
# SIDE-BY-SIDE COMPARISON OF HAIL DAMAGE MITIGATION

KYLE REITER  
MICHAEL BOLEN  
DAVE DOERNER

## FIELD DEMO SNEAK PEAK

### MOTIVATION

- Damage to large-scale solar plants caused by hailstorms in the United States has created significant financial risks for insurers and stakeholders.
  - Hail damage accounts for over 50% of solar plant losses with an average of \$58 million per claim (1).
  - Insurance company premiums have increased as much as 400% while simultaneously lowering coverage caps (2,3).
- Hail impact can compromise the PV module resulting in power loss and/or safety hazards. (4)
- Climate change is increasing hailstorm severity and frequency. Larger hail stones are becoming more common (5).
  - Larger hail stones have more kinetic energy due to increased mass and terminal velocity, which increases damage potential.
- Knowledge sharing is leading to improved hail mitigation strategies to reduce damage claims and improve resiliency.
- SB Energy has designed and constructed a field-based experiment to do a side-by-side analysis of hail damage mitigation.



### METHODOLOGY

- SB Energy is testing the capability to measure and mitigate hail damage at their Innovation Center by implementing different hail stow angles (60, 0, -60 degrees) in addition to using different front sheet glass thicknesses (2, 2.8, 3.2, 4.0 mm) in a side-by-side field experiment.
- SB Energy is testing the capability to measure and mitigate hail damage at their Innovation Center by implementing different hail stow angles (60, 0, -60 degrees) in addition to using different front sheet glass thicknesses (2, 2.8, 3.2, 4.0 mm) in a side-by-side field experiment.
- Hail-stow away panel positioning will be triggered by a forecasting system where localized hail alerts will automate hail mitigation to a pre-programmed stow position best suited for that geographical location.
- The kinetic energy of natural hail stones will be measured using plane-of-array hail sensors.
- I-V, IR, and EL measurements will be taken before and after a natural hail storm, which typically happens a couple times per year at the site.
- The results of this experiment will inform:
  - Relative efficacy of active and passive hail mitigation options
  - Technologies to deploy at large-scale commercial plants in hail-prone regions.

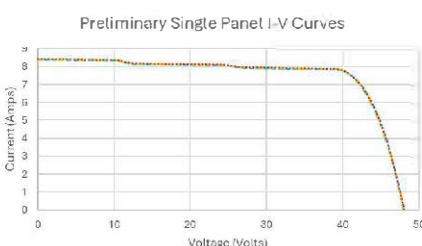


| Glass to Glass PV Modules |            | Glass to Backsheet PV Modules |            |
|---------------------------|------------|-------------------------------|------------|
| Glass Thickness           | Row/Angle  | Glass Thickness               | Row/Angle  |
| 2.0 mm                    | Row 4/ 0°  | 3.2mm                         | Row 6/-60° |
| 2.0 mm                    | Row 2/60°  | 3.2mm                         | Row 5/ 0°  |
| 2.0 mm                    | Row 1/-60° | 3.2mm                         | Row 4/ 60° |
| 2.0 mm                    | Row 1/ 0°  | 3.2mm                         | Row 3/ 60° |
| 2.0 mm                    | Row 2/ 0°  | 4mm                           | Row 2/ 60° |
| 2.8 mm                    | Row 4/ 0°  | 4mm                           | Row 6/-60° |
| 2.8 mm                    | Row 5/-60° | 4mm                           | Row 5/ 0°  |
|                           |            | 4mm                           | Row 4/ 60° |



### MEASUREMENTS

#### I-V

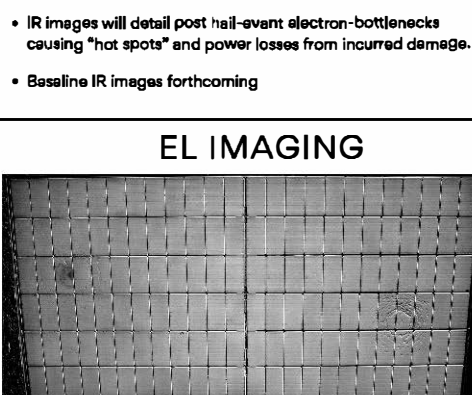


Example preliminary I-V curve measurement of solar panels.

| I-V Run  | Voc (V) | Jsc (A/m²) | FF    | Pmax (W) | Vmp (V) | Imp (A/m²) | Rs (Ω) | Rsh (Ω) |
|----------|---------|------------|-------|----------|---------|------------|--------|---------|
| Module 1 | 48.02   | 8.40       | 77.14 | 311.01   | 40.40   | 7.70       | 77.76  | 0.53    |
| Module 2 | 48.05   | 8.40       | 77.10 | 311.13   | 40.35   | 7.71       | 111.28 | 0.71    |
| Module 3 | 47.99   | 8.42       | 76.77 | 310.29   | 40.24   | 7.71       | 111.28 | 0.70    |
| Module 4 | 48.02   | 8.41       | 76.93 | 310.53   | 40.27   | 7.71       | 81.56  | 0.53    |

- Initial I-V traces provide a PV module performance baseline. After a hail event I-V measurements will be taken to assess the reduction in performance and provide guidance on what hail damage mitigation method was most effective.

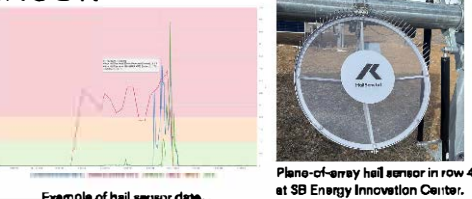
#### IR IMAGING



#### EL IMAGING

- EL imaging will provide understanding of unexpected recombination after a hail event from defects or cracks.

#### HAIL SENSOR



### SUMMARY AND FUTURE WORK

- Active and passive hail damage mitigation techniques are being compared side-by-side in the field at SB Energy's Innovation Center.
- Results, following a natural hail event, will provide valuable insights into the efficacy of market-ready technologies and support business decisions regarding the deployment of hail mitigation techniques for large-scale solar plants in hail-prone areas.



1 GRITZO, L., DR. (2024, JULY 10). MOTHER NATURE CHALLENGES RENEWABLE ENERGY INSURANCE/. FORBES. RETRIEVED FEBRUARY 6, 2025, FROM <https://www.forbes.com/sites/leslong/2024/07/10/mother-nature-challenges-renewable-energy-insurance/>

2 DEGENNARO, H. (2024, JULY 30). HAIL RISE MAY BRING FINANCIAL INSTABILITY TO SOLAR PROJECTS. POWER MAGAZINE. RETRIEVED FEBRUARY 6, 2025, FROM <https://www.powermag.com/best-practices-for-mitigating-hail-damage-to-solar-projects/>

3 SUPRAWA CHAKRABORTY, AVINASH KUMAR HAL DIKAR, NAI JAPANEKI MANOJ KUMAR, ANAJI YBIS OF THE HAIL IMPACTS ON THE PERFORMANCE OF COMMERCIALLY AVAILABLE PHOTOVOLTAIC MODULES OF VARYING FRONT GLASS THICKNESS. RENEWABLE ENERGY, VOL 100, 2023, PAGES 345-356, ISSN 0960-1481, HTTP://DOI.ORG/10.1016/J.RENENE.2022.12.061

4 GENSINI, V.A., ASHLEY, W.S., MICHAELIS, A.C. ET AL. HAILSTONE SIZE DICHOTOMY IN A WARMING CLIMATE. NPJ CLIM ATMOS SCI 7, 185 (2024). HTTP://DOI.ORG/10.1038/s41562-024-00728-3

# Fluctuating PV Module Wind Loads

Yarrow Fewless  
Principal  
yfewless@cppwind.com

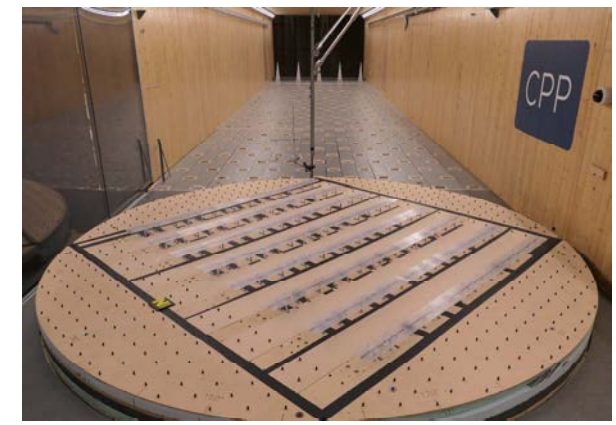
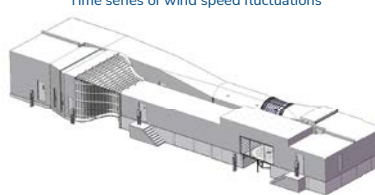
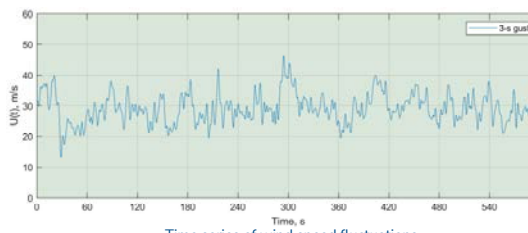
CPP WIND ENGINEERING CONSULTANTS

## Introduction

There is considerable interest in the health of solar photovoltaic (PV) modules in the field. One of the main concerns is that current module testing standards only consider a steady load (non-fluctuating) applied with an even distribution, i.e. with no asymmetry, when it is well known that the wind fluctuates and in typical ground mount applications the loading on a module is significantly asymmetric in many cases. This is especially true for modules in single portrait orientation (1P) where a single module experiences the full gradient from the leading edge to the trailing edge.

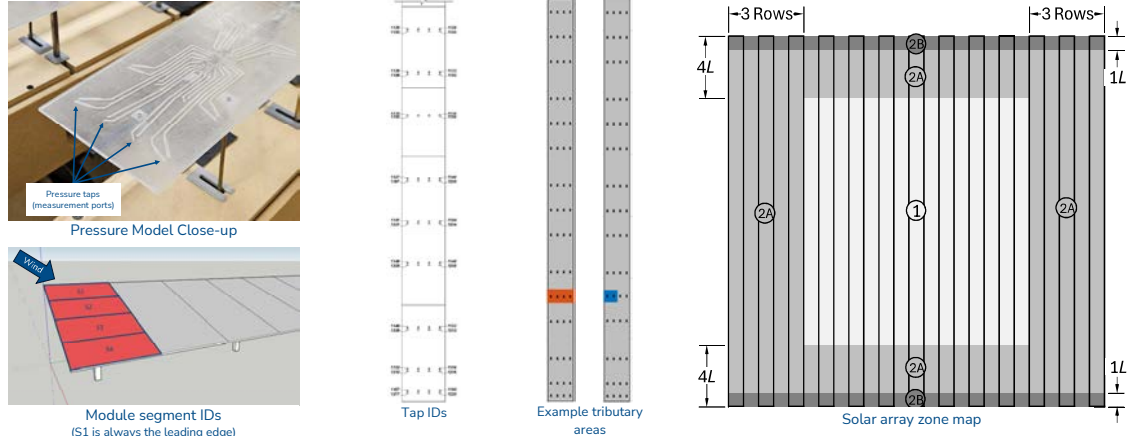
This poster presents load patterns on modules in the 1P configuration. The results are based on wind tunnel tests carried out in one of CPP's atmospheric boundary layer wind tunnels. This type of wind tunnel is designed to reproduce the gustiness of the wind at model scale.

The desired outcome from presenting this poster is to inspire improvement of the testing methods so we can have faith that module reliability can be predicted.



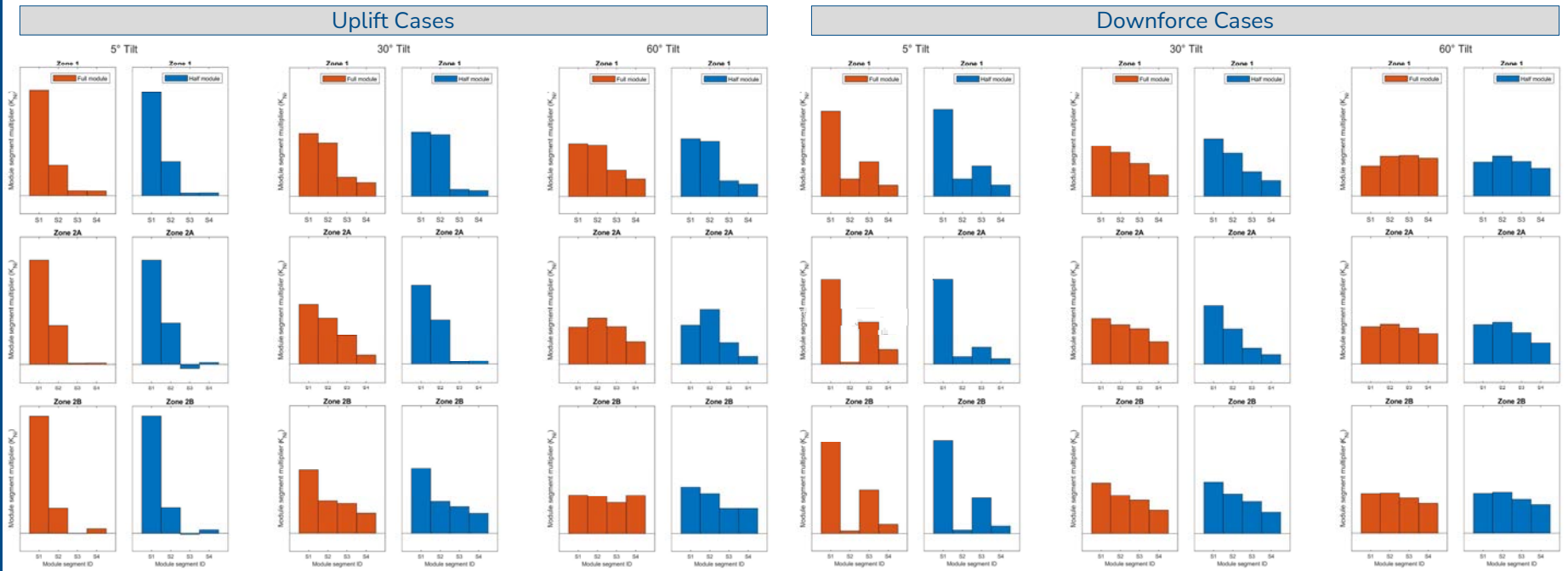
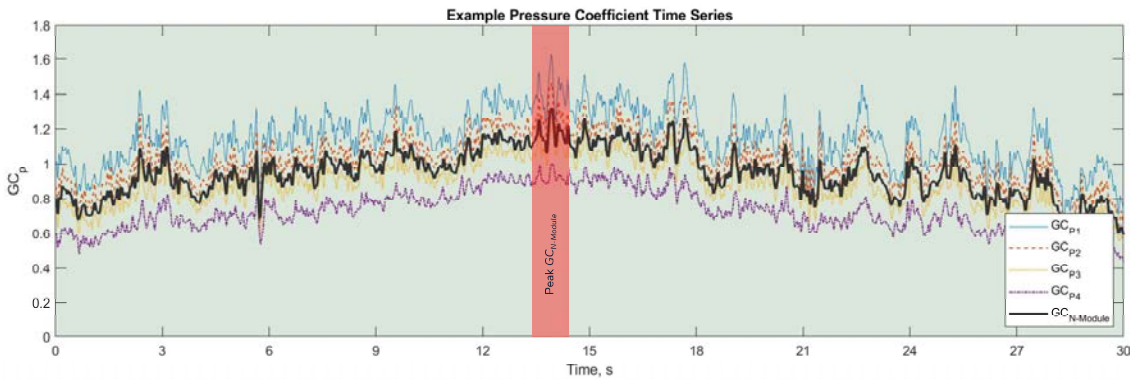
## Methods

- Model the array at ~1:20 scale, incorporating pressure measurement instrumentation.
- Test in 10° increments of approach wind direction in an atmospheric boundary layer wind tunnel set up for the model scale.
- Test tilts from 0° to 75° (only 5°, 30°, and 60° are presented); range of GCR/height
- Analyze the data to find the peak load on a module or half of a module in different array zones. See array zone map at far right.
- Divide the module area into four segments and extract the pressure distribution, then normalize the pressures by dividing by the peak full-module pressure.
- Present results as four equally sized 'module segment multipliers' ( $K_{Ni}$ ). The average of  $K_{Ni}$  ( $i=1$  to 4) for the full-module case is 1.00.



## Results

- A short example timeseries of the fluctuating pressure coefficients on the module is shown at right. This is a case with the nose up into the wind, i.e. an uplift case.
- The four  $GC_{Ni}$  series are the fluctuating pressure coefficients in the four segments of the module.
- The  $GC_{N-Module}$  series is the area averaged normal force coefficient on the full module area.
- Considerable fluctuation and asymmetry is evident.
- Normalized load cases are shown below. Notes:
  - Lower tilts show greater asymmetry.
  - Downforce at steep tilts show the most symmetrical load, though in most cases still somewhat unbalanced.



## Conclusions

- Loads fluctuate considerably in time and are usually significantly asymmetric
- Tilt has a significant effect on the load pattern, with lower tilts more asymmetric
- Uplift and downforce are different enough to not be lumped together
- Inertial loads from vibration are not presented here, and can vary considerably depending on the system design. They can make the loading more asymmetric. They can be determined through analysis of the wind tunnel data for application in the physical loading test.
- It's important to question if the symmetric sandbag test has any relevance given the asymmetry and fluctuations. Asymmetric and fluctuating (cyclical) testing may be required.



# Comparative Dust Soiling Assessment for PV systems: Evaluating Multiple Methodologies



Sha Li<sup>1</sup>, Brett Pendleton<sup>1</sup>, Thore Müller<sup>2</sup>

<sup>1</sup>Leeward Renewable Energy, Dallas, Texas, USA, <sup>2</sup>PVRADAR, Munich, Germany

## Abstract

Dust accumulation on solar panels reduces the amount of sunlight reaching the photovoltaic (PV) cells, therefore decreases energy production and overall system efficiency. Various methods, such as optical or electrical sensors, manual cleaning comparisons, and different soiling models can be used to quantify soiling losses. In this study, we present a comparative study of different soiling assessment strategies at two PV power plants in California. The methodologies of each strategy and their potential and the limitations are discussed in this study, to support a comprehensive, data-driven soiling assessment approach. The findings from this study offer valuable insights into optimizing cleaning schedules and strategies for operating assets and improving soiling model accuracy for development assets in future PV plants.

## Methodology and Assumptions

The two PV power plants are located in Antelope Valley, California. The two sites have never been washed since commissioning was complete. The major PV array equipment on site are thin-film frameless modules that are placed on single axis trackers. Both power plants have optical soiling devices installed but the data has obvious issues. Therefore, we are evaluating the following methodologies in order to accurately assess the soiling level on-site.

1) Kimber Model<sup>1</sup>: 0.03%/day soiling rate, with 6mm rain cleaning threshold and no grace period nor manual cleaning (default model parameters).

2) Humboldt State University (HSU) Model<sup>2,3</sup>: Assuming 6mm rain cleaning threshold for direct comparison with Kimber model. Particle concentrations data (PM2.5 & PM10) is sourced from MERRA-2.

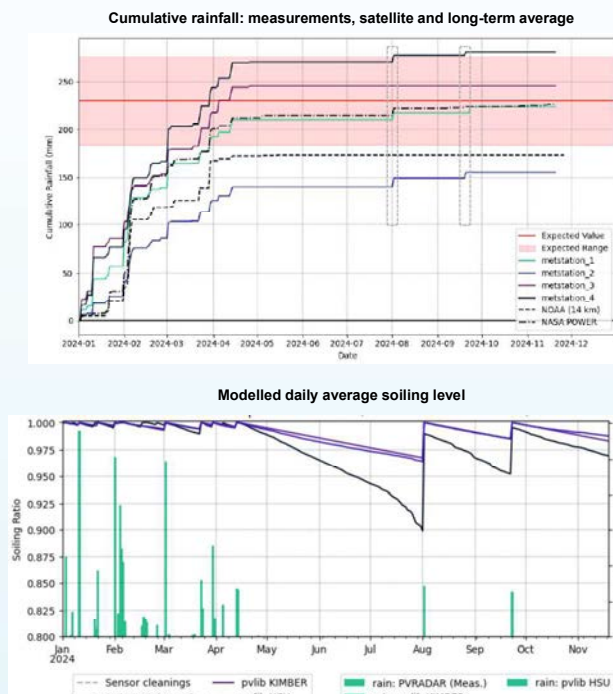
3) PVRADAR Model<sup>4</sup>: Proprietary physical soiling model primarily based on particle concentrations from MERRA-2, incorporating meteorological factors and plant design characteristics.

On-site rain measurements have been processed/aggregated to be compared with the satellite data to determine agreement and exclude faulty data. The best-fit rain measurement was selected as input for all three models above.

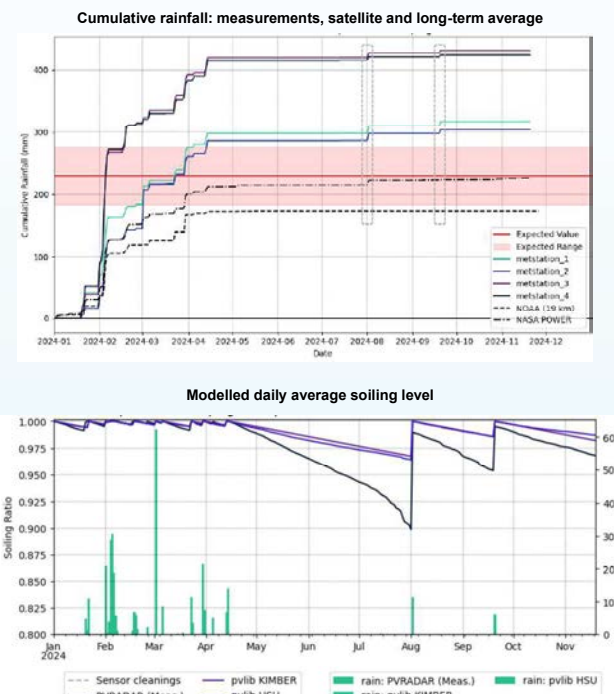
4) I-V curve trace individual modules and strings at different locations spread across the PV power plants before and after wash the modules and compare the results. This method is a classical method to measure soiling, therefore has been used to validate the modeling results.



## Results Project 1



## Results Project 2



## Avg. soiling loss factors in % for each month of the modelled period from all three soiling models and as measured.

| Project   | Method                     | 24-Jan | 24-Feb | 24-Mar | 24-Apr | 24-May | 24-Jun | 24-Jul | 24-Aug | 24-Sep | 24-Oct | 24-Nov |
|-----------|----------------------------|--------|--------|--------|--------|--------|--------|--------|--------|--------|--------|--------|
| Project 1 | Kimber Model               | 0.12   | 0.26   | 0.25   | 0.21   | 0.93   | 1.84   | 2.76   | 0.55   | 0.9    | 0.67   | 1.3    |
|           | HSU Model                  | 0      | 0.1    | 0.19   | 0.2    | 1.29   | 2.17   | 3.1    | 0.58   | 0.73   | 0.68   | 1      |
|           | PVRADAR                    | 0.17   | 0.11   | 0.43   | 0.39   | 2.29   | 4.56   | 7.28   | 2.23   | 3.14   | 1.63   | 2.67   |
|           | IV Curve Tracing early Nov |        |        |        |        |        |        |        |        |        |        | 2.84   |
|           | IV Curve Tracing late Nov  |        |        |        |        |        |        |        |        |        |        | 1.93   |
| Project   | Method                     | 24-Jan | 24-Feb | 24-Mar | 24-Apr | 24-May | 24-Jun | 24-Jul | 24-Aug | 24-Sep | 24-Oct | 24-Nov |
| Project 2 | Kimber Model               | 0.12   | 0      | 0      | 0      | 1      | 1.9    | 2.81   | 0.52   | 0.63   | 0.81   | 1.5    |
|           | HSU Model                  | 0.16   | 0      | 0      | 0.17   | 1.29   | 2.17   | 3.1    | 0.58   | 0.63   | 0.77   | 1      |
|           | PVRADAR                    | 0.36   | 0.1    | 0.32   | 0.39   | 2.29   | 4.56   | 7.28   | 2.2    | 2.8    | 1.8    | 2.8    |
|           | IV Curve Tracing early Nov |        |        |        |        |        |        |        |        |        |        | 2.84   |
|           | IV Curve Tracing late Nov  |        |        |        |        |        |        |        |        |        |        | 3.4    |

## Conclusion and Future Work

In this study, we compared different soiling assessment approaches at two PV power plants in California. The PVRADAR model matches well with I-V curve tracing result which was conducted in Nov 2024. Both Kimber and HSU Model underestimates soiling level for both projects.

We aim to build a database with available soiling measurements from Measurement Campaigns at different project locations/climate and further validate and stress test different models. By coupling on-site measurements with modeling efforts, this process enables a data-driven approach to accurately assess soiling levels on-site for operational assets. The approach also enhances our confidence in predicting soiling level for future development assets and arranging/optimizing cleaning schedules for operational assets by using the best-fit model with tuned parameters.

- Kimber model results heavily rely on input assumptions such as soiling loss rate (energy lost due to one day of soiling), rain cleaning threshold (amount of daily rainfall required to clean the panels) and grace period (# of days after a rainfall event when it is assumed the ground is damp, and so it is assumed there is no soiling). Different combinations of these input parameters will yield different results. Most of the time, such parameters might be changing month over month (i.e. different monthly soiling loss rate). Partial cleaning occurs because light rain might not fully wash everything away. The above-mentioned reasons pose challenges in determining accurate input assumptions and therefore impact accuracy of the final soiling results.
- HSU model has similar limitations as specifying accurate input assumptions (rain cleaning threshold, deposition or settling velocity of particulates)
- PVRADAR's soiling model is location-specific, based on particulate matter concentrations, meteorological conditions, and plant design parameters. Instead of assuming a fixed soiling rate as input, it dynamically calculates soiling by integrating multiple physical processes. It first determines the rate at which particles deposit on the module surface, accounting for factors such as tilt angle, time-varying tilt for trackers, night stow position, and humidity. It then models how these deposited particles accumulate on the glass, incorporating the effects of precipitation and partial cleaning by light rain. Finally, it calculates how accumulated particles attenuate incoming irradiance as a function of their optical properties. The soiling rate can be derived as the rate of change of the soiling level over time.
- I-V curve tracing dirty and clean modules is used to validate which models are more accurate. The primary issue with this method is the cost and labor-intensive associated with manually washing and I-V curve tracing modules, which results in limited data point throughout the year. Effective operational practices to handle I-V curve tracing must be implemented to ensure accuracy and repeatability. I-V curve data needs to be properly processed (irradiance, temperature adjustment). Both short circuit current and maximum power drop needs to be compared and studied.

## References

- [1] A. Kimber, L. Mitchell, S. Nogradi, and H. Wenger, "The Effect of Soiling on Large Grid-Connected Photovoltaic Systems in California and the Southwest Region of the United States," 2006 IEEE 4th World Conference on Photovoltaic Energy Conference. 2006. doi: [10.1109/wcpv.2006.279690](https://doi.org/10.1109/wcpv.2006.279690)
- [2] M. Coello and L. Boyle, "Simple Model for Predicting Time Series Soiling of Photovoltaic Panels," IEEE Journal of Photovoltaics, vol. 9, no. 5, pp. 1382–1387, Sep. 2019. doi: [10.1109/jphotov.2019.2919628](https://doi.org/10.1109/jphotov.2019.2919628)
- [3] L. Boyle, H. Flinchbaugh, and M. P. Hannigan, "Natural soiling of photovoltaic cover plates and the impact on transmission," Renewable Energy vol. 77, pp. 166–173, May 2015. doi: [10.1016/j.renene.2014.12.006](https://doi.org/10.1016/j.renene.2014.12.006)
- [4] <https://pvradar.com/>

## Contact

Sha Li, [Sha.Li@LeewardEnergy.com](mailto:Sha.Li@LeewardEnergy.com)  
Brett Pendleton, [Brett.Pendleton@LeewardEnergy.com](mailto:Brett.Pendleton@LeewardEnergy.com)  
Thore Müller, [thore.mueller@pvradar.com](mailto:thore.mueller@pvradar.com)

# MANTIS: From Multiscale Metrology and Analysis to Next Generation Thin Film Module Inspection Systems

K. Lu, E. Ignatovich, P. Miller, **G. Horner**  
S. Johnston, D. Kern  
K. Davis, S. Venkat, M. Liggett  
M. Bolen, E. Brosz

Tau Science Corporation, OR  
National Renewable Energy Laboratory, CO  
University of Central Florida, Orlando, FL  
SB Energy, CA

## Abstract

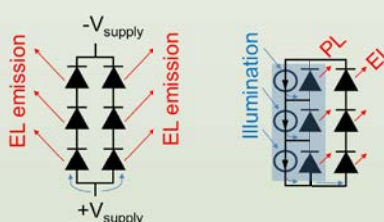
The three-year MANTIS project was launched in Q4'24 to develop outdoor inspection techniques for CdTe PV power plants. The techniques are being developed with the help of multiscale analysis, where defect root cause is assessed using an array of instruments ranging from aerial IR imaging to microscopic analysis, assisted by machine learning that was first developed for silicon module inspection. In this poster we report on the first laboratory results, including non-contact EL (**nc-EL**) imaging and infrared thermography (**nc-IR**). Feedback and discussions are welcome and encouraged as we collect input from current owner-operators of CdTe facilities. This feedback is an important part of the project, as we seek to improve the tools available for operational decision making.

## Key Project Deliverables

|                |  |
|----------------|--|
| <b>Year 1:</b> | Characterize set of CdTe modules prior to accel. test.<br>Deploy non-contact EL ( <b>nc-EL</b> ) imaging system for field test                   |
| <b>Year 2:</b> | Publish midpoint report on accel. test results and defect root causes<br>Deploy non-contact shunt imaging system ( <b>nc-IR</b> ) for field test |
| <b>Year 3:</b> | Publish survey paper and hold industry workshop on CdTe field monitoring, results, best practices  |

## Non-contact Outdoor Imaging

Modern CdTe modules are configured in the 'butterfly' layout, where two sections of the module are electrically connected in parallel. This provides an opportunity to optically pump one half of the module while capturing emission from the second half. The technique eliminates the need to filter pump wavelengths from the emission, and it can be operated either in daylight or at night.

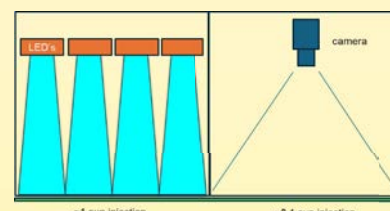


Conventional EL (left) is contrasted with butterfly nc-EL (right) (ref's 1-4).

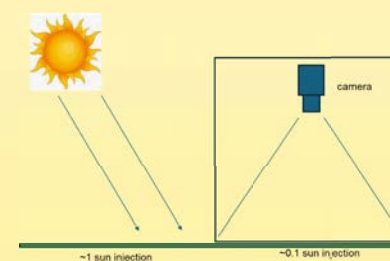
Using this butterfly bias approach, the team is developing a set of metrology systems tailored to inspect CdTe modules both indoors and outdoors.

### Roles

|             |  |
|-------------|--|
| NREL        | Accelerated test, imaging method development, defect root cause analysis                     |
| UCF         | Defect root cause analysis, machine learning to tie module performance to field imaging data |
| Tau Science | Imaging method development, acquisition and defect recognition software                      |

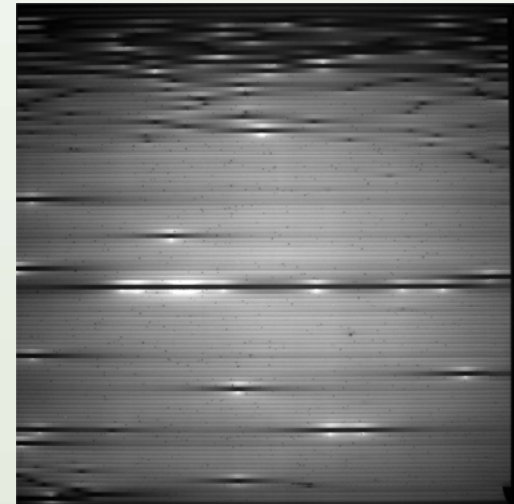


Indoor butterfly imaging

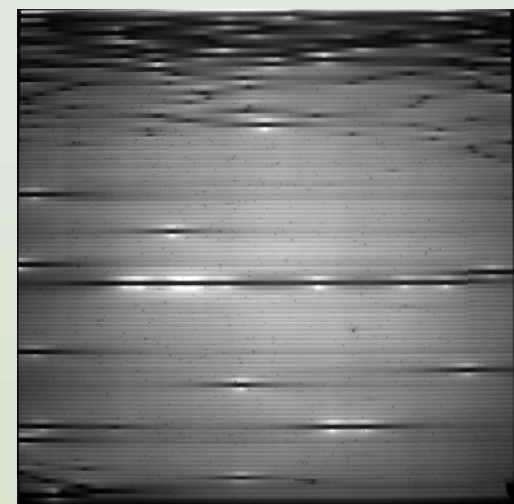


Outdoor butterfly imaging

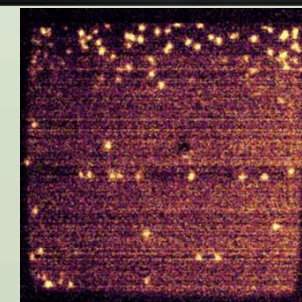
Conventional EL @ $0.1^* I_{sc}$



Butterfly nc-EL @1-sun pump



Butterfly nc-IR @1-sun pump



### References

1. S. Johnston, "Contactless Electroluminescence Imaging for Cell and Module Characterization," 42nd IEEE PVSC, New Orleans, 2015.
2. Alliance for Sustainable Energy, LLC, US Patent 9641125B2
3. K. Davis *et al.*, "Electroluminescence Excitation Spectroscopy: A Novel Approach to Non-Contact Quantum Efficiency Measurements," 44th IEEE PVSC, Washington DC, 2017.
4. M. Koentges *et al.*, "Applicability of Light Induced Luminescence...," IEEE JPV 1 May 2022.

This work supported in part by DOE Office of Energy Research via Award DE-EE0011425.

# Inline, Non-contact EL Scanner for Module Inspection and Quality Control

K. Lu, E. Ignatovich, P. Miller, L. Vasilyev, A. Dirriwachter, G. Horner  
J. Williams, T. Frank, E. Schneller  
S. Johnston, D. Kern

Tau Science Corporation, Cornelius, OR  
Silfab Solar Inc., Burlington, WA  
National Renewable Energy Laboratory, Golden, CO

## Abstract

EL and PL imaging systems typically use a CMOS Silicon camera to collect images. However, the dynamic range and signal to noise ratio (SNR) are often poor. In addition, EL imaging requires electrical connection to the sample- sometimes inconvenient and at other times impossible. This work uses an NREL patented technology and incorporates an InGaAs linescan camera to substantially improve the SNR and dynamic range of both EL and PL images.

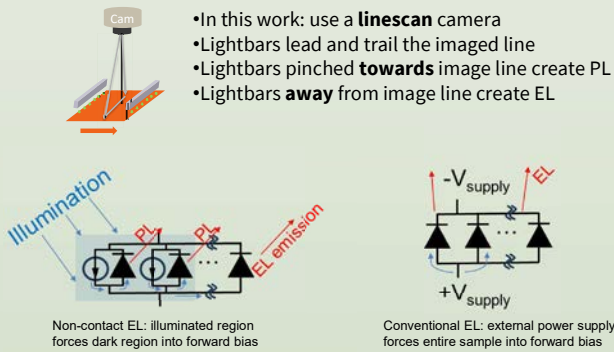
### EL vs non-contact EL

Non-contact EL (nc-EL) has several advantages:

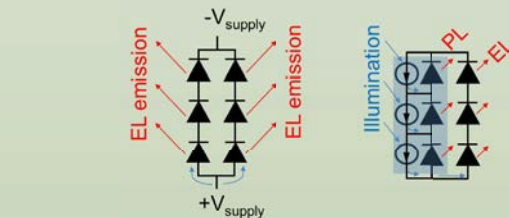
- Older MC4 connections may be brittle and break when handled- nc-EL requires no connection.
- Handling MC4's entails some safety risk. Some utility sites require string level Lock Out/Tag Out even at night due to the risk of inverter back-feed.
- Some cell designs (like Metal Wrap Through) offer no opportunity to perform EL before lamination- non-contact EL can be used to find chipped & defective cells even without solder interconnects

Non-contact EL can be implemented in two ways:

- **Within-cell EL**: illuminate a fraction of the cell, collect emission from non-illuminated region



- **Within-module or "Butterfly EL"**: illuminate  $\frac{1}{2}$  the module and collect EL emission from the second  $\frac{1}{2}$ . Note that this requires a series/parallel layout, common in today's  $\frac{1}{2}$ -cell and thinfilm modules:



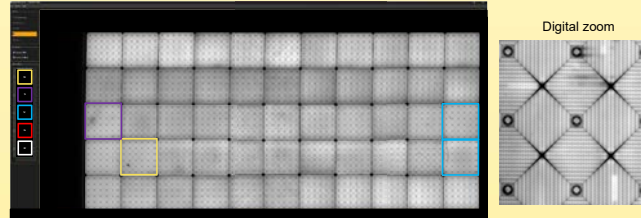
### Project Overview

This DOE-funded project has developed the linescan nc-EL technique and completed Budget Period 1 with the following milestones:

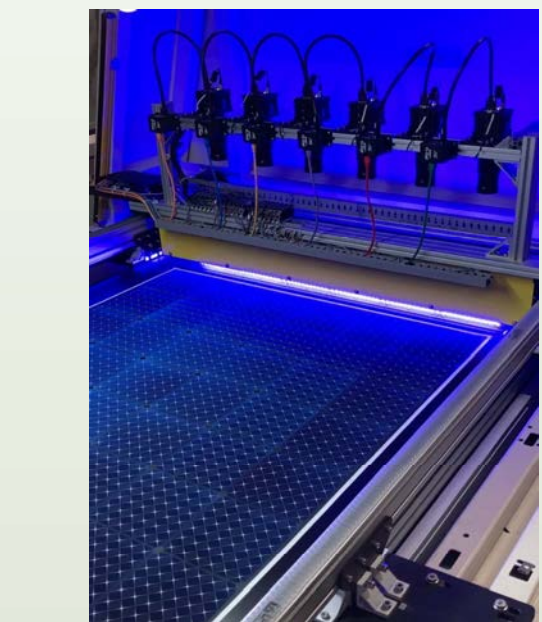
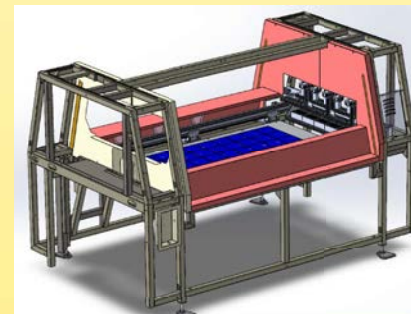
- Desktop system delivered to US R&D cell lab.
- Mini-module scanner delivered to US manufacturer for 24x7 quality control



- Machine learning classifies defects

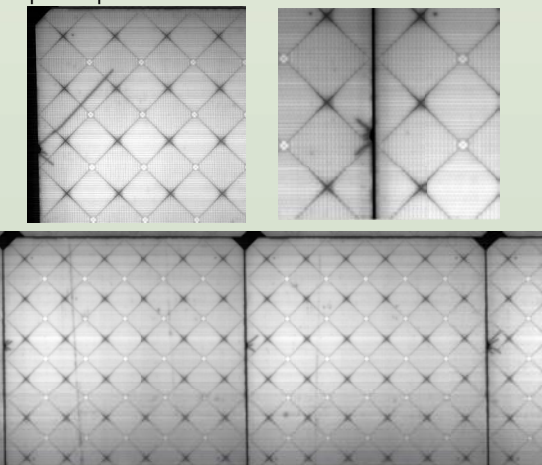


- Inline module scanner delivered to Silfab



### Next Development Steps

- Increase scan speed from 0.25 m/sec to 2 m/sec.
- Modules shuttle between process bays @ ~2 m/sec: cameras will remain fixed & sense motion w/ encoder.
- Develop larger defect library for various end-users. Edge chip example:



- Develop portable outdoor scanner

### References

1. S. Johnston, "Contactless Electroluminescence Imaging for Cell and Module Characterization," 42nd IEEE PVSC, New Orleans, 2015.
2. Alliance for Sustainable Energy, LLC, US Patent 9641125B2
3. K. Davis *et al*, "Electroluminescence Excitation Spectroscopy: A Novel Approach to Non-Contact Quantum Efficiency Measurements," 44th IEEE PVSC, Washington DC, 2017.
4. M. Koentges *et al*, "Applicability of Light Induced Luminescence...," IEEE JPV 1 May 2022.

This work supported in part by DOE Office of Energy Research via Award DE-EE0009635.

# Low Cost & Meaningful Solar PV Module & Mounting Joint Testing

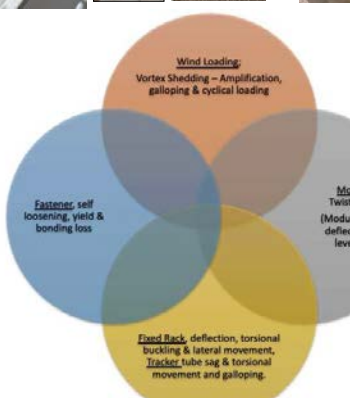
## Capturing Systems Dynamic Effects - Secure & Protective Module Mounting

Gerald Robinson, LBNL // Jon Ness, Matrix Engineering // James Cormican, terrasmart // Chris Needham, Azimuth Advisory Services



### Industry Challenge – Systems Affects

Failures are multifaceted (e.g. installation, design, procurement) however, systems affects are the least understood and represent significant knowledge gaps.



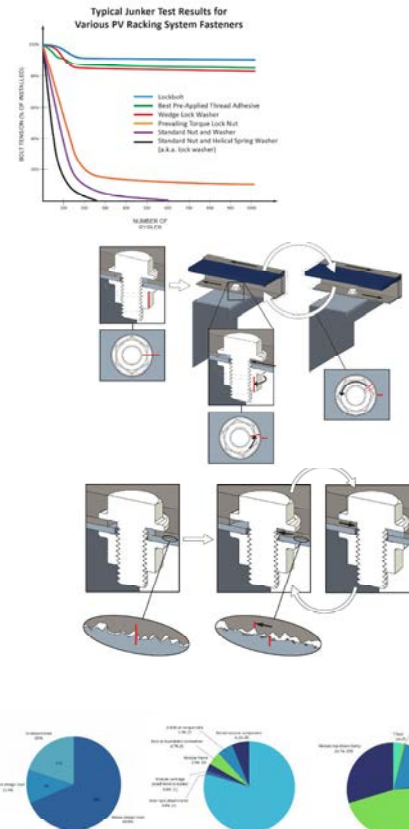
### Mounting Systems



### Module Behavior (Examples)



### Fastener Behavior (Examples)

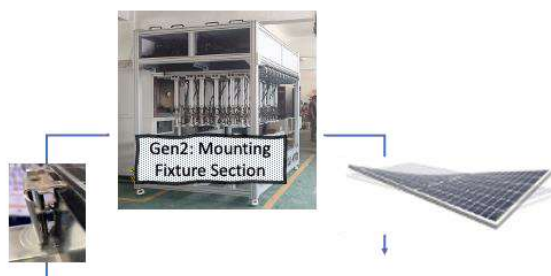


### The Vision: PV Module Mounting System Dynamic Simulator

Creating a test process (IEC/UL) and rack that encompasses system-wide effects for fastener and module both:

- ✓ Testing is affordable.
- ✓ Testing provided by industry labs that support stakeholders.
- ✓ Inclusive of systems demands imparted to fastener.
- ✓ Inclusive of loads imparted into modules; twist, bend.
- ✓ Test rack is manufactured and sold by test equipment manufacturer.

**GEN 2: Module & Module Mounting Test Rack**



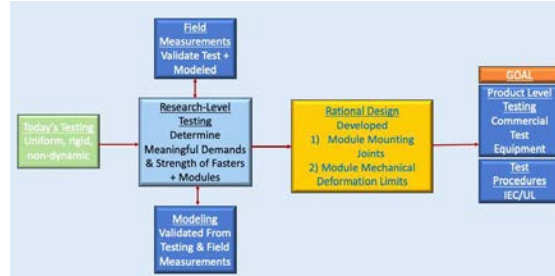
New or revise UL standard focused mounting system reliability

New or revise IEC standard focused mounting performance & aging

### Innovation & Impact

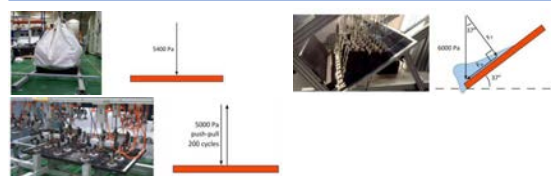
- ✓ **Reduced LCOE: CAPEX and OPEX**
  - ✓ CAPEX: Optimized design for climate zones.
  - ✓ OPEX: 30-Year + assets W/O retightening and module replacements due to mechanical damage.
  - ✓ Fill knowledge gaps to create “Rational Design Basis” for stronger solutions in fastening and module support.
- ✓ Inform future product-level testing standards from SDOs (UL, ASCE, IEC, SEIA, etc.)
- ✓ Create controlled test conditions of structures, which would enable the development of better simulation methods.
- ✓ The testing provides a meaningful visualization to bring broader recognition to failure mechanisms.

### Realizing The Vision



### Fastener & Module Testing Today

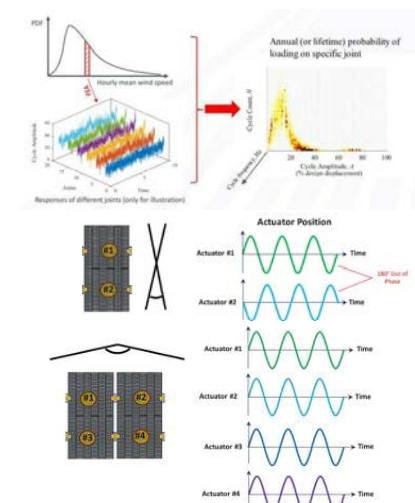
Fasteners Testing (UL 2703) & Module Testing (IEC 62782)



### Phase 1 Testing Fixture



### Phase 1 Testing Protocol



### Contact Info

Gerald Robinson, LBNL – [grobinson@lbl.gov](mailto:grobinson@lbl.gov)  
 Jon Ness, Matrix Engineering – [jness@matrixengrg.com](mailto:jness@matrixengrg.com)  
 James Cormican, terrasmart – [jcormican@terrasmart.com](mailto:jcormican@terrasmart.com)  
 Chris Needham, Azimuth Advisory Services – [chris@azimuth-ventures.com](mailto:chris@azimuth-ventures.com)

# Developing a UV Spot Test for Years of Equivalent Exposure

Ingrid Repins, Steve Johnston, Tim Silverman, Ellie Palmiotti, Michael Deceglie, Ashley Gaulding  
 National Renewable Energy Laboratory

## Current Module UV Tests are Insufficient

- Module design qualification (IEC 61215) contains a UV dose designed to reproduce layup tape delamination observed in the 1980's.
- The dose ( $15 \text{ kWh/m}^2; \lambda = 280 - 400 \text{ nm}$ ) is equivalent to 2 to 3 months of outdoor exposure.
- Some tests apply more UV (e.g. IEC 63209,  $187 \text{ kWh/m}^2$ ). However, this brings just the testing time to around 3 months to get only ~2 years equivalent exposure.
- Modules are expected to degrade minimally for 25 years and beyond.

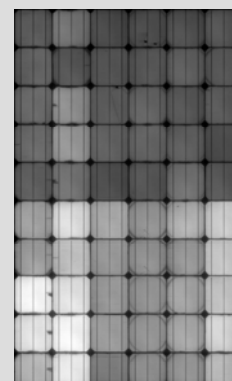
A different approach is needed to:

- minimize testing delays and expense: large UV sources only provide acceleration factors less than 10.
- extend equivalent test doses closer to the module lifetime.
- enable quick quality assurance tests. Untested changes to bills of materials are causes of field underperformance.<sup>1</sup>

## New Technology, New Degradation Modes

More rigorous UV testing is needed to screen for degradation modes in modern cells, including:

- Damage to the passivation layer. This effect has been observed in the lab<sup>2</sup>, and suspected cause of egregious degradation found in some n-PERT modules.<sup>3</sup> →
- Increased series resistance for some BOM's when TOPCon stressed with moisture and UV.<sup>4</sup>
- Partially reversible  $V_{OC}$  degradation has been seen in TOPCon exposed to UV and DH.<sup>5</sup>



EL from n-PERT module where top half exposed to 4000 hours UV.<sup>3</sup>

## Equipment



Fiber-fed arc lamp typically used for curing epoxies

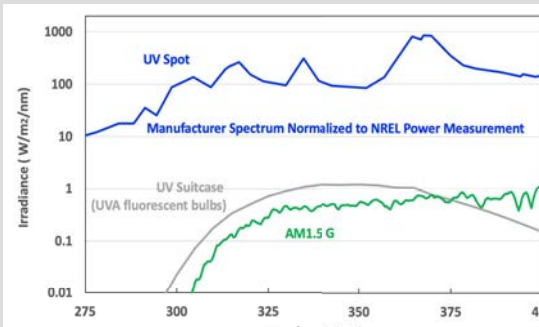


Enclosed fiber tip exposing a thin film module at NREL

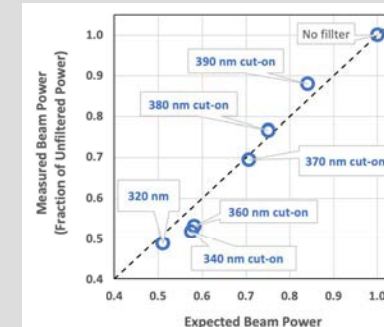


Thermopile for monitoring spot power

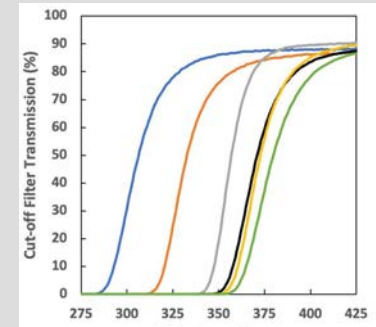
## UV Spot Exposure Characteristics



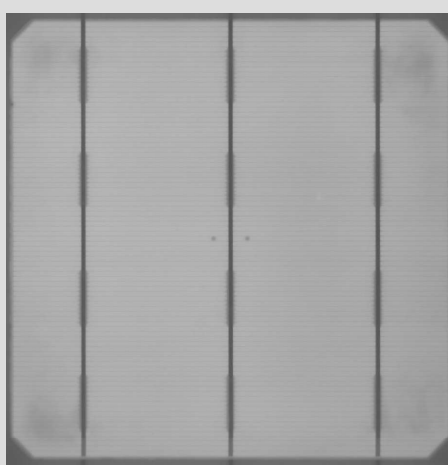
~300x more intense (i.e. faster) than typical sources  
 In 19 hours, the spot center experiences 5 years UVA equivalent field exposure.



Manufacturer spectrum verified by passing spot through different optical filters (above) during power measurement and comparing with expected transmitted power.



## Plans for Evaluating the Results



- We can't use a module power measurement to evaluate the impact of UV if only a small (6 mm FWHM) spot is exposed.
- Therefore, perform high resolution EL of exposed cell before and after UV.
- Hope to reproduce 50% decrease in EL intensity seen after 6000 hours UVA fluorescent exposure in n-PERT study, but 300x faster.
- First EL on fielded module not expected to degrade has been performed. (~200 μm resolution)
- Full-width half maximum spot size is 6 mm.
- Spot exposure of control module is up next.

## Conclusions and Path Forward

- Equipment for a possible UV spot test was identified and characterized.
- Power and spectral measurements confirm that the spot center will receive a 5 year field equivalent UV dose in 19 hours.
- Degradation will be evaluated by high resolution EL before and after stress.
- Preliminary tests are underway.

## References

- M.G. Deceglie et al., Bill of Materials Variation and Module Degradation in Utility-Scale PV Systems, *IEEE JPV* 12(6), 2022.
- Witteck et al., UV-induced degradation of PERC solar modules with UV-transparent encapsulation materials, *Progress in PV* 25, 2017.
- E.A. Gaulding et al., "UV + Damp Heat Induced Power Losses in Fielded Utility N-Type Si PV Modules," submitted to *Progress in PV*, 2025.
- C. Sen et al., "Buyer aware: Three new failure modes in TOPCon modules absent from PERC technology," *Sol. Mat.* 272, 2024
- Gebhardt, "Reliability of Commercial TOPCon PV Modules—An Extensive Comparative Study," *Progress in PV*, 2024.

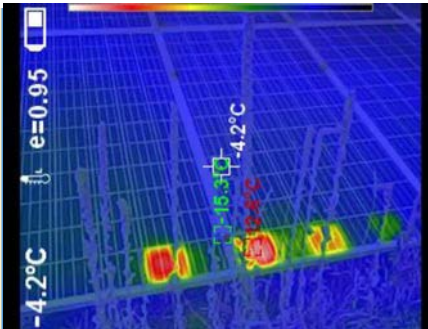
# Residual Effects of Long-Term Vegetation Shading on a Ground Mount PV Array

Rich Strömberg, Interdisciplinary PhD Student, Univ. of Alaska Fairbanks and Founder at Solar Reuse Test Lab™

## BACKGROUND

Vegetation of various types (grasses, mullein, sunflowers) was observed growing close to the lower module rows of a 6-year-old ~1MW fixed solar array in the Rocky Mountain region. This vegetation was casting shadows on modules, causing reverse biasing of cells along the bottom row as seen in infrared thermographs (ground- and aerial-based imaging). A trained eye could detect subtle discoloration of the encapsulant layer on some of these bottom row cells which was confirmed with nighttime UV fluorescence. Only modules on the bottom row of the fixed mount arrays were found to exhibit any thermal IR, UV fluorescent and faint visual signatures. Most still had adjacent vegetation corresponding with the observed signatures.

A subsequent site visit was conducted to better analyze affected modules under visual, UV and infrared inspection, followed by electroluminescence imaging and electrical characterization to determine if there were lasting, residual impacts to the affected modules after vegetation was cleared in front of the array.



## RESEARCH QUESTIONS

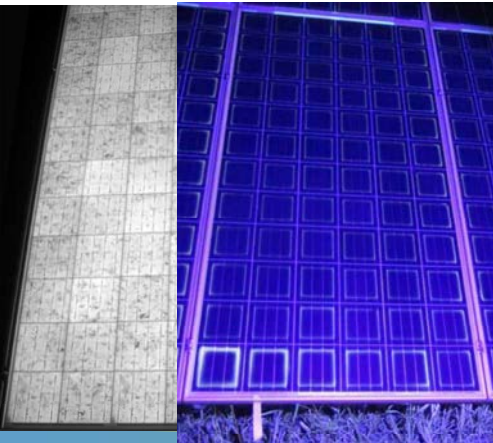
Is the bottom row UVF signature present on only the bottom module?

Does EL imaging show lower power output on affected cells?

Is there a measurable power loss for affected modules? Does the IR hot cell remain after vegetation is removed?

## METHODS

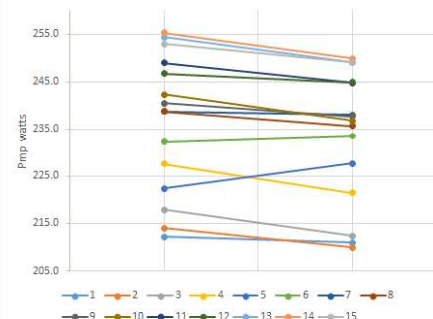
- Identify and label PV modules with 1) tall vegetation casting shadows on module cells, 2) hot cells associated with the shading as indicated with a handheld IR camera and 3) visual signs of encapsulant browning only along the bottom row of cells of that module (likely a very faint level of discoloration). Modules were labeled with orange masking tape on lower frame front as well as the racking rails on the back side of the array to be easily detectable day or night.
- Use a dust mop to clean affected bottom module. (Mop could only reach about 1/3<sup>rd</sup> of the top module, so there will be minor soiling on the top/control module.)
- Collect IR thermographs during daylight hours.
- Remove vegetation in front of modules under evaluation with landscaping shears.
- Disconnect affected strings at DC combiner and disconnect affected modules from their string during daylight hours.
- Conduct nighttime UV fluorescence imaging and electroluminescence imaging (most at 5 amps with one repeated at 1 amp) on all modules.
- Measure simultaneous power output of affected bottom modules and the module mounted immediately above it on the top row with EY1800W IV curve meters during full sunlight.
- Reconnect all strings and close circuit on DC combiners.



## RESULTS

- UVF images reveal between 1 and 5 cells on the bottom row with enhanced encapsulant fluorescence.
- Only bottom row modules show the UVF and IR signature.
- 20 minutes after vegetation is cleared in front of module, the IR signature is no longer visible.
- There was no clear cell correlation between UVF images and EL images.
- Results from electrical measurements of all 15 pairs of modules (top=control and bottom=vegetation shading) return a t-value of 0.00152, rejecting the null hypothesis.
- The average difference between the electrical performance of the control modules and vegetation shading modules is a reduction in Pmp of 1.54%.

PV Module Power - Ctrl(Top) vs Veg(Bot)

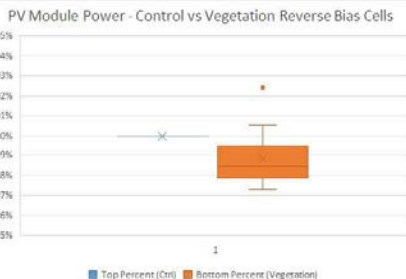


## UNKNOWNs

There is no prior data to know the original power performance of any modules.

It is not possible to know how much of the time over the past 6 years that vegetation has been shading any particular module or row of modules nor the severity of shading.

The pattern of skip stringing modules along both the upper and lower racking rows prevents comparing IV curve traces to detect electrical differences between shaded and unshaded modules.



## CONCLUSIONS

- Shading of PV module cells is known to cause reverse biasing of the affected cells [1] with can cause elevated cell temperature, encapsulant discoloration, reduced power output real-time and a possible increase in annual power degradation rate. [2].
- Partial cell shading of this magnitude can cause 30-35% power losses in real time for a PV module.
- There is a clear correlation between cells shaded by vegetation and encapsulant discoloration as revealed under nighttime ultraviolet light fluorescence.
- Degradation in PV module power output across 15 pairs (vegetation shaded and adjacent unshaded) showed a small (1.54%) total reduction in module output but with high confidence (t-value 0.00152).
- This small power loss was not discernable under field EL imaging.

## REFERENCES:

- [1] Z. Liu, Y. Gong, Z. Wang, Y. Li, and D. Liu, "Revealing the Intrinsic Mechanisms of Hot and Cold Spots within a Locally Shaded Photovoltaic Module Based on Micro-Electrical Characteristics," *Energies*, vol. 17, p. 4462, Sep. 2024, doi: 10.3390/en17174462.
- [2] M. Islam, M. Jadin, A. A. Mansur, S. Zain, and M. A. Haq, "Analysis of Photovoltaic Module Degradation: An Experimental Investigation on the Correlation Between Partial Shading, Hot Spots, and EVA Discoloration," 2024, pp. 263–274. doi: 10.1007/978-981-97-3847-2\_23.

Contact: Rich Strömberg [restromberg@alaska.edu](mailto:restromberg@alaska.edu)

# Measuring stow effectiveness in-situ with collocated horizontal and plane of array (POA) GroundWork® Eyewitness instruments at an operating solar plant



Travis Morrison, Colin Sillerud, Douglas Robb, Julie Chard, Alex Bryan, Ann Will  
GroundWork Renewables, Inc.

## MOTIVATION: HAIL DATA KNOWLEDGE GAP

Hail events at utility-scale solar facilities can lead to devastating damage which may lead to large downtime and near un-insurable assets (Chakraborty et al 2023). Figure 1, highlights the widespread risk of hail in the USA during the project lifecycle. To curb the risk of damage to photovoltaic (PV) modules during an event, owners and tracker manufacturers are working together to defend their assets by placing their modules into a defensive stow ahead of convective cells with a high probability of producing hail.

Despite defensive stow practices, in-situ observations of hail stone impact energy and diameters are extremely limited for operational solar plants. Therefore, there is a high demand for industry-specific observations of hail stone kinetic energy, effective diameter, and count at both horizontal and at POA.

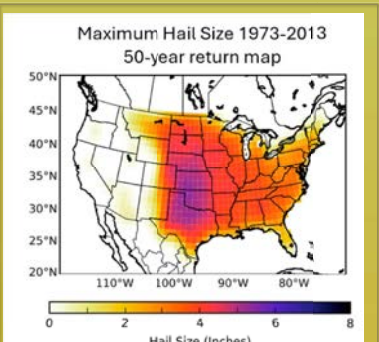


FIG: 50-year maximum hail return map in the USA derived based on a collection of spotter and radar data. Note that over half the country is at risk for damaging hail (>2 inches) during the life cycle of a solar asset (Reprinted from Allen et al., 2017)

## QUANTIFYING STOW EFFECTIVENESS AND EFFECTIVE FALL ANGLE

The form factor and autonomous features of the GroundWork Eyewitness allow the device to be readily deployed on the end of a tracker row. Allowing the device to track with the modules. When deployed with a near horizontal device nearby (10 deg South), the difference in impact energy of hail may be quantified by assuming similar fall angles, diameters, and geometries over a sampling period.

Projected two-dimensional, or effective fall angles, are also measured through a minimization of the force between the two sensors and knowing the angle of the devices. By assuming similar kinematics between observation sites, we can also infer if hail is falling towards the stowed module or into/towards the stowed module. See the comparison between the time series data of Collocation Site 1 and 2 from 0016 UTC to 0035 UTC.

## CONTACT

Travis Morrison  
GroundWork Renewables, Inc.  
tmorrison@grndwork.com

© GroundWork Renewables, Inc. | All Rights Reserved

## GROUNDWORK EYEWITNESS

The GroundWork Eyewitness in-situ hail monitoring device is composed of four piezo-electric force transducers behind 6 mm glass and a solar cell which allows measurement of each hail stone. The low-power device sleeps until struck by a hail impact, collects data, then reports the event to the cloud.



FIG: Photo of the GroundWork Eyewitness. The device is 42 cm by 42 cm and weighs approximately 4.6 kg.

### Device details:

- Measures kinetic energy and diameter for each individual hail strike
- Has an observable diameter range from 10.4 mm to 70 mm
- Is self-powered and with a global SIM card
- Includes an onboard inclinometer for stow verification

## DEPLOYMENT METHODOLOGY

Systems are deployed across the facility based on siting recommendations from GroundWork Renewables, which accounts for site geographic location, size, and historical meteorology.

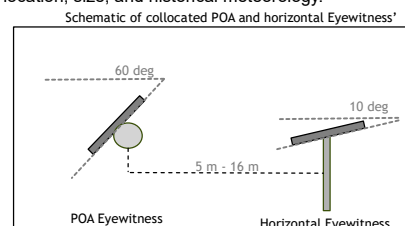


FIG: (above) Schematic of the collocated horizontal and POA Eyewitness sensors. Sensors are placed within a 6 m – 15 m radius



FIG: GroundWork Eyewitness deployed at horizontal on a pile (above), and at POA on the end of a tracker row (right)

## CONCLUSION AND FUTURE WORK

In-situ measurements of collocated horizontal and POA instruments can help the utility-scale solar industry understand stow efficacy, the direction of stow, and the stow angle, improving solar plant survivability in the likely event of a hail storm in hail-prone regions. Future work will include:

- Instrumentation of more sites to increase storm data.
- Inclusion of in-situ wind speed and direction measurements to enhance the analysis
- Correlation of this and other events with third-party data to better understand and capture storm microphysics and stow efficacy

## REFERENCES

- Allen, J.T., Tippett, M.K., Kahlert, Y., Sobel, A.H., Lepore, C., Nong, S., and Muehlbauer, A. An extreme value model for hailstone size. American Meteorological Society, 4(2016). DOI: 10.1175/MWR-D-17-0119.1
- NOAA National Weather Service, Radar Operations Center (1991). NOAA Next Generation Radar (NEXRAD) Level 2 Base Data. NOAA National Centers for Environmental Information.
- Helius, J.J. and Collins, S.M. JGRS (2016). DOI: 10.5334/jgrs.119
- Uz, M.E. Modeling the effect of hailstones on steel roofing membranes for residential buildings. Sci Rep (2023). DOI: 10.1038/s41598-023-23210-w
- Marshall, J.S., and Palmer, W. M.C. The distribution of raindrops with size. Journal of Meteorology, 5 (1948).
- Chakraborty, S., Halder, A.K., and Kumar, N.M. Analysis of the hail impacts on the performance of commercially available photovoltaic modules of varying front glass thickness. Renewable Energy, Vol 203, 2023, ISSN 0960-1481. DOI: 10.1016/j.renene.2022.12.061.

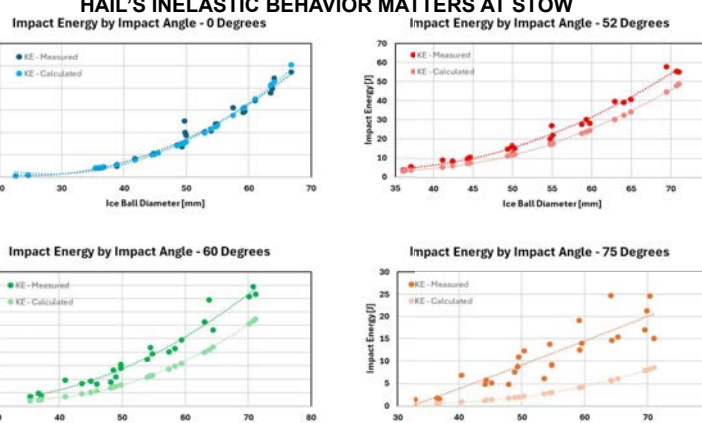
## LABORATORY TESTING

Laboratory ice balls ranging from 25 mm – 70 mm in diameter were used to compare the measured kinetic energy of ice impacts with calculated values using the kinetic energy equation for an elastic collision. Readings from the GroundWork Eyewitness sensor matched the calculated kinetic energy at normal incidence to within +/- 10% ( $k=2$ ) across the tested range. However, the simple elastic kinetic energy model ( $\frac{1}{2}mv^2\cos(\theta)^2$ ) underestimated the energy delivered to the Eyewitness sensor under angled impacts due to hail's inelastic collision by up to 69%. Furthermore, the greater the impact angle offset, the greater the discrepancy between the measured and calculated values.

**TAB:** Hail strike impact angle and the corresponding ratio of calculated kinetic energy for an elastic collision to the measured kinetic energy

| Impact Angle (Degrees) | Kinetic Energy: Elastic model/Measured (%) |
|------------------------|--|
| 0                      | +2.86 %                                    |
| 52                     | -20.84 %                                   |
| 60                     | -38.36 %                                   |
| 75                     | -68.96 %                                   |

## HAIL'S INELASTIC BEHAVIOR MATTERS AT STOW



Uz (2022) proposes energy transferred for hail strikes into plates requires an understanding of the hail's plastic deformation and vibrational energy transferred to the plate. Future work will aim to better model and measure the inelastic collisions of hail with solar modules as there is a direct correlation between modeling this physics with probable maximum loss modeling for project survivability and insurance.

FIG: Measured kinetic energy for a range of hail diameters and incident angles. Lighter circles indicated kinetic energy assumed from elastic collision

Watch an inelastic hail strike at a 75-degree strike angle

## IN FIELD OBSERVATIONS OF STOW EFFECTIVENESS

### EVENT DETAILS:

In the spring of 2024, an operating plant in northern Texas, densely instrumented with 10 Eyewitness sensors observed a hail event. The site was instrumented with 8 study areas. Two study areas contained collocated sensors at POA and horizontal, Collocation Site 1 and Collocation Site 2. Time series data highlighted from these two study areas from this event is presented (below) and NEXRAD data from the storm front (right).

### Kinetic Energy Timeseries of Hail Event: Stow and Horizontal

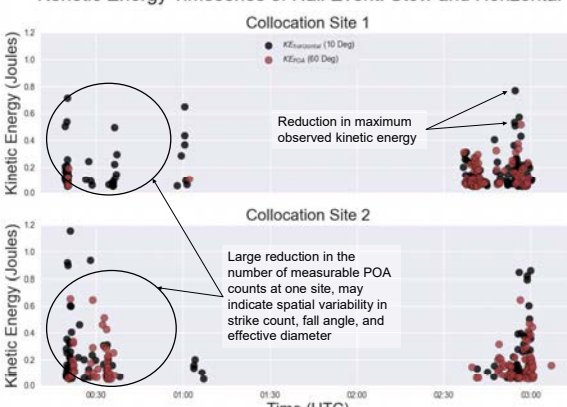


FIG: Time series of the kinetic energy from Collocation Site 1 (top) and Collocation Site 2 (bottom). The black circles indicate the horizontal sensor, while the red circles indicate the POA sensor.

### Histograms of Hail Event: Stow vs Horizontal

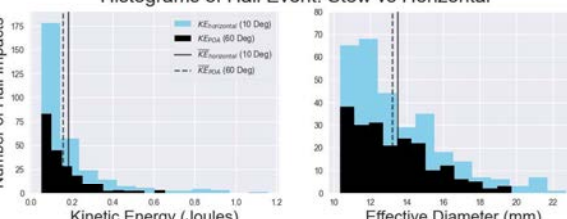


FIG: Histograms of the kinetic energy and effective diameter from Collocation Sites 1 and 2 separated by data collected from the horizontal and stowed devices. Note the power law distribution of hail size (Marshall and Palmer, 1948) and kinetic energy (Heymsfield et al, 2018)

### NEXRAD Level 2 RHI Scans

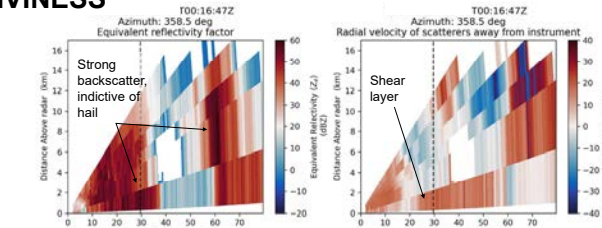


FIG: RHI scans from the nearest NEXRAD, 29 km from the observational site. Note the coarseness of the data, with single data points in the vertical transect every 2 km. Of interest is the large observed shear layer 2 km above the site during the storm front

### EVENT DISCUSSION

Large variations in projected fall angle highlight strong intra-storm wind speed and direction variability. This is consistent with the strong shear layers observed in the radial velocity RHI radar scan, and the early variability in hail stone strike count between POA sensors at Collocation Sites 1 and 2. The POA Eyewitness sensors reported a stow angle of 60 degrees and measured anticipated distributions of hailstone size and kinetic energy that may allow extrapolation below the instrument's lower-end sensitivity. Results from the elastic kinetic energy model for deriving fall angles may overestimate fall angles based on laboratory results (above).

**TAB:** Calculated percent differences for effective diameter and kinetic energy between horizontal and stowed (POA) sensors from hail event at Collocation Sites 1 and 2

|         | Eff. D (mm) - Horizontal | Eff. D (mm) - Stow | Percent Change (%) | KE (J) - Horizontal | KE (J) - Stow | Percent Change (%) |
|---------|--------------------------|--------------------|--------------------|---------------------|---------------|--------------------|
| Count   | 297                      | 204                | -31.3              | 297                 | 204           | -31.3              |
| Maximum | 22.8                     | 19.7               | -13.3              | 1.16                | 0.66          | -43.4              |
| Minimum | 10.4                     | 10.4               | 0.0                | 0.05                | 0.05          | 0.0                |
| Mean    | 13.5                     | 13.2               | -2.0               | 0.18                | 0.16          | -14.2              |
| Median  | 12.7                     | 12.8               | 0.4                | 0.11                | 0.12          | 1.8                |

### Effective Fall Angle

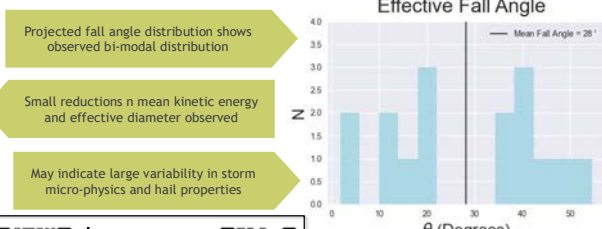


FIG: Effective fall angle derived from elastic model computed on one-minute averages. The vertical black line indicates the mean value

Learn more about module testing and hail monitoring

# What is a polyolefin? A critical overview of ethylene copolymers as PV module encapsulants

Gernot Oreski<sup>1</sup>, Chiara Barretta<sup>1</sup>, Petra Christöfl<sup>1</sup>, Paul Gebhardt<sup>2</sup>, Karl-Anders Weiß<sup>2</sup>, David C. Miller<sup>3</sup>, Soňa Uličná<sup>3</sup>, Michael Kempe<sup>3</sup>, Laura S. Bruckman<sup>4</sup>, Alessandro Virtuanj<sup>5</sup>, Hengyu Li<sup>5</sup>, Brian Habersberger<sup>6</sup>, Jeff Munro<sup>6</sup>, Kristof Proost<sup>7</sup>, Marcel Kühne<sup>8</sup>

<sup>1</sup> Polymer Competence Center Leoben; <sup>2</sup> Fraunhofer ISE; <sup>3</sup> National Renewable Energy Laboratory; <sup>4</sup> Case Western Reserve University; <sup>5</sup> Swiss Center for Electronics and Microtechnology (CSEM); <sup>6</sup> DOW Chemical; <sup>7</sup> IP Fab; <sup>8</sup> Hanwha Q CELLS

## Should we call “polyolefin” encapsulants that way?

A **polyolefin** is any of a class of polymers produced from **olefins** (also called an **alkene** with the general formula  $C_nH_{2n}$ ) as monomers

Are all polyolefin encapsulants “polyolefins”?

Term “Polyolefin” has different meaning in PV industry than in material science

- Thermoplastic polyolefins: Non-crosslinked polyolefins that contain crystallinity associated with - most typically - polyethylene (PE), ethylene/α-olefin copolymers, or polypropylene (PP)
- Polyolefin elastomers (POE): Polyolefins with low amounts of crystallinity, such as polyisobutylene (PIB), ethylene/α-olefin copolymers, and ethylene propylene diene monomer rubber (EPDM rubber), that are often but not always chemically cured

## What is the main issue?

### How PV community sees it!

| Component    | Encapsulants       |                           |     |
|--------------|--------------------|---------------------------|-----|
| Category     | Polyolefin         | Ethylene/polar copolymers | ... |
| Sub-category | Peroxide cured POE | Peroxide cured EVA        | ... |
| Product      | POE 1              | EVA 1                     | ... |

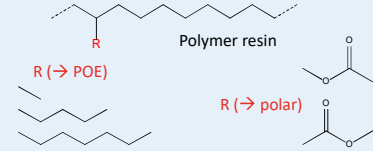
### How polymer community sees it!

| Component    | Encapsulants       |                           |     |
|--------------|--------------------|---------------------------|-----|
| Category     | Polyolefin         | Ethylene/polar copolymers | ... |
| Sub-category | Peroxide cured POE | Peroxide cured EVA        | ... |
| Product      | POE 1              | EVA 1                     | ... |

Chemical composition (base polymer & additives) is not considered – lack of comparability

## What are “polyolefin” encapsulants made of?

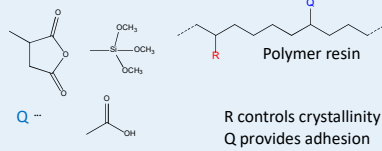
### Cured/crosslinked encapsulants



#### Characteristics

- Additives: Peroxide, coagents, adhesion promoters, antioxidants, UV absorbers & stabilizers
- Film produced at **low temperature** (below peroxide composition temperature)
- Film **crosslinks** during lamination

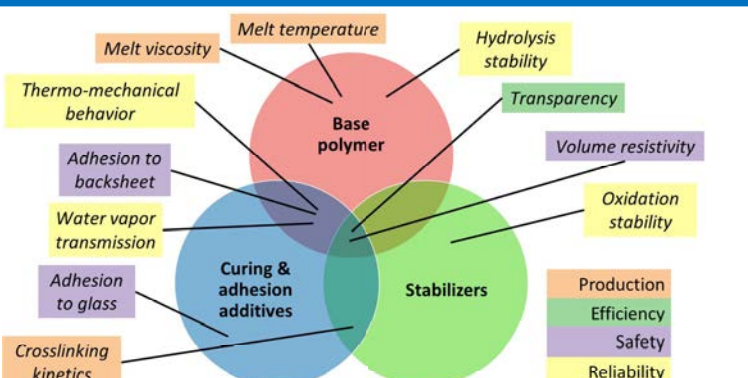
### Non-cured encapsulants



#### Characteristics

- Additives: Antioxidants, UV absorbers & stabilizers
- Film can be produced at **high temperatures**
- Fast lamination** – no need for crosslinking
- Latent crosslinking** vs. **thermoplastic behavior**
  - Crosslinking may occur post-lamination over time (example Q = alkoxy silane)

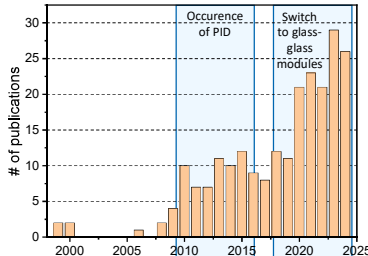
## Properties of polyolefin encapsulant films



Only few publications investigate the role of additives and stabilizers in reliability of encapsulant films

## Inventory of polyethylene copolymer encapsulants

- 228 indexed publications mentioning polyolefin encapsulants between 1999 and 2024

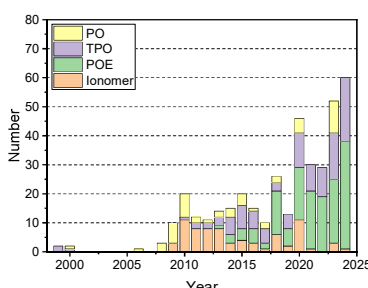


- 391 encapsulant films have been investigated

- POE - 152 mentions
- TPO - 113 mentions
- PO - 53 mentions
- Ionomer - 73 mentions

- Out of 391 investigated encapsulant films

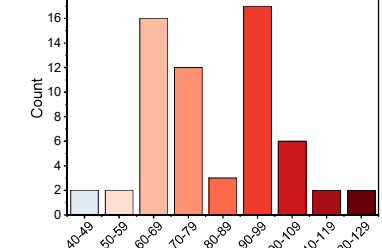
- For 62 (~15.8%) materials the manufacturer is listed
- Only for 45 (~11.5%) cases information on the chemical composition of the base polymer is given



- Market inventory: 75 different types from 26 manufacturers (as of October 2024)

- Inventory does not cover the entire market, but only verified materials characterized by the co-authors' institutions and companies).

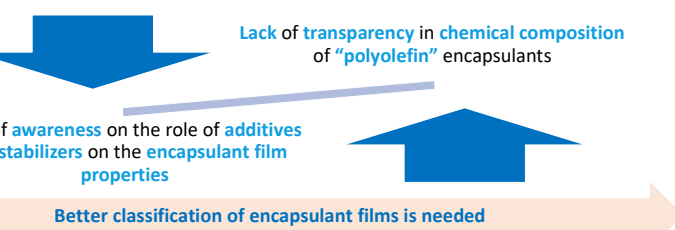
- Five different base polymers
- Two different curing chemistries (peroxide and silane based) as well as non curing, thermoplastic encapsulants
- Variations in material softening onset and shear viscosity
- UV transparent (UV-T), UV blocking (UV-B) and white (W) versions
- Melting temperatures ranging from 49 °C to 121 °C
- Production dates ranging from 2006 to 2024



### Interesting observations

- Comparison of the same brand name of one encapsulant film for different production years showed differences in melting temperature → change in comonomer content

## SUMMARY & CONCLUSIONS



**Module lamination**

- Similar chemical structure, e.g. ethylene α-olefin copolymer, does not lead to the same **thermo-mechanical** properties
- Lamination conditions need to be optimized according to the **property profile**

**Reliability**

- Long-term stability of the encapsulation materials is determined by the **additives** and **stabilizers**
- Encapsulant properties directly and indirectly influence most **module degradation modes**

**Comparability of results**

- Too generic designation of polyolefin encapsulant films
- Reported findings from one “polyolefin” encapsulant cannot be directly compared to other “polyolefin” encapsulants

| Resin          | Ethylene Polymers                         | Categorization of some common encapsulants using a two-dimensional taxonomy |  |
|----------------|---|---|--|
|                |   | Cured   | Non-cured  |
| Other Polymers | Polyolefin                                | Peroxide cured POE  |  |
|                | Ethylene/polar copolymers and terpolymers | Peroxide cured EVA  | Ethylene/acrylate/VTMS terpolymer                              |
|                | Grafted or Post-reactor modified polymers |   | VTMS-g-POE   |
|                | Silicone                                  |   | • Ionomer<br>• MAH-g-POE<br>• Ethylene/acrylate/GMA terpolymer |
|                |   |   | • PVB<br>• TPU   |

Abbreviations: VTMS – vinyltrimethoxysilane; MAH-g-POE – maleic anhydride grafted POE; GMA – glycidyl methacrylate; PDMS – polydimethylsiloxane; PVB: polyvinyl butyral; TPU – thermoplastic urethane.

This work has been carried out with support from the Horizon Europe projects PEPPERONI and MC2.0



This project is co-financed by the European Union. Views and opinions expressed are however those of the author(s) only and do not necessarily reflect those of the European Commission. European Union, European Institute of Infrastructure and Environment Agency (EIT) and the European Union nor the granting authority can be held responsible for them. The project is also supported by the Swiss State Secretariat for Education, Research and Innovation (SERI).



Polymer Competence Center Leoben GmbH (PCCL), Sauraustrasse 1, 8700 Leoben, Austria  
Corresponding Author: Gernot.oreski@pccl.at

Part of this work was contributed by the National Renewable Energy Laboratory, operated by Alliance for Sustainable Energy, LLC for the U.S. Department of Energy (DOE) under Contract No. DE-AC36-08GO28308. Funding was provided by U.S. Department of Energy Office of Energy Efficiency under agreements 330308, 325009, 343509, 382609, and 52785.



Co-financed by the European Union

# Analysis the Performance of PV Modules with Different Failures under Longtime Outdoor Condition

Bingnan Wang, Sai Li, Jinyu Tao

National Centre of Inspection on Solar Photovoltaic Products Quality (CPVT), P.R. China

## Introduction

Crystalline silicon photovoltaic (PV) modules are susceptible to degradation during long-term outdoor operation due to environmental and operational factors such as temperature fluctuations, humidity, ultraviolet (UV) radiation, chemical corrosion, and mechanical stress. Table 1 summarizes typical failure modes of PV modules. These factors may lead to structural degradation, including crystal defects, ribbon corrosion, and encapsulation aging, ultimately affecting performance and lifespan. Such issues pose challenges to the stable operation of PV systems.

To take a deep research on the reliability and economic efficiency of PV system, appropriate design, material selection, installation, maintenance and performance monitoring are essential. Empirical studies on the performance and degradation of damaged PV modules are critical for reliability assessments and life-cycle evaluations. This research investigates the performance degradation patterns under outdoor conditions, providing practical data to refine degradation models and lifetime prediction algorithms. The findings are expected to offer theoretical foundations for optimized material selection and sustainable recycling strategies in PV module manufacturing.

| Failure Type         | Description  | Failure Mechanism   | Performance Impact                                     |
|----------------------|--|---|--|
| Physical Damage      | Natural disasters (heat, cold, wind, etc.)   | Accidental impact, during transportation/Installation       | Cell cracks and fragmentation/Mobile structural damage |
| Material Degradation | Aging of encapsulation (e.g., EVA), backsheet materials, and solar cells over time | Reduced light transmittance/Decreased electrical efficiency |  |
| SHD                  | Power loss induced by shadow field effects (internal or external to module)        | Decreased cell performance/darkening                        |  |
| Hot-Spot Formation   | Current voltage mismatch caused by partial shading or cell mismatch                | Localized overheating/Cell burning                          |  |
| Mechanical Stress    | Thermal expansion coefficient mismatch under temperature cycling                   | Solder joint failure/Cell micro-cracks                      |  |
| Cell Defects         | Intrinsic material process defect during manufacturing                             | Initial performance deficiency/Reduced lifespan             |  |

## Method

This study evaluates the operational performance and degradation characteristics of PV modules with different failure types. Field-tested modules were collected from 23 large-scale PV plants in Northwest China (arid climate; high irradiation, significant temperature fluctuations, and UV exposure). According to NEA data, photovoltaic systems in this region demonstrate annual peak hours ranging from 1,460 to 1,617, and aging modules (5–10 years in operation) exhibit representative failure patterns. The research is initiated with:

- Independent micro-inverters for each sample
- Real-time meteorological/electrical data acquisition (Feb 2021-Oct 2024)
- Periodic IEC 61215-compliant evaluations:

The field deployment configuration is illustrated in Figure 1.

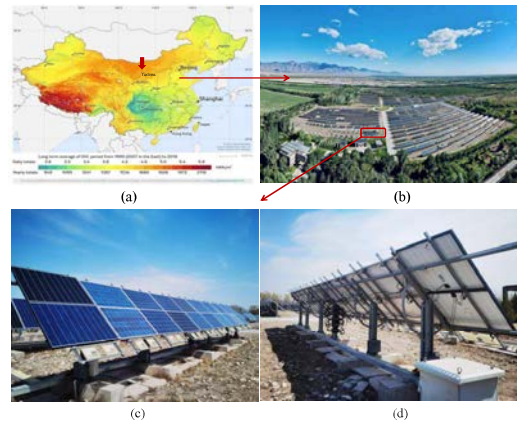


Fig. 1 (a) Location of the test site in China; (b) PV outdoor site; (c) Front view of the platform; (d) Rear view of the platform.

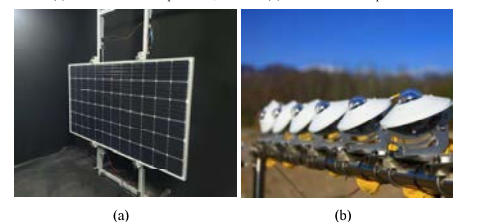


Fig. 2 (a) STC testing; (b) Pyranometers with different angles;

### Indoor Laboratory Testing

- Power rating: HALM AAA-class solar simulator following IEC 60904-1 procedures.
- Periodic degradation monitoring: 8-month interval STC power reassessment (Figure 2a)
- Diagnostics: NTEL2400 Electroluminescence (EL) Imaging System, FLIR Ti400 Infrared (IR) Thermography System:

### Outdoor Field Monitoring:

- Individual microinverter integration for module-level MPPT
- Pyranometer (Fig. 2b)
- Ambient temperature sensor.

## Data & Analysis

From February 2021 to October 2024, 15 samples were subjected to long-term monitoring under actual conditions. Considering that some samples lacked the actual initial power, the measured degradation rate was calculated based on the on-site measured power and the rated power.

As can be seen from Table 2, the EL test results of the samples with cracks in the cells all show abnormalities. Since the samples are only shipped after the EL test results show no cracks during the production line, it can be inferred that the cracks in the cells may have been caused during the transportation or installation process. However, most of the samples with cracks have a degradation of 3%–6% during the period from 2021 to 2024, such as sample 1, 2, and 15. Therefore, it can be concluded that cracks will not directly cause significant power loss of the sample in the short term.

Table 2 The degradation of the samples

| Sample | Failure/Defects                  | Operation Years | Rated Power (W) | Initial Degradation (%) | Degradation (%) | Accumulated Degradation (%) |
|--------|----------------------------------|-----------------|-----------------|-------------------------|-----------------|-----------------------------|
| 1      | Cell micro-cracks/None           | 1.1             | 300             | 12.8%                   | 13.1%           | 15.2%                       |
| 2      | Small cell/cell micro-cracks     | 1.1             | 300             | 12.8%                   | 13.1%           | 15.2%                       |
| 3      | Cell micro-cracks/Backsheet      | 1.1             | 230             | 3.6%                    | 22.4%           | 24.4%                       |
| 4      | Cell fragmentation/Backsheet     | 1.1             | 230             | 15.9%                   | 70.6%           | 73.7%                       |
| 5      | Cell micro-cracks/None           | 1.1             | 230             | 4.6%                    | 5.8%            | 6.4%                        |
| 6      | Small cell/cell micro-cracks     | 1.1             | 230             | 9.2%                    | 91.5%           | 96.3%                       |
| 7      | Glass breaking/Cell micro-cracks | 1.1             | 240             | 45.0%                   | 34.6%           | 78.9%                       |
| 8      | Glass breaking/None              | 1.1             | 230             | 78.54%                  | 94.0%           | 96.2%                       |
| 9      | Fragmentation, Backsheet         | 1.1             | 230             | 36.8%                   | 95.9%           | 98.6%                       |
| 10     | Cell micro-cracks/None           | 1.1             | 230             | 36.8%                   | 95.9%           | 98.6%                       |
| 11     | Cell micro-cracks/None           | 1.1             | 230             | 36.8%                   | 95.9%           | 98.6%                       |
| 12     | Corrosion damage                 | 30              | 230             | 5.28%                   | 16.35%          | 20.63%                      |
| 13     | Cell backsheet                   | 30              | 270             | -1.6%                   | 40.1%           | 41.4%                       |
| 14     | Glass breaking/Cell micro-cracks | 30              | 270             | 3.8%                    | 8.4%            | 12.2%                       |
| 15     | Backsheet deformation            | 30              | 270             | 3.8%                    | 8.4%            | 12.2%                       |
| 16     | Cell micro-cracks/None           | 230             | 15.10%          | 20.5%                   | 20.5%           | 20.5%                       |

Glass scratches directly affect the light transmittance of the front side of the module, which in turn affects  $I_{SC}$  and  $V_{OC}$ , and has an impact on the output power finally. In the operation and maintenance of the PV power plant, modules with obvious and serious scratches and glass fragmentation will be replaced during daily operation and maintenance. The degree of glass scratches inspected this time has a limited impact on the light transmittance of the samples. It can be seen that the power output of the samples with small glass scratch areas and no cell fragmentation has not significantly decreased. However, there is a great difference in the power of different glass damages. As shown in Figure 3, sample 6 and 13 are both with glass damage. Sample 6 was impacted by external force and showed a radial damage, causing a large area of cell fragmentation, and its initial test power degradation reached 92.54%, basically losing the power generation ability. Sample 7 and 8 also showed the same situation. The glass of sample 13 was spider web-like damaged, but the cells had a small number of cracks with an initial test power degradation of 12.65%, and a cumulative degradation of 6.4% during the test period, which was significantly different from sample 6.

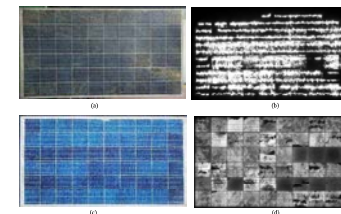


Fig. 3 a. Sample 6 Appearance b. Sample 6 EL  
c. Sample 13 Appearance d. Sample 13 EL

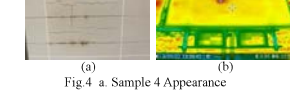


Fig. 4 a. Sample 4 Appearance b. Sample 4 Infrared Photo

Therefore, in the process of power station construction and grid-connected operation, it is necessary to avoid the problems of glass damage and cell fragments in the samples as far as possible, and regularly carry out the detection of sample power degradation during the later operation and maintenance process. When the power degradation reaches the economic balance point of technological transformation benefits, the modules with glass damage and cell fragmentation should be replaced in time.

The typical defects of the backsheet include scratches and cracks. Since all the selected samples were installed on fixed racks, it can be inferred that the physical damage of backsheet scratches mainly occurred during the transportation and installation stages. Scratches and cracks in the backsheet can allow moisture and air to enter the sample, where they react chemically with the encapsulant (EVA) to form acetic acid and corroded metal conductors and accelerates the power degradation of the sample. Based on extensive research experience, in arid and hot climate conditions with low ambient humidity, the likelihood of moisture entering the interior of a PV module through a single backsheet crack is relatively low, and thus the probability of metal corrosion is also small. However, the backsheet cracks found in this research, along with the more severe power degradation, are speculated to be due to the combination of backsheet cracks and cell fragments. This causes long-term current mismatch between cells and multiple hot spots in different areas, which significantly accelerates the power degradation of the sample. As shown in Figure 4, the temperature of the hot spot in Sample 4 during operation reached 64.9°C, more than 30 degrees higher than that of a normally operating sample. The cumulative degradation during the test period reached 53.8%.

Table 3 The Peak Hours of the samples

| Date | Failure/Defects                        | 2021/8/31 | 2021/9/30 | 2021/10/31 | 2021/11/30 | Accumulated Peak Hours (h) |
|------|--|-----------|-----------|------------|------------|----------------------------|
| 1    | Accumulated irradiation                | 1118.57   | 1226.74   | 1451.31    | 917.70     | 4700.41                    |
| 2    | Cell micro-cracks/None                 | 1000.00   | 992.40    | 988.57     | 789.47     | 3049.42                    |
| 3    | Small cell/cell micro-cracks           | 1055.12   | 995.31    | 995.01     | 977.41     | 3045.70                    |
| 4    | Cell micro-cracks/Backsheet cracks     | 1022.54   | 993.82    | 1000.32    | 971.4      | 3777.89                    |
| 5    | Cell fragmentation/Backsheet cracks    | 956.87    | 974.82    | 993        | 97.68      | 1801.66                    |
| 6    | Cell micro-cracks/Backsheet cracks     | 989.78    | 983.25    | 1120.76    | 984.1      | 3777.79                    |
| 7    | Glass breaking/Cell micro-cracks       | 286.72    | 218.48    | 302.11     | 99.84      | 866.15                     |
| 8    | Glass breaking/Cell fragmentation      | 755.48    | 760.1     | 378.9      | 305.1      | 1870.98                    |
| 9    | Backsheet cracks/Backsheet deformation | 17.09     | 1245.9    | 1317.05    | 111.59     | 2501.74                    |
| 10   | Acidic Ices infiltration               | 147.81    | 0         | 0          | 0          | 147.81                     |
| 11   | Cell micro-cracks/None                 | 1017.82   | 1024.83   | 996.01     | 786.70     | 3715.56                    |
| 12   | Corrosion damage                       | 1002.42   | 981.89    | 1012.76    | 864.06     | 4113.57                    |
| 13   | Cell backsheet                         | 1000.42   | 981.71    | 982.76     | 864.06     | 3984.91                    |
| 14   | Glass breaking/Cell micro-cracks       | 978.24    | 956.71    | 791.42     | 879.97     | 3865.11                    |
| 15   | Backsheet deformation                  | 992.21    | 984.03    | 1109.25    | 688.21     | 3714.23                    |
| 16   | Cell micro-cracks/None                 | 999.42    | 938.31    | 1007.57    | 626.1      | 3951.79                    |

As can be seen from Table 4, since Sample 11 was a control sample, its degradation rate during the test period was 0.96%, hence its peak hours was relatively high. Samples with junction box abnormalities had significantly lower peak hours than other samples due to the instability of the electrical connections. Moreover, the peak hours of samples with multiple damages (such as cracks in cells + backsheet cracking + burning) was significantly lower than that of samples with single failure.

## Typical Cases Analysis

During the implementation of this research, several typical failure cases were identified through analysis, such as samples 3, 8, and 9, which exhibited different behaviors during the degradation and aging process than expected. The analysis is as follows:

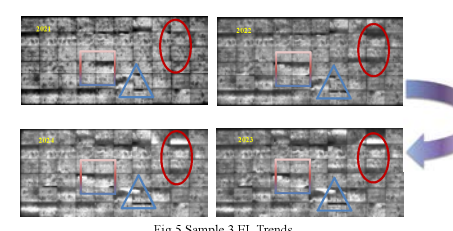
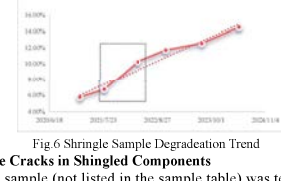


Fig. 5 Sample 3 EL Trends

## ◆ Degradation Caused by Cell Defects and Backsheet Cracking

Sample 3 had partial edge dark areas in the cells (cutting damage) of the initial state, as shown in Figure 5. During the operation, the three marked dark areas showed a gradual increase and were accompanied by the appearance of fragments. The corresponding changes in the sample degradation shown in Figure 6. It can be seen that after August 2021, there was a rapid power degradation rate, which was higher than the average degradation trend indicated by the red dashed line, and was the same as the EL imaging change trend in 2022. Subsequently, it remained relatively stable. Therefore, it can be inferred that compared to hidden cracks in the cells, the fragments caused by cutting damage to the cells have a more severe impact on PV modules.

The degradation trend of sample 3



## ◆ Impact of Single Cracks in Shingled Components

There is a shingled sample (not listed in the sample table) was tested in the research. During the installation process, the backsheet of this sample was scratched, as shown in two cracks within the cells, as shown in Figure 7. However, the width of the cracks gradually increased after months, forming a small number of fragments. This is related to the connection structure of shingled module as it cuts the intact cells into multiple narrow and long strips, which are horizontally stacked and connected through conductive adhesive. The stress distribution in the stacking area is uneven, and the junction is prone to cracks due to deformation. However, STC power tests indicated that the power of the sample decreased from 304.92W to 303.49W from 2021 to 2024. It is evident that under low humidity environmental conditions, a single crack has a relatively low impact on the power of the sample.

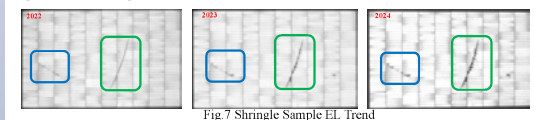


Fig. 7 Shingle Sample EL Trend

## ◆ Impact of Damaged Junction Box Samples

The junction box is a core component of electrical connection and protection of a PV module, it can trigger a multitude of issues when failed, covering aspects such as safety, power generation efficiency, and component reliability. In this research, Sample 9 experienced intermittent open circuits in its electrical structure during the testing process, as shown Figure 8. The blue curve had an amplitude of 0 for some periods. After maintenance, it returned to normal. A similar situation occurred during indoor testing, where the power value displayed was 0. Therefore, the failure of the junction box seal (such as due to the aging of the adhesive) can lead to the ingress of moisture, causing corrosion of the internal terminals or cables, a decrease in insulation resistance, and even short circuits between metal components, resulting in leakage current, increasing the risk of fire.

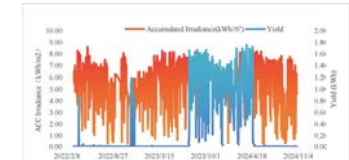


Fig. 8 Shingle Sample Degradation Trend

## Conclusions

Crystalline silicon PV modules, when exposed to outdoor environments over the long term, are subject to damage caused by a variety of factors, including external environmental conditions and installation operation factors. This project focuses on the degradation mechanisms and power generation capability trends of modules that have already suffered different types of failure during operation. Through long-term laboratory and outdoor testing and analysis of 15 types of PV modules that have been in operation for 5–10 years, it can be observed that in arid and hot regions, where cracks are the most common type of failure, the impact of a single cell crack on the sample is relatively low. However, if influenced by external forces, the cracks in the cells can develop into fragments, which significantly affect the power and generation capability. A single glass scratch has a limited impact on the power of the PV module, but when glass damage is combined with cell fragments, it can cause severe failure. It was also found in the tests that failure to the junction box not only has a significant impact on the power generation capability of the samples but is often accompanied by backsheet burning during operation, leading to the formation of high-temperature hot spots, accelerating the material aging process, and easily causing short circuits between metal components, resulting in leakage current and increasing the risk of fire.

Due to the limited samples in this research, it is necessary to expand the sample size or conduct repeated experiments in the future to enhance the reliability of the conclusions. For example, introducing TOPCon and HJT samples, future research will further combine material micro-characterization (such as defect analysis and environmental endurance testing) to explore the mechanisms.

## Acknowledgments

This research was generously supported by the National Centre of Inspection on Solar Photovoltaic Products Quality (CPVT). We are grateful to our research group members for their active participation in the data collection and analysis.

E-mail: ggbn@163.com

# Low-Cost Daytime Electroluminescence Imaging

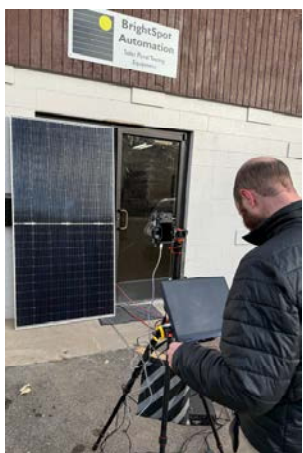
Jared D. Friedl, Rich Landy, and Andrew M. Gabor

BrightSpot Automation, Boulder, CO, USA



## 1. Background/Motivation

- Most outdoor electroluminescence (EL) imaging of solar panel defects is performed at night to avoid noise light from the sun overwhelming the signal from the panels

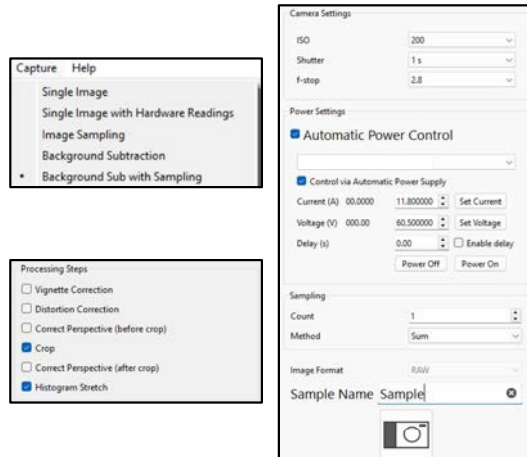


TravEL-Spot

- Daytime measurements are desired by some groups
  - Daytime solutions exist, but are generally expensive and have low resolution
  - Even for indoor testing, sunlight and fluorescent light can add noise
- We present a low-cost approach to taking low-noise EL images in high-noise conditions using IMPEL software which controls both the high-resolution camera and the power supply. An **image pair** is captured with the power supply on, then off, and a **Difference image** is generated by subtracting these images on a pixel-by-pixel basis to remove noise
- If the signal-to-noise ratio (SNR) of a single **Difference image** remains inadequate, multiple **image pairs** are produced sequentially, and their **Difference images** are summed together to improve SNR

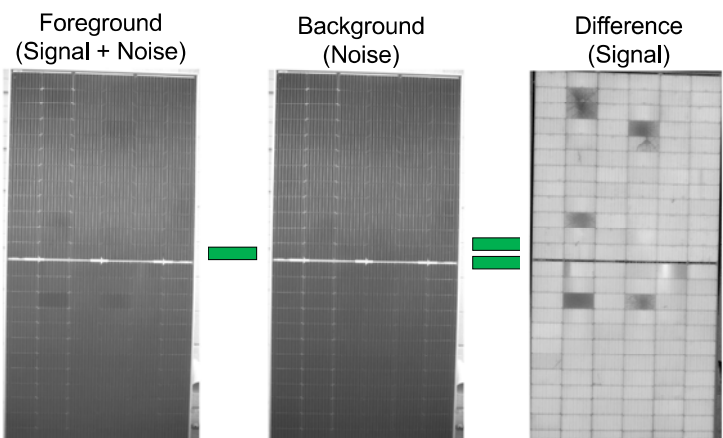
## 2. Implementation in IMPEL Software

- IMPEL software controls and coordinates camera and power supply with user-defined settings
- Multiple background subtractions can be sampled to generate final Difference image
- Image contrast is enhanced via a user defined histogram stretch



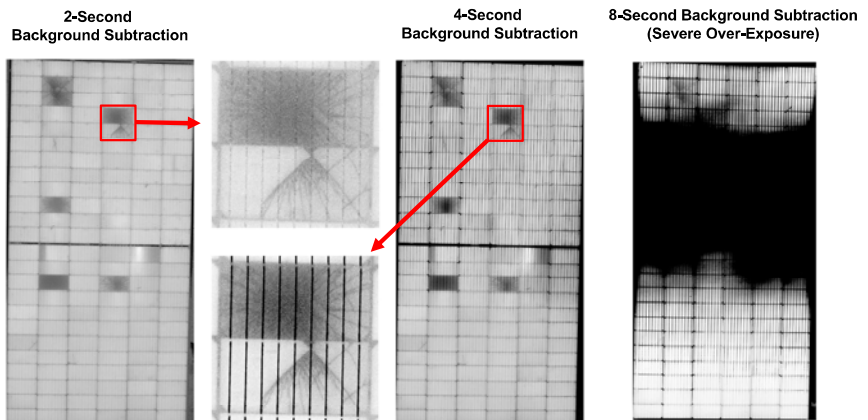
## 3. Background Subtraction

- Background subtraction effectively extracts EL signal even when noise light is far brighter
- Histogram stretch improves contrast of EL-only image and reveals damaged or degraded cells



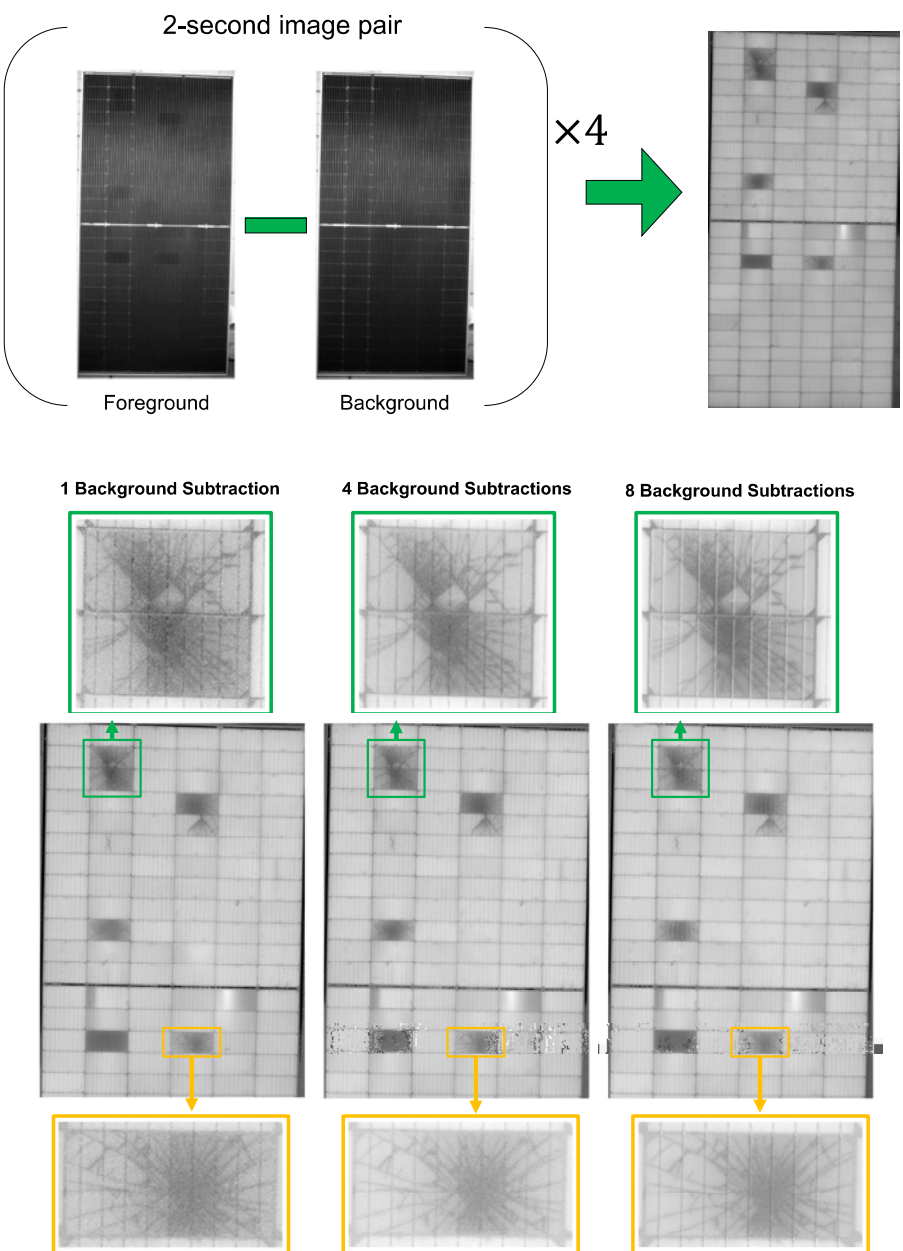
- Longer exposure times improve quality of background-subtracted Difference image, but:

- Pixel saturation on inactive areas of the module – wires and backsheet – produces visual artifacts in the Difference image without invalidating active area signal
- It is important to avoid pixel saturation in the active area of the module



## 4. Background Subtraction With Sampling

- Multiple Difference images from shorter-exposure image pairs are easily summed to improve EL image quality



- Background subtraction with sampling isolates EL signal in especially noisy conditions, such as outdoors in the sun, while a short duty cycle suppresses the effects of variable noise



# A Tool to Create High-Fidelity and Adaptive Finite Element Meshes for PV Systems

Xin He (NREL), Walid Arsalane (NREL), Munjal Purnkant Shah (NREL), Ethan Young (NREL)

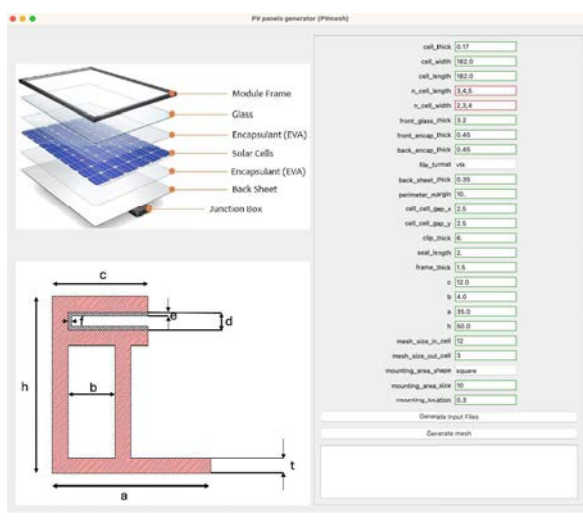
## Motivation

The finite element (FE) method has been widely employed to assess the reliability and durability of PV modules. Theoretically, the **accuracy of simulation results is intrinsically linked to the quality of the mesh** used in the FE model, necessitating the development of high-fidelity FE meshes. However, generating an optimal mesh for PV panels presents significant challenges due to their complex geometrical configurations. To address this issue, a **Python-based tool utilizing GMSH has been developed to create high-fidelity, flexible FE meshes for PV systems**. The developed tool, called **PVMesh**, offers the following advantages: it allows for improved control over mesh size across various domains, thereby **enhancing overall mesh quality**; it supports generating mesh files in multiple formats to facilitate **compatibility across different platforms**; and it accepts input lists to generate meshes for models with diverse geometries, thereby **streamlining parametric studies**.

## PVMesh Package

The graphic user interface (GUI) triggers a background process in which the code **generates an input file** based on users' inputs, **creates the geometry**, **generates the mesh**, and automatically **saves the mesh file in various formats**.

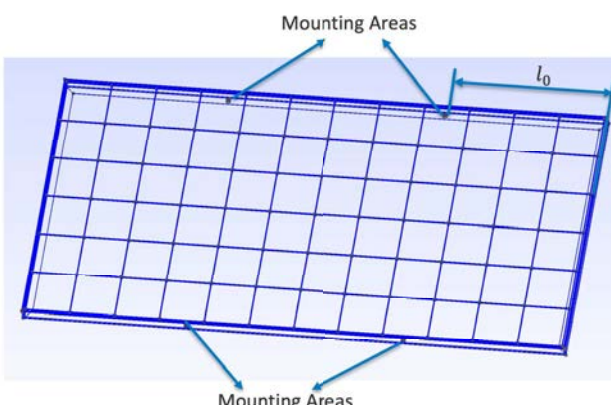
- Facilitating compatibility: the mesh file is saved in **.msh**, **.vtk**, **.inp**, and **.bdf** formats which are widely used across different FE packages.
- Streamlining parametric studies: allow users to input lists for each parameter. PVMesh considers all combinations of input parameters, generating one mesh file for each combination.



The GUI of PVMesh.

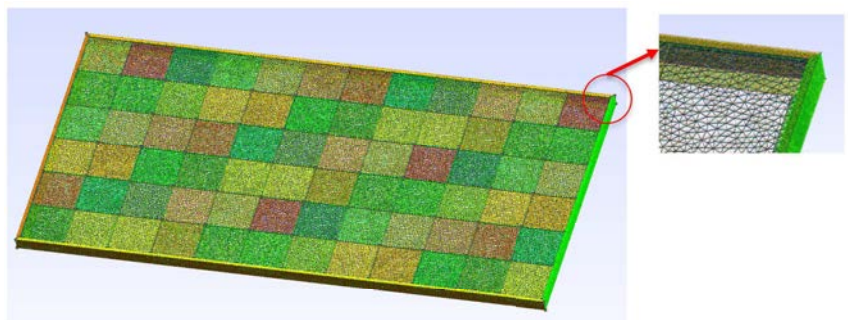
## Meshing Strategies

To mitigate the issue of discontinuous mesh sizes, all layers are partitioned according to the configuration of the cell layer, resulting in a uniform arrangement across all layers.



Partitioned geometry based on cell layer's configuration.

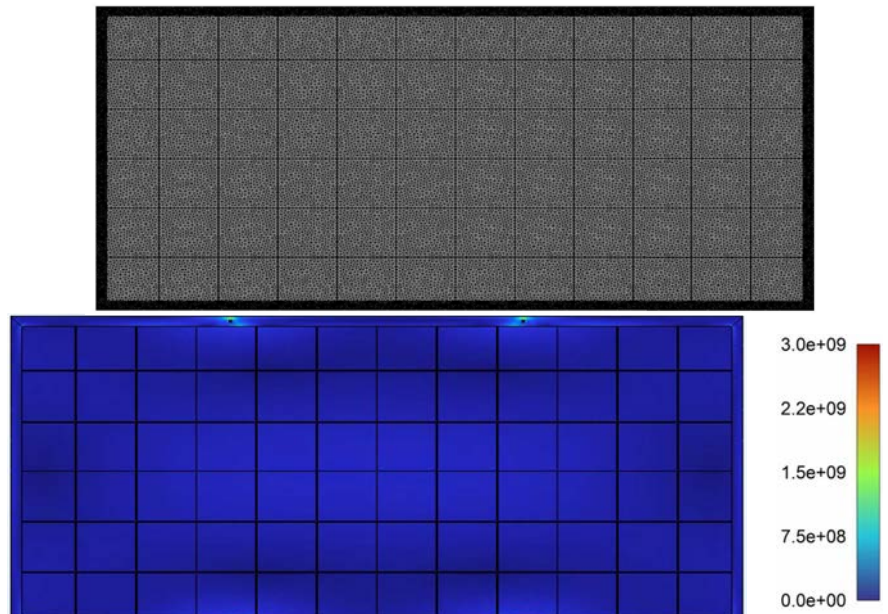
To enhance user flexibility in meshing, PVMesh allows users to specify mesh sizes for different domains. A finer mesh is used for the frame and gap areas to accurately capture their complex geometries while a coarser mesh is applied to the regions within the cell domain across its entire thickness to reduce the total number of elements or degrees of freedom.



Generated mesh with ~500K nodes in a panel consisting of 12 by 6 cells, coarse mesh size is applied to cell domains

## Mesh Verification

The generated mesh from PVMesh is imported into various commercial software packages to verify its integrity. A simple simulation was conducted in which all domains were assigned elastic material properties ( $E = 100\text{GPa}$ ,  $\nu = 0.3$ ). In this simulation, the displacements at the mounting areas were constrained, and a uniform pressure of  $10\text{MPa}$  was applied to the top surface, excluding the surfaces of the frames.



(Top) The mesh imported to three different solvers: COMSOL, ANSYS, and FENiCSx, (Bottom) an example of the simulated Von Mises stress, note the stress concentrations near the mounting areas due to the applied boundary conditions. The successful execution of this simulation indicates the high quality of the mesh.

## Conclusions

We developed an open-source tool, named PVMesh, in response to the challenges associated with generating high-quality meshes for PV panels. PVMesh offers enhanced control over mesh size across domains, thereby improving overall mesh quality. It exports mesh files in multiple formats, facilitating compatibility with various commercial software packages. Additionally, PVMesh accepts list inputs to enable the generation of multiple mesh configurations for parametric studies on geometry or mesh density.

## References

- [1] E. Young, et al., "A fluid-structure interaction solver for investigating torsional galloping in solar-tracking photovoltaic panel arrays," Journal of Renewable and Sustainable Energy, vol. 12, no. 6, 2020.
- [2] X. He and N. S. Bosco, "Finite element simulation of mixed-mode pv encapsulant delamination based on cohesive zone model," National Renewable Energy Lab.(NREL), Golden, CO (United States), Tech. Rep., 2018.
- [3] M. Deceglie, N. Bosco, T. Silverman, and M. Springer, "Whatscracking [swr-23-03]," National Renewable Energy Laboratory (NREL), Golden, CO (United States), Tech. Rep., 2023.





# IEC PV Standards Activities



John Wohlgemuth  
PowerMark Corporation

## Summary

IEC Technical Committee (TC) 82 writes International PV Standards

PowerMark serves as the Technical Advisor (TA) to US TAG of TC82 under NREL Agreement SUB-2025-10028.

In 2024 TC 82 published 1 International Standard, 4 Technical Specifications and 4 Corrigendum/Amendments to existing standards.

## IEC PV Standards published in 2024

**IEC 62788-1-1:** ED 1 - Measurement procedures for materials used in photovoltaic modules - Part 1-1: Encapsulants - Polymeric materials used for encapsulation

## IEC PV TS's published in 2024

**IEC TS 60904-1-2:** ED 2 -Photovoltaic devices - Part 1-2: Measurement of current-voltage characteristics of bifacial photovoltaic (PV) devices

**IEC TS 62257-9-5:** ED 5 - Renewable energy off-grid systems – Part 9-5: Integrated systems – Laboratory evaluation of stand-alone renewable energy products for rural electrification

**IEC TS 62788-2:** ED 2 - Measurement procedures for materials used in photovoltaic modules - Part 2: Polymeric materials - Frontsheets and backsheets

**IEC TS 62788-8-1:** ED 1 - Measurement procedures for materials used in photovoltaic modules - Part 8-1: Electrically conductive adhesive (ECA) - Measurement of material properties

## New TC 82 Projects

**Floating PV** – System design, module and component qualifications

**Safety for Higher Voltage Modules** (up to 3000 volts)

**Revision of Module Qualification** (IEC 61215 series)

**Revision of module energy rating system** (IEC 61853 series)

**Connecting PV systems to grid** (IEC 63409 series)

**About half of all the projects being worked on in TC82 involve maintenance of older documents.**

## 2024 Corrigendum & Amendments

**IEC 60891:2021/COR1:2024** - Corrigendum 1 - Photovoltaic devices - Procedures for temperature and irradiance corrections to measured I-V characteristics

**IEC 61730-2:2023/COR1:2024** - Corrigendum 1- Photovoltaic (PV) module safety qualification - Part 2: Requirements for testing

**IEC 62788-7-3:2022+AMD1:2024 CSV** - Measurement procedures for materials used in photovoltaic modules - Part 7-3: Accelerated stress tests - Methods of abrasion of PV module external surfaces

**IEC TS 62915:2023/COR1:2024** - Corrigendum 1 - Photovoltaic (PV) modules - Type approval, design and safety qualification - Retesting

## Requirements for Participation in IEC Standards Activities

Join your National TAG

In US this means joining the ANSI TAG for IEC TC82 & paying the \$325 annual dues

For more information contact John Wohlgemuth at [JWPVReliability@ieee.org](mailto:JWPVReliability@ieee.org)

# Soiling loss modeling in regions across the United States

ALEX BERLINSKY, SENIOR ENGINEER, PERFORMANCE ENGINEERING

PIERRE METAUT, DIRECTOR, PERFORMANCE ENGINEERING

CHRISTINE BORDONARO, PH.D. SENIOR MANAGER, PERFORMANCE & TECHNOLOGY

TAYLOR ROMSHEK, OWNER'S ENGINEER



## Introduction

- Soiling of PV modules from dirt or dust can be a cause 0%-7% performance loss for utility scale projects, so it is important to understand expected losses in early-stage development.
- The industry standard method of estimating soiling losses comes from the "Kimber Model" <sup>(1)</sup>.
- The algorithms referenced in the Kimber Model require a characteristic daily soiling rate, rainfall cleaning threshold, and grace period for each project design and location.
- The Kimber Model proposes typical values for systems in geographies across the desert southwest but does not provide guidance for other US locations. In absence of formalized standards, the industry often uses inputs from the paper uniformly across the US.
- Clearway maintains weather stations at all development locations for a period of 24 months, which include soiling sensors which undergo weekly cleaning. We used data from 10 of these locations to extract inputs to the Kimber Model and compare assumed project losses to "default" inputs referenced in the paper.

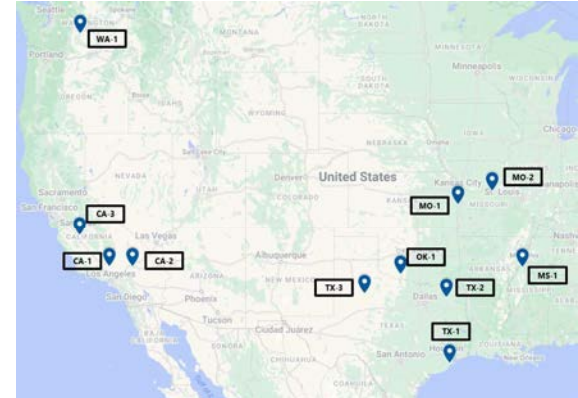


Figure 1: Sites examined in this study

## Methodology

- We developed a python script which extracts the 1-minute GHI, rainfall, and soiling ratio data collected during our met campaigns.
- The script aggregates the data to daily timesteps and uses iterative calculations to determine the optimal input parameters which best align predicted Kimber Model soiling to the observed soiling on site.
- Figure 2 shows the observed soiling ratio and rainfall from the soiling station with the estimated soiling ratio using the optimal Kimber inputs overlayed.
- The inputs determined from that analysis can be applied to a timeseries rainfall dataset with 25 years of historic record to find monthly soiling loss estimates.
- Figure 3 shows a sample from 1999 of the historic rainfall record at the project site and displays the estimated soiling ratios when using the optimal Kimber inputs and the default Kimber inputs.

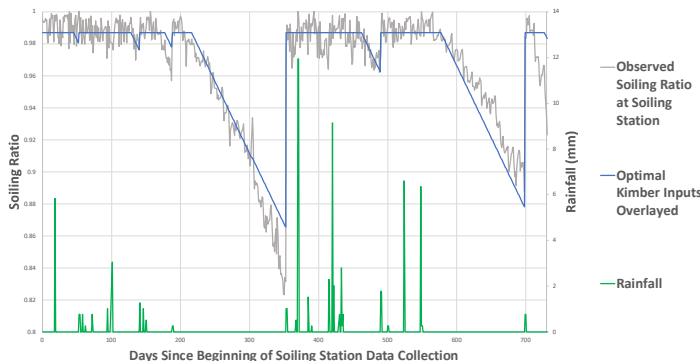


Figure 2: Soiling ratio and rainfall observed at soiling station for CA-3 over 2-year campaign with optimal Kimber Model input assumptions overlayed

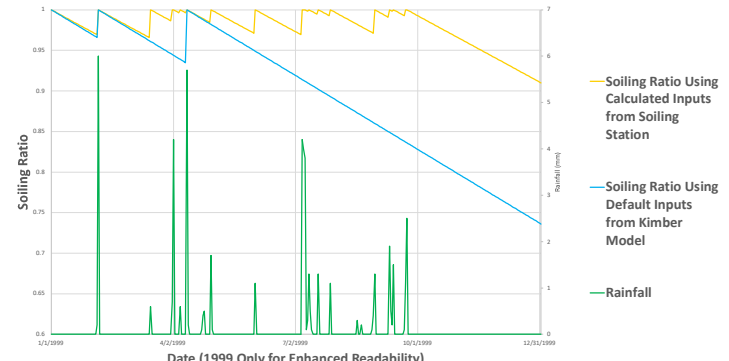


Figure 3: 1999 Rainfall at CA-3 plotted with expected soiling ratios found using soiling station determined optimal Kimber Model input assumptions (yellow) and default Kimber Model inputs (blue)

## Results

Table 1: Soiling Loss Factor results

| Project | Default Inputs from Kimber Paper | Site-Specific Inputs from Met Campaign | Delta  |
|---------|----------------------------------|--|--------|
| WA-1    | 4.67%                            | 0.33%                                  | 4.34%  |
| CA-1    | 8.34%                            | 0.95%                                  | 7.39%  |
| CA-2    | 13.46%                           | 1.56%                                  | 11.91% |
| CA-3    | 12.20%                           | 2.44%                                  | 9.76%  |
| TX-1    | 0.75%                            | 0.03%                                  | 0.72%  |
| TX-2    | 0.83%                            | 0.35%                                  | 0.48%  |
| TX-3    | 1.93%                            | 0.23%                                  | 1.70%  |
| MO-1    | 0.63%                            | 0.19%                                  | 0.44%  |
| MO-2    | 0.60%                            | 0.09%                                  | 0.51%  |
| OK-1    | 1.35%                            | 0.12%                                  | 1.22%  |
| MS-1    | 0.59%                            | 0.23%                                  | 0.36%  |

- Our results show the following:

- Projects in California exhibited the largest deviations from the default Kimber inputs in large part due to the conservative nature of the default 5mm rainfall cleaning threshold.
- For the example project (CA-3) shown in Figure 2 and Figure 3, a threshold of ~1 mm was shown to reset the soiling rate in the measured data. Rainfall cleaning threshold appears to have the biggest impact on example project CA-3.
- Greater alignment between the Kimber Inputs and site-specific inputs for regions with more rainfall.
- However, it can be challenging to extract the inputs from a 2-year met campaign in these regions, as soiling may not have a chance to meaningfully accumulate between rainfall events showing trends.
- Project by project considerations should be made. Projects with less than 0.5% soiling loss factor in any given month after site-specific study may be rounded up to ensure estimates are reasonable.
- A well-maintained soiling station during the met campaign can help yield more accurate preconstruction energy estimates.
- Further areas of study:
  - Comparison of operational data to model inputs.
  - Case studies in additional regions with varying rainfall.

<sup>(1)</sup> "The Effect of Soiling on Large Grid-Connected Photovoltaic Systems in California and the Southwest Region of the United States" by Kimber et. al (2006)

# Adaptable Silicon Solar Cell Metrology in the Age of the Inflation Reduction Act

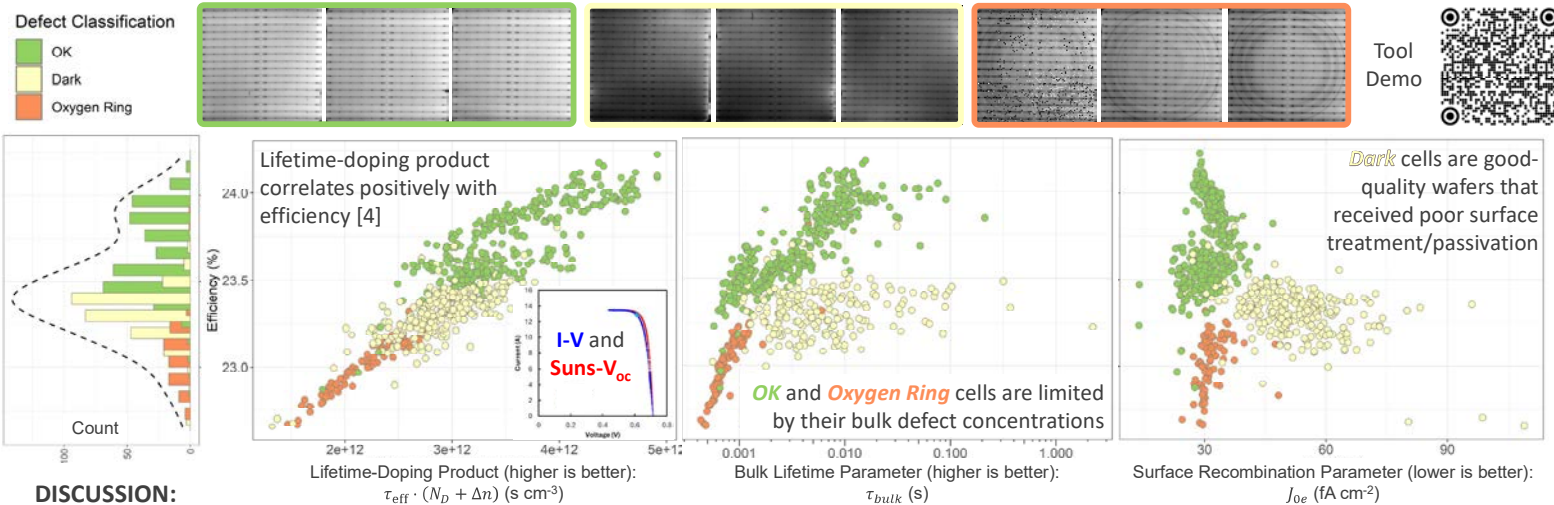
Harrison Wilterdink, Adrienne Blum Karpen, Nick Degenhart, Lena Bruno, Wes Dobson, and Ron Sinton  
Sinton Instruments, Boulder, CO, U.S.A.

**ABSTRACT:** In January 2025, the Solar Energy Industries Association reported annual production capacities of approximately 50 GW for US modules and 1 GW for US cells [1], which suggests that up to 49 GW of cells are being imported annually by the nascent US module manufacturing industry incentivized by the 2022 Inflation Reduction Act (IRA). While cell imports will likely continue in the short-term, module manufacturers may gradually transition to new domestic cell suppliers in order to benefit from the IRA's domestic content provisions. Among the changing landscape of cell suppliers, module manufacturers must implement and maintain quality control measures to weed out defective cells that would compromise module quality.

We present a case study in quality control by leveraging the capabilities of a nearly-contactless solar cell sorter that provides comprehensive cell characterization including light I-V, reverse dark I-V, Suns-V<sub>oc</sub>, substrate doping, carrier recombination lifetime, and power loss analysis by mechanism. A fully contactless line scan photoluminescence image of the cell complements these measurements by allowing visual identification of defects such as cracks, broken fingers, oxygen rings, and low-lifetime regions. The "contact-light" nature of this system means it can more easily adapt to changing cell designs and cell suppliers, while the suite of measurements means module manufacturers can implement better quality control with fewer tools.

## METHODS AND ANALYSIS:

- We measure the I-V curve, Suns-V<sub>oc</sub> curve, and line scan PL image of 1000 industrial TOPCon cells on the Sinton Instruments FCT-1000 [2][3] in order to report efficiency and carrier recombination lifetime parameters as a function of the top three visual defect classes.



## DISCUSSION:

- What is the best strategy to sort these cells into modules?

This depends on whether each defect class degrades differently in the field, which was unfortunately outside the scope of this study. We modeled two basic strategies:

- Sort by efficiency only—Most modules will contain a mix of defect classes.
- Sort by defect class and efficiency—Most modules will contain only cells of a single defect class, potentially leading to more uniform and predictable long-term degradation characteristics.
- Both strategies have comparable cell-to-module power losses due to current mismatch [6].

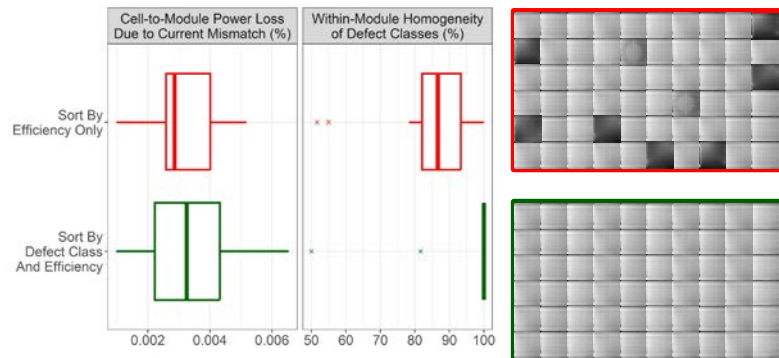


Illustration of modules resulting from different cell sorting strategies

**CONCLUSIONS:** Domestic module manufacturing requires thorough quality control of incoming cell supply. We have developed a **next-generation cell sorter** that utilizes contactless and near-contactless test methods to accommodate the widest possible variety of cell types, including modern cell designs with vanishing silver content such as multi-busbar, busbarless, and backside-contact. The tool can sort on all conventional I-V cell parameters, Suns-V<sub>oc</sub>/lifetime parameters, as well image-based visual defect classes to enable optimal quality control of incoming cells.

## REFERENCES:

- [1] SEI Solar and Storage Supply Chain Dashboard, accessed 21-Jan-2025: <https://seia.org/research-resources/solar-storage-supply-chain-dashboard/>
- [2] H. Wilterdink, R. Sinton, A. Blum, K. Dapprich, N. Degenhart, W. Dobson, "Near-Contactless Production I-V Testing of Silicon Solar Cells", 50<sup>th</sup> IEEE PVSC, 2023 (Puerto Rico).
- [3] A. Blum Karpen, H. Wilterdink, R. Sinton, N. Degenhart, L. Bruno, W. Dobson, "Characterization Solutions for the Next Generation of Solar Cells", Workshop on Crystalline Silicon Solar Cells and Modules: Materials and Processes, 2024.
- [4] A. Blum, R. Sinton, W. Dobson, H. Wilterdink, J. Dinger, "Lifetime and Substrate Doping Measurements of Solar Cells and Application to In-Line Process Control", 43<sup>rd</sup> IEEE PVSC, 2016 (Portland).
- [5] D. Kane and R. Swanson, "Measurement of the Emitter Saturation Current by a Contactless Decay Method", 18<sup>th</sup> IEEE PVSC, 1985 (Las Vegas).
- [6] R. Evans, K. Kim, X. Wang, A. Sugianto, X. Chen, R. Chen, M. Green, "Simplified Technique for Calculating Mismatch Loss in Mass Production", Solar Energy Materials & Solar Cells, 2015.



# X-Ray Imaging as a Tool for Understanding Photovoltaic Connector Failures

Steven J. DiGregorio, Laurie Burnham, Bruce H. King

Sandia National Laboratories, Albuquerque, NM

## Background and Motivation

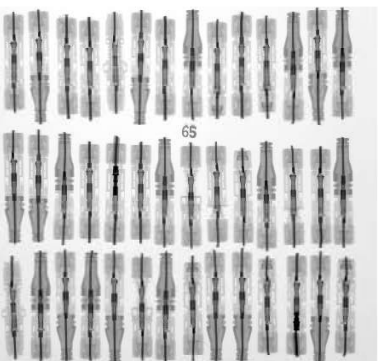
Connector failures are a major cause of power loss, safety hazards, and fires in the photovoltaic industry. Understanding the reasons for these failures is crucial for improving reliability. Traditional forensic methods often involve destructive testing, which limits the number of samples available for analysis. This study uses non-destructive, high-throughput X-ray imaging to analyze over 3,000 fielded connectors. The X-ray analysis method developed in this study can serve as a valuable tool for addressing PV connector issues.

## Objectives

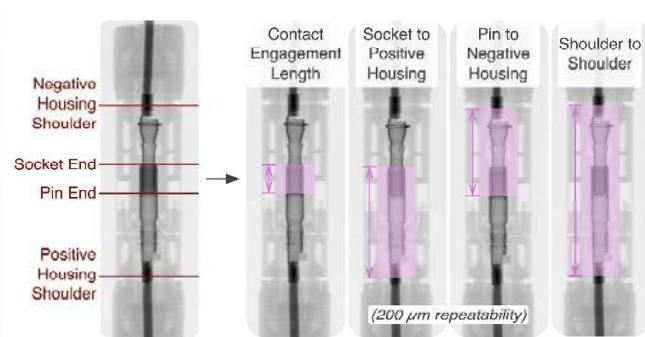
- Develop a non-destructive forensic analysis method for connector failures
- Identify failure modes of fielded connectors
- Measure parameters such as contact displacement and engagement lengths
- Correlate these parameters with resistance measurements to identify key factors contributing to connector performance issues

## Experiment

4. Layout connectors for simultaneous X-ray imaging

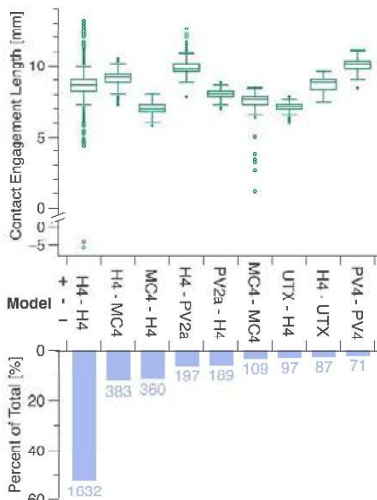


5. Image analysis - manually select 4 points per X-ray image



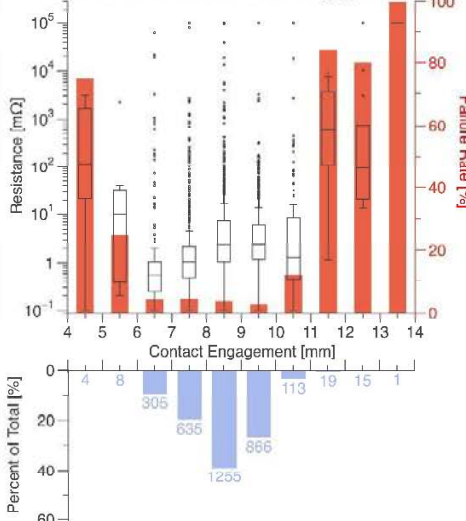
## Results

### Contact Engagement vs. Connector Model

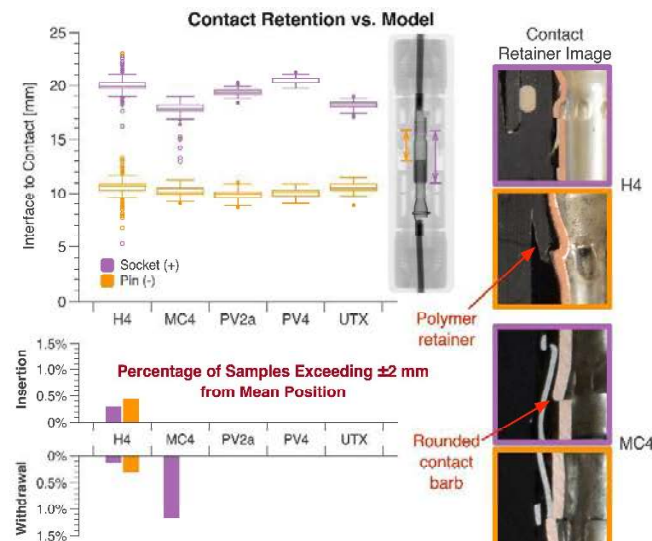


- Mean engagement lengths differ by 3.5 mm
- Negative values indicate complete separation despite normal external appearance.
- H4 - H4 connectors most numerous (52%)

### Performance vs. Contact Engagement



- Failure criteria = resistance > 100 mΩ or signs of melting
- Over and under-insertion correlate with high resistance and failure rates
- 8 ± 2 mm is optimal
- Over-insertion correlates strongly with thermal damage (high heating may cause over-insertion)



- Cross-mating and contact displacement impact engagement lengths
- Displacement > 2 mm may lead to issues
- H4's metal socket retainer outperforms the polymer pin retainer
- Rounded contact barbs can lead to withdrawal failure
- Other models were too few to draw conclusions

## Conclusions and Future Work

- Developed high-throughput forensics method for field-harvested connectors
- Contact engagement length matters (optimal = 8 ± 2 mm)
- Factors that impact engagement length = cross-mating and contact retention
- Future work: cable tension experiments to compare different strain relief and contact retainer designs

## Acknowledgments

This material is based on work supported by the U.S. Department of Energy's Office of Energy Efficiency and Renewable Energy (EERE) under the Solar Energy Technologies Office Award Number 38531.



# Performance Evaluation of a Brazil Research Floating PV Power Plant

Denio Alves Cassini<sup>1</sup>, Antonia Sônia A.C. Diniz<sup>1</sup>, Vinícius Camatta Santana<sup>1</sup>

Daniel Sena Braga<sup>1</sup>, and Lawrence L. Kazmerski<sup>1,2</sup>

<sup>1</sup>Pontifícia Universidade Católica de Minas Gerais (PUC Minas) Belo Horizonte, Brasil

<sup>2</sup>Renewable and Sustainable Energy Institute (RASEI), University of Colorado Boulder, Colorado USA

## Background, Purpose, and Rationale

Brazil's cumulative PV installations surpassed 50-GW<sub>p</sub> at the end of 2024 [1]. This represents ~21% of the country's electrical power, second only to the major hydroelectric sector. With this significant PV-market growth, new applications, including floating PV (FPV) ("fotovoltaics") are emerging [2]. This market segment is important in Brazil because of government & utility interest to gain PV access to existing hydroelectric reservoirs for electric-power expansions. This study evaluates a research-FPV plant (capacity of 1.3-MW<sub>p</sub>) on the Santa Marta CEMIG reservoir (-16.45°, -42.89°), Minas Gerais State, & connected to the energy distributor's electrical system (monitored since March 2022).

**Objectives:** (1) To identify the advantages and disadvantages of using FPV solar systems installed in a reservoir linked with a hydroelectric plant, (2) To evaluate various PV technologies to assess their specific operation in this environment, and (3) To implement a research plan to monitor and identify any degradation processes related to this type of application/installation under the semi-arid tropical climate and the varying environment of the aquatic biome. The conditions leading to potential induced degradation (PID) and unanticipated temperature anomalies associated with the installation design/configuration are analyzed and reported.

## Observations for FPV System



### FPV Module Operating Temperatures and Conditions

- These track ambient temperatures
- Lower than ground-mounted reference modules
- Noticeable increase in aquatic life under FPV structure

FPV Santa Marta: Average Ambient and Module Temperatures Between 11:00 and 14:00

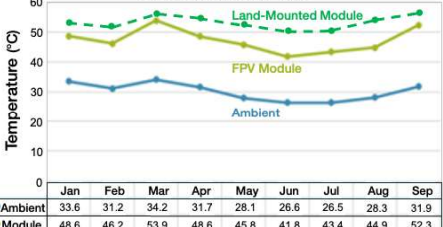


Figure 1. Comparison of average FPV module operating to ambient temperatures. Comparison to local reference ground-mounted module operating temperature is included to show benefit of FPV power benefits

### Access for Characterization and Maintenance

- More limited than ground-mounted system
- Additional safety equipment
- Requires training

## Thin-Film and Bifacial Modules



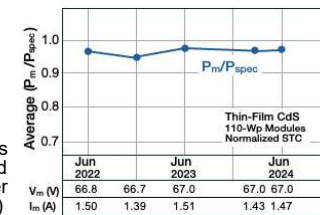
Figure 4. Photos of FPV systems showing mounting of thin-film CdTe modules. Inset also shows the bifacial module positioning,

### Thin Film CdTe Modules: No degradation

- 10 110-W<sub>p</sub> Modules
- Installed April 2022

### Bifacial Modules:

- 2 450-W<sub>p</sub> Modules
- PERC cells
- Installed November 2024
- No degradation (but still being monitored; early in process)



### Thin-Film CdTe I-V Characteristics

Figure 5. Thin-film CdS modules indicating stability over 2-year period on FPV platform. (Average power compared to spec sheet, with V<sub>m</sub> & I<sub>m</sub>)

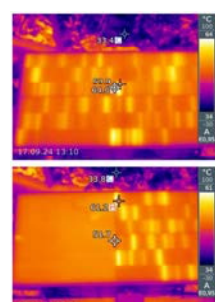
## Crystalline-Si Module Issues

### Affecting Monocrystalline-Si PERC Modules

#### Observations and Measurements Confirming PID [3]

##### A. Drone IR-Thermographic Inspection

- IEC 62446-3
- Hot spots on affected modules (April 2023)
- Area affected: Cells near negative edge of string; hear edges of modules



##### B. I-V characteristics

- Reduction in MPP voltage & current (P<sub>m</sub>)
- Increased R<sub>s</sub> and significantly lower R<sub>sh</sub> for individual modules (Table)

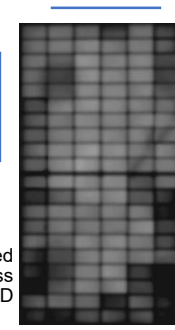
Figure 2. Left: Drone scans of portion of FPV system showing higher temperature (hot spots) regions on modules. And, corresponding degraded I-V characteristics for typical two modules (power loss). Below: Tabulation of the I-V parameters for the 2 modules, with decreased R<sub>sh</sub> and increased R<sub>s</sub>.

| Modules    | Irrad. (W/m <sup>2</sup> ) | Temp. (°C) | I <sub>sc</sub> (A) | V <sub>oc</sub> (V) | I <sub>mp</sub> (A) | V <sub>mp</sub> (V) | P <sub>max</sub> (W) | FF   | R <sub>s</sub> (Ωm) | R <sub>sh</sub> (Ωm) |
|------------|----------------------------|------------|---------------------|---------------------|---------------------|---------------------|----------------------|------|---------------------|----------------------|
| Data Sheet | 1000                       | 25         | 11.6                | 43.6                | 11.1                | 36.2                | 400                  | ---  | 0.32                | 800                  |
| Module 01  | 988                        | 51.0       | 11.0                | 21.1                | 9.9                 | 13.8                | 135.9                | 0.59 | 0.62                | 12.4                 |
| Module 04  | 928                        | 39.7       | 10.8                | 20.4                | 9.6                 | 14.4                | 137.7                | 0.63 | 0.42                | 29.0                 |

##### C. EL imaging

- Selected individual PERC modules analyzed
- PID cells darker images (less light emission)
- Correspond to higher temperature cells

Figure 3. EL image of selected Si PERC module showing loss (darker) regions due to PID (negative edges of string)



[1] ABSOLAR, Energia Solar Fotovoltaica no Brasil, No. 74, Dec.10, 2024. Available through the link: <https://www.absolar.org.br/mercado/informativo/>

[2] Wood Mackenzie, "Floating solar landscape 2024," Nov. 8, 2024. <https://www.woodmac.com>

[3] Sitemark, Unveiling Potential Induced Degradation (PID): Causes, Detection, and Effective Mitigation for PV Modules. <https://doi.org/10.1039/C8RA07071G>

Acknowledgements: The authors would like to thank the collaborators of the GREEN Laboratory (Energy Study Group), the Graduate Program in Mechanical Engineering of the Pontifícia Catholic University of Minas Gerais, and especially CEMIG for their support and collaboration on this project. This work was carried out with the support of CNPq and CAPES (Brazil), CEMIG, and the Fulbright Scholar Program.

This poster contains no sensitive or proprietary information.

## System Soiling Observations



Figure 7. View of floating-PV system, with open-area (potato field) on opposite shore. This area is a source of soiling, with prevalent winds directed over FPV system.

Location, Location, Location!

### Soiling Comparison

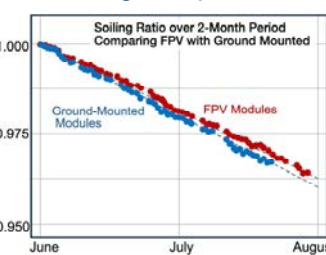


Figure 9. Soiling ratios measured on land-based reference modules are nearly the same as for the FPV modules. Soiling rates are relatively low, less than 0.06%/day.

# MODULE MOUNTING DESIGN QUALIFICATION CHALLENGES

Authors: Jim Sorensen and Sumanth Lokanath

## THE CURRENT SITUATION:

### MODULE MANUFACTURERS

- ▶ Issue mount-specific and sometimes project-specific approvals based on opaque requirements
- ▶ Approval requirements vary by manufacturer, frequently based solely on the module SMLT (IEC 61215, MQT 16)
- ▶ Modules delivered to a project may differ physically from modules tested, but no change in datasheet or model number. For instance: glass thickness, glass stress, frame cross section, material supplier quality, etc.

### TRACKER MANUFACTURERS

- ▶ As experts in wind loading, have little influence on module qualification requirements.
- ▶ Some tracker manufacturers have established high quality standards and rigorous durability protocols demonstrating reliable track records, while other low-cost manufacturers experience much higher failure rates.
- ▶ Unwilling to take module breakage risk
- ▶ Unwilling to make conservative product changes that erode competitiveness. The industry needs to apply consistent requirements.

### FIELD EXPERIENCE

- ▶ Increasing observance of glass breakage at wind conditions well below design wind speeds [1][2]
- ▶ Module frame buckling during strong, but below design wind speeds
- ▶ Module frame fatigue failures [3]
- ▶ Module fastener pull through at mounting points
- ▶ Module fastener loosening



### REFERENCES:

- [1] H. Hieslmair, F. Samara, and M. Jovanovic, "Stress concentrators," DNV, 2023. [Online]. Available: <https://www.dnv.com/article/stressconcentrators/>
- [2] D. Wang, A. Hermawan, and E. Woolard, "Correlation between mid-level wind speed and rear glass breakages on non-large-format bifacial PV modules on trackers in a solar farm," in Proc. IEEE 52nd Photovolt. Specialist Conf., 2024, pp. 0064-0067.
- [3] Y. Yu, "Glass breakage study on large module plus typical tracker system", IEC WG9 committee presentation , 2024
- [4] C. Sillerud, "Modern Methods for Testing Mechanical Durability of PV Modules", NREL/PVWR Proceedings, 2024
- [5] S. Van Pelt, "Module wind load resistance: Standards vs Reality", PV Magazine Webinar, 2021, <https://www.pv-magazine.com/webinars/module-wind-load-resistance-standards-vs-reality/>
- [6] M. Hutchins, "Weekend Read: Temper Tantrum", PV Magazine, 2024, <https://www.pv-magazine.com/2024/01/06/weekend-read-temper-tantrum/>
- [7] J. Raoult, B. Dalatre, "Fatigue equivalent load approach for fatigue design", MATEC Web Conf. 300 02003 (2019), DOI: 10.1051/matecconf/201930002003

## TESTING:

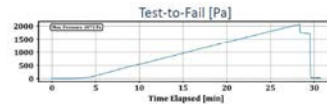
### MOUNTING CONSIDERATIONS:

- ▶ Testing a single module mounted on two mounts, does not represent the typical in-use condition. Mounts are loaded at 50% of expected. Loads are unbalanced. The effect on module can be unpredictable.
- ▶ Must pass component-level testing (not covered here) separate from Module + Mounting testing.
- ▶ Modules also experience stress due to torque tube twist and sag when fixed, or due to movement of the structure. These are currently not considered in testing.

### ASSESSMENT OF TRUE SAFETY FACTOR FOR UNIFORM LOAD:

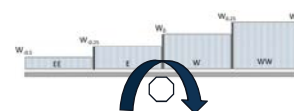
- ▶ Typical test loads are 1.5X design loads, following IEC 61215...
- ▶ Often testing is conducted only to a desired limit, but not up to failure, due to the time and cost of testing
- ▶ Recommend using TTF method proposal [4]

- **Test-to-Failure**
  - Goal: Bound the issue with a max load
  - Duration: 1 hour



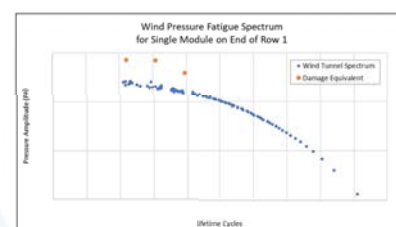
### NON-UNIFORM LOADING:

- ▶ Typical tracker loading is not uniform. It has been assumed that this is adequately captured in the average uniform load requirement and associated safety factor. However, this is widely recognized as inadequate [5][6].
- ▶ With advances in module load test equipment, conducting non-uniform loading is easily performed
- ▶ Industry agreement is needed on universal testing determination and levels



### CYCLICAL FATIGUE LOADING:

- ▶ Most often, no cyclical testing is conducted. In other cases, the DML cycle is used from IEC 61215, which is significantly inadequate for metal fatigue and/or fastener evaluation.
- ▶ Industry agreement is needed on universal testing determination and levels
- ▶ Test equipment now exists for more complex cyclical loading
- ▶ Propose using a damage equivalent approach to setting test levels [7]



## THE PROBLEM

The utility PV industry generally relies on mounting-specific approvals issued by module manufacturers often at pressures well below those required by IEC and UL (61215, 61730, etc). Owner's engineers and project due diligence often require these documents ostensibly to reduce the risk of module breakage and incompatible mounting configurations. However, the process of obtaining these letters and the conditions necessary for satisfactory approval are generally a black box process and not governed by a transparent industry standard.

As an industry, we need to implement a more rigorous qualification testing protocol for different mounting conditions. The reliance on a simple uniform pressure static loading test is insufficient to identify common failure mechanisms seen in the field today.

## PROPOSED TESTING CHANGES

The Interface (Module + Mounting) Test Protocol needs to be expanded:

- ▶ Implement module side-by-side testing
- ▶ Implement a true assessment of safety factor in uniform load testing (TTF)
- Implement baseline non-uniform load testing
- Implement realistic cyclical fatigue loading cycle
- Stop assuming 2400Pa testing is required and necessary

## NEXT STEPS

- Assemble a team of experts committed to contribute to solving this problem.
- Plan to restart IEC Module-Structure Interface standard.

Let us know!

**ARRAY**  
ARRAYTECHINC.COM

# 17 Years of Investigating Fires in PV Systems: A Synopsis of Experience

## Bill Brooks, PE, Principal, Brooks Engineering

After 37 years of experience working with PV systems and having personally investigated about 50 fires in the past 17 years where PV systems were implicated, the author pauses for a moment to recollect what this unique experience has afforded. Specific names and products cannot be shared due to a host of non-disclosure agreements (NDAs). The more beneficial approach for the PV industry is to summarize the experience and categorize the failures and the root causes so that changes to safety standards and construction codes can be more effectively informed. This is not to say that all fire failures require a change to safety standards and construction codes, but it is simply to provide additional information as these important safety-related documents are revised and updated. Since so many fires, euphemistically called "thermal events" are protected by NDAs, it is unfortunate the underlying messages are squelched. This presentation is intended to alleviate this dearth of information with information that is accurate but free of specific names and product failures.

### PV on Fire: Ground-Fault Fires



Bakersfield Fire—Ground-Fault Blindspot—2009

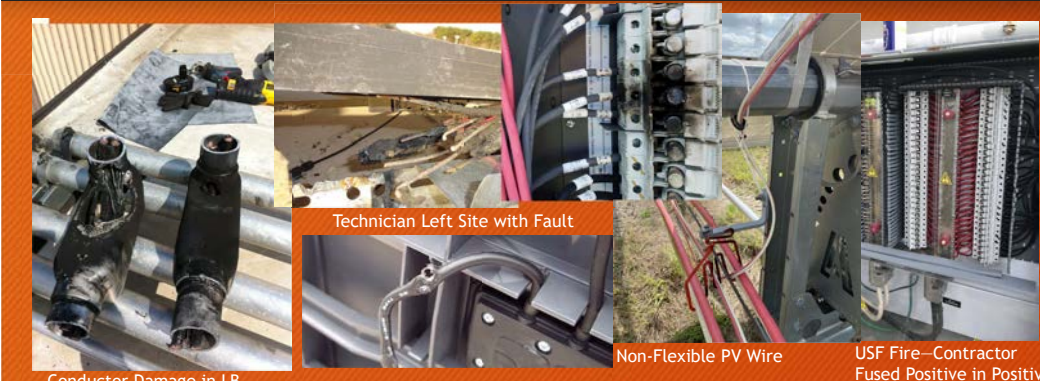


Mt. Holly Fire—Ground-Fault Blindspot—2011



Delanco Fire—Arc or Ground-Fault Blindspot—2013

### PV on Fire: Construction Mistake Fires



Conductor Damage in LB

Technician Left Site with Fault

Non-Flexible PV Wire

USF Fire—Contractor Fused Positive in Positive Grounded System



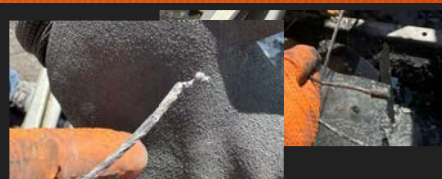
Reverse Polarized String

Bare Grounding Conductor Contacting Negative Bus

### PV on Fire: Connector Fires



Field-Installed Connectors—#1 Reason for PV Fires



Recent Connector Fire—Connector Not Fully Seated



Typical Damage from Connector Fires

### PV on Fire: Product Failure Fires



BIPV Product Failures—Undersized Diodes—Bad Connections

1000Vdc Rooftop Inverter Failures

Likely Origin of Arcing Fire



1500Vdc Inverter Failures

## Decoding PV Module and Tracker Deformation: FEA Insights for Enhanced Durability

Dieter BILLET<sup>1</sup>, Gauvain JAGO<sup>1</sup>

1: ENGIE Laborelec, Rue de Rhode 125, 1630 Linkebeek, Belgium

\* Corresponding author : gauvain.jago@engie.com

### BACKGROUND AND MOTIVATION

- Larger PV modules face structural challenges, leading to visible deformation.
- Mechanical stress and environmental factors can cause spontaneous glass breakage.
- Flexing module and mechanical loads may accelerate crack propagation.
- Modern tracking systems exert higher static and dynamic forces, increasing module vulnerabilities.
- Current standards do not fully account for real-world deformations, necessitating updated evaluation methods.
- No maximum allowable deformation is currently defined in existing norms.



Fig 1: Observed onsite deformation of large, flexible modules.



Fig 2: Measurement of module deformation observed onsite.

### PV PLANT AND CONFIGURATION

- ENGIE's 196 MWp PV plant in the Atacama Desert, COD in 2022.
- Tracker: 2V42 with bifacial PERC 540W modules (2256 × 1133 mm).
- Onsite measurement campaign conducted on 50 modules.
- Multiple measurement methods tested to assess deformation.
- Observed deformation: Ranged from 2.7 mm to 7.5 mm.
- Manufacturer specification: Maximum curvature tolerance of 10 mm under gravitational loads.



Fig 3: Locations of deformation measurements across the PV plant.

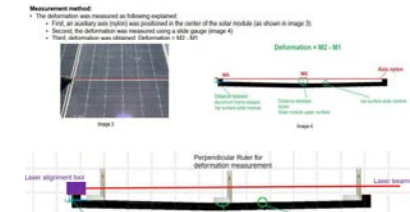


Fig 4: Comparative assessment of different measurement techniques

### MODELISATION

- A tracker and module model was developed in ANSYS, based on tracker specifications and incorporating PV module BOM data.
- Experimental measurements were used for model validation.
- Silicon cells were simplified as a layer matching the glass size, leading to approximate stress estimations for the cells.
- Symmetric semi-section applied for computational efficiency.
- Pressure loads ranging from 1200 Pa to 2400 Pa were applied to the surface.

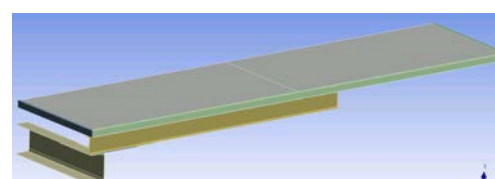


Fig 5: Symmetric model representation of the module and tracker structure.



Fig 6: Cross-sectional view of the module representation, highlighting key structural details.

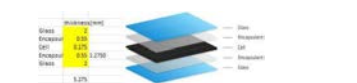


Fig 7: Solar module representation with five simplified layers for structural analysis.

### PRELIMINARY RESULTS

- Gravitational loads: Maximum deformation of 6.5 mm, with 3 MPa stress on bottom glass (low).
- Structural limit: the PV panel almost reaches the material limits for a load of 2000 Pa.
- Maximum stress zones: Located along long edges near the omega bar (top/bottom glass) and slightly below center (rear glass), facilitating post-wind event inspections.
- Silicon positioning: In glass-glass modules, silicon is at the neutral fiber, minimizing stress, whereas in monofacial modules, it is closer to the edge, making it more vulnerable to bending stresses.

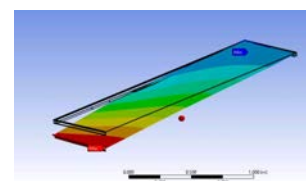


Fig 8: Vertical deformation of 5 mm under gravitational load, measured at a 45° angle at the designated PV park site.

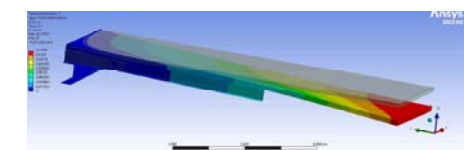


Fig 9: Deformation under a 2000 Pa load on the upper glass, with a maximum deflection of 13.8 cm. The uniformly applied load may underestimate real-world conditions.

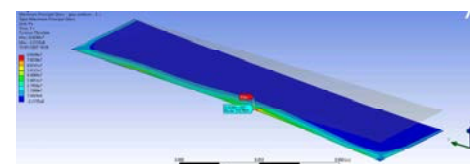


Fig 10: Maximum stress of 88 MPa observed at the end of the omega bar under a 2000 Pa load, with peak levels along the upper side of the glass near the aluminium frame.

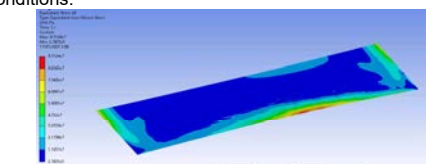


Fig 11: Maximum stress of 97 MPa in the silicon layer near the end of the omega bar under a 2000 Pa load (using a simplified silicon plate model).

### CONCLUSION

- This project identifies overload conditions for PV modules mounted on trackers, linking structural stress to deformation risks.
- Greater emphasis is needed on PV structural integrity, as modules are becoming more flexible and vulnerable to mechanical loads.
- Additional manufacturer data, including wind tunnel tests and detailed evaluation reports, is essential for better model validation.
- Further insights on glass quality and maximum glass strength are necessary to enhance durability assessments and failure predictions.

### NEXT STEPS

- Develop laboratory protocol to mitigate risks related to module deformation.
- Enhance cell modeling to evaluate crack propagation.
- Analyze the impact of glass quality on module deformation and crack propagation.
- Assess the Whatscracking tool for predictive capabilities of cracks.
- Simulate dynamic loads on a simplified tracker model and explore excitation mitigation strategies.

### REFERENCES

- Effects of wind load on the mechanics of a PV Power Plant, Pascal Romer, Kishan Bharatbhai, Andreas J. Beinert, Fraunhofer Institute for Solar Energy Systems ISE, 2022.
- Vortex Shedding Dynamics Behind a Single Solar PV Panel Over a Range of Tilt Angles in Uniform Flow, Jose Luis Suárez, David Cadenas, Higinio Rubio, Pablo Ouro, University of Oviedo, University of Manchester.

### YOUR OPINION

- Would 1300 mm panel provide sufficient resistance under field conditions ?
- Should fully tempered glass be required for larger PV modules ?
- What laboratory testing methods best assess module deformation risks ?
- Are current industry standards sufficient for defining deformation limits ?

# Low-Cost Vibrational Sensors for in-situ High-wind Detection and Analysis

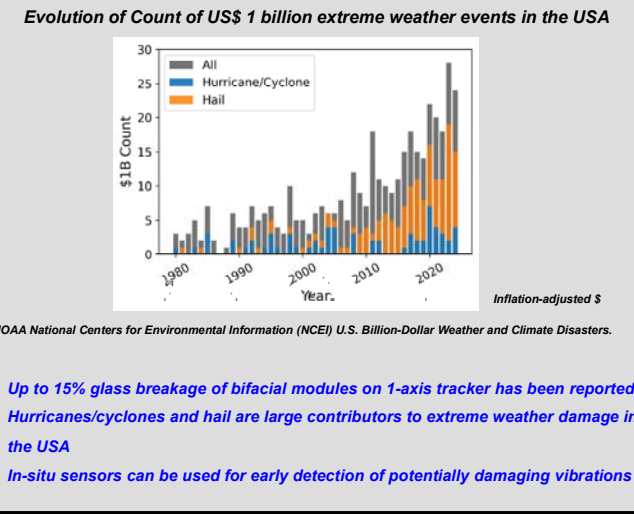
Dirk C. Jordan<sup>1</sup>, Ryan M. Smith<sup>2</sup>, William Sekulic<sup>1</sup>, Hubert Seigneur<sup>3</sup>

<sup>1</sup>National Renewable Energy Laboratory, Golden, CO 80401, USA

<sup>2</sup>Pordis LLC, Austin, Texas, 78729, USA

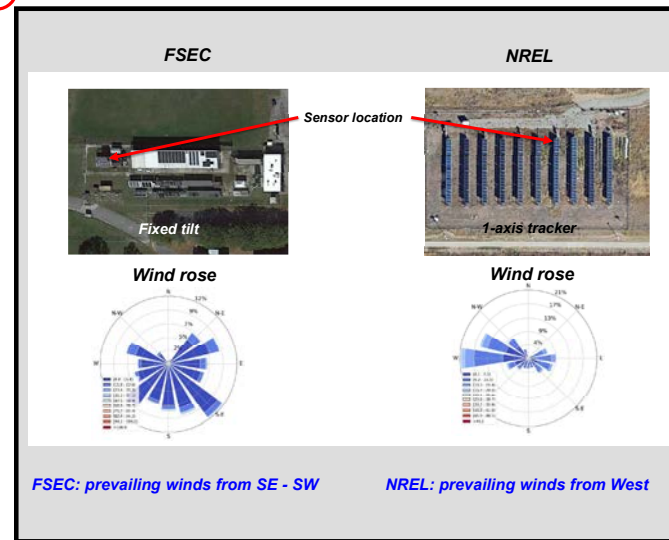
<sup>3</sup>Florida Solar Energy Center, University of Central Florida, Cocoa, FL 32922, USA

## 1 Introduction

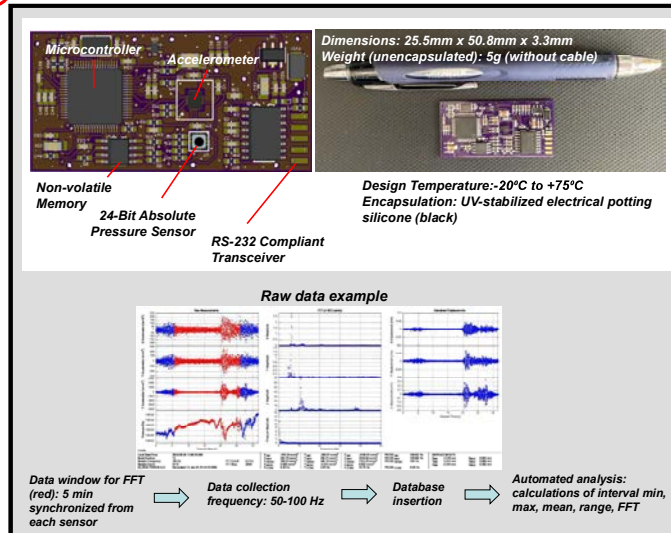


<sup>1</sup>D.Wang, A. Hermawan, and Evan Woolard, DNV, PVSC, 2024.

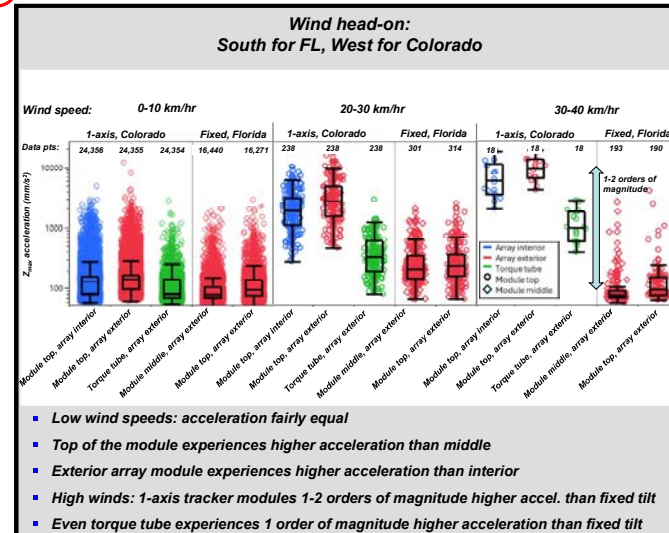
## 4 Sensor Locations & Wind



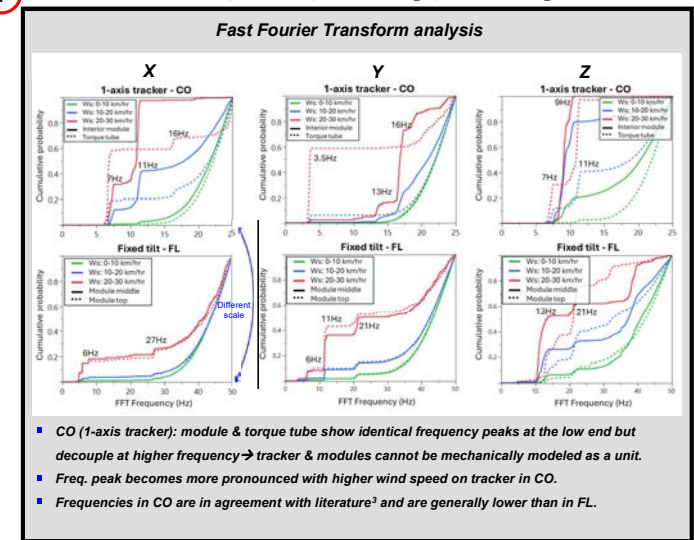
## 2 Vibration Sensor Design



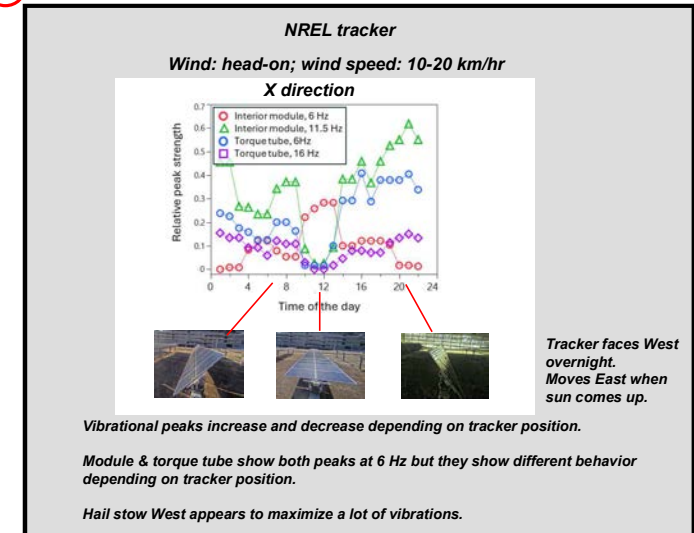
## 5 Head-on Acceleration



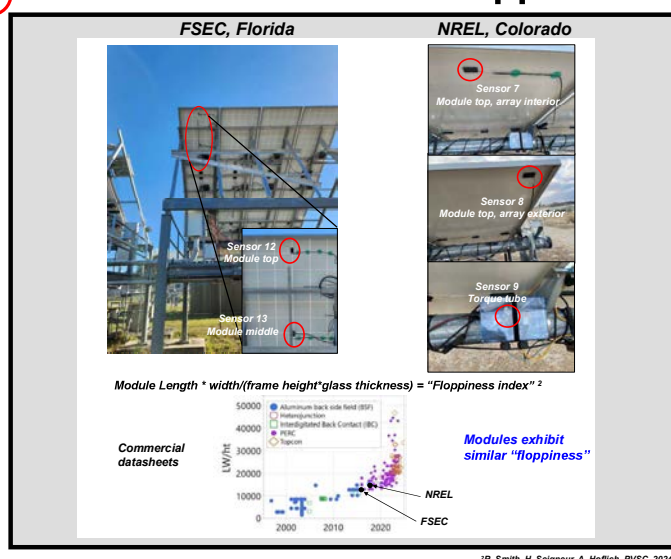
## 7 Modal (Frequency) Analysis



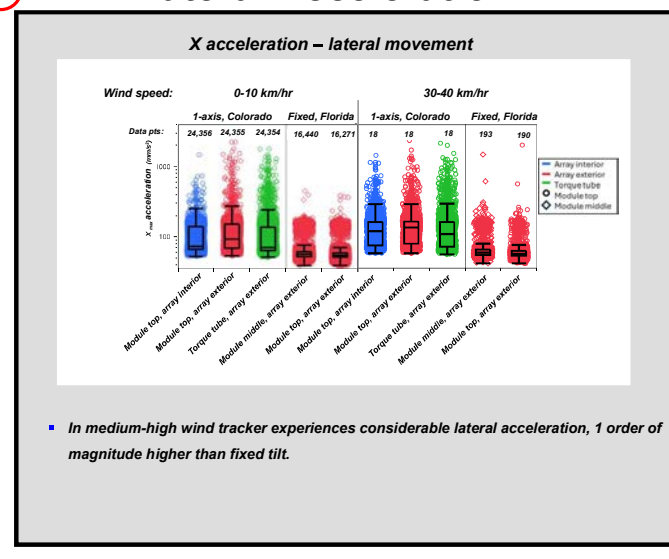
## 8 Tracker Position Effect



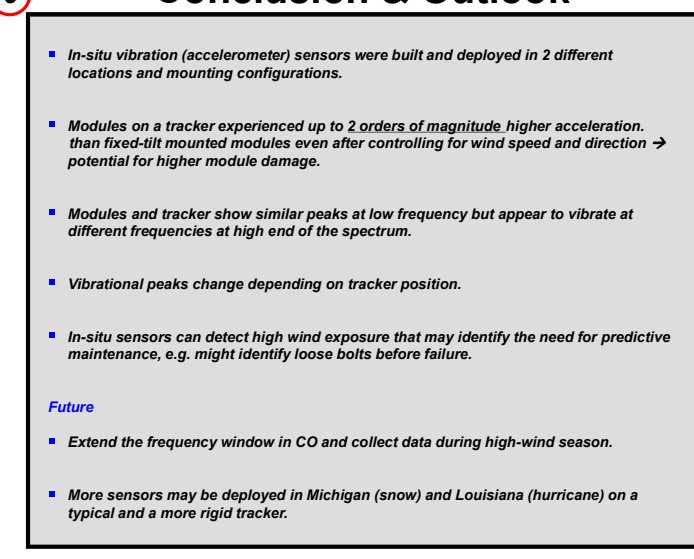
## 3 Sensor Locations & “Floppiness”



## 6 Lateral Acceleration



## 9 Conclusion & Outlook



# Feasibility of Passive MOSFET Paralleling for Photovoltaic Current-Voltage Curves

Alden Mapes, William Sekulic, Byron McDanold, Josh Parker  
 National Renewable Energy Laboratory, Golden, CO 80401 USA

## Introduction

- Current-Voltage (IV) curves are an essential method of characterizing photovoltaic (PV) cells and modules that captures the current output of the device at a range of output voltages [1].
- The FLEA load was developed as a low-cost way to capture IV-curves and track maximum power for a wide range of PV devices, from small research cells to large modules.

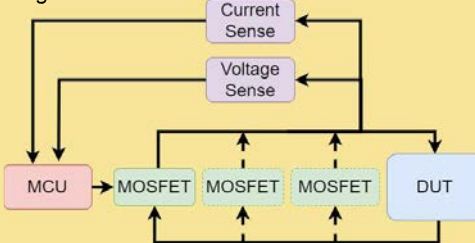


Fig 1 A block diagram of the modified FLEA system

- The FLEA is being developed with the goal of being fully open source and adaptable.
- MOSFETs are used as active resistors, controlling current through the module.
- For high-power modules, it becomes impractical to dissipate the power in a single MOSFET so paralleled MOSFETs are needed [2].
- When MOSFETs operate in the linear mode, they can experience positive feedback between current and temperature, which can cause a single MOSFET to monopolize current and fail [3].
- We evaluate passive circuit solutions to parallel MOSFETs for low cost IV-curve tracing and maximum power point tracking.

## Discussion

- While it is feasible to use passively controlled parallel MOSFETs for IV curve tracing, other operations like continuous maximum power tracking an active control scheme may provide control for higher power modules.
- An active operational amplifier control scheme is almost a requirement to adjust each MOSFET gate ( $V_{GS}$ ) and reduce current imbalance.
- It is recommended to oversize MOSFETs to account for the high temperatures which they may experience during operation, as well as expected deviations in power-sharing.
- Using heat sinks analogous to those used to cool CPUs is an effective way of dissipating heat from MOSFETs.
- Binning MOSFETs by device characteristics is an effective way to ensure currents are well-matched between devices.

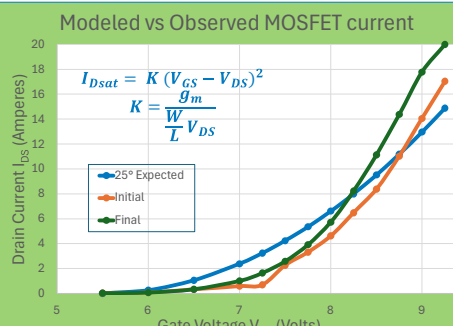


Fig 6 Comparison between initial and final current flow and modeled current flow at a given gate voltage

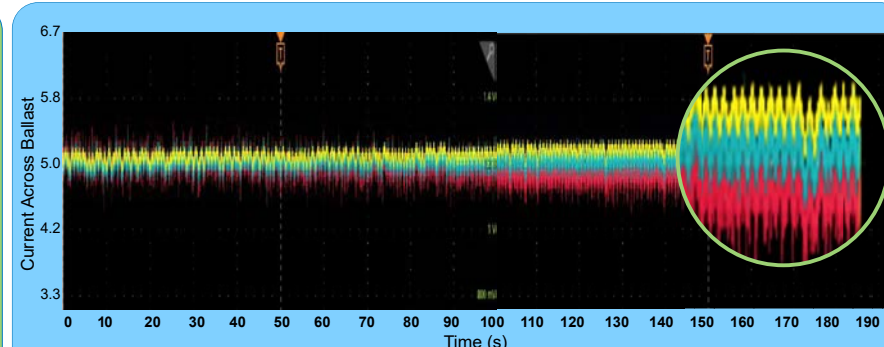


Fig 7 A slow deviation between the currents of three devices during outdoor testing final difference ~8%

## Methods

- We monitored temperature and current flow through each MOSFET.
- MOSFETs with an extended Forward Bias Operating Area were used to allow linear operation.
- Each MOSFET had a separate gate resistor to control for transient effects and a ballast resistor to help balance the power-sharing.
- For outdoor IV-curves, we modified a FLEA load with an external voltage divider and an amplifier to drive the higher gate voltages of these Linear MOSFETs.
- We characterized a generic 260W multi-crystalline silicon module and a 575W monocrystalline silicon bifacial module.
- To cool the MOSFETs, we used heat sinks mounted to fans
- A model of the behavior of the MOSFETs at a certain threshold voltages is shown compared to observed voltages in figure 5.

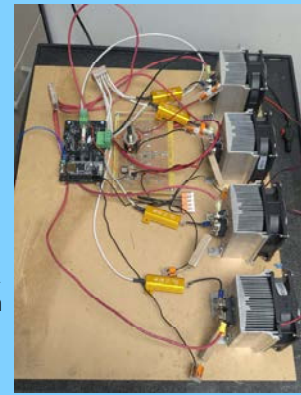


Fig 2 The outdoor 4 MOSFET setup

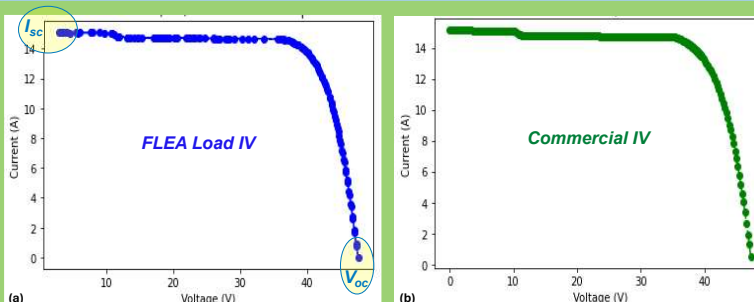


Fig 3 showing IV curves taken on a 575 W module outdoors using 4 MOSFETs with a modified FLEA load [a] compared with an IV curve taken consecutively using a commercially available unit [b]

## Results

- We were able to characterize a 575W module outdoors
- Rapid thermal runaway was avoidable with proper circuit design and oversizing.
- The number of MOSFETs did not impact the FLEA's accuracy beyond the decreased  $I_{sc}$  due to lower  $R_{DS(on)}$
- Slow unbalancing of current between devices occurred outside.
- While device characteristics affected current sharing, this did not cause breakdown.

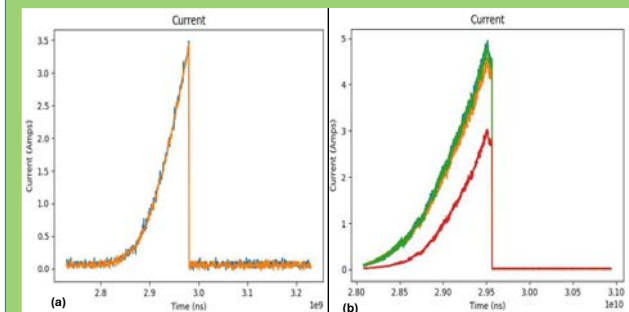


Fig 4 current sharing between 2 well matched MOSFETs (a) compared to 4 MOSFETs with more deviation in device characteristics

- A heatsink without a fan was unable to dissipate the heat from generated.
- FLEA loads are capable of measuring currents of 15 amps without external MOSFETs.

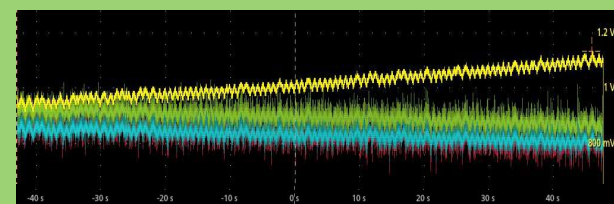


Fig 5 current sharing after intentionally disconnecting a fan during an outdoor test

## References

- [1] ASTM Standard G 1036-02. Standard Test Methods for Electrical Performance of Nonconcentrator Terrestrial Photovoltaic Modules and Arrays Using Reference Cells. West Conshohocken, PA: ASTM International. 2019
- [2] J. B. Forsythe, "Paralleling of Power MOSFETs for Higher Power Output," 1981 Annual Meeting Industry Applications Society, Philadelphia, PA, USA, 1981, pp. 777-796.
- [3] AN11599 Using power MOSFETs in parallel, Nexperia, Nijmegen, Netherlands, Rev 1, 7 July 2015, Available: <https://www.mouser.com/pdfDocs/AN11599.pdf>.

## Acknowledgments

The authors would like to thank Greg Perrin for his help building the modified FLEA. We extend our thanks to Timothy Silverman, Chris Deline, and Quin Guy for their invaluable advice and feedback.

# Updates on PV Bio-Soiling in the Southeast U.S.

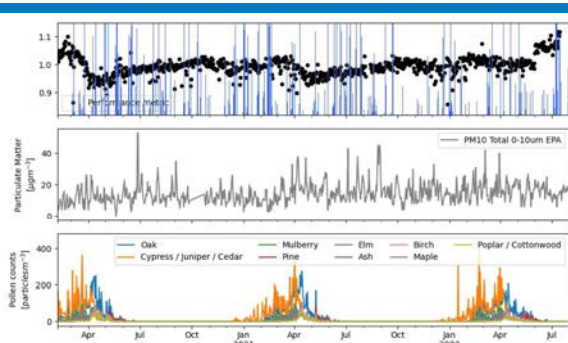
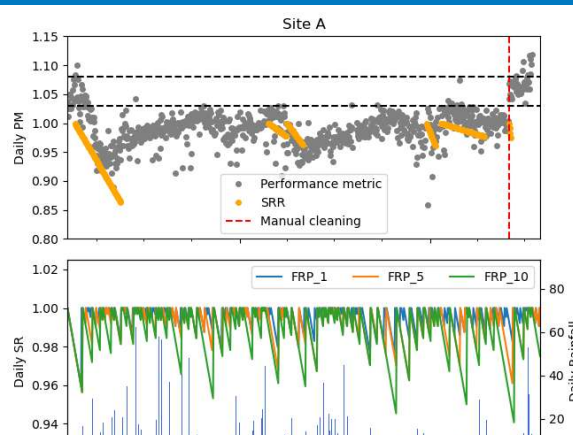
Matthew Muller<sup>1</sup>, Alexandra Rivera<sup>2</sup>, Michael Valerino<sup>2</sup>,

<sup>1</sup>National Renewable Energy Laboratory, <sup>2</sup>Solar Unsoiled

**PROBLEM:** Current PV sawtooth soiling models have been proven to be incorrect for the Southeast United States. Whereas previous models predict negligible soiling losses in the Southeast, the authors have demonstrated a number of sites in the region with sustained soiling losses greater than 10%. It is currently unclear what factors drive the most extreme losses and if there are alternatives to mechanical cleaning to prevent these losses.

**HYPOTHESIS:** Pollen is responsible for short term losses in the spring season with slow recovery into the summer months while bio-soiling losses from fungus and bacteria build up over months and years to create sustained soiling losses. Fungus and bacteria build up require mechanical cleaning to remove.

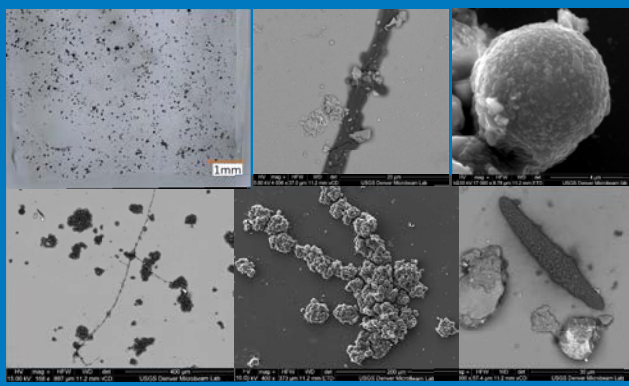
MECHANICAL CLEANINGS AT SEVERAL SITES IN THE S.E. DEMONSTRATE PERFORMANCE IMPROVEMENTS OF 5-12%, LEADING TO AN ONGOING BIO-SOILING INVESTIGATION



SOLAR UNSOILED HAS CAPTURED MICROSCOPIC IMAGES FROM 100s OF SITES TO BETTER UNDERSTAND THE SUSTAINED SOILING LOSSES



GLASS SHARD SEM: BLACK MATERIAL ~3.3% AREA COVERAGE, PRIMARILY CARBONACEOUS/ORGANIC, ~5 µm SPHERES CONSISTENT WITH FUNGAL SPORES, TRACE AMOUNTS OF MINERAL PARTICLES, EVIDENCE OF CORN OR WHEAT SMUT



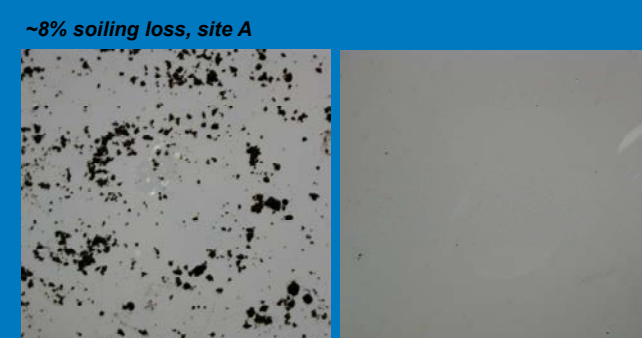
MODULES WITH HIGH LOSSES (13-14% BELOW) DO NOT LOOK DIRTY, AS FUNGUS IS OFTEN A DARK COLOR THAT DOESN'T CONTRAST AGAINST DARK CELLS.



POLLEN, ON THE OTHER HAND, CAN MAKE MODULES LOOK EXTREMELY SOILED EVEN THOUGH THEY CONTRIBUTE LESS LOSSES (5-10% BELOW). POLLEN IS SOMEWHAT TRANSPARENT WHILE BLACK FUNGUS IS NOT.



MECHANICAL CLEANING CAN FULLY REMOVE FUNGUS AND BACTERIAL WHILE RAINFALL DOES NOT (IMAGES BEFORE/AFTER CLEANING)



## RESULTS AND ONGOING WORK

- Pollen soiling can be slowly removed by rainfall while fungus and bacterial film soiling is less easily removed by rainfall.
- Systems can reside at a sustained 5-12% soiling loss, but mechanical cleaning demonstrates a full recovery.
- Cleaning is necessary in the Southeast but asset owners must accurately assess soiling losses to make economically optimal cleaning decisions.
- It is still unclear which locations are at most risk for sustained bio-soiling.
- A new study is beginning to understand if different glass types and surface coatings have an impact on fungal and bacterial film growth.

# Test-to-Failure Protocol for PV Module Hail Damage

## Integrating Weibull Analysis and Impact Mechanics

**Authors:** Tyjal DeWolf-Moura, Jon Previtali, Peter Bostock » VDE Americas; Cherif Kedir, Saeed Arash Far, Adrian Hernandez, Manpreet Kaur, Jesse Rodney Reynolds » RETC (Renewable Energy Test Center); Ronald Fritz » InSite Technologies; Michael Pilliod » Central Tension

### PV Reliability Workshop 2025

#### Abstract

The growing solar power industry faces significant challenges from hail damage, necessitating robust testing protocols to assess module resilience. While current hail resiliency tests conforming to IEC 61215 standards provide pass-fail data, they do not produce test results across a sufficiently broad range of impact energies to generate comprehensive hail resiliency curves, like the one shown in **Figure 1**, reflecting real-world conditions. In response, VDE Americas, RETC, and Central Tension have collaborated to develop an enhanced testing methodology incorporating a Weibull test-to-failure (TTF) approach, which requires a minimum of 25 randomly selected modules for statistical significance. The team's research addresses challenges associated with manufacturing freezer ice balls (FIBs) according to IEC 61215 specifications, maintaining compliance with FIB requirements, and momentum limitations. Alternative testing using synthetic ice balls with various polymer materials and silicone pad combinations has proven unsuccessful due to point load issues producing divergent resiliency curves. Concurrent with these protocol developments, VDE is investigating whether momentum or kinetic energy serves as the primary determinant of glass breakage during hail impact events. This relationship could be tested through variable impact angle testing, which would create different ratios of normal and tangential forces while maintaining consistent kinetic energy levels, potentially illuminating the fundamental physics of hail-induced glass failure mechanisms and informing future test protocol development. This experimental approach would build upon established research methodologies in the field, including previous studies that combined steel ball drop testing with finite element analysis.

#### Test Protocol

1. Using RETC's hail test equipment, we can input x-y coordinates that the machine automatically targets. Using this functionality, the test protocol randomly generates coordinates within specific allowed areas for each shot, as shown in **Figure 2**.
2. The protocol tests each module using FIB shots that gradually increase kinetic energy, selecting FIB sizes that allow the shots to be as close as possible to IEC 61215 standard.
3. A vertical pressure gun fires the FIB shots, allowing for a wide range of ice ball sizes, velocities, and relatively high shot precision.
4. An adjustable mount allows the sample PV module to be tilted to test resilience at different angles of incidence, which will be used in future experimentation.
5. Test results indicate that the edge of the module and the junction box area will have different strength characteristics from the other interior module areas. Therefore, we propose testing these areas separately to allow for the calculation of a separate failure distribution for the module edges and junction box area.

#### Freezer Ice Balls vs. High-Density Polyethylene Balls

1. Before beginning Weibull TTF experiments, we experimented with replacing FIBs with high-density polyethylene (HDPE) balls as a potential way to improve operational efficiencies and test reliability.
2. Based on this study, we determined that the impacts of HDPE balls are fundamentally different from FIB for several reasons; we have yet to find a satisfactory equivocation between these materials to allow for substitution.
3. An important factor may be that HDPE balls do not shatter on impact, effectively delivering a greater percentage of impact energy into the glass and allowing for higher peaks in the characteristic forces.
4. We attempted to use a rubber or silicon sheet over the glass to compensate for the differences in impact characteristics. Because the impacts are still clearly different, as shown in **Figure 3**, we have, for now, continued to use FIBs.
5. We also tested rubber balls but found these to be impractical and dangerous due to ricochet.

#### Kinetic Energy vs. Momentum

1. As shown in **Figure 4**, normal kinetic energy decreases as a cosine squared function of the impact angle of the hail with the panel, while the normal momentum decreases as a cosine function only. This means there are significant differences in potential damage mitigation of tilt depending on which quantitate is more relevant.
2. VDE Americas is developing a TTF experiment to answer this question.

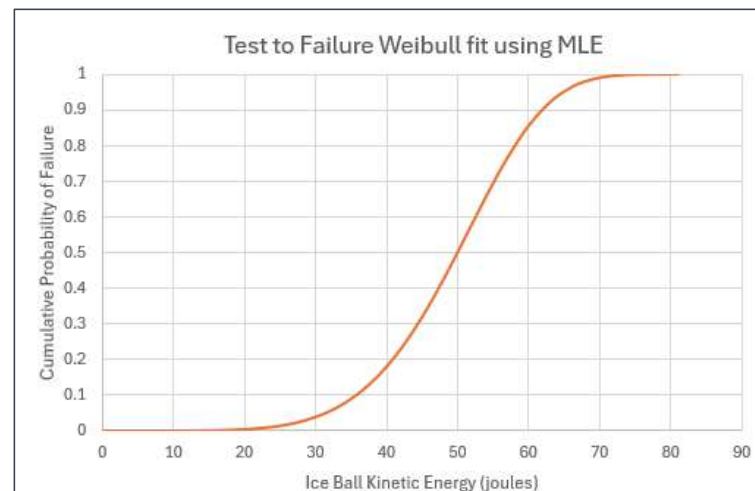


Figure 1. A Weibull distribution calculated from test-to-failure (TTF) data.

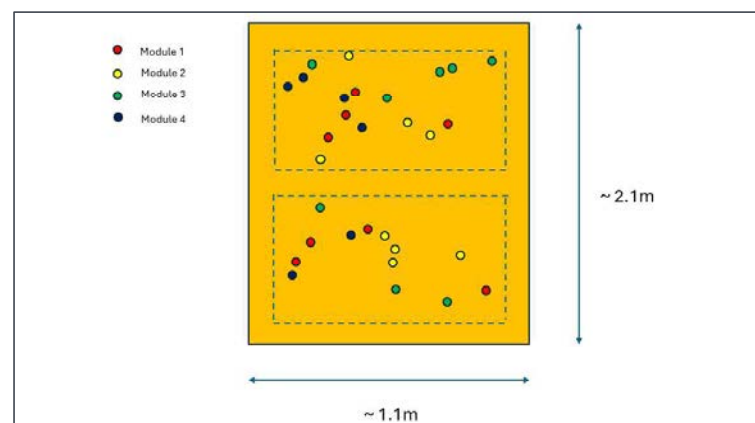


Figure 2. Example diagram of randomly generated shot coordinates. The coordinates are generated such that they avoid both the edges of the panel and the junction box area, where the breaking characteristics are different.

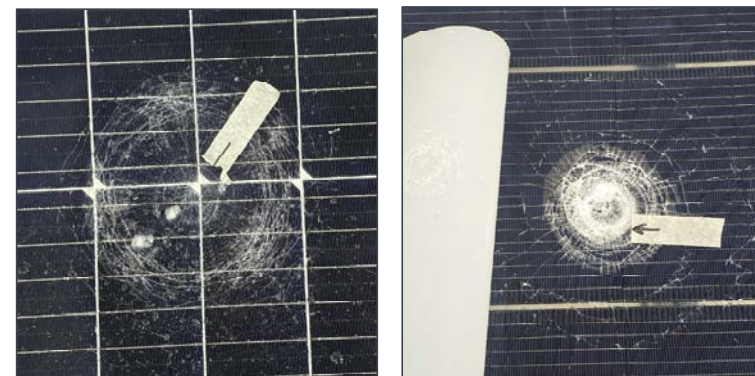


Figure 3. FIB impact (left) versus HDPE impact (right).

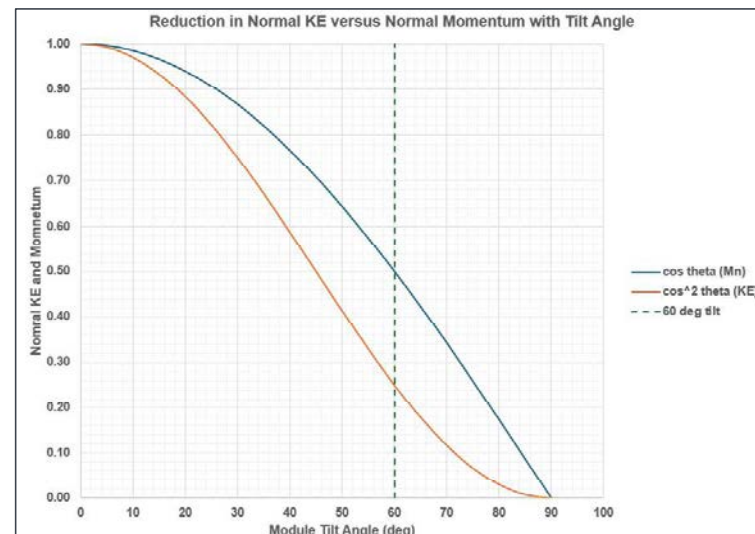


Figure 4. Normal KE vs Normal Momentum as a function of impact angle

# Reliable Module Design Cost Reductions for Vertical Bifacial PV

March 2025 PVRM, by Joseph McCabe, P.E., Fellow

## ABSTRACT

The paradigm of orienting bifacial photovoltaic (PV) modules vertically opens up reliable module cost reduction opportunities. This presentation investigates module design ramifications of lower short circuit currents ( $I_{sc}$ ), lower installed normal operating cell temperatures (iNOCT), lower probability of hail damage, and increased bifaciality factors. Cost reduction opportunities include using thinner glass, changing glazing type, reducing encapsulation costs, eliminating aluminum framing and j-box strategies. Levelized cost of energy improvements (LCOE) from less land usage (agrivoltaics), increased bifaciality factors, reduced soiling, patterned glass and reduced metal requirements for structures are presented.

### Current, Temperature, Hail, Wind

Vertical means 25% less full sun which also means lower currents and temperatures, significantly lowered probability of a perpendicular strike from hail falling from the sky, virtually eliminated up lift wind forces to name just a few.

STRING  $I_{sc}$ : In Denver,  $I_{sc}$  for Vertical has maximum 12.6 amps, average 4.4 amps. Latitude tilt south has max 15.2 amps, average 5.5 amps, a 25.6% difference in  $I_{sc}$ .

TEMPERATURE: In Denver, iNOCT for Vertical has max 59.2 C with average 19.8 C; Latitude tilt south has max iNOCT of 61.8 C and average 24.8 C, a 5 C or 25% C difference in average iNOCT.

Cost Reductions: The cross sectional areas of wires (grids, interconnections, diodes, pig tails) can have their cross sectional areas reduced because of 25% lower amperages. Extreme and average module temperatures are reduced for two reasons, because full sun is reduced and the vertical orientation increases convection heat transfer to ambient air on both sides. Materials chosen because of high module temperatures can now be chosen for reduced long term temperatures at a lower cost. Reduced extreme temperature fluctuations can help reduce warranty exposure. Actual bifacial cell design changes are not considered.

Low site specific winds justify lower structural costs. Uplift forces are basically eliminated for vertical surfaces. Holding modules rigid requires metal. Vertically orienting, especially if allowed to swing naturally in the wind, reduce metal costs, eliminating frames.

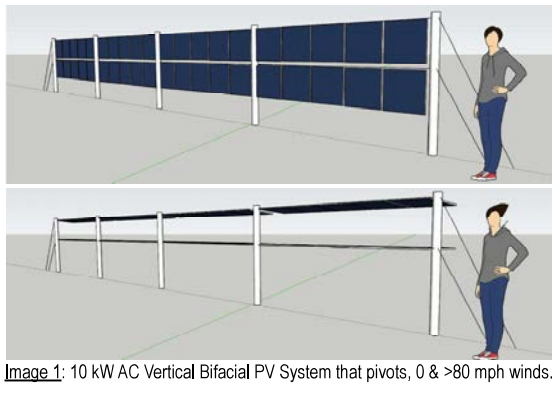


Image 1: 10 kW AC Vertical Bifacial PV System that pivots, 0 & >80 mph winds.

## Module Material Cost Reduction Opportunities

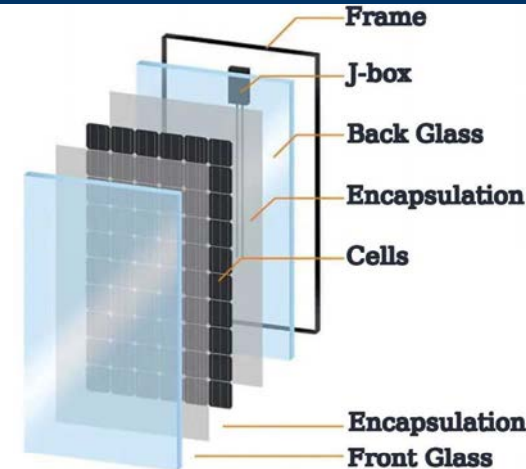


Image 2: PV Module Materials, j-box different location(s) for bifacial. Image courtesy of <https://pv-manufacturing.org/>

We used NREL's Detailed Cost Analysis Model (DCAM <https://dcam.openei.org/>) to evaluate total module cost reduction opportunities compared to the 2024 baseline model. Only modifying the module material costs below, the total module costs were reduced 27% for a USA made module and 32% for a low cost China module:

- Two encapsulant reduced from \$1.00 to \$0.75 per square meter
- Front and back glass reduced from \$2.40 to \$2.00 per square meter
- Ribbon reduced from \$0.60 to \$0.50 per module
- String connectors and partial metalization reduced from \$1.25 to \$1.00
- Aluminum frame reduced (eliminated) \$6.82 to \$0.02 for clips
- J-box reduced \$1.70 to \$1.50 each.

## Cell Modifications

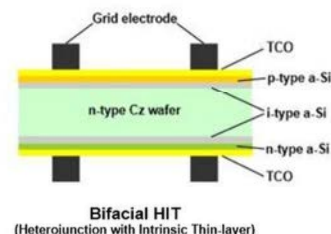


Image 3: Bifacial HIT PV cell, courtesy of [Mateo Flecha](#).

There are many ways to manufacture a bifacial PV cell. Image 3 shows one that can produce a high bifaciality factor (BF), which has an additional grid electrode compared with a monofacial cell. High BF is important for performance, including the leveled cost of energy (LCOE). Any additional backside processing and grid electrode was not included in the above module cost reduction analysis.

## Levelized Cost of Energy Improvements

LCOE improvements can include module capital cost reductions already discussed. Land usage optimization (agrivoltaics), increased bifaciality factors, no soiling, use of patterned glass and higher DC/AC ratios can also improve LCOE for vertical bifacial PV. Insurance is lower with less potential for hail damage and lower capital costs.

Patterned Glass: Patterned glass is glass with a light-focusing surface structure and low reflection. Specific orientation of patterned glass can help to capture more photons as opposed to reflecting them. If modules are vertical, the path of the sun is likely to be above the top edge, so patterns in glass can help direct the sun into the cells. "This Side Up" directions on modules would be needed. Vertical bifacial has, "nearly zero soiling in Mumbai."

Diodes: Early morning and late afternoon sun might shade sequential rows of vertically mounted systems. Diodes for lower rows can be customized, optimized, for the highest value by reducing losses due to known daily shading patterns. Modules without diode protection like CdTe are not recommended for installations with known shading (orientation matters).

Bifaciality Factors: At [RE+ 2024](#), BYD exhibited standard 90% bifaciality factor modules. Achieving higher bifaciality factors can be accomplished by an additional backside binning activity during module manufacturing.

Land value and revenue can be increased using rows of vertical bifacial PV and farming in between. See Image 4.

More vertical bifacial PV modules in front of lower rated inverters, like a 1.76 DC/AC ratio, can improve the LCOE for PV systems with storage. Energy is clipped into storage twice per day, because of the dual hump production curve in the morning and nighttime. This helps to reduce curtailments. 10 kW AC system with 10 kW / 20 kWh storage in Denver, [NREL SAM](#) calculates 27,903 kWh/yr which is a 31.7% capacity factor. Electrical BOS costs are reduced. Image 5.



Image 4: Rows of vertical bifacial PV, courtesy of [Thomas Hickey](#).

## High DC/AC Usage

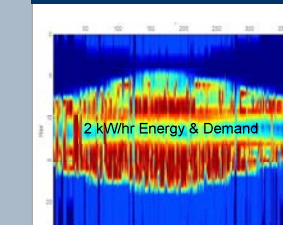
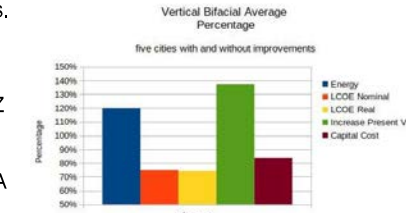


Image 5: The dark blue hours show when electricity from a generator or the grid would be needed if using 2 kWhr 24/7/365. Appropriate for water pumping, evaporative cooling and refrigeration which are used more in the summertime.

## Values

Using the potential module cost reductions of 27% (\$0.430 to \$0.314/watt), bifaciality factor increases (70% to 90%), BOS reductions (inverter and structural \$0.35 to \$0.25/watt), land costs reduction (100% to 10%), 5%/yr to zero soiling, and using all the other latest industry default numbers from version 2024.12.12 of [NREL SAM](#), LCOE were evaluated for five locations. Comparing vertical bifacial with and without updates the energy per year increased about 20%, LCOE was lower by 25%, Present Value significantly increased 30 to 45% depending upon location because of weather, and capital costs were reduced 16%. Pattern glass, diode improvements, higher DC/AC ratios and lower insurance were not evaluated, but could further increase these economic values for vertical bifacial with the system improvements.



LCOE was about the same for lower cost vertical bifacial as for fixed tilt at latitude standard bifacial modules without the suggested cost reductions justified by a vertical orientation; but 16% less expensive to install. The higher the latitude the better.

## CONCLUSION

USA PV module costs can be reduced 27% for vertical bifacial PV designs. LCOE can be improved 25%. A white paper with more details on these concepts is available by writing to [energyideas@gmail.com](mailto:energyideas@gmail.com). Other presentations on the topic are freely available at [agrisoltaics.com](http://agrisoltaics.com).



AgriSoltaics™

## ACKNOWLEDGEMENTS

Thanks to Ron [Sinton](#), Mateo Flecha, David Feldman, Michael Woodhouse, Jacob Cordell, Thomas Hickey, [NREL](#)'s SAM & BCAM groups, and [pv-manufacturing.org](https://pv-manufacturing.org/).

Rabin Dhakal & Wayne Li

## Introduction and Background

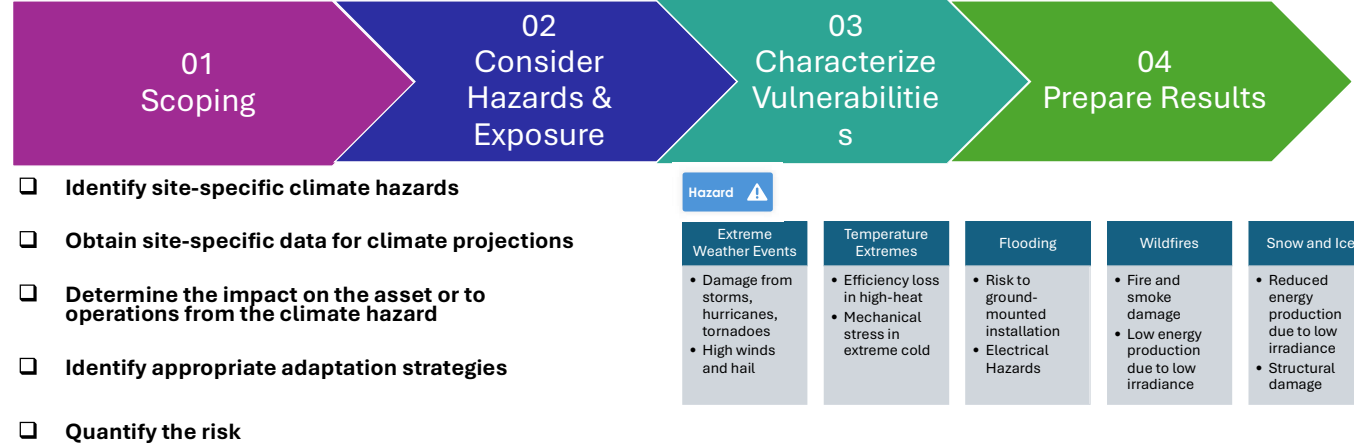
- Primary objective:** To understand the high-temperature impact on Solar PV inverter performance and reliability.
- Why It Matters:**

- Rising temperatures due to climate change
- Increased stress on PV systems
- Potential for decreased performance and reliability

## Method



Adapted from IPCC AR6 (Simpson et al. 2021).



### Vulnerability

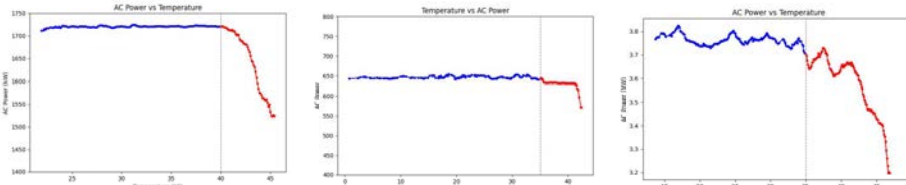
To describe the vulnerabilities on the inverter of utility scale PV plant due to the high temperature following performance and reliability data were accessed

- Inverter-level performance data (e.g., power output, temperature, efficiency).
- Ambient temperature and irradiance measurements.
- Site-level SCADA data for operational insights.
- Maintenance logs to identify potential reliability issues.

### Purpose of the Data:

- Evaluate high-temperature impacts on performance and reliability.
- Correlate environmental conditions with inverter behavior.
- Support simulation models with real-world operational data.

## Result



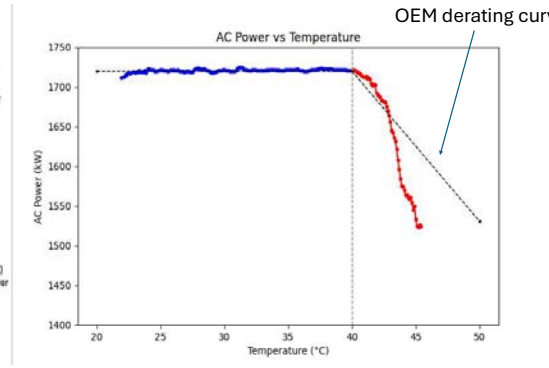
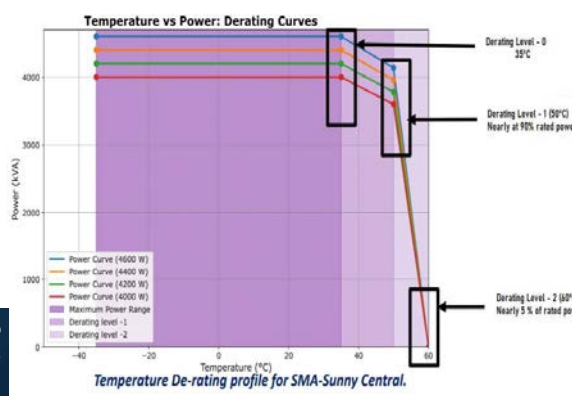
The temperature related derating degrades the system's performance. EPRI study on 7 different case study sites with more than 300 central inverters of size range 600 kW to 4200 kw shows that the electricity loss can be up to 5 % due to temperature-related derating.

| Solar Plant Location | Inverter                   | Derating Time in % | Energy Loss/Year (%) |
|----------------------|----------------------------|--------------------|----------------------|
| Middle East          | Inverter A                 | 3.85               | 0.83                 |
| Nevada               | TMEIC 630 kW               | 1.53               | 0.15                 |
| Southern California  | SMA 800 kW                 | 1.2                | 0.17                 |
| New Mexico           | SMA 630 kW                 | 0.8175             | 0.13                 |
| Arizona1             | Inverter B                 | 10.75              | 5.23                 |
| Arizona 2            | Inverter C                 | 8                  | 1.5                  |
| Arizona 3            | SMA Sunny Central 4200 kVA | 11.68              | 3.4                  |

| OEM Name          | Model Name      | Offered Power Ranges (kVA) | MPPT Range (V) | Derating Level-0 Temperature (°C) | Derating Level-1 Temperature (°C) | Derated Power at Level-1 (%) | Derating Level-2 Temperature (°C) (0-5% power) |
|-------------------|-----------------|----------------------------|----------------|-----------------------------------|-----------------------------------|------------------------------|--|
| SMA Energy System | Sunny Central   | 4000 to 4600               | 880-1325       | 35                                | 50                                | 90                           | 60   |
| Sungro w          | SG3150U D       | 3300 to 8800               | 875-1500       | 40                                | No Info                           | No Info                      | No Info  |
| Siemens           | Gamesa Electric | 4100 to 4700               | 835-1500       | 40                                | 55                                | 88.82                        | 65   |
| FIMER             | PVS980-58       | 1818 to 2091               | 850-1500       | 50                                | 55                                | 80                           | 60   |

Source: PV Inverter Scorecard, EPRI, Palo Alto, CA, 2024, 3002029885

Selecting the proper inverter is crucial to prevent energy loss due to temperature-related derating, especially considering different inverters have varying derating profiles



## Conclusion/Future Works

This study presents a quantitative discussion of the risks associated with high-temperature operation of inverters, underscoring the necessity for a deeper understanding of PV inverter asset performance and reliability. Enhanced access to standardized, high-quality data, along with more mature data sets, is crucial for conducting a reasonable and quantifiable risk assessment. The study is limited to analyzing the AC power output of inverters under high-temperature conditions. Therefore, to comprehensively assess the overall losses due to high-temperature operation of solar PV systems, the following studies are recommended:

- DC Power Loss Analysis, Clipping Loss Study, Enhanced Simulation Models including future load profile, Comprehensive reliability data collection etc.

This material is based upon the case study of Climate READi initiative of EPRI. The team would especially like to acknowledge Jeff Thomas from EPRI; we would also like to acknowledge the support of the industry partner SRP and DEWA.

# Watts the Hype? AI's Role in Powering Solar Reliability

Mike Mousou, kWh Analytics

## Introduction

- Artificial Intelligence (AI) models, particularly large-language models (LLMs), are transforming data analysis across industries.
- The solar industry processes millions of operational events annually, but manual classification of these events has become a significant bottleneck to understanding what drives production losses.

## Methods

### 1. Data Collection & Preprocessing

- compiled, cleaned, and standardized an extensive dataset of ~190,000 energy loss events down to ~10,000 to ensure high quality and diverse examples.

| Event Notes  | Classification Category |
|--|-------------------------|
| Inverter 2 offline due to ground fault and SEL relay fault | Equip. Outage           |
| Loss of communication between inverters 3 and 4            | Comms Loss              |
| Plant was curtailed to 10 MW as directed                   | Curtailment             |

### 2. Dataset

- Split into training and validation datasets via randomized 80/20 stratified split.

### 3. Fine-Tuning

- Train out of the box LLM with ~8,000 labeled events.

### 4. Evaluation

- Assess accuracy using validation dataset of ~2,000 events.



Acknowledgement: This material is based upon work supported by the U.S. Department of Energy's Office of Energy Efficiency and Renewable Energy (EERE) under the award number DE-EE0009827.

Legal Disclaimer: The views expressed herein do not necessarily represent the views of the U.S. Department of Energy or the United States Government. The views expressed herein do not necessarily represent the views of the U.S. Department of Energy or the United States Government.

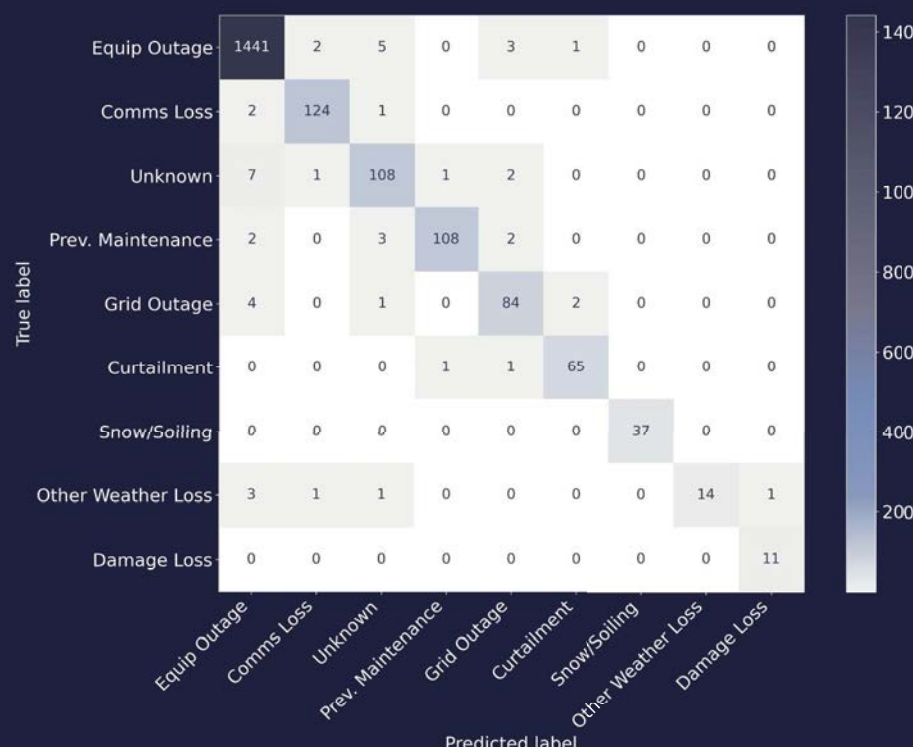
# Leverage a Specialized Dataset to Achieve up to 98% Classification Model Accuracy—for Under \$5



This plot compares the F1-Scores across all classification categories for the fine-tuned model and various base models when tested against the validation set

## A Powerful Model at a Low Cost

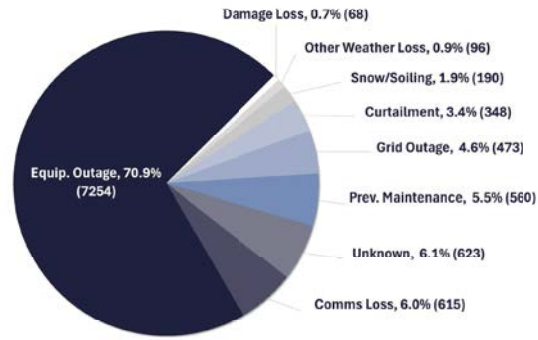
- Base model - gpt-4o-mini-2024-07-18
- Trained tokens- 2,016,561
- Total Fine-Tuning cost = **\$4.97**
- Post-Production Activity:
  - Total Tokens → 64,719
  - Total API Requests → 1,039
  - Total Cost → \$2.21
  - Cost per Request/Event Classification → **\$0.0021**



## Classification Metrics By Category



## Distribution of Event Categories in Full Dataset



## Additional Information

- Model Hyperparameters:
  - Supervised training
  - Epochs - 3
  - Batch Size - 16
  - LR multiplier - 1.8

## Discussions / Takeaway

- Accessibility & Affordability of fine-tuning LLMs enables broad utilization across the industry, replacing labor-intensive work.
- Any text-based classification work can be automated with a high degree of accuracy and speed.
- Fine-Tuned Models have demonstrated superior performance compared to even the most advanced models, underscoring the value of leveraging domain-specific data—in this case PV.

# Investigating the Oxygen Barrier Properties of Desiccated Edge Sealants for Protection of Perovskite Solar Modules

by Lori Postak, M.Sc., Quanex IG Systems, Inc.

**Materials being tested:** Desiccated edge sealants, such as Quanex SolarGain Edge Sealant SET LP03, are polyisobutylene and butyl rubber adhesives with integrated desiccant that reduce moisture ingress thereby protecting cells, connections, and transparent conductive oxide coatings from corrosion and degradation in many PV module types certified to IEC 61215 & IEC 61730. Depending on formulation, these sealants can be UV stable, durable, solid electrical insulators.

## Module designers and modelers seek material property data for oxygen transmission rate (OTR)

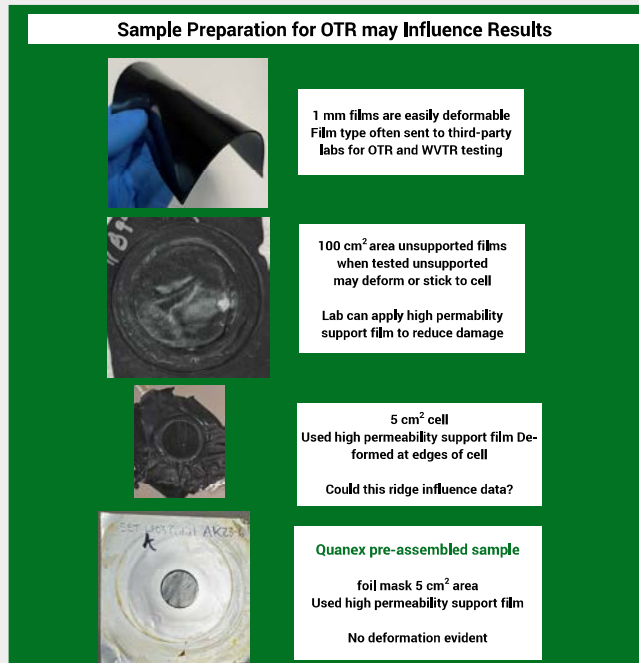
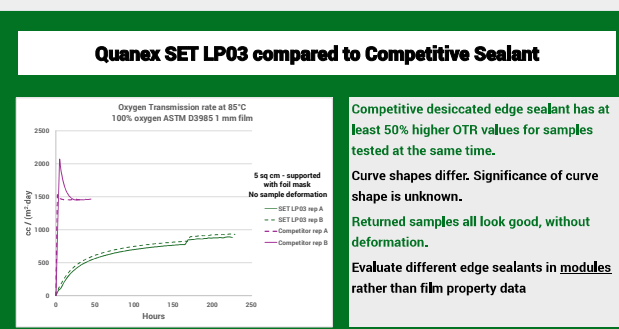
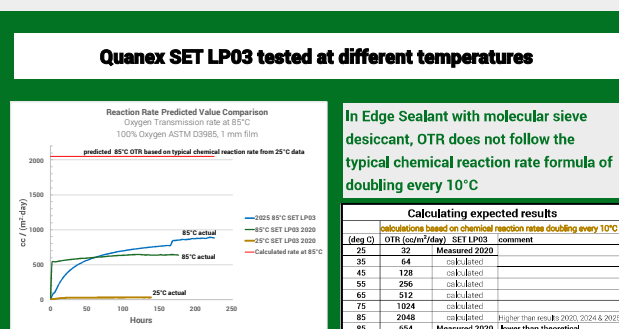
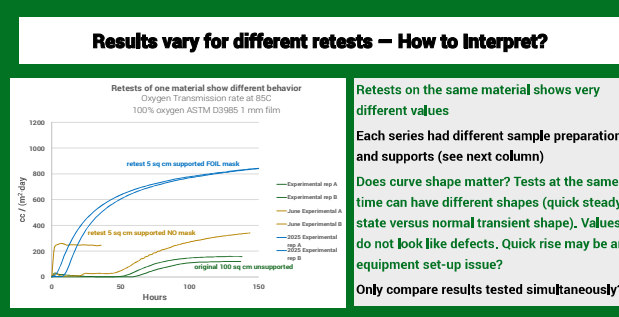
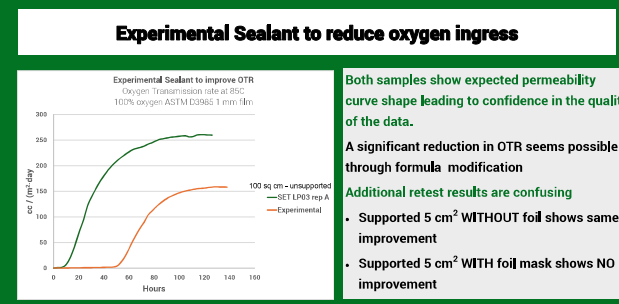
Conceptually easy to enable comparison of different materials

Reality proves that testing thin, easily deformable films is difficult and data may be unreliable even from a third-party lab

## Testing of Films - ASTM D3985 Dry Oxygen Transmission Rate

Poster contents:

- Share Quanex experience regarding OTR testing
- Highlight variability of the data within samples tested at the same time
- Illustrate significant change in data for materials tested at a different time
- Demonstrate differences in the shape of a curve from standard transient curves to curves with immediate jump to steady state
- Provide examples of sample preparation methods
- Recommend necessary information to make decision about the quality of OTR data
- Propose additional tests for evaluation of oxygen ingress



## RECOMMENDATIONS WHEN TESTING FILMS

| Third party laboratories   | Recommendations for Users   |
|--|---|
| Expect expertise in stated method  | Request machine printout to assess issues or normal permeation curves, not just the certificate report<br><br>Carefully inspect charts to understand permeation behavior and any machine glitches   |
| May not have protocols to handle easily deformable sealants  | Request a support film be used during testing as described in IEC 62788-6-2 or supply sample to third-party lab with high permeability film <sup>1</sup> already applied.<br><br>Request samples to be returned so that you can assess whether samples are damaged                  |
| OTR Default test time stops at 120 hours or sooner if steady state reached earlier   | Edge sealant may need 240 hours or longer to reach steady state. Contract to run until steady state.  |
| Lab Disclaimer:<br>Results only apply to sample tested<br><i>Experience discussed in this poster shows this to be true</i> | Samples or series submitted at the same time are likely to be most reliable to directly compare materials. Replicates tested in the same series are usually within 20% of one another.<br><br>Tests run at different times may not yield similar results even on the same material. |
|  | When performing additional tests at a different time, resubmit a previous sample with each series as a reference for comparison to possibly scale the new data.   |

<sup>1</sup> Y. Hu, et. al. *J Appl Polym Sci* 81: 1624–1633, 2001

## QUESTION: Does Edge Sealant OTR need improvement?

Perovskite Solar Cells are sensitive to degradation from oxygen

Desiccated Edge Sealants butyl rubber backbone provides an oxygen barrier along with moisture barrier properties.

Blocking oxygen ingress via edge sealant will not prevent degradation from oxygen trapped inside the module during assembly.

The solution to increasing PSC stability need to start at the cell and encapsulation levels.

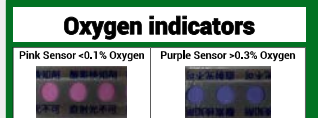
**Is an improvement in Edge Sealant OTR needed for >25 year PSC stability?**

Quanex requests market/user feedback. Please contact the author.

## Testing to evaluate module performance

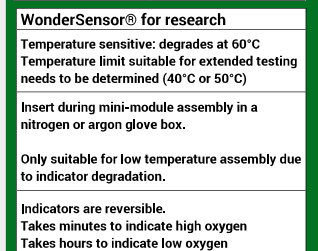
### Edge sealant oxygen resistance performance is better assessed via module testing.

- Eliminates issues experienced with test film deformation
- Module testing includes influence of adhesion which is critical to module performance



IEC 62788-5-2 differentiates moisture effects in a module from heat effects at 85°C.

An oxygen pressure chamber permits direct study of oxygen permeation through the sealant into a module.



## Accelerate Oxygen Exposure via pressurized chamber

Several ASTM methods utilize Oxygen-Pressure Vessels.

ASTM F2003 Accelerated Aging of Ultra-High Molecular Weight Polyethylene after Gamma Irradiation in Air  
ASTM D3632 Accelerated Aging of Adhesive Joints by the Oxygen-Pressure Method

Both require 70°C. Each ASTM method uses a different pressure. (5 bar or 20 bar)  
Regulate chamber temperature via external heating and insulation of the vessel.

A 5 Gallon ASME Stainless Steel Pressure Tank can hold mini-modules up to 30 cm x 30 cm

Learn more about desiccated edge sealants at [www.Quanex.com/solar](http://www.Quanex.com/solar)

Contact Lori.Postak@Quanex.com or Mark.Molinaro@Quanex.com



# Edge Sealed Photovoltaic Modules: Matching Thermal and Optical Properties of Traditional Encapsulation

David Durney,<sup>1</sup> Ryan Ruhle,<sup>1</sup> Larry Maple,<sup>1</sup> Steve Johnston,<sup>2</sup> Dana Kern,<sup>2</sup> and Walajabad Sampath,<sup>1</sup>

<sup>1</sup> Colorado State University (CSU), Fort Collins, Colorado 80523, US

<sup>2</sup> National Renewable Energy Laboratory (NREL), Golden, Colorado 80401, US

## Abstract

Photovoltaic (PV) energy production is experiencing rapid growth, necessitating innovations in module design to enhance cost efficiency, reliability, and recyclability. This study introduces a novel edge-sealed module (ESM) architecture that eliminates traditional vacuum lamination and cross-linked encapsulants. Accelerated testing has been accomplished in collaboration with the National Renewable Energy Laboratory (NREL). Preliminary results demonstrate that this architecture matches the thermal and optical performance of traditional modules, addressing degradation issues such as yellowing, delamination, and potential-induced degradation (PID). Utilizing internal nano-scale textures, the ESM design achieves low reflectance and improved heat dissipation without the need for advanced anti-reflective coatings. Outdoor testing using an in-situ data logger validates the thermal and optical performance of the ESM modules, showing comparable open-circuit voltage ( $V_{oc}$ ) and short-circuit current ( $I_{sc}$ ) to conventional modules. This architecture holds promise for meeting the Department of Energy's goal of 50-year module lifespans while enabling cost-effective and sustainable manufacturing practices. Further testing and increased sample sizes are required to refine and validate these findings.

## CSU's Advanced Fabrication

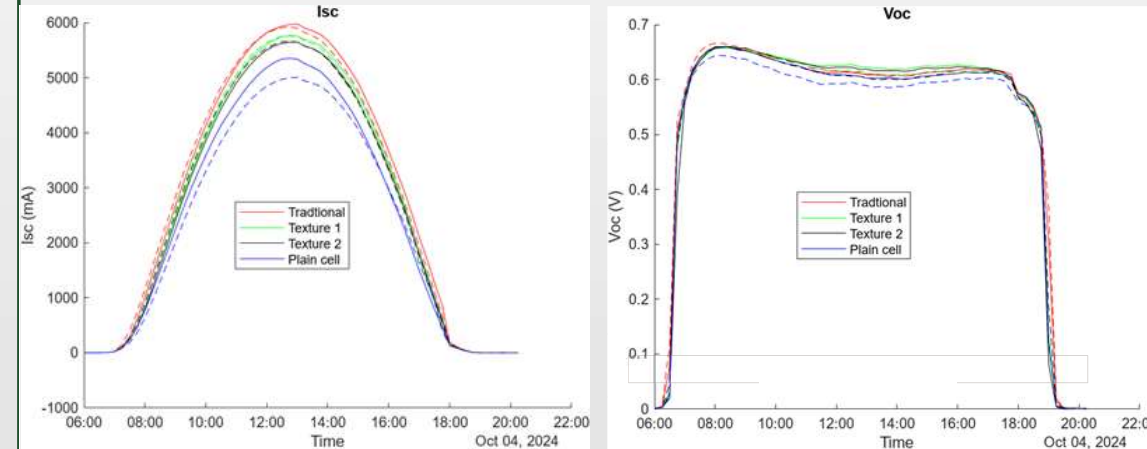


- Above is the manufacturing equipment at CSU
- Advanced Edge Seals have been demonstrated, passing 5000hr Damp Heat
- 30s cycle time has been demonstrated

## Benefits of Edge Sealed Modules

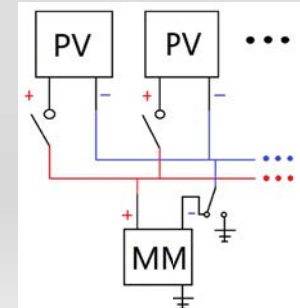
- Improved barrier against moisture ingress (~50 years in humid climates).
- Process cycle time for each manufacturing step is less than 30 seconds.
- ~20x smaller manufacturing tool footprint compared to current methods
- Increased mechanical strength (~2x) and better tolerance to glass temper distortion
- Reduced process conditions for Perovskite and c-Si/perovskite tandem configurations.
- Ability rapidly prototype novel cell architectures.

## Recent C-Si Results



In-Situ Data Logger data from October 04, 2024. This day was chosen due to the lack of cloud cover. Textured modules show increased optical performance and thermal performance, matching traditional modules within experimental error. Potentially showing increased thermal performance from traditional samples

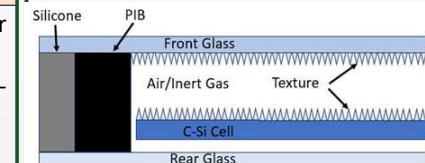
## In-situ Data Logger



- Outdoor tester mounted on the CSU PV test field close to a NOAA weather station for real time weather monitoring
- Powered by a raspberry pi, puts each sample into short circuit ( $I_{sc}$ ) condition and open circuit condition ( $V_{oc}$ )
- INA260 multimeter chip reports the  $V_{oc}$  and  $I_{sc}$  of each sample every fifteen minutes.
- $V_{oc}$  decreases with temperature
- $I_{sc}$  is a measure of how much light is collected by the solar cell
- Eight samples are tested. Two samples of nano texture 1, nano-texture 2, cells encapsulated in optical silicone, and plain cells are used



## Nano-Structure Technology



- Nano-Structures reduce reflection loss at the glass-air interface
- Nano-structures increase internal convection of the cells, improving thermal performance of the cell
- Nano-Structured modules eliminate the need for traditional encapsulation, which reduces degradation of solar cells
- Typical degradation due to encapsulants include Potential Induced Degradation, stress induced microcrack formation due to glass temper distortion and high pressures, yellowing from acidic acid buildup and delamination.

## Acknowledgments

We would like to thank David McDougall and our partners at HB Fuller for their support, research and products.

## Conclusions

- Edge sealed modules have potential for high longevity, lower cost, improved manufacturability.
- Edge seal modules eliminate the need for traditional state-of-the-art encapsulants, increasing module longevity
- Nano-Structured modules improve the optical performance of the cell by redirecting light into the module, reducing reflectance.
- Thermal performance is improved by nano-structures due to increased internal convection
- Decreased manufacturing cost due to the elimination of traditional encapsulants, enabling low-cost, competitive manufacturing

# Data-driven insights into solar production performance

Phoebe Hwang, kWh Analytics

## Introduction

It has been shown that solar underperforms from 7-13% on average across the US in Year 1 with little to no improvements in the following years [1]. Given that solar deployments have experienced an average annual growth of 26% in the last decade [2], we wanted to see how this trend has evolved by examining performance index (PI) over a few axes, highlighting trends by year, vintage, and region.

[1] kWh Analytics, "2022 Solar Generation Index," 2022.

[2] SEIA, "Solar Market Insight Report Q4 2024," Dec. 2024.

## Methods

1. We analyzed data from monthly operating reports (MORs) spanning over 35000 system-months from 2011 to 2023.
2. We compared historical actual generation vs. the P50 expectation to calculate performance index (PI).
3. The PI was adjusted for insolation using GHI data from Clean Power Research SolarAnywhere database, forming weather-adjusted PI (WA PI).

Table 1. Avg. WA PI by Vintage & Operational Year

| Vintage | 2011  | 2012   | 2013  | 2014  | 2015  | 2016   | 2017  | 2018  | 2019   | 2020  | 2021   | 2022  | 2023  | Operational Year |
|---------|-------|--------|-------|-------|-------|--------|-------|-------|--------|-------|--------|-------|-------|------------------|
| 2010    | 96.7% | 99.3%  | 98.8% | 96.8% | 93.5% | 98.9%  | 99.9% | 96.6% | 95.3%  | 95.2% | 101.4% | 84.2% | 95.6% |                  |
| 2011    | 97.0% | 100.3% | 99.2% | 98.3% | 99.6% | 102.7% | 95.2% | 94.2% | 97.6%  | 96.3% | 97.0%  | 95.5% | 87.8% |                  |
| 2012    | 98.2% | 98.0%  | 96.6% | 93.1% | 98.5% | 97.9%  | 95.1% | 97.0% | 96.4%  | 96.1% | 97.1%  | 96.1% |       |                  |
| 2013    | 98.1% | 98.4%  | 98.0% | 96.8% | 95.7% | 94.4%  | 95.6% | 93.7% | 96.5%  | 97.6% | 95.4%  |       |       |                  |
| 2014    |       | 103.8% | 96.3% | 95.5% | 94.7% | 94.6%  | 94.8% | 92.4% | 102.4% | 87.7% | 84.4%  |       |       |                  |
| 2015    |       |        | 93.4% | 92.4% | 92.7% | 91.7%  | 90.7% | 89.1% | 84.8%  | 85.5% | 84.9%  |       |       |                  |
| 2016    |       |        |       | 90.8% | 91.9% | 91.7%  | 91.1% | 90.2% | 87.5%  | 87.6% | 89.6%  |       |       |                  |
| 2017    |       |        |       |       | 88.1% | 87.1%  | 88.1% | 88.2% | 88.0%  | 85.8% | 85.1%  |       |       |                  |
| 2018    |       |        |       |       |       | 88.9%  | 87.7% | 93.4% | 92.8%  | 88.6% | 90.1%  |       |       |                  |
| 2019    |       |        |       |       |       |        | 94.9% | 94.2% | 93.8%  | 92.0% | 94.1%  |       |       |                  |
| 2020    |       |        |       |       |       |        |       | 88.2% | 89.8%  | 89.2% | 90.6%  |       |       |                  |
| 2021    |       |        |       |       |       |        |       |       | 92.4%  | 86.1% | 88.4%  |       |       |                  |
| 2022    |       |        |       |       |       |        |       |       |        | 89.1% | 88.4%  |       |       |                  |

→ Overall performance has not improved as more assets get installed each year. New builds continue to suffer from underproduction as well.

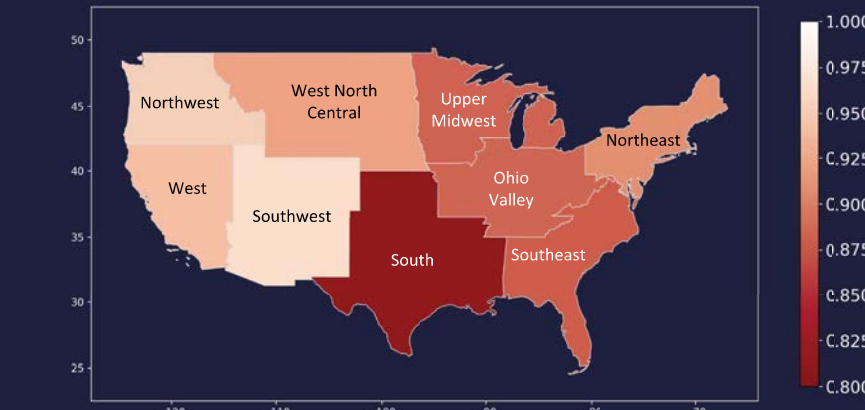


Acknowledgment: This material is based upon work supported by the U.S. Department of Energy's Office of Energy Efficiency and Renewable Energy (EERE) under the Solar Energy Technologies Office Award Number DE-EE0009827.

Legal Disclaimer: The views expressed herein do not necessarily represent the views of the U.S. Department of Energy or the United States Government. The views expressed herein do not necessarily represent the views of the U.S. Department of Energy or the United States Government.

# PV sites are averaging 91.8% PI, as sites around the country continue to underperform.

Figure 1. Lifetime WA PI by Climate Regions



→ The South is experiencing underperformance the most, while the Southwest leads in PV site performance nationwide.

Table 2. Avg. WA PI by Region & Operational Year

| Climate Region     | 2011   | 2012   | 2013   | 2014   | 2015   | 2016  | 2017   | 2018  | 2019  | 2020  | 2021  | 2022  | 2023  | Operational Year |
|--------------------|--------|--------|--------|--------|--------|-------|--------|-------|-------|-------|-------|-------|-------|------------------|
|                    |        |        |        |        |        |       |        |       |       |       |       |       |       |                  |
| NorthWest          | 112.9% | 110.8% | 108.2% | 104.8% | 99.6%  | 93.5% | 95.5%  | 91.5% | 96.3% | 94.2% | 96.7% | 82.1% |       |                  |
| Northeast          | 84.2%  | 93.6%  | 92.7%  | 92.9%  | 90.2%  | 94.7% | 92.9%  | 91.2% | 91.6% | 93.7% | 89.8% | 88.7% | 89.7% |                  |
| Ohio Valley        |        |        |        |        | 87.9%  | 92.0% | 90.6%  | 88.8% | 87.0% | 87.8% | 88.3% | 89.1% | 86.6% |                  |
| South              |        |        |        |        |        | 96.3% | 87.3%  | 85.9% | 84.6% | 86.4% | 82.0% | 80.9% | 76.4% | 74.7%            |
| Southeast          |        |        |        |        | 104.4% | 90.7% | 86.9%  | 87.5% | 92.7% | 89.6% | 88.0% | 87.6% | 87.2% | 84.4%            |
| Southwest          | 98.9%  | 98.5%  | 99.6%  | 98.7%  | 97.8%  | 97.8% | 97.3%  | 95.5% | 94.3% | 96.5% | 96.8% | 97.6% | 94.0% | 94.0%            |
| Upper Midwest      |        |        |        |        |        |       | 88.9%  | 81.5% | 76.0% | 88.6% | 91.1% | 87.6% | 91.6% |                  |
| West               | 98.9%  | 101.0% | 100.8% | 99.1%  | 99.1%  | 97.2% | 95.8%  | 93.1% | 93.6% | 90.6% | 92.2% | 84.1% | 85.3% |                  |
| West North Central |        |        |        |        |        |       | 100.2% | 87.7% | 95.1% | 86.7% | 91.5% | 96.5% | 96.9% |                  |

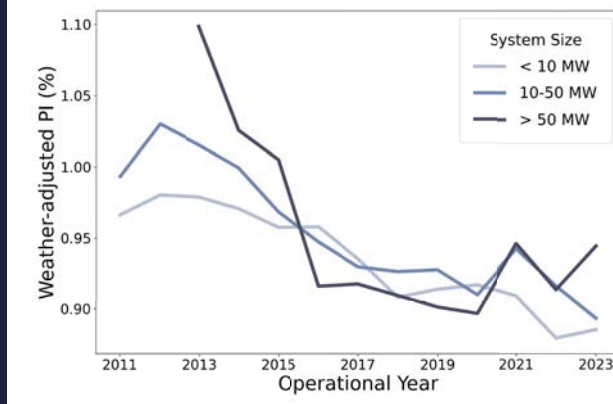
→ While solar performance remains stable in some regions, it has declined in key areas with high solar deployment, such as the South and the West.

Table 3. Avg. WA PI by Region & Operational Month

| Climate Region     | 1     | 2     | 3      | 4      | 5     | 6     | 7     | 8     | 9     | 10    | 11     | 12     | Month |
|--------------------|-------|-------|--------|--------|-------|-------|-------|-------|-------|-------|--------|--------|-------|
|                    |       |       |        |        |       |       |       |       |       |       |        |        |       |
| NorthWest          | 95.1% | 98.8% | 96.0%  | 94.2%  | 90.7% | 92.7% | 94.1% | 91.9% | 90.2% | 97.4% | 102.4% | 100.9% |       |
| Northeast          | 78.8% | 78.6% | 94.6%  | 95.5%  | 96.9% | 94.0% | 94.1% | 94.1% | 95.7% | 92.3% | 94.3%  | 81.8%  |       |
| Ohio Valley        | 82.5% | 85.5% | 90.5%  | 91.8%  | 89.8% | 88.9% | 88.9% | 89.8% | 90.6% | 90.3% | 91.0%  | 82.0%  |       |
| South              | 89.0% | 76.7% | 78.0%  | 80.1%  | 86.2% | 82.4% | 81.7% | 81.4% | 81.6% | 80.0% | 84.7%  | 75.4%  |       |
| Southeast          | 86.3% | 85.3% | 90.1%  | 95.4%  | 88.7% | 89.5% | 88.9% | 85.6% | 84.3% | 89.3% | 91.6%  | 81.4%  |       |
| Southwest          | 93.4% | 93.9% | 101.8% | 100.8% | 97.8% | 95.7% | 95.8% | 98.5% | 97.8% | 97.2% | 93.1%  | 90.2%  |       |
| Upper Midwest      | 73.1% | 79.1% | 88.9%  | 89.6%  | 92.5% | 93.8% | 92.2% | 92.6% | 92.0% | 95.1% | 91.9%  | 75.0%  |       |
| West               | 93.5% | 99.7% | 95.6%  | 94.4%  | 93.8% | 99.3% | 94.0% | 91.7% | 91.1% | 91.6% | 91.1%  | 92.8%  |       |
| West North Central | 88.2% | 82.6% | 88.2%  | 95.3%  | 96.8% | 95.8% | 94.4% | 97.4% | 95.7% | 92.1% | 89.9%  | 86.8%  |       |

→ Sites across the States are underperforming in the winter, especially in the Northeast and Midwest regions.

Figure 2. Avg. WA PI by System Size



→ Sites are suffering from low WA PI, regardless of system sizes.

## Discussion / Takeaway

- Current MORs often lack the necessary detail to pinpoint the primary factor driving the underperformance. Some hypotheses could explain the overestimated P50 projections:
  1. **Underestimated Losses** - Extreme weather losses and curtailment may not be accurately reflected in modeling.
  2. **Overly Optimistic Availability Assumptions** - Many models assume high system availability without fully accounting for downside scenarios.
  3. **Misaligned Incentives** - Higher P50 values are often rewarded with better project financing terms, creating an implicit incentive for inflated production estimates.
- We encourage the industry to prioritize accuracy in energy production estimates. This could reduce long-term risks to debt coverage, strengthen investor confidence and public support for solar projects, and ensure a sustainable growth by aligning financial models with real-world performance.
- Have you observed similar trends in underperformance? We'd love to hear insights from across the industry and foster a more data-driven dialogue on improving solar performance.

## Introduction

When modeling PV systems in PVsyst® [1], the performance of PV modules is determined by detailed electrical characteristics specified in PAN files. PVsyst® uses PAN file parameters and one-diode model assumptions to generate an IV curve which determines module performance behavior. See Figure 1 for an example I/V curve. PAN files can come from a variety of sources, including PVsyst's internal database, module manufacturers, and third-party module testing labs. They can also be created manually in PVsyst® with default settings and generic performance parameters. Not all of the parameters needed for a PAN file are listed in manufacturer module datasheets. Unlisted parameters include key resistance parameters that can either be estimated with PVsyst's default methods or are provided directly within a PAN file from a manufacturer or third-party testing lab.

These resistance parameters, Rshunt and Rseries, directly impact the module's modeled low-light performance, which can have significant impacts on the final modeled PV system generation. Figure 2 shows example module efficiencies over a range of irradiance levels. This curve is largely determined by the Rshunt and Rseries parameters. The default method for PVsyst® to determine this curve is to target a relative efficiency @ 200 W/m<sup>2</sup> of -3% [2]. Manufacturers and third-party labs can also provide their own resistance parameters. As the true values of these parameters are not typically disclosed or standardized, the industry generally must accept the values provided in a given PAN file as correct and accurate.

Another often uncertain characteristic of PAN files is the temperature behavior which is related to a heat loss factor U and the muPmpp factor of the PV module. The muPmpp factor is by default an output of the one-diode model but can be corrected to the value provided on manufacturer module specification sheets. Figure 3 shows an example plot of module voltage and maximum power varying with temperature.

To evaluate the performance variability resulting from PAN file specifications, we ran a series of PVsyst® energy models where we tested manufacturer or third-party provided PAN files against ones created with default performance parameters.

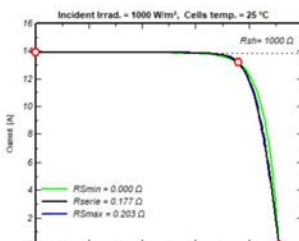


Figure 1: Example I/V curve, PVsyst

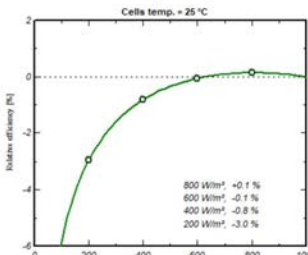


Figure 2: Module relative efficiency versus irradiance level, PVsyst

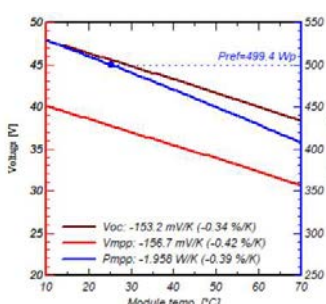


Figure 3: Module voltage and maximum power versus temperature, PVsyst

## Results and Discussion

### PAN Performance Comparison

Figure 5 plots the PVsyst output of *Loss due to Irradiance Level* between the sampled and default PAN file sets for the Maine site location. It shows a high variability of loss in the sampled PAN file set, while the default PAN file set loss remains relatively consistent around 0.5%. The same trend is shown in Figure 6 for the Arizona site location, although at a lower overall loss due to the warmer climate.

The PVsyst default method for determining resistance parameters seems a reasonable estimate as the default results lie relatively in the middle of the sampled results. However, the variability in non-default PAN file low-light performance, may indicate a need for further standardization of how resistance parameters for PAN files are measured and implemented in the industry. Project designs could unknowingly choose modules that will model and/or perform up to 2% lower than others due to inconsistent specifications.

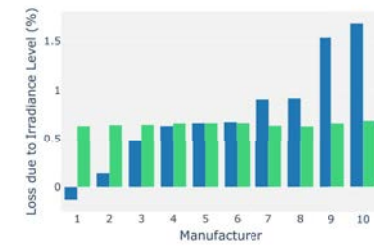


Figure 5: Loss due to Irradiance Level for sampled and default PAN file sets in the Maine site location

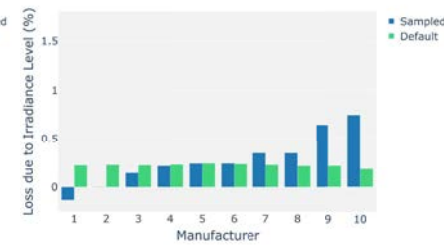


Figure 6: Loss due to Irradiance Level for sampled and default PAN file sets in the Arizona site location

The *Loss due to Temperature* system output is much more aligned between the PAN file sets as shown below in Figures 7 and 8, with the overall losses more significant in the warmer climate of Arizona.

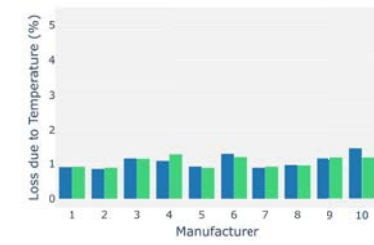


Figure 7: Loss due to Temperature for sampled and default PAN file sets in the Maine site location

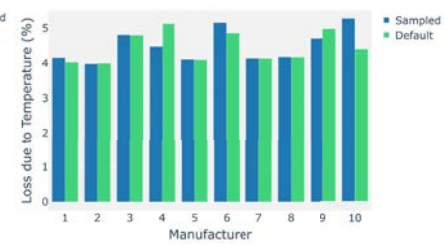


Figure 8: Loss due to Temperature for sampled and default PAN file sets in the Arizona site location

Overall, there is more variability in the low-light performance than the temperature behavior between the PAN file sets. Additionally, the loss impact due to irradiance level is more significant in areas with more total global irradiance and temperature losses are more significant in warmer climates.

### Sensitivity Analysis

Figure 9 shows the impact on *Loss due to Irradiance Level* when varying Rshunt for both site locations. The curves exhibit exponential behavior, with a significant loss increase at lower Rshunt values compared to the limited loss decrease at higher Rshunt values. This behavior is more pronounced, with a higher overall loss, for the Maine site location. The exponential nature indicates that a small change in resistance parameters has the potential for a significant change in losses, further reinforcing the conclusion from the PAN file comparison above that there may be a need for standardization of methods to determine these parameters. Figure 10 shows the impact on *Loss due to Temperature* when varying muPmpp. The curve behavior is linear, with a higher overall loss and steeper slope for the Arizona site location. This indicates that variation in muPmpp is more impactful in warmer climates.

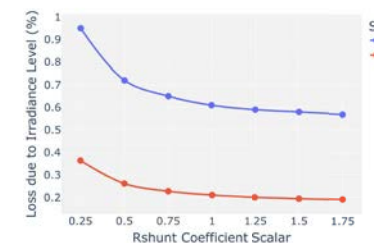


Figure 9: Loss due to Irradiance Level when scaling Rshunt for Maine and Arizona site locations

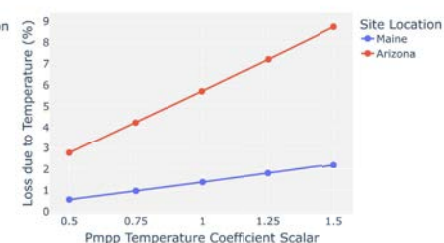


Figure 10: Loss due to Temperature when scaling muPmpp for Maine and Arizona site locations

## Conclusions:

Our analysis highlights the impact of PAN file parameter variations on modeled PV system performance. Differences in resistance parameters primarily affect low-light behavior, leading to variation in irradiance-related losses that are more significant in areas with more total irradiance. The PVsyst default method for low-light behavior provides a reasonable estimate, but the differences in PAN files suggest a need for more scrutiny on key parameters throughout the industry.

## References:

1. PVsyst – Photovoltaic Software. PVsyst SA, Satigny, Switzerland. <https://www.pvsyst.com/>
2. "Rseries and Rshunt determination procedure", PVsyst 7 Help Documentation. PVsyst SA, Satigny, Switzerland. <https://www.pvsyst.com/help-pvsyst7>

Table 1: Tracked PAN parameters and PVsyst outputs

### Sensitivity Analysis:

A sensitivity analysis was conducted by independently applying scaling factors to the shunt resistance and muPmpp temperature coefficient in PVsyst's generic Si-mono 500 W Twin half-cells bifacial module PAN file and comparing performance across the range of scaling factors for both site locations.



Disruptive Acceleration Science

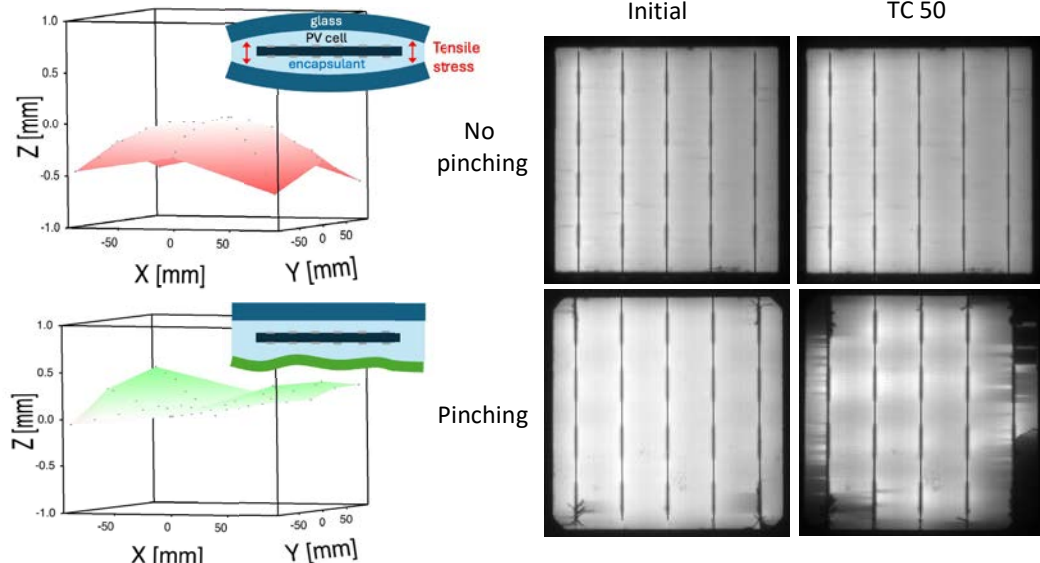
# Edge pinch in mini-modules:

## What it is, why it happens, and how to stop it

Michael Owen-Bellini, John Mangum, Xavier Hanna, David C. Miller, Kent Terwilliger, Rebecca Wai, Sona Ulicna, Laura Schelhas, Dennice Manchester Roberts, Dana B. Kern

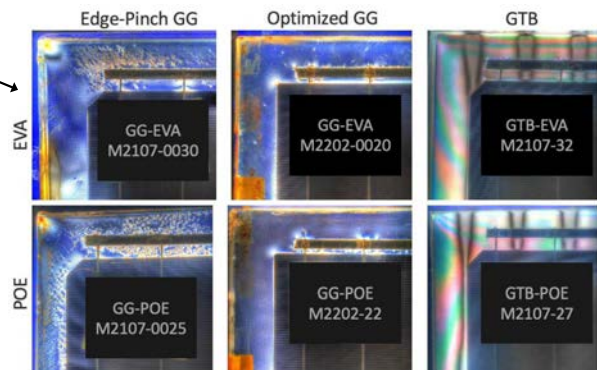
### What it is: a tapering thickness from the center to the edge of a mini-module

- Pinching is observed as a tapered thickness and bowing across glass-glass modules
- Pinching applies additional stress to the cells in mini-modules
- This is not observed in modules with polymer backsheets which are able to conform to the shape of the module as needed



**Pinching in research-scale mini-modules might lead to false negative results and lost time**

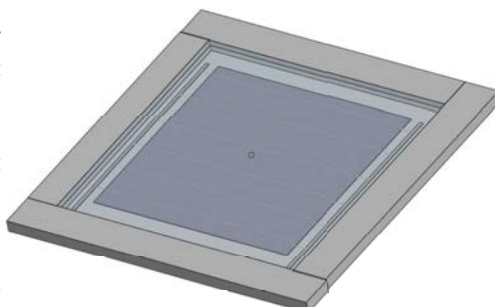
### Why it happens: pressure is applied non-uniformly over the edge of modules in vacuum-laminators with bladders


Photoelasticity!  
Cool!


- During lamination using a bladder vacuum-laminator, the bladder inflates to apply pressure to the module
- Without support, the bladder conforms over the edge of the module and pinches the edges closer together

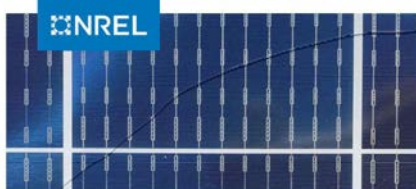
### How to stop it: using appropriate supports around the module will prevent the bladder from applying pressure over the edge

- Placing a frame around the module assembly before lamination prevents the bladder from conforming over the edges of the module to restrict pinching
- The frame can also help to prevent extrusion of the encapsulant from the edges
- Tape around the edge of the module assembly can further assist with preventing extrusion



### Does pinching matter for commercial scale modules?

"Oh, it definitely does" – Ellie Palmiotti  
"Yes I think it's a problem" – Tim Silverman



**Tough Break: Many Factors Make Glass Breakage More Likely**

Timothy J Silverman,<sup>1</sup> Elizabeth C. Palmiotti,<sup>1</sup>  
Martin Springer,<sup>1</sup> Nick Bosco,<sup>1</sup> Mike Deceglie,<sup>1</sup>  
Ingrid Repins,<sup>1</sup> and Ashley Gaudling<sup>1</sup>

<sup>1</sup>National Renewable Energy Laboratory

# Beyond Energy Gains: The Reliability Impacts of Diffuse Stowing in PV Trackers

Riccardo Adinolfi Borea<sup>1</sup>, Tobin Ford<sup>2</sup>, Silvana Ovaitt<sup>2</sup>, Vincenzo Cirimele<sup>1</sup>, Francesco Melino<sup>1</sup>, Giosuè' Maugeri<sup>3</sup>  
 Alma Mater Studiorum – University of Bologna, Italy<sup>1</sup>; NREL – National Renewable Energy Laboratory<sup>2</sup> RSE – Ricerca sul Sistema Energetico<sup>3</sup>  
[riccardo.adinolfi2@unibo.it](mailto:riccardo.adinolfi2@unibo.it)

## Abstract

When overcast sky conditions occur, the lack of directionality of the global irradiance component leads the photovoltaic (PV) module optimal tilt angle for power production to be close to 0°. This led to the development of the so-called diffuse-stow tracking strategy, which orients the module horizontal with overcast conditions. However, its effectiveness depends on the local weather dynamics.

Using an hourly weather dataset – equal to considering hourly movement of the tracker – and state-of-the-art modeling tools, we show that diffuse-stow generally improves energy yield and reduces cumulative tracker movement compared to conventional back-tracking. For Golden, CO, using TMY data, diffuse-stow can increase annual energy yield by 0.26% while decreasing cumulative angular movement by 9.2%. However, when sub-hourly (5-minute) data is considered, the results change. The energy gain increases to 0.36% and the angular movement, instead of decreasing, increases to 100.2%. This shift is attributed to Golden's weather, characterized by short-lived overcast periods.

This study defines the irradiance threshold where diffuse-stow provides meaningful energy gains with minimal impact on tracker movement. Furthermore, it contributes to a broader discussion on single-axis tracker longevity by considering the implications of cumulative angular movement.

## Tracking Strategies for Diffuse Conditions

While tracking optimizes PV orientation toward the Sun, diffuse tracking strategies orient the module horizontal during overcast conditions, due to lack of radiation directionality. However, the threshold of overcast conditions at which changing the module orientation becomes beneficial is not well defined. To evaluate this, the optimal tilt angle for a bifacial PV module is analyzed under varying diffuse and direct irradiance conditions, via PVlib's infinite sheds algorithm [1], modeled using  $C_{dir}$ :

$$C_{dir} = DNI / DNI_{clear}$$

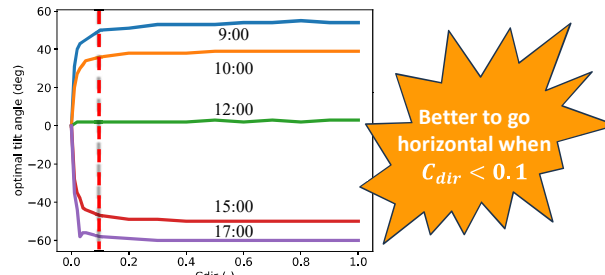


Fig.1 Optimal tilt angle variation for different time of the day and different value of  $C_{dir}$

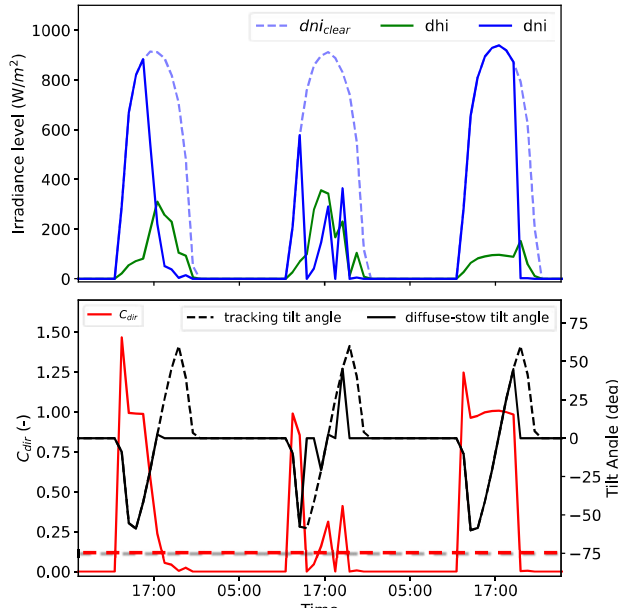


Fig.2 (top) Radiation components for two days, with the (bottom) resulting  $C_{dir}$  and tracker angle based on the diffuse tracking strategy

## Conclusions

Diffuse-stow strategies increase the energy yield of a PV system with single-axis tracker by up to 1.4%. The improvement of energy yield is strongly related with the weather condition of the location, being diffuse-stow meaningful when overcast condition occurs.

However, the cumulative angular movement, that a tracker executes during the year, changes as well. Depending on the weather data resolution considered, indeed, the cumulative angular movement of the tracker changes drastically. While using weather datasets with hourly resolution results in a decrease of the angular movement of 9.2% with diffuse-stow, using 5 minutes resolution results in an increase of 100.2%. Such discrepancy is related with weather condition variability. In particular, the higher is the variability and the higher is the discrepancy. Therefore, using diffuse-stow can cause a higher angular movement of the tracker, which could affect its lifespan and reliability.

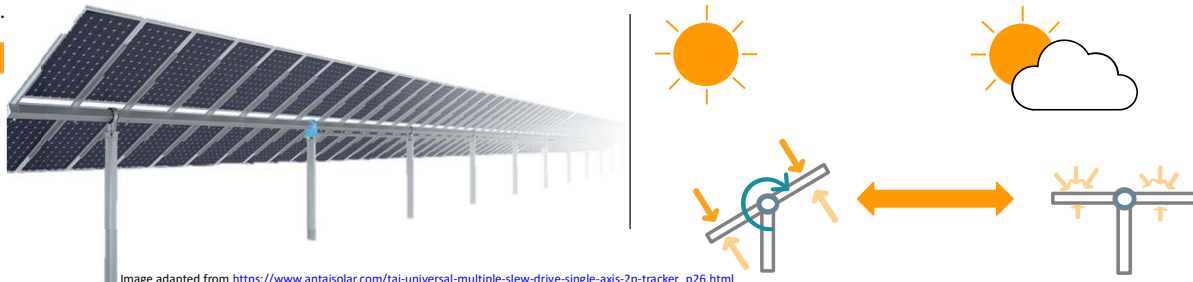


Image adapted from [https://www.antaisolar.com/tai-universal-multiple-slew-drive-single-axis-2p-tracker\\_p26.html](https://www.antaisolar.com/tai-universal-multiple-slew-drive-single-axis-2p-tracker_p26.html)

## Tracking routine results

We first compare the yearly energy improvement and cumulative angular movement change for diffuse-stow tracking at hourly (60 min) and sub-hourly (5 min) intervals in Golden, CO, and Richmond, VA. The blue bars indicate the percentage energy improvement from diffuse-stow tracking. Green-Red bars represent the cumulative angular movement change of the tracker under diffuse stow conditions.

$$\Delta Energy [\%] = \left( \frac{\sum Energy_{diffuse-stow}}{\sum Energy_{tracking}} - 1 \right) \times 100$$

$$\Delta Movement [\%] = \left( \frac{\sum Movement_{diffuse-stow}}{\sum Movement_{tracking}} - 1 \right) \times 100$$

Diffuse stow provides a net energy gain in all cases, but the magnitude varies between hourly (60 min) and sub-hourly (5 min) datasets. While sub-hourly adjustments yield higher energy gains, they also result in significantly increased tracker movement due to more frequent adjustments. This effect is also seen for our simulation of the whole US below. This increase in tracker movement can potentially impacting reliability. The trade-off between energy optimization and mechanical wear highlights the need for optimized scheduling strategies to balance performance and durability.

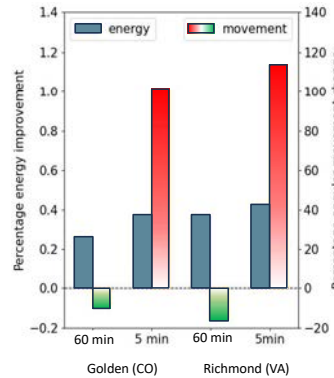
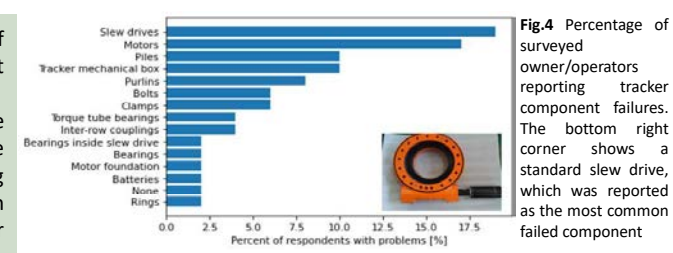
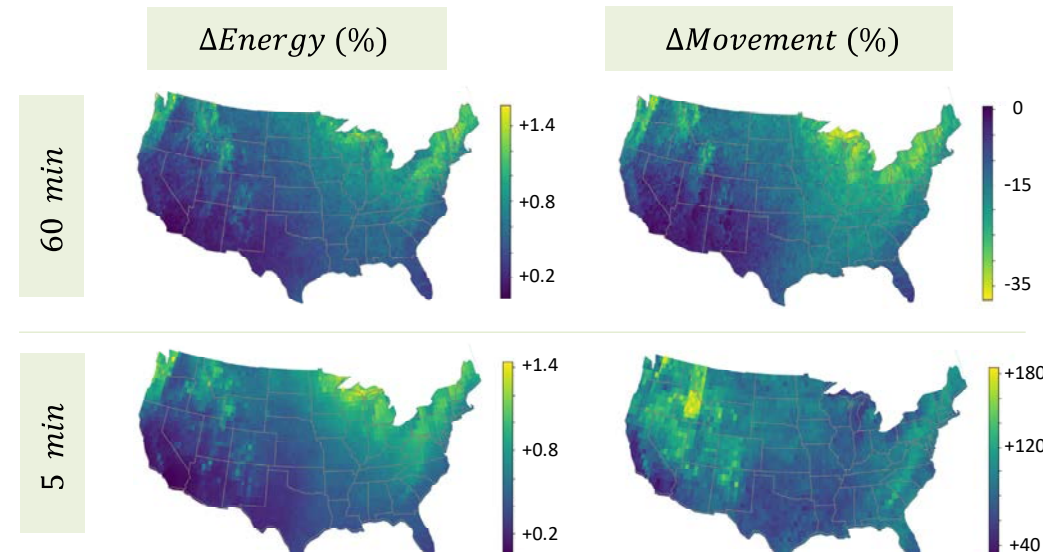


Fig.3 Comparison on yearly energy improvement and cumulative angular movement change for diffuse-stow tracking at hourly (60 min) and sub-hourly (5 min) intervals in Golden, CO, and Richmond, VA.



Taken from IEA PVPS Task13 report <https://doi.org/10.69766/OIK1919>



Colorado State  
University

# Improving Solar Tracker Resilience with Wind Nowcasting and Aerodynamic Mitigations

**UB** University at Buffalo

Pejman Fatehi<sup>1</sup>, Mahmoud Elnahla<sup>1</sup>, Yanlin Guo<sup>2</sup>, Teng Wu<sup>3</sup>, James Elsworth<sup>4</sup>, and Scott Dana<sup>4</sup>

<sup>1</sup>Graduate Student, Dept. of Civil and Environmental Engineering, Colorado State Univ, <sup>2</sup>Associate Professor, Dept. of Civil and Environmental Engineering, Colorado State Univ, <sup>3</sup>Professor, Dept. of Civil, Structural and Environmental Engineering, University at Buffalo, <sup>4</sup>National Renewable Energy Laboratory

## Introduction:

- Extreme weather events such as high winds, threaten single-axis tracker (SATs) solar PV systems.
- Enhancing wind resilience of SATs by improving aerodynamic stability avoids damage, allows higher stow speeds, reduces maintenance costs, and minimizes downtime.
- Strengthening SATs' structural and aerodynamic performance could lower the levelized cost of energy (LCOE), making solar power more reliable and cost-effective in extreme conditions.

## Motivation:

- High wind events cause 44% of extreme weather impacts on PV systems.<sup>1</sup>
- Over 50% of insurance claims in PV facilities stem from extreme weather.<sup>2</sup>
- Wind damage can lead to up to 60% energy loss and long-term performance degradation.<sup>3</sup>
- Disruptions impact electricity supply, safety, health, economy, and environment.<sup>4</sup>
- Enhancing wind resilience of SAT solar systems increases reliable energy generation and minimizes risks.<sup>5</sup>

## Part I: Better prediction of wind speeds to guide tracker operation and design

### Wind data collection:

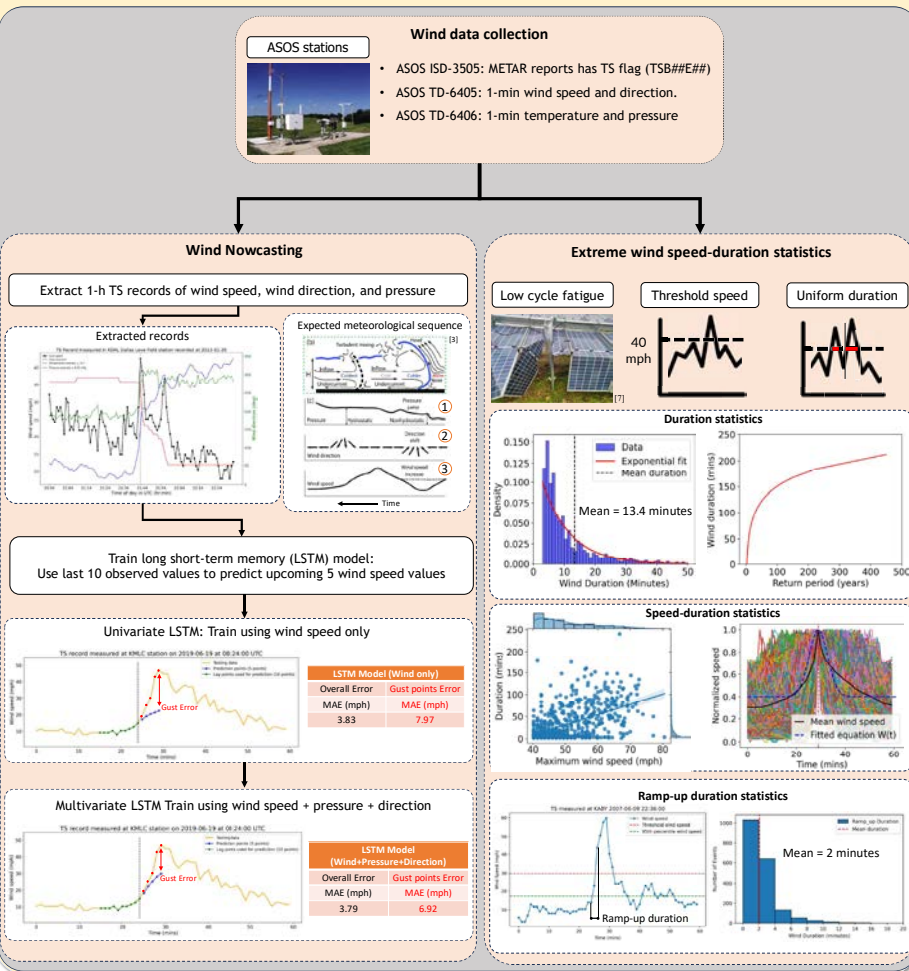
- Three ASOS<sup>6</sup> datasets were used to extract extreme thunderstorm wind records with gust speeds exceeding 25 knots (30 mph).

### Wind nowcasting:

- Extracted time series thunderstorm (TS) records were used to train a wind forecasting model. Using the last 10 observed values, the model predicts the next 5 wind speed observations, enabling timely stow.
- The model trained with wind speed alone struggled to predict gusts accurately. Since TS are thermodynamically driven, incorporating pressure and wind direction improved performance. Wind nowcasting, combined with digital twin modeling, could enhance emergency response capabilities.

### Extreme wind duration statistics:

- Extreme wind duration statistics are critical for assessing low-cycle fatigue effects.
- Ramp-up duration analysis (mean: 2 minutes) shows how quickly wind intensifies, emphasizing the need for rapid response and accurate forecasting to mitigate sudden loading effects.



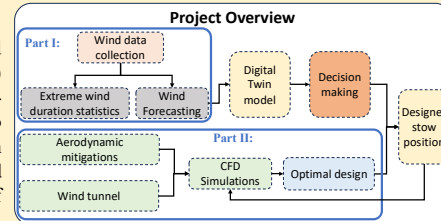
## Conclusion:

- The LSTM model accurately nowcasts 5-minute wind speed using the last 10 observed data points, achieving an overall mean absolute error of 3.79 mph and a gust mean absolute error of 6.92 mph which enables real-time wind forecasting.
- Based on forecasted wind conditions, the stow position is adjusted to either low or high attack angles to minimize aerodynamic instability.
- The developed mitigation framework identifies effective aerodynamic mitigators that increase critical flutter speed and reduce structural vibrations, enhancing tracker resilience.
- These performance of aerodynamic mitigators are validated through OpenFOAM simulations and will be validated using wind tunnel tests, ensuring reliable performance under extreme wind conditions.

## Project Objective and Overview :

- Enhance the aerodynamic performance and wind resilience of solar SATs by integrating wind data analysis, digital twin modeling, and aerodynamic optimization.
- Collect and analyze wind data to forecast extreme wind conditions, developing and testing aerodynamic mitigators through CFD simulations and wind tunnel experiments, and refining tracker designs for optimal stability.

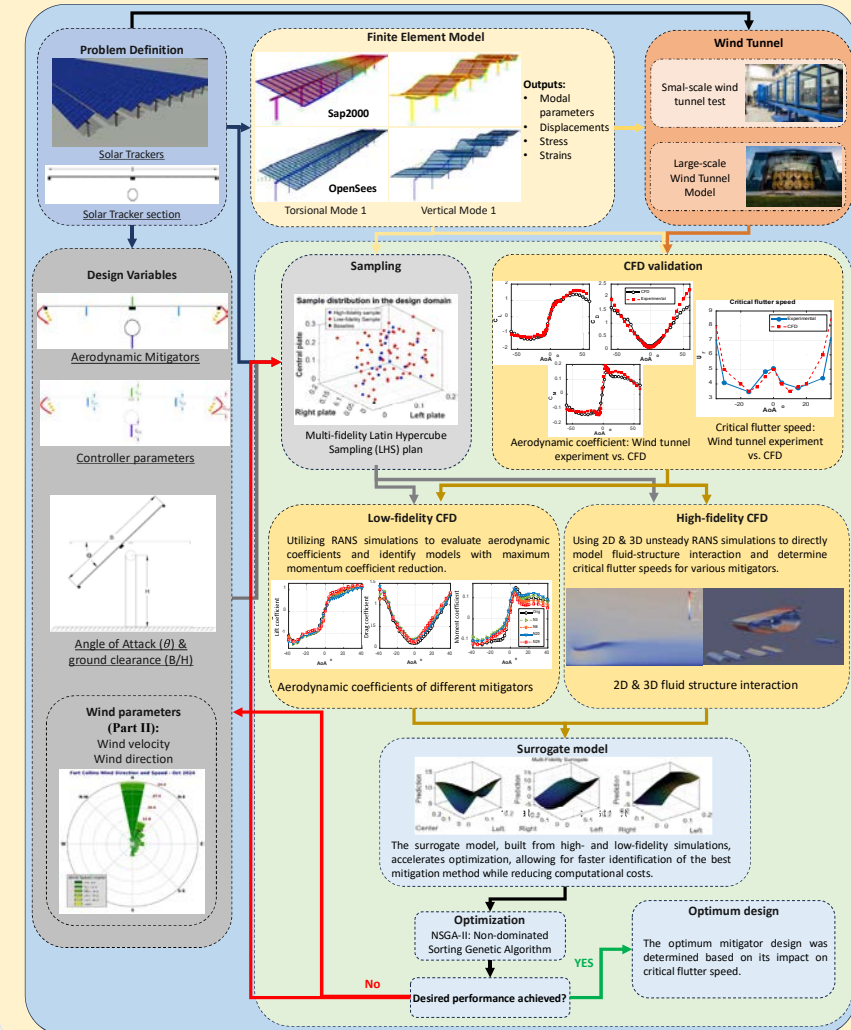
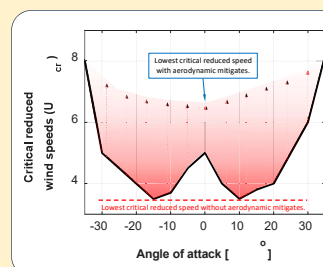
A digital twin model integrates real-time wind forecasting, computational fluid dynamics (CFD) results, and structural analysis to support decision-making regarding tracker stow. The goal is to determine the best strategies to improve system performance under varying wind conditions based on wind forecasts and implementation of aerodynamic mitigators.



## Part II: Aerodynamic mitigator to decrease tracker instabilities

OpenFOAM simulations assess aerodynamic performance of various mitigators through aerostatic force analysis and 2D/3D fluid-structure interaction (FSI).

- Initial steady Reynolds-averaged Navier-Stokes (RANS) simulations evaluate aerodynamic mitigators before detailed FSI studies.
- Promising mitigators undergo in-depth 2D/3D FSI analysis to assess aerodynamic and structural performance, with results integrated into a surrogate model for optimization.
- Using the NSGA-II<sup>8</sup> optimization algorithm, the optimal design was identified and validated through high-fidelity CFD simulations.



## Future Work:

- Extend CFD simulations to multi-row solar tracker farms, evaluating different aerodynamic mitigators for each row to address varying wind effects.
- Enhance wind forecasting by incorporating radar, satellite, into the deep learning nowcasting model.
- Develop a digital twin model for efficient simulations of various what-if scenarios, optimizing emergency response strategies under extreme winds.
- Analyze cost-effectiveness by assessing LCOE reduction when implementing the proposed mitigation strategies compared to baseline systems.

# Photovoltaic Module Backsheet Burns Attributed to Misaligned Busbar Wires

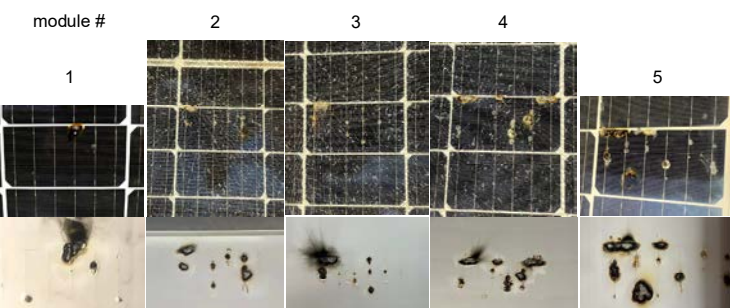
Steve Johnston, Dana B. Kern, Rebecca B. Wai, Harvey Guthrey, Steven P. Harvey, and Ingrid L. Repins

National Renewable Energy Laboratory, Golden, CO, 80401, U.S.A.

## Module backsheet burn

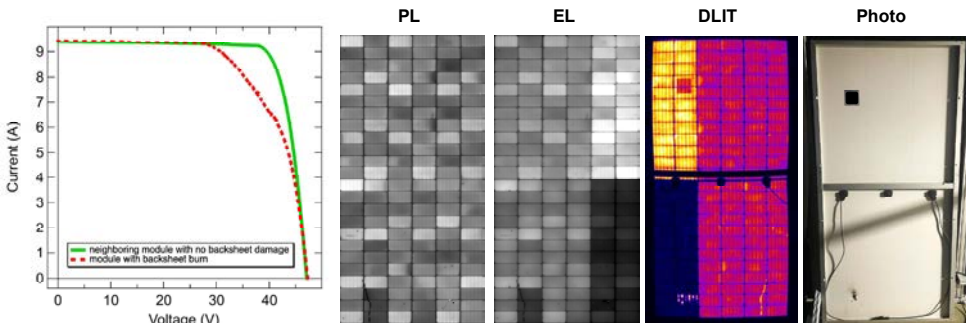


## Five example modules with backsheet burns



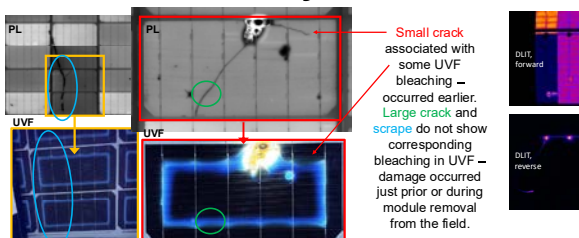
Front images on top and rear images on bottom. The front glass is sometimes broken due to the thermal stresses of the hot spots. Burn marks are located in lines along busbars. The rear side photos have been horizontally flipped so that the burn patterns match the views from the front.

## I-V curve and luminescence and thermal imaging



The current-voltage (I-V) curve of the burned module shows fill factor loss compared to a neighboring undamaged module. The module has three junction boxes as shown in the photo on the right. There are top and bottom parallel strings of cells. The photoluminescence (PL) and electroluminescence (EL) images are collected from the front side, while the dark lock-in thermography (DLIT) image and photo are from the rear side. The EL and DLIT images show that current cannot flow easily through the string with burn marks and damaged cell, as a higher ratio of current flows through the upper string. DLIT shows heating along busbars of the burned-area cell.

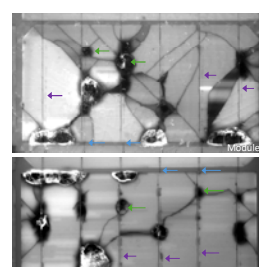
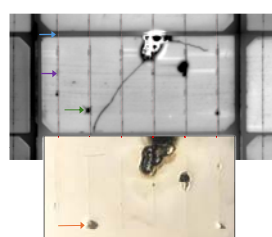
## UV fluorescence showing cell crack history



## Reverse bias with no significant hot spots

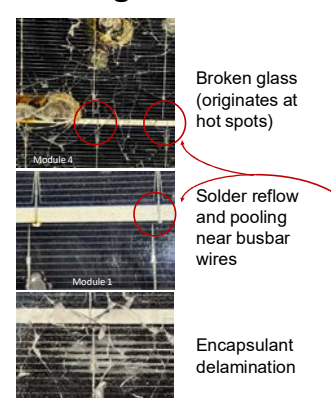
DLIT images show heating due to current flow with more current through the parallel upper left string due to the defects on the burned cell areas in the lower string. In reverse bias, current flows through the bypass diodes. The right image shows a neighboring module. When the bypass diodes are disconnected, reverse bias can force current through the cells and show localized areas of early breakdown. These reverse-bias hot spots are overlaid on the module's EL image. The spots do not heat enough to induce damage (outdoor fielding) and are only weakly detectable with DLIT.

## Misaligned wires observed on cells that have backsheet burns



The rear-side photo is horizontally flipped to match the front PL image. Misalignment is observed where wires wrap from cell to cell (blue arrow and red dashed lines). Dark lines on the PL image arise from rear-side wires misaligned from the busbar (purple arrow). Burn marks are offset from front-side busbars (green arrow). Burn marks are aligned with raised bubbles and dimples in the backsheet and co-located with the rear-side wires (orange arrow).

## Other issues related to misaligned wires



## Laser-scribed isolated cell areas from:

### Nominal cell

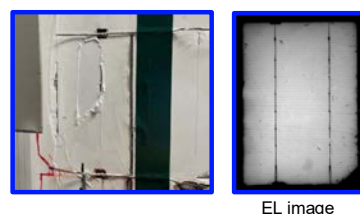
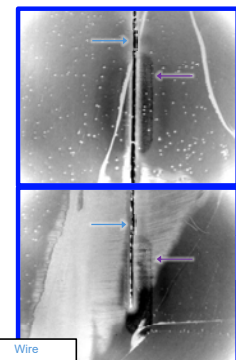
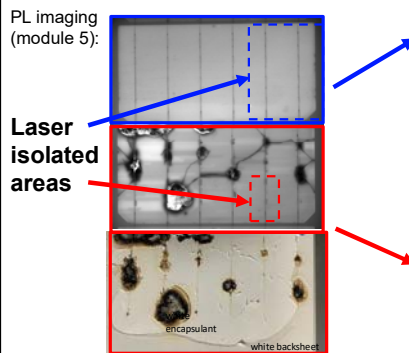


### Image wire alignment through back encapsulation

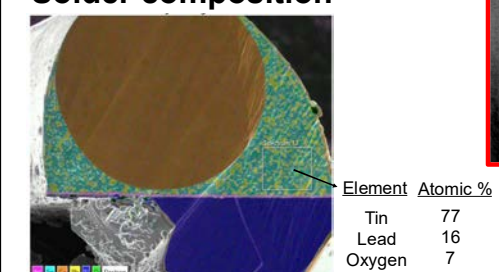


## Peel backsheet areas from nominal cell and burned/misaligned wire cell

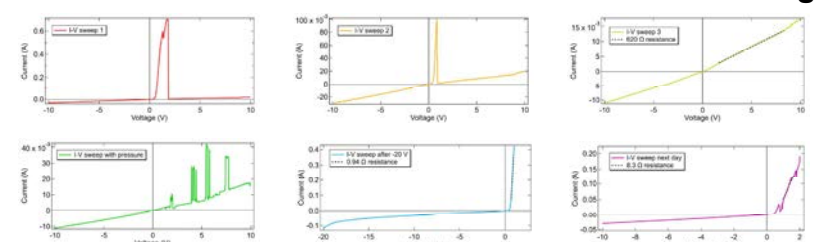


The backsheet has been partially peeled off over the burned cell, but the rear encapsulation is white and not transparent. The rear-side photo is horizontally flipped to match the orientation

## Solder composition



## Measure I-V of laser-scribed isolated cell area with misaligned wire



Consecutive I-V curves initially show a momentary spike of current and nominal diode resistance, followed by high resistance as applied voltage increases. However, by the third sweep, the resistance remains high (~600 Ω). Pressing on the wire correlates to current spikes. A large reverse bias of -20 V has led to a temporary low resistance and diode-like curve. However, high resistance returns after no current is run overnight.

## Summary and Recommendations

- Misaligned busbar wires led to hot spots that burned through the backsheet and often shattered the front glass of the affected modules.
- The observed hot spots are not attributed to partial shading, reverse breakdown, or failed bypass diodes.
- The solder has a conventional tin and lead composition and not a low-temperature variety.
- The solder pads show evidence that the busbar wires were initially attached to the solder pads.
- It is speculated that the lamination process provided force to shift the wires off the solder pads, perhaps shearing a strip of the solder pad from the cell.
- The misaligned busbar wires show inconsistent contact quality. It is also speculated that the wires had pressure from the lamination to maintain good contact long enough to pass final flash testing and EL imaging and initially perform adequately in the field.
- Visual inspections for misaligned wires should be performed to prevent this problem in the future. Soldering quality should be well controlled and verified. Inspections could be part of automated factory imaging (visible and/or infrared). Installers should perform visual spot checks when modules are received.**

The increased complexity of half-cell modules raises the likelihood of soldering-related defects, making robust quality control even more essential. Weak soldering, in particular, is concerning due to its latent nature—it is often difficult to detect during production but can deteriorate over time under operational stress or long-term field conditions. These challenges highlight the need for rigorous material inspections, process validation, and consistent process control to ensure long-term module reliability and safety.

F. Lu, M. Mohammadnezhad, and D. Cowan, "The 2025 PV Module Manufacturing Quality Report," Kiwa PI Berlin, kiwa.com/pi-berlin, 2025.

# Off track: performance impacts of PV tracker mishaps

Sara MacAlpine, JUWI Solar

Simulated annual energy losses for a single-axis tracking bifacial PV array located in sunny Tucson, AZ

## STALLS!



| ANNUAL SIMULATED ENERGY LOSS |      |         |         |
|------------------------------|------|---------|---------|
| Stow Angle                   | 0°   | +/- 45° | +/- 60° |
| Blocks Affected              |      |         |         |
| 1%                           | 0.2% | 0.3%    | 0.3%    |
| 10%                          | 2.2% | 3.0%    | 3.3%    |
| 25%                          | 2.9% | 7.5%    | 8.3%    |

## STOWS!



### Simplified Stow Strategy:

- Stow at 30°/30mph, 40°/40mph, 50°/50+mph
- Tracker moves 5 degrees/minute
- Spend minimum 15 minutes in stow once initiated

Energy  
Loss: 0.4%

### Double Minimum Time Spent In Stow:

Energy  
Loss: 0.56%

### Increase All Stow Tilts by 10°

Energy Loss: 0.56%

### Decrease Wind Stow Threshold by 5mph

Energy Loss: 1.0%

### by 10mph

Energy Loss: 2.2%

## SHADINGS!



| Cross Axis Tilt | 28% GCR               |                          | 35% GCR               |                          |
|-----------------|-----------------------|--------------------------|-----------------------|--------------------------|
|                 | Standard Backtracking | Slope Aware Backtracking | Standard Backtracking | Slope Aware Backtracking |
| 0.5°            | 1.0%                  | 0.0%                     | 1.1%                  | 0.0%                     |
| 1.0°            | 2.1%                  | 0.0%                     | 2.6%                  | 0.0%                     |
| 2.0°            | 3.1%                  | 0.1%                     | 4.3%                  | 0.1%                     |
| 3.0°            | 3.5%                  | 0.2%                     | 4.8%                  | 0.2%                     |
| 5.0°            | 4.5%                  | 0.6%                     | 5.9%                  | 0.5%                     |

Conservative cross axis tilt in slope aware backtracking could minimize risk of shading losses with little downside

### Continuing Work:

- Automated identification of tracker issues
- Validation of pvlib self shading simulation results
- Investigation of further uses for the pvlib self shading and tracking modeling tools

This work uses pvlib code as provided and described in  
Going beyond stuck trackers: how well do your trackers work?  
W. Hobbs and K. Anderson. Photovoltaic Reliability Workshop  
March 4-6 2025, Denver Colorado USA.